

General Strong Coupled Mode Theory For Multiwaveguide Nonlinear Directional Couplers

by

Farshid Farjady



**Department of Electronic and Electrical Engineering
University College London**

Submitted in accordance with the requirements of the University of
London for the degree of Doctor of Philosophy

October 1996

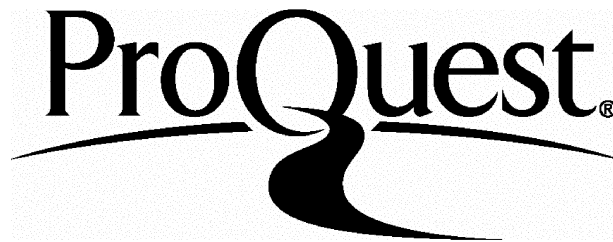
ProQuest Number: 10046046

All rights reserved

INFORMATION TO ALL USERS

The quality of this reproduction is dependent upon the quality of the copy submitted.

In the unlikely event that the author did not send a complete manuscript and there are missing pages, these will be noted. Also, if material had to be removed, a note will indicate the deletion.



ProQuest 10046046

Published by ProQuest LLC(2016). Copyright of the Dissertation is held by the Author.

All rights reserved.

This work is protected against unauthorized copying under Title 17, United States Code.
Microform Edition © ProQuest LLC.

ProQuest LLC
789 East Eisenhower Parkway
P.O. Box 1346
Ann Arbor, MI 48106-1346

To my parents

ACKNOWLEDGEMENTS

Firstly I am indebted to my supervisor Prof Mike Wilson for introducing me to this field of research, and for his continuous advice, guidance, and encouragement throughout my PhD.

I am very grateful to my PhD advisor Dr Paul Radmore for technical suggestions and discussions throughout my PhD, and for valuable advice on mathematical methods and technical writing.

Special thanks goes to Dr David Haigh for his help and encouragement throughout my PhD.

I would also like to thank Prof Roy Cole for his help and support since the early days I came to UCL.

I wish to thank Dr Marco Federighi for several valuable discussions.

I wish to thank many of my past and present friends and colleagues for contributing to a lively and enjoyable environment conducive to research. I would especially like to mention Dr Mike Plissi, Dr Brian Stothard, and Dr Danny Webster.

I am very grateful to EPSRC for financing my PhD.

Finally, I wish to thank my parents for giving me unlimited support and encouragement throughout my entire education.

ABSTRACT

Three main topics are covered in this thesis.

The first part of this thesis concerns new theoretical work on strong coupled mode theory for the multiwaveguide nonlinear directional coupler (NLDC). The coupled mode equations for the general case including all the guides interacting are derived for the first time and expressed in the form of a new single-line matrix equation. The matrix form allows the physics of the NLDC to be immediately apparent. We discuss an error in the literature regarding the strongly coupled two guide case. Two new identities for the NLDC are derived. We propose an improvement on the coupled mode theory model by taking into account the power held in the overlap. We show for the first time analytical solutions for the strong coupling case, and derive a new accurate analytical formula for the switching power.

We numerically check our equations against other methods and against beam propagation method simulations for both weak and strong coupling regimes. We also study in detail the variation of the coefficients appearing in the equations against different parameters.

The second part concerns a new soliton generator based on graded nonlinearities. It is shown that this device leads to cleaner and more efficient single-soliton generation, and can be used to improve the efficiency of soliton couplers. Our device has the advantage that it prevents multisoliton emission effects normally associated with uniform nonlinear devices. It is also a linear scanner in contrast with previous uniform nonlinear devices which were angular scanners.

We next propose a novel three guide graded-nonlinear soliton coupler. It is simpler to operate and more efficient than a previous published device which used uniform nonlinearity. It operates solely by means of the power of the propagating optical beam, whereas the previous published device required an additional control beam.

CONTENTS

Acknowledgement	3
Abstract	4
Table of contents	5
Table of figures	11
General introduction	14
1 Nonlinear Materials	17
1.1 Introduction.....	17
1.2 Bound-electron nonlinearities (the Kerr effect)	17
1.3 Dynamic nonlinearities.....	19
1.3.1 Nonlinearity due to free carriers.....	19
1.3.2 Bandfilling nonlinearities.....	20
1.3.3 Exciton enhanced nonlinearities.....	20
1.4 Two photon absorption	21
1.5 Nonlinear materials.....	21
1.5.1 Semiconductors	21
1.5.1.1 Below bandgap (non-resonant) nonlinearities	22
1.5.1.2 Multi-Quantum wells	23
1.5.2 Glasses	23
1.5.3 Semiconductor-doped glasses	24
1.5.4 Erbium doped glasses.....	24
1.5.4.1 Review of erbium doped fibre lasers and amplifiers	24
1.5.4.2 Using erbium-doped silica in integrated optics	26
1.5.4.3 Nonlinearity in erbium-doped fibres	26
1.5.4.4 Semiconductor laser amplifiers	27
1.5.5 Liquid crystals	27
1.6 Conclusions	28
References	29
2 Spatial and temporal solitons	36
2.1 Introduction	36
2.2 Spatial solitons	36
2.2.1 Bright spatial solitons	36
2.2.2 Dark spatial solitons	37
2.2.3 Interaction between vector spatial solitons	38
2.2.4 Light carrying light via cross-phase-modulation	38
2.2.5 Light carrying light using photo-refractive materials	39
2.2.6 Spatial soliton x-junctions and couplers	40
2.2.7 Optical vortex solitons	40
2.2.8 Spiralling spatial solitons	41
2.2 Temporal solitons	41

References	43
3 Linear strong coupled mode theory.....	46
3.1 Introduction	46
3.2 Linear strong coupled mode theory	47
3.3 Coupled mode equations	48
3.3.1 Strong coupled mode equations	49
3.3.2 Weak coupled mode equations	51
3.4 Physical consequences of the overlap integrals	52
3.5 Multiwaveguide case	53
3.5.1 Comparison between different notations	53
3.6 The modification coefficient	56
3.7 Relative magnitudes of coefficients	57
3.8 Lossless systems	57
3.9 Prior weak coupled mode theories in hindsight	59
3.10 Solution of coupled mode equations	59
3.11 Conclusions	62
References.....	63
4 The nonlinear directional coupler: Review of the literature	65
4.1 Introduction	65
4.2 The nonlinear coupler: the basics and general review of the literature	65
4.3 Pulsed operation of nonlinear directional couplers	68
4.4 Incorporation of other effects	69
4.4.1 Diffusion	69
4.4.2 Saturation	69
4.4.3 Asymmetric nonlinearities/waveguides	69
4.4.4 Incorporation of gains and losses	70
4.4.5 Multiwaveguide nonlinear couplers	71
4.4.6 Non-parallel nonlinear couplers	72
4.5 Practical nonlinear directional couplers	72
References	72
5 New formalism and identities for nonlinear coupled mode equations	78
5.1 Introduction	78
5.2 Definition of the nonlinear coefficients	79
5.3 Power dependent coefficients	83
5.4 Derivation of new identities	83
5.4.1 Lorentz reciprocity theorem	83
5.4.2 Derivation of new identities	84
5.4.2.1 Nonlinear-nonlinear identity	84
5.4.2.2 Linear-nonlinear identity	87
5.4.2.3 Linear-linear identity	89
5.4.2.4 Applications of the identities	91
5.4.2.5 Relationship between the three identities	93

References	94
6 Strong CMT for multiwaveguide nonlinear couplers	96
6.1 Introduction	96
6.2 Derivation of the nonlinear coupled mode equations	100
6.3 Description of the multiwaveguide system under consideration	101
6.4 The two-guide case	105
6.4.1 Comparison with Meng and Okamoto	105
6.4.2 Comparison with Fraile-Pelaez	106
6.5 Three waveguides	107
6.6 Four waveguides	109
6.7 Assuming interaction between all the waveguides	109
6.8 Conclusions	110
References	111
7 In matrix form	113
7.1 Introduction	113
7.2 Adjacent guide interactions	113
7.2.1 The formulation	113
7.3 Matrix form- assuming interaction between all the guides	116
7.3.1 Two guide operation	118
7.3.2 The three guide coupler	118
7.4 Lossless case: violation of conservation of power in key papers	119
7.5 Conclusions	121
References	122
8 Beam propagation method and coupled mode theory programs	124
8.1 Introduction	124
8.2 Beam propagation method algorithm	124
8.2.1 Introduction	124
8.2.2 The beam propagation method algorithm	125
8.2.3 The computer model	128
8.2.4 Optimizing the beam propagation method program	129
8.2.5 The input field to the nonlinear directional coupler	129
8.2.6 Absorbing edges	131
8.3 Runge-Kutta solution of coupled mode equations	132
8.3.1 Introduction	132
References	138
9 Power independent coefficients.....	140
9.1 Introduction	140
9.2 The slab waveguide	140
9.2.1 Eigenvalue equation	141
9.3 Calculating the propagation coefficient	142

Contents

9.4 Relating amplitude to total power	142
9.5 Two waveguides	143
9.6 Calculating the linear coefficients	144
9.6.1 Overlap integral.....	144
9.6.2 The coupling coefficient.....	146
9.6.1 The modification coefficient	147
9.7 Calculating the nonlinear coefficients	147
9.7.1 The self-phase-modulation.....	147
9.7.2 The larger-cross-phase-modulation coefficient.....	148
9.7.3 The cross-phase-modulation coefficient	149
9.8 Comparison between the nonlinear coefficients.....	150
9.9 Conclusions	152
References	152
10 Coefficients incorporating nonlinear TE modes.....	153
10.1 Introduction	153
10.2 Nonlinear guided waves- Literature survey	153
10.2.1 Miscellaneous NLGWs.....	155
10.2.2 Practical NLGWs.....	155
10.2.2.1 Launching requirements	155
10.2.2.2 Effects of losses, saturation, and diffusion.....	156
10.2.2.3 Nonlinear mode along a curved interface.....	156
10.2.3 Soliton interaction with nonlinear interfaces and waveguides.....	156
10.2.4 Soliton emission from nonlinear waveguides.....	157
10.2.5 Spatial soliton emission from tapered waveguides.....	158
10.2.6 Gain	158
10.3 The nonlinear slab waveguides	159
10.3.1 Nonlinear waves in a self-focusing nonlinear medium	159
10.3.2 Linear core with nonlinear cladding on both sides.....	161
10.3.4 Linear core with nonlinear cladding on one side.....	165
10.3.5 Calculating the total power	166
10.3.6 Comparing the field amplitude with that calculated in chapter 9.....	171
10.4 The nonlinear directional coupler	171
10.5 Variation of coefficients with input power.....	173
10.5.1 Overlap integrals.....	174
10.5.2 Coupling coefficient.....	175
10.5.3 Nonlinear modification coefficients (NLMC).....	177
10.5.4 The nonlinear cross-coefficients.....	178
10.6 Conclusions for chapter 10.....	182
References.....	183
11 Analytical solution to nonlinear coupled mode equations.....	187
11.1 Introduction	187
11.2 Transforming to Stokes parameters	188

11.3 Constants of motion	192
11.3.1 Calculation of the total power	192
11.3.2 The Poincaré equations (spheres, ellipsoids, and paraboloids)	193
11.3.2.1 Strong coupling case	194
11.3.3 The parabolic surface	196
11.4 Critical power formula.....	197
11.4.1 Intersection between the two geometrical surfaces	197
11.4.2 Physical explanation for the coupled mode formula	200
11.4.2.1 Effects of linear and nonlinear coefficients	200
11.5 Power curves.....	202
11.5.1 Power as a function of distance	202
11.5.1.1 Below critical power	203
11.5.1.2 Above critical power	204
11.6 Conclusions	206
References	207
12 Numerical comparison of coupled mode theory with BPM.....	208
12.1 Introduction	208
12.2 Critical power curves.....	208
12.2.1 Varying the guide thickness	209
12.2.2 Comparison with BPM for a ‘thick’ guide.....	211
12.2.3 Comparison with BPM for a ‘thin’ guide.....	214
12.3 Some notes on the BPM analysis.....	217
12.4 Conclusions.....	218
References	219
13 Novel graded-nonlinear scanner and single soliton generator.....	220
13.1 Introduction	220
13.2 Graded nonlinear waveguides	221
13.3 Conclusions	225
References.....	226
14 Novel tri-state spatial soliton switch using graded nonlinearities.....	227
14.1 Introduction	227
14.2 New graded-nonlinear tri-state switch	228
14.3 Device geometry.....	229
14.4 Results.....	232
14.5 Conclusions.....	235
References	236
15 Conclusions and future work	237
15.1 Summary of results and conclusions	237
15.1.1 Conclusions (part 1): Coupled mode theory for the multiwaveguide nonlinear	

Contents

directional coupler.....	237
15.1.2 Conclusions (part 2): Graded nonlinear soliton generator.....	239
15.1.3 Graded nonlinear three guide soliton coupler.....	239
15.2 Future work and some novel devices	239
References	242
Appendices	244
Appendix 1 Summary of results and conclusions	247
Appendix 2	248
Appendix 3 Z-reversal concept.....	249
Appendix 4 Lorentz' reciprocity theorem.....	250
Appendix 5	251
Appendix 6	252

TABLE OF FIGURES

Chapter 3

Fig. 3.1 a-c	Illustrating the permittivity profiles	49
Fig. 3.2	Symmetrical guides	52
Fig. 3.3	Asymmetrical guides	53
Fig. 3.4	Asymmetrical weakly coupled guides	53
Fig. 3.5	Effect of modification coefficient	57
Fig. 3.6	Effect of modification coefficient	57

Chapter 5

Fig. 5.1	Power dependent mode shapes (nonlinear film region)	83
Fig. 5.2	Power dependent mode shapes (nonlinear coupling region).....	83
Fig. 5.3	Perturbing a nonlinear guide.....	85
Fig. 5.4	Illustrating the unperturbed and the perturbed systems.....	87
Fig. 5.5	Perturbing one linear waveguide to form another	90

Chapter 6

Fig. 6.1	Illustrating the aligned and non-aligned waveguide geometries	98
Fig. 6.2	Constructing the perturbed system	101
Fig. 6.3	Showing the perturbed and the unperturbed systems.....	102

Chapter 8

Fig. 8.1	Illustrating the BPM algorithm	128
Fig. 8.2	Exciting the guide with a non-modal field shape.....	130
Fig. 8.3	Multisoliton emission	130
Fig. 8.4	Exciting the guide with the correct nonlinear TE mode shape.....	131

Chapter 9

Fig. 9.1	The slab waveguide arrangement	140
Fig. 9.2	Parallel slab directional coupler	143
Fig. 9.3	Variation of the overlap integral with guide width.....	146
Fig. 9.4	Variation of the coupling and modification coefficients	147
Fig. 9.5	Variation of SPM coefficient with increasing guide separation.....	148
Fig. 9.6	Variation of larger XPM coefficient with guide separation	149
Fig. 9.7	Variation of XPM coefficient with guide separation.....	150
Fig. 9.8	Comparison between the different coefficients	151
Fig. 9.9	Comparison between the different coefficients	151
Fig. 9.10	Variation of different coefficients with input power.....	152

Chapter 10

Fig. 10.1	The nonlinear directional coupler.....	159
Fig. 10.2	Illustrating linear core with nonlinear claddings.....	161

Table of figures

Fig. 10.3	Illustrating the linear core, and nonlinearity in region 1 only.....	165
Fig. 10.4	Dispersion diagram.....	167
Fig. 10.5	BPM simulation. Power=72 Watts/m (state (i)).....	168
Fig. 10.6	BPM simulation. Power=72 Watts/m (state (ii))	169
Fig. 10.7	BPM simulation. Power=72 Watts/m, (state (iii))	169
Fig. 10.8	Illustrating total power/unit length against x_{01} for $d = 2.0\mu m$	170
Fig. 10.9	Illustrating power/unit length against x_{01} for $d = 1.0\mu m$	170
Fig. 10.10	Mode shapes for three powers	173
Fig. 10.11	Variation of overlap integral with input power	174
Fig. 10.12	Variation of coupling coefficients with input power	177
Fig. 10.13	Variation of Q_1 and Q_1^m with guide thickness and input power.....	178
Fig. 10.14	Variation of Q_2 with input power $d = 2.0\mu m$	179
Fig. 10.15	Comparison between Q_2 and Q_3 with input power	180
Fig. 10.16	Comparison between $Q_{2,av}^m$ and Q_3^m	181
Fig. 10.17	Comparison between Q_1 , Q_2 , and Q_3	181.
Chapter 11		
Fig. 11.1	The Poincaré sphere.....	194
Fig. 11.2	The effect of the overlap integral on the ellipsoid.	196
Fig. 11.3	Intersection between the two constants of motion.	198
Fig. 11.4	Trajectories resulting from the intersection between the two geometric surfaces for different input powers.....	199
Fig. 11.5	Effect of increased coupling on the critical power.....	201
Fig. 11.6	Effect of increasing SPM on the critical power	202
Fig. 11.7	Power vs propagation distance	205
Chapter 12		
Fig. 12.1	Critical power vs guide separation for different thicknesses.....	210
Fig. 12.2	Comparison between different methods for $d = 2\mu m$	212
Fig. 12.3	Effect of various coefficients on the critical power. $d = 2\mu m$	213
Fig. 12.4	Comparison between different methods for $d = 0.5\mu m$	214
Fig. 12.5	Effect of various coefficients on the critical power. $d = 0.5\mu m$	215
Fig. 12.6	Improved accuracy using normalised fields	216
Fig. 12.7	Crit power vs guide separation for guide thicknesses $d = 0.5\mu m$. ..	217
Chapter 13		
Fig. 13.1	The graded-nonlinear waveguide converting a linear TE mode to nonlinear TE mode in a $d = 1.0\mu m$ waveguide (input power=200 W/m).	222
Fig. 13.2	Generation of a single soliton using the graded-nonlinear waveguide (input power=200 W/m).....	224
Fig. 13.3	Variation of waveguide power with propagation distance for different input powers in uniform-nonlinear waveguide	224
Fig. 13.4	Improved switching using a graded-nonlinear waveguides	225

Table of figures

Chapter 14

Fig. 14.1	A schematic of the device geometry.....	231
Fig. 14.2	The variation of the nonlinearities in the two cladding with distance.	231
Fig. 14.3	BPM diagram for 50 Watts/m input power	233
Fig. 14.4	Power switches to the right hand guide at 90 Watts/m	233
Fig. 14.5	Power switches to the left hand guide at 130 Watts/m	234
Fig. 14.6	Switching characteristics	135

Appendices

Fig. A4.1	Illustrating Lorentz theorem	231
------------------	------------------------------------	-----

GENERAL INTRODUCTION

In the eighties dispersion was the main limitation in the exploitation of the huge bandwidth of the optical fibre ($\sim 10^{15} \text{ Hz}$) for long distance communications. Dispersion resulted in distortion of the transmitted pulses, which meant that electronic repeaters were required for their periodic reshaping and amplification. Apart from being very expensive, electronic repeaters acted as an obstacle against increasing the transmission rate of pulses because of the limited response time of electronics. Today, many of the problems which initially beset all-optical transmission have been overcome. The introduction of erbium doped fibre amplifiers has resulted in cheap and fast all-optical amplification instead of expensive and slow electronic amplification. The employment of temporal soliton pulses has led to distortion free pulse transmission. The main problem which used to limit soliton transmission rate, ie the Gordon-Haus jitter (a frequency modulation on the lightwave caused by amplifier noise interacting nonlinearly with the lightwave) has now been overcome using frequency filters. All-optical long distance transmission exploiting most of the bandwidth of the fibre now seems to be within reach. The exploitation of the huge bandwidth of the optical fibre is still however practically of little use because once the light reaches the end of the fibre, it is then converted into electrical signals and then processed with electronics (which is slow due to capacitive delays). Therefore ways are being explored to replace electronic components with all-optical components for signal processing. Such all-optical components will make use of nonlinear materials which have intensity dependent refractive indices. A beam of light travelling through such a nonlinear optical device temporarily changes nonlinearly, the refractive index (which defines the device), and in turn alters the optical characteristics of the device. Therefore the nature of transmission for that beam of light (or also for another beam) travelling through the device is changed. In summary, in all-optical devices the propagation of an optical beam is controlled optically rather than electronically.

In the past couple of decades rapid progress has been made in the search for all-optical components. All-optical switches, transistors, filters, scanners, and pulse compressors are to name a few. Many of these components will also be used as parts of a future all-optical computer (to be constructed hopefully within the next few decades). The operational speed of these computers will be several orders of magnitude faster than electronic computers today.

In this thesis several new all-optical components are studied. The first is the nonlinear directional coupler (NLDC) which is perhaps the most useful all-optical

device. For maximum generality, the strongly-coupled multiwaveguide coupler is considered (for the first time). By introducing matrix formalism, the full coupled mode equations of the general multiwaveguide case are combined into a single matrix equation. An improved coupled mode theory is proposed which is more consistent and accurate than previous attempts found in the literature. We show that a serious error exists in the methods of some important papers in the literature regarding the two guide case. In the final two chapters of the thesis, we study two novel devices: the graded nonlinear soliton generator and the three guide graded-nonlinear soliton coupler. The graded nonlinear soliton generator is capable of linear scanning, leads to single soliton emission, and is more efficient for switching in soliton couplers. The three guide graded-nonlinear soliton coupler makes use of graded nonlinearities in achieving two-side soliton generation. A brief overview of the thesis is now given.

Chapters 1-4 are review chapters setting the background for the rest of the thesis. Recent papers in the literature regarding nonlinear materials, spatial and temporal solitons, linear strong coupled mode theory, and nonlinear directional couplers are reviewed. Chapters 5-7 concern nonlinear coupled mode theory for multiwaveguide nonlinear couplers. In particular, chapter 5 introduces the formalism for the coefficients and derives new identities for the nonlinear coupler. In chapter 6, the nonlinear coupled mode equations of the multiwaveguide coupler are derived. This theory is accurate for the cases of strong coupling, and applies to coupling between all the guides. In chapter 7 the coupled mode equations are repackaged into an elegant single-line matrix format. In chapter 8, the beam propagation method program used later in the thesis is explained, as well as the numerical procedure for integrating the nonlinear coupled mode equations using Runge-Kutta. In chapter 9, the power independent linear and nonlinear coefficients are calculated. The variations of these coefficients with change in parameters including guide separation and guide thickness are investigated. In chapter 10, the power dependent linear and nonlinear coefficients are calculated which are then compared with those of chapter 9. In chapter 11 an analytical solution for the full nonlinear coupled mode equations is derived using elliptical functions. It is shown that two constants of motion can be extracted, one of which is an ellipsoid. An accurate formula for the critical power is also derived. In chapter 12 we compare the accuracy of results obtained using the critical power formula against those using the beam propagation method. We discuss in detail a serious flaw in the literature regarding the inconsistent inclusion of the overlap integral in the coupled mode equations.

In chapter 13 there is a shift in topic towards soliton devices. A novel graded

nonlinear soliton scanner is studied. This scanner is capable of single soliton generation, and can be used for linear scanning purposes instead of angular scanning. Switching in these scanners is much sharper than in previous uniform nonlinear scanners.

In chapter 14 we propose a novel three guide soliton coupler which makes use of graded nonlinearity. This coupler is simpler to operate and more efficient than ones found in the literature which make use of uniform nonlinearities. The switching here is dependent entirely on the input power rather requiring an additional control beam.

Conclusions and further work are finally presented in chapter 15.

CHAPTER 1

NONLINEAR MATERIALS

1.1 INTRODUCTION

The all-optical components studied in this thesis all make use of nonlinear materials with intensity dependent refractive indices (Kerr effect). In this chapter, the origin of the intensity dependent refractive index is discussed, starting from the ideal Kerr effect originating from bound-electron effects. Other effects which also lead to intensity dependent refractive index changes in practical materials, such as free carriers, bandfilling, and two photon absorption are next described, followed by a review of a selection of nonlinear materials including semiconductors, semiconductor doped glasses, active semiconductor materials, glasses, erbium doped glasses, and liquid crystals.

1.2 BOUND-ELECTRON NONLINEARITIES (THE KERR EFFECT)

The classical model for nonlinear effects in materials is the Lorentz forced oscillator model. The electric field of the light provides a driving force which drives oscillators consisting of electron clouds bound to their respective atomic nuclei. For this discussion we assume that the light is single frequency and that it propagates inside an isotropic dielectric medium. The electric field shifts the electron clouds from their equilibrium positions creating separated positive and negative charges or dipoles. At low light intensities, the displacement of each electron cloud varies linearly with the electric field. Each electron cloud therefore oscillates around its equilibrium position at the same frequency as the incident oscillating field. The oscillation of the dipole is accompanied by absorption and temporary storage of energy from the incident light as the displacement is increasing, and release of this energy back into medium when decreasing. The frequency of the radiated light is the same as the frequency of the oscillating dipole and the incident light. However it is phase-shifted with respect to the incident light because of the absorption and radiation processes. Macroscopically the material appears to have a refractive index which induces a phase-shift on the light propagating through it.

The electron clouds oscillate with larger amplitudes for higher light intensities.

When the light intensity becomes very large, the displacement of the electron cloud becomes a nonlinear function of the driving field at the extremities of displacement. In effect the oscillation of the electron cloud resembles a sinusoidal wave with distorted peaks and troughs. Since the oscillation is therefore no longer purely sinusoidal it is no longer oscillating at a single frequency. In other words, each dipole oscillates at several different frequencies simultaneously and radiates all these frequencies back into the medium. These emitted frequencies are all phase-shifted with respect to the incident light. In addition to the linear contribution at the fundamental frequency ω , there is a nonlinear contribution at frequency ω (proportional to the intensity of the light) due to third-order nonlinear effects (mixing of ω , $-\omega$, and ω field components), plus nonlinear contributions at dc and 2ω due to second-order nonlinear effects, and components at multiples of the fundamental frequency such as 3ω , 4ω etc. Normally only the linear and nonlinear components at the fundamental frequency ω build up cumulatively. The higher frequency components (which give rise to second, third harmonic generation etc) only build up if there is some kind of phase matching.

All materials exhibit third-order nonlinear effects, whereas only non-centrosymmetrical materials exhibit second-order effects. In centrosymmetrical materials such as SiO_2 optical fibres, where there is an inversion symmetry, an intense light beam distorts the oscillation of the dipoles equally in both directions that it is applied. This means that dc components are absent in these cases and therefore second-order nonlinearities, which are responsible for dc components, are also absent.

The greater the order of the nonlinearity, the smaller the nonlinear effect. Third-order nonlinearities which give rise to intensity dependent refractive indices are normally quite weak effects. Large intensities are needed to exploit them. Apparently this might require large powered pulsed lasers, making it seem impractical outside the laboratory. However optical fibres and integrated optical waveguides with thicknesses of the order of microns have made nonlinear optics at low powers a practical reality. Since the fields are confined to narrow regions, moderate powers can now produce very intense beams. The intensities become so high, that appreciable refractive index changes can be induced in the medium [1-6]. Moreover, use of waveguides allows diffractionless propagation for sufficient distances to allow nonlinear effects to fully take place.

Recently it has been shown that it may be possible for fields to travel inside a bulk medium without need for a waveguide. These fields 'create' their own waveguides in the nonlinear medium and are called spatial solitons. The application of spatial solitons for ultrafast signal processing systems still awaits the search for suitable nonlinear materials. At present materials do exist which support spatial solitons at low powers but

are either too slow or lossy. Eventually suitable materials will be found opening up new possibilities unavailable to integrated nonlinear optics today.

1.3 DYNAMIC NONLINEARITIES

The bound electron nonlinearities so far are not associated with real exchange of energy between the light and the medium. The energy is only temporarily stored in the dipoles before being released again. Dynamic nonlinearities [7], on the other hand refer to cases where real exchange of energy takes place between the light and the medium as in absorption of light to generate free carriers.

1.3.1 Nonlinearity due to free carriers

The nonlinearities associated with the Kerr effect are weak. They can be enhanced by using the resonance oscillation frequencies of the dipoles. These frequencies are associated with large absorption. Since absorption is related to refractive index via the Kramers-Krönig relationship, the refractive index also increases near the resonance. As the frequency of the field approaches the resonance frequency, the electrons oscillate with greater amplitudes, and finally break off to form free carriers.

As more free carriers are produced in the material the refractive index reduces. This is because the increased free carriers cause the density of bound-electrons to reduce, and since bound electrons contribute to refractive index (as explained in section 1.2 above), the reduced bound-electron density causes a lowering of the refractive index. An empirical formula for the nonlinear refractive index can be derived. Firstly the refractive index is calculated in terms of the free carrier density using Lorentz' model (or Drude model as it is also known [8]). The free carrier density is then related to the absorption by considering a two level atom, and equating the rate of carrier generation (which is proportional to absorption of light) to the rate of carrier recombination. Once the number of free carriers is calculated in terms of the absorption coefficient, it can be substituted back into the formula for refractive index derived by the Drude model to derive the nonlinear refractive index in terms of absorption to give [7-9]

$$n_2 = -\frac{e^2 \alpha T_1}{2n_0 m^* \hbar \omega^3 \epsilon_0}$$

where α is the absorption, T_1 the recombination time, and n_2 the nonlinear refractive index defined by the refractive index $n = n_0 + n_2 I$, where n_0 is the linear refractive index, and I the light intensity. We note from the equation above that the magnitude of n_2 is proportional to absorption and the recombination time. Also that, since n_2 is

negative, an increase in intensity causes a reduction in the refractive index.

1.3.2 Bandfilling nonlinearities

There is another kind of nonlinearity associated with resonance. It is due to bandfilling and is most often encountered in semiconductors. Free carriers are generated by the light intensity. They fill up the lower energy levels of the conduction band and block the transition of further electrons. Consequently the material becomes less absorbing. The reduction in absorption can then be related to a reduction in refractive index via the nonlinear Kramers-Krönig relationships [10-11]. The reduction in absorption and refractive index are both proportional to intensity. At very high intensities, the absorption reduces so much that the material becomes transparent.

The nonlinearities associated with bandfilling are quite large, but are not strictly $\chi^{(3)}$ processes. Photogenerated carriers unfortunately diffuse resulting in the non-local nature of the nonlinearity. The nonlinearities are also accompanied by a great deal of loss. In addition they saturate (material becomes transparent at large intensities), and the nonlinearities are slow (dependent on recombination times of the order of ns to μs).

1.3.3 Exciton enhanced nonlinearities

The nonlinearity in multiquantum well (MQW) semiconductor materials is enhanced just below the bandgap due to excitonic effects. Excitons are formed due to the coulombic attraction between photogenerated electron-hole pairs. The required binding energy leads to a resonance peak just below the bandgap. In bulk semiconductors at room temperature, there is a reduction in the lifetime of the electron-hole pair, which leads to the exciton peak reducing and widening. Since in bulk materials the exciton peak is very close to the bandedge, the two edges smear into each other, and excitonic effects appear insignificant. MQW materials however consist of many thin layers of alternating bandgap materials, and the difference between the bandgaps confines the electrons and holes to the lower bandgap materials. The resulting localisation increases the lifetime of the exciton and therefore increases the binding energy which causes the excitonic peak to be further away from the bandedge. Consequently at room temperature, the exciton peak remains distinct from the bandedge.

The exciton resonance peak can be used for nonlinear effects. Here the light intensity causes an increase in the photogenerated carrier density which leads to a reduced absorption peak. The reduction in the absorption peak occurs because the increased carrier density introduce fields into the medium which 'screen' the field components holding the excitons together, thereby reducing their lifetimes.

1.4 TWO PHOTON ABSORPTION

Two photon absorption (TPA) [12-16] is a positive non-resonant nonlinearity. It occurs when two photons assist the virtual transition of an electron from the valence band to the conduction band. The first photon enables the transition from the valence band to a virtual level within the bandgap. The electron stays there only for a short time and if a second photon arrives in the intervening time, it can complete the transition of the electron to the conduction band. The process is dependent on the number of photons available, as the more photons there are the more chance that it occurs. Therefore TPA is an intensity dependent absorption process which can be related to the intensity dependent nonlinear refractive index via the nonlinear Kramers-Krönig relationships. The absorption is given by

$$\alpha = \alpha_0 + \beta_2 I$$

where α_0 is the linear absorption coefficient, β_2 the two-photon absorption coefficient and I the intensity of light. The magnitude of the nonresonant nonlinearity has a maximum near the TPA edge [17] at the half-bandgap. The nonlinearity at or below the TPA edge is positive. The nonlinearity associated with substantially above the TPA edge is negative in semiconductors.

Since TPA is not dependent on photogenerated carriers, it results in very little absorption, and consequently associated with only a small nonlinear refractive index. TPA is also a very fast process since it is a virtual process, not limited by the recombination times of photogenerated carriers or thermal effects.

1.5 NONLINEAR MATERIALS

A selection of some of the more commonly used nonlinear materials is now reviewed, including semiconductors, multiquantum well materials, glasses, semiconductor-doped glasses, erbium-doped glasses, and liquid crystals.

1.5.1 Semiconductors

Semiconductors are of interest since their properties are well-known from electronics and linear optics. They have giant nonlinearities near the bandgap resonance. Theoretical reviews can be found in [18-19].

Above the bandgap, the nonlinearity is enhanced due to bandfilling. When free carriers become generated, they rapidly fill the lower energy levels by exchanging energy with each other (electron-electron and hole-hole interactions) and with the lattice, on a time scale of $<300\text{fs}$ until they reach a quasi-equilibrium state. As the

recombination time is quite slow, the quasi-equilibrium population of excited carriers is maintained by the optical excitation preventing further excitation of carriers. The bandfilling reduces the absorption, saturating it completely at the bandedge (resulting in a blue-shift in the bandedge being observed- the dynamic Moss-Burstein shift). Resonant (above bandgap) nonlinearities are large but they are also quite slow compared with nonresonant (below bandgap) nonlinearities, since the speed of the nonlinearity is limited by the long carrier recombination time (of the order of ns to μs).

There is also a large nonlinearity associated with heating, due to the carrier-carrier collisions, but the nonlinearity is slow and positive (opposite sign to the bandfilling nonlinearity).

Finally, there is a nonlinearity associated with the bleaching of the excitonic absorption peak. However this nonlinearity is negligible in bulk semiconductors at room temperature, and is mostly observed in MQW materials.

1.5.1.1 Below bandgap (non-resonant) nonlinearities in semiconductors

Below the bandgap the nonlinearities are mostly due to bound-electrons and TPA. TPA is large for photon energies above the half-bandgap, but small for photon energies below the half-bandgap. The peak in the nonlinear refractive index occurs exactly at the half-bandgap. The absorption associated with TPA deteriorates the switching of devices. In order to make use of the nonlinearity associated with TPA, but avoid the dissipation, the device should be operated just below the half-bandgap [20]. The sign of the nonlinearity associated with TPA is positive above the half-bandgap (and negative below). Bound-electron nonlinearities (the true $\chi^{(3)}$ effect) are naturally positive in sign.

It was found in ref. 21 that above the half-bandgap, TPA imposes severe limitations on the maximum phase change obtained via ultrafast nonlinearities, irrespective of the physical length of the device. In ref. 22 a GaAs/GaAlAs MQW waveguide was operated near the half-bandgap resonance to minimise TPA. Large nonlinearities were observed, but with low absorption. The nonlinearity was of the order of $n_2 = 9 \times 10^{-14} \text{ cm}^2/\text{W}$ at $1.55\mu\text{m}$.

Nonlinear directional couplers have also been fabricated using the nonlinearity just below the TPA edge [23], where the nonlinearity was high ($n_2 = 6 \times 10^{-18} \text{ m}^2/\text{W}$) but the absorption low. A $1.5\mu\text{m}$ thick $Al_{0.18}Ga_{0.82}As$ guiding layer of length 6.25mm was used. The switching was fast (response time of $< 100 \text{ fs}$) and associated with very low losses.

All-optical demultiplexing of 500 fs pulses has also been demonstrated in a 2cm

length *AlGaAs* nonlinear coupler at $1.55\mu\text{m}$ [24].

1.5.1.2 Multi-Quantum Wells

MQW structures exhibit exciton resonances near the band-edge. The nonlinearity is larger than in bulk [25-26] due to the saturation of the exciton peak via coulomb screening of the plasma and bandfilling. Although the nonlinearities are large for the resonant effect, the drawbacks include losses, saturation, long recovery times, and thermal effects. The nonlinearity is around $n_2 = 10^{-11} - 10^{-12} \text{ m}^2/\text{W}$, and loss coefficient $\alpha = 12.9 \text{ cm}^{-1}$ [27].

Nonlinear directional couplers have been modelled [28] and constructed [29-32] in GaAs-AlGaAs MQWs. In order to obtain large nonlinearities the wavelength was chosen to be close to the bandedge, but due to high absorption large losses were incurred. In [29-32] the losses were especially large because the nonlinearity was situated in all regions of the device. In order to minimise the losses but still make use of the enhanced bandedge nonlinearity, only the coupling region can be made nonlinear [33-35].

Picosecond all-optical switching using excitonic enhancement was observed by Jin et. al. [36] in *GaAs/AlGaAs* MQWs. Nearly complete switching occurred. The power requirement was around 10W for a 1.2mm coupling length. A cavity dumped dye laser synchronously pumped by a mode-locked frequency-doubled *Nd:YAG* laser was used to generate the 10ps pulses of variable repetition rates.

1.5.2 Glasses

Although the nonlinearity in glasses is low, they can be drawn into long lengths of fibre. They can also be doped to allow for resonant nonlinearities (as in semiconductor doped glasses described below). The response time of the nonlinearity would then be related to the fluorescence time of the dopant. The non-resonant nonlinearity in glasses is very close to the ideal $\chi^{(3)}$ processes since it is of bound-electron origins. Although it is very small, it is also very fast (10^{-15} s).

The first demonstration of a NLDC capable of substantially complete all-optical switching at subpicoseconds was made in dual core fibre [37]. The switching power was 850W , and the coupler length 2.0m . NLDCs with 100fs switching times have also been demonstrated in a dual-core-fibre nonlinear couplers [37]. The length of the device was very short 0.5 cm , but required large switching powers, 32kW . A colliding-pulse mode locked dye laser and a copper-vapour-laser pumped dye amplifier system was used. The laser produced the 100fs pulses at a wavelength of 620nm ,

amplified at an 8.6kHz repetition to 100nJ. The nonlinear refractive index was $n_2 = 3.3 \times 10^{-20} \text{ m}^2/\text{W}$. They mentioned that the switching power could be reduced to much lower values by using higher nonlinearities, longer coupling lengths, and smaller core sizes, so that mode-locked semiconductor lasers could be used instead.

Spatial solitons have been observed in glasses [38-39]. Using a gaussian field, it was found that spatial solitons were formed at around 400kW. At low powers however, the effect of the nonlinearity was small, and the field diffracted. At much higher powers (around 1.25MW) TPA affected the shape of the spatial soliton. Since TPA is an intensity dependent absorption, the peak of the soliton goes through a more lossy material than the sides. Therefore the peak reduces with increased input power, whereas the sides increase (forming a three-peaked distribution). Eventually the centre of the field reduces to zero, and two spatial solitons are formed on either side of the peak, which move away with distance or with power. The system used 75fs pulses at a repetition rate of 8.6kHz and a wavelength of 620nm. A colliding-pulse mode-locked dye laser and copper-vapour-laser pumped dye amplifier arrangement was used to excite the sample. The arrangement resulted in several microjoules. The waveguide layer was 5.0μm thick, and the nonlinearity $n_2 = 3.4 \times 10^{-20} \text{ cm}^2/\text{W}$.

1.5.3 Semiconductor-doped glasses

Semiconductor doped glasses have large nonlinearities (due to bandfilling) which are very fast (tens of picoseconds). The nonlinearity is of the order of $n_2 = 10^{-13} \text{ m}^2/\text{W}$ [40] in $\text{CdS}_x\text{Se}_{1-x}$ doped glasses [41-42] at a wavelength of around 0.49μm (ie large bandgap). Because of long free carrier lifetimes, large quasi-equilibrium carrier population can be developed, which allows semiconductor doped glasses to be suitable as saturable absorbers in Q-switched lasers.

1.5.4 Erbium doped glasses

Erbium-doped laser amplifiers have high positive nonlinearities of the order of a thousand to a million times greater than those of silica [43]. The linear amplifying properties of erbium-doped lasers (EDL) and amplifiers (EDLA), are now reviewed before discussing the nonlinear effects.

1.5.4.1 Review of erbium doped fibre lasers and amplifier

The advantage of using fibres and waveguides for optical amplification is that the cross-sectional area of the core is very small allowing high population inversions to be developed for moderate pumping powers. Rare earth doping of silica leads to the material becoming active (reviews of general rare-earth-doped fibre lasers and

amplifiers can be found in [44-47]).

Erbium doped lasers and amplifiers are of particular interest since they lase at two important wavelengths $1.54\mu\text{m}$ and $2.7\mu\text{m}$. The wavelength $1.54\mu\text{m}$ is useful for long distance communications, since it is situated in the low loss window of silica fibres and in the anomalous dispersion region for fibres where bright solitons exist. The $2.7\mu\text{m}$ wavelength corresponds with the low loss window for fluoride glass. It is also a wavelength where laser light is strongly absorbed by water, making it suitable for medical applications and for eye-safe lasers (the water layer covering the eye absorbs the laser light before it reaches the retina).

Erbium doped lasers and amplifiers are essentially three level systems. A pump beam excites erbium ions Er^{3+} to a high energy pumping level, from where they relax rapidly (by interacting nonradiatively with the lattice and releasing phonons) to a lower metastable level ${}^4I_{13/2}$. The lifetime of the ions at the metastable level is quite long (10 – 15ms), and so a large quasi-equilibrium population inversion can be formed allowing the material to become active. (As a side-note, the long recombination (fluorescence) time of erbium makes this material useful for Q-switching applications (where the bandfilling blocks absorption [48] and makes the material transparent)).

The erbium-doped laser has a high quantum efficiency (for converting the pump power to the laser power), and has a very broad fluorescence spectrum (80nm [49]), a very narrow lasing wavelength, and an output power which can range from milliwatts to more than watts depending on the pumping power.

The pumping of EDLs can be implemented using laser diodes [50] at three possible wavelengths 807nm, 980nm, and 1480nm. Unfortunately the 807nm pump band is problematic due to excited-state absorption (ESA), ie. the pumping causes ions in the upper lasing level (${}^4I_{13/2}$) to be promoted to still higher levels, thereby reducing the pumping efficiency.

Erbium doped fibre amplifiers (EDFAs) [51-52] have high single-pass gains (45dB) due to high population inversions resulting from the long upper-state lifetime and narrow optical confinement. EDFAs have polarisation independent gains [53], and low noise figures (near quantum limit [54]), and are associated with very little cross-talk between signals of different wavelengths even deep in saturation. EDFAs also have high output power saturation [55] (greater than 0 dBm). The output power saturation is due to amplified spontaneous emission (ASE), resulting from the saturation of the gain due to depletion of the upper state. The output saturation power can be increased by increasing the pumping power (this causes the population inversion to be restored before it is depleted).

1.5.4.2 Using erbium-doped silica in integrated optics

For some applications, it is desirable to have erbium-doped silica in integrated waveguide form instead of optical fibre (for example for observing bright spatial solitons). In these cases the distances have to be short; one does not have the luxury of unlimited lengths as afforded by optical fibres (eg. 10 metres as in [52]). However, since the lengths are so short in integrated form, the gains achieved are small unless the erbium concentration is increased significantly. However, in pure silica there is a certain limit to which the ion concentration can be increased. When there is a high concentration of ions, the close proximity of the ions causes them to interact. The ions may form microcrystals ('clustering') removing available ions for the population inversion. The close proximity of excited ions also causes them to interact via 'up-conversion' [56-57]. Here exchange of energy between two ions results in one ion being excited to a still higher state, whilst another ion relaxes down to the ground state. This process also leaves less ions available for population inversion.

Due to clustering and upconversion, the maximum doping concentration is limited. Until a few years ago it was believed that the minimum length for rare-earth doped fibre to achieve useful gains was around 1m, clearly unsuitable for integrated optics applications.

The problems have recently been resolved by use of co-dopants such as *Al* or *P* [58-59], and anti-clustering co-dopants [60]. Very high rare-earth concentrations have been demonstrated in a variety of hosts obtained by different fabrication processes [61-63]. Gains of around 21dB over 2.4cm [62] have been reported recently.

1.5.4.3 Nonlinear refractive index in erbium-doped fibres

The nonlinearity in erbium-doped laser amplifiers is quite high, of the order of a thousand to a million times greater than those of silica [43], but unfortunately it is accompanied by saturation and loss. The nonlinearity is due to changing of the relative population densities between the upper lasing level and the lower lasing level [43, 64-65]. This is achieved by altering the pumping intensity, so that the population of the upper lasing state is altered, thereby varying the refractive index [65] (recall there is a nonlinearity associated with changes in carrier density). The nonlinearity is also to a lesser extent due to the gain saturation, ie at high powers the stimulated emission depletes the upper state population reducing the gain. The reduction in gain causes an increase in the refractive index [64].

A theoretical calculation of the nonlinear refractive index was given in [43, 64]. A nonlinearity of the order of $n_2 = 7.0 \times 10^{-15} \text{ m}^2/\text{W}$ was estimated [43]. Nonlinear effects in erbium doped glasses have been studied here at UCL using the Finite Element

Method in combination with Runge-Kutta [10,66].

All-optical switches have been demonstrated experimentally in erbium doped integrated fibres and waveguides. Optical switching in twin-core erbium-doped fibres was reported in ref. 67. The switching power was $< 1mW$ using a fibre length of $2.26m$ and a measured nonlinear refractive index of $n_2 = 3.917 \times 10^{-15} m^2/W$. The saturation power was $5mW$. In ref. 68 an InGaAsP laser diode was used to pump a nonlinear switch using a two-mode erbium-doped fibre. The pump power was in the milliwatt range. In ref. 69 all-optical switching in an elliptical-core two-mode fibre was observed with pump powers of $1.6W$ with $33m$ long fibres. In ref. 70 the nonlinear refractive index of erbium-doped Y_2O_3 integrated-optical devices was estimated to be $1.4 \times 10^{-14} m^2/W$ but with a slow relaxation time of $6ms$.

All-optical switching has also been observed in an $8mm$ long Nd -doped two-mode channel waveguide [73]. The switching time was around $410\mu s$ at a repetition rate of $1kHz$. The nonlinear refractive index was estimated at $10^{-17} m^2/W$, with a pump power of around $7mW$. The gain of the waveguide was around $15dB$ at $1064nm$.

1.5.4.4 Semiconductor laser amplifiers

Semiconductor laser amplifiers exhibit instantaneous negative nonlinearities, and slow positive nonlinearities. The instantaneous negative nonlinearity is due to dynamic carrier heating (DCH) [72-79], where ‘hot’ electrons are generated from free-carrier absorption[†] and TPA. The electrons then relax rapidly to the bottom of the conduction band (cooling process) and block the absorption of further electrons, so reducing the refractive index via Kramers-Krönig [64]. Since the processes are all either ‘virtual’ or intraband, the nonlinearity is instantaneous.

There is also a slow (interband) positive nonlinearity due to spectral hole burning, ie. the intense field leads to high stimulated emission rates depleting the upper state population and reducing the gain [80], leading to an increase in the refractive index via Kramers-Krönig [64]).

Typical values for nonlinearity in InGaAsP optical amplifiers, are $n_2 = -3. \times 10^{-16} m^2/W$ [80], or $n_2 = -2. \times 10^{-15} m^2/W$ [79].

[†] Free carrier absorption occurs when free carriers are excited to still higher energies by incoming photons or by phonons to produce what are known as ‘hot carriers’ [8, 81]

1.5.5 Liquid crystals

Liquid crystals have large positive nonlinearities and have been used in experiments to demonstrate nonlinear guided waves [82], bright spatial solitons [83-84], and for

modelling nonlinear directional couplers [85]. The nonlinearities originate from thermal and orientational effects. Some of the liquid crystals which have been considered so far include MBBA and CS_2 . Liquid crystal MBBA has a large positive nonlinearity of the order of $10^{-9} m^2/W$ [82], and capable of exceptionally large index changes before saturation. However the nonlinearity is very slow ($\sim 5s$) and accompanied by large losses (loss coefficient $\alpha = 20cm^{-1}$). MBBA has been used in experiments to demonstrate nonlinear guided waves [82], using powers of the order of $50mW$. Another material, CS_2 has a smaller nonlinearity than MBBA, $n_2 = 3 \times 10^{-18} m^2/W$, but a much faster response time ($2ps$) and has been used to demonstrate bright spatial solitons [83-84].

1.6 CONCLUSIONS

There has been rapid progress in the search for suitable nonlinear materials. However the search has still far to go. The materials studied so far all have trade-offs. The materials with the largest nonlinearities are either very lossy or slow. The ones which are fast and lossless have small nonlinearities and require pulsed lasers to exploit them. For some applications it is required that the nonlinearity should be positive in sign (for example to study bright spatial solitons). However many of the large nonlinearities are due to resonance enhancement and are negative in sign.

Liquid crystal MBBA has a large positive nonlinearity, but is not suitable for ultrafast signal processing since the nonlinearity is very slow. CS_2 is much faster, but unfortunately has a small positive nonlinearity.

Erbium doped glasses look promising. They result in positive nonlinearities reported to be a million times greater than glass.

Recently cascaded nonlinearities [eg. 86] have been proposed where large nonlinear phase-shifts can be induced with very little absorptive losses. Cascaded nonlinearity is implemented using the second-order susceptibility in non-centrosymmetric materials [87] by up-converting light to its second-harmonic and then subsequently down-converting it back to the fundamental. Large nonlinear phase-shifts of the order of π to 2π have been observed in quasi-phase-matched KTP waveguides [88].

REFERENCES

- [1] G. I. Stegeman, and C. Seaton, "Nonlinear integrated optics", J. Appl. Phys., vol. 58, no. 12, 1985, pp. R57-R78
- [2] G. I. Stegeman, "Overview of nonlinear integrated optics", in Nonlinear Waves in Solid State Physics, edited by A. D. Boardman et. al., Plenum Press, New York, 1990, pp. 463-494.
- [3] G. I. Stegeman, E. M. Wright, N. Finlayson, R. Zanoni, and C. T. Seaton, "Third-order nonlinear integrated optics", J. Light. Technol., vol. 6, no. 6, 1988, pp. 953-968.
- [4] G. I. Stegeman, and E. M. Wright, "All-optical waveguide switching", Opt. Quant. Electron., 1990, pp. 95-122; E. Wright, and G. I. Stegeman, "Nonlinear planar waveguides", Anisotropic and nonlinear optical waveguides", in Anisotropic and Nonlinear Optical Waveguides, edited by C. G. Someda and G. Stegeman, Elsevier Science Publishers B. V., 1992, pp. 117-141.
- [5] C. T. Seaton, X. Mai, G. I. Stegeman, and H. G. Winful, "Nonlinear guided wave applications", Optical Engineering, vol. 24, no. 4, 1985, pp. 593-599.
- [6] G. Assanto, "All-optical integrated nonlinear devices", J. Modern Optics, vol. 37, no. 5, 1990, pp. 855-873.
- [7] P. N. Butcher and D. Cotter, "The elements of nonlinear optics", Cambridge studies in modern optics, Cambridge University Press, 1990
- [8] S. Desmond Smith, "Optoelectronic devices", PrenticeHall International series in optoelectronics (UK), 1995.
- [9] C. Kittel, "Introduction to Solid State Physics", New York, Wiley, pp. 34, 247-8, 253, 254, 255, 272
- [10] M. Montagna, S. Selleri, and M. Zoboli, "Nonlinear refractive index in erbium-doped optical amplifiers", Opt. and Quant. Electron., vol. 27, 1995, pp.871-880.
- [11] D. C. Hutchings, M. Sheik-Bahae, D. J. Hagan, and E. W. Van Stryland, "Kramers-Krönig relations in nonlinear optics", Opt. and Quant. Electron., Vol. 24, 1992, pp. 1-30.
- [12] J. S. Aitchison, M. K. Oliver, E. Kapon, E. Colas, and P. W. E. Smith, "Role of two-photon absorption in ultrafast semiconductor optical switching devices", Appl. Phys. Lett., Vol. 56, No.14, April 1990, pp. 1305-1307.
- [13] A. Villeneuve, M. Sundheimer, N. Finlayson, G. I. Stegeman, S. Morasca, C. Rigo, R. Calvani, and C. De Bernardi, "Two-photon absorption in $In_{1-x-y}Ga_xAl_yAs/InP$ waveguides at communication wavelengths", Appl. Phys. Lett., Vol. 56, No. 19, 1990, pp. 1865-1867.

- [14] E. W. Van Stryland, M. Vanherzeele, M. A. Woodall, M. J. Soileau, A. L. Smirl, Z. Guha, and T. F. Boggess, "Two-photon absorption, nonlinear refraction, and optical limiting in semiconductors", *Opt. Eng.*, Vol. 24, No. 4, 1985, pp. 613-623.
- [15] C. R. Pidgeon, B. S. Wherrett, A. M. Johnston, J. Dempsey, and A. Miller, "Two-photon absorption in Zinc-Blende semiconductors", *Phys. Rev. Lett.*, Vol. 42, No. 26, 1979, pp. 1785-1788.
- [16] R. W. Munn, and C. N. Ironside, "Principles and applications of nonlinear optical materials", Blackie academic and professional, 1993
- [17] M. Sheik-Bahae, D. C. Hutchings, D. J. Hagan, and E. W. Van Stryland, "Dispersion of bound electronic nonlinear refraction in solids", *IEEE J. Quant. Elect.*, Vol. 27, No.6, June 1991, pp. 1296-1309.
- [18] H. Haug, "Theory of optical semiconductor nonlinearities", *SPIE vol. 881 Optical Computing and Nonlinear Materials*, 1988, pp. 102-106; N. Peyghambarian, "Materials for fast switching and logic devices", *SPIE vol. 769 Workshop on Photonic Logic and Information Processing*, 1986, pp. 28-40.
- [19] B. R. Bennett, R. A. Soref, and J. A. Del Alamo, "Carrier-induced change in refractive index of InP, GaAs, and InGaAsP", *IEEE J. Quant. Electron.*, vol. 26, no. 1, 1990, pp. 113-122
- [20] J. M. Arnold, "Nonlinear guided waves", *Radio Science*, vol. 28, no. 5, 1993, pp. 885-890
- [21] K. W. DeLong, G. I. Stegeman, "Two-photon absorption as a limitation to all-optical waveguide switching in semiconductors", *Appl. Phys. Lett.*, vol. 57, 1990, pp. 2603-2604.
- [22] H. K. Tsang, R. S. Grant, R. V. Penty, I. H. White, J. B. D. Soole, E. Colas, H. P. Leblanc, N. C. Andreadakis, M. S. Kim, and W. Sibbett, "GaAs/GaAlAs Multiquantum well waveguides for all-optical switching at $1.55\mu\text{m}$ ", *Electron. Lett.*, Vol. 27, no.22, October 1991, pp. 1993-1995.
- [23] J. S. Aitchison, A.H. Kean, C. N. Ironside, A. Villeneuve, and G. I. Stegeman, "Ultrafast all-optical switching in $\text{Al}_{0.18}\text{Ga}_{0.82}\text{As}$ directional coupler in $1.55\mu\text{m}$ spectral region", *Electron. Lett.*, Vol. 27, No.19, September 1991, pp. 1709-1710.
- [24] A. Villeneuve, K. Al-Hemyari, J. U. Kang, C. N. Ironside, J. S. Aitchison, and G. I. Stegeman, "Demonstration of all-optical demultiplexing at 1555 nm with an AlGaAs directional coupler", *Electron. Lett.*, vol. 29, no. 8, 1993, pp.721-722.
- [25] S. Schmitt-Rink, "Linear and nonlinear optical properties of semiconductor quantum wells", *Adv. Phys.*, Vol. 38, No. 2, 1989, pp. 89-188.
- [26] D. S. Chemla, D. A. B. Miller, and P. W. Smith, "Nonlinear optical properties of GaAs/GaAlAs multiple quantum well material: phenomena and applications", *Opt.*

Eng., Vol. 24, No. 4, 1985, pp. 556-564.

[27] P.R. Berger, P.K. Bhattacharya, and S. Gupta, "A waveguide directional coupler with a nonlinear coupling medium ", IEEE J. Quant. Electron, Vol. 27, No. 3, pp. 788-795, 1991.

[28] W.M. Gibbons, and D. Sarid, "Model of a nonlinear directional coupler in gallium arsenide", Appl. Phys. Lett, Vol. 51, No. 6, August 1987, pp. 403-405.

[29] P. Li Kam Wa, J. E. Stitch, N. J. Mason, J. S. Roberts, and P. N. Robson, "All optical multiple-quantum well waveguide switch", Electron. Lett., vol. 21, 1985, pp. 26-27

[30] P. Li Kam Wa, J. H. Marsh, P. N. Robson, J. S. Roberts, and N. J. Mason, "Nonlinear propagation in GaAs/GaAlAs multiple quantum well waveguides", SPIE, vol. 578, Boston, MA, 1985

[31] P. Li Kam Wa, P. N. Robson, J. P. R. David, G. Hill, P. Mistry, M. A. Pate, and J. S. Roberts, "All-optical switching effects in a passive GaAs/GaAlAs multiple quantum well waveguide resonator", Electron. Lett., vol. 22, pp.1129-1130, 1986

[32] P. Li Kam Wa, P. N. Robson, "Nonlinear multiple quantum well waveguide devices", Proc. SPIE, vol. 800, Novel Optoelectron. Devices, 1987, pp. 43-49.

[33] M. Cada, R. C. Gauthier, B. E. Paton, and J. Chrostowski, " Nonlinear guided waves coupled nonlinearly in a planar GaAs/GaAlAs multiple quantum well structures", Appl. Phys. Lett., vol. 49, 1986, pp. 755-757

[34] M. Cada, B. P. Keyworth, J. M. Glinski, A. J. Springthorpe, and P. Mandeville, " Experiment with multiple-quantum well waveguide switching element", J. Opt. Soc. Amer. B, vol. 5, 1988, pp.462-466.

[35] M. Cada, J. D. Begin, "An analysis of a planar optical directional coupler with a lossless Kerr-like coupling medium", IEEE J. Quantum Electron., vol. 26, 1990, pp. 361-371.

[36] R. Jin, C. L. Chuang, H. M. Gibbs, S. W. Koch, J. N. Polky, and G. A. Pubanz "Picosecond all-optical switching in single-mode GaAs/AlGaAs strip-loaded nonlinear directional couplers", Appl. Phys. Lett., Vol. 53, No.19, November 1988, pp. 1791-1793.

[37] S. R. Friberg, A. M. Weiner, Y. Silberberg, B. G. Sfez, and P. S. Smith, "Femtosecond switching in a dual-core-fibre nonlinear coupler", Opt. Lett., Vol. 13, No.10, October 1988, pp. 904-906; S. R. Friberg, Y. Silberberg, M. K. Oliver, M. J. Andrejco, M. A. Saifi, and P. W. Smith, "Ultrafast all-optical switching in a dual-core fibre nonlinear coupler", Appl. Phys. Lett., Vol. 51, No.15, October 1987, pp. 1135-1137.

[38] J. S. Aitchison, Y. Silberberg, A. M. Weiner, D. E. Leaird, M. K. Oliver, J. L.

- Jackel, E. M. Vogel, and P. W. E. Smith, "Spatial optical solitons in planar glass waveguides", J. Opt. Soc. Am. B, Vol. 8, No.6, June 1991, pp. 238-240.
- [39] J. S. Aitchison, A. M. Weiner, Y. Silberberg, M. K. Oliver, J. L. Jackel, D. E. Leaird, E. M. Vogel, and P. W. E. Smith, "Observation of spatial optical solitons in a nonlinear glass waveguide", Optics Letters, Vol. 15, No.9, May 1990, pp. 471-473.
- [40] V. Leutheuser, U. Langbein, and F. Lederer, "Optical response of a nonlinear bent directional coupler", Optics. Comm., vol. 75, no. 3,4, 1990, pp. 251-255.
- [41] N. Finlayson, W. C. Banyai, C. T. Seaton, G. I. Stegeman, M. O'neill, T. J. Cullen, and C. N. Ironside, "Optical nonlinearities in CdS_xSe_{1-x} -doped glass waveguides", J. Opt. Soc. Am. B, Vol. 6, No.4, April 1989, pp. 675-684.
- [42] L. H. Acioli, A. S. L. Gomes, J. R. Rios Leite, and C. B. Araujo, "Ultrafast $\chi^{(3)}$ - related processes in semiconductor doped glasses", IEEE J. Quant. Electron., Vol. 26, No. 7, 1990, pp. 1277-1284.
- [43] R. A. Betts, T. Tjugiarto, Y. L. Xue, and P. L. Chu, "Nonlinear refractive index in erbium doped optical fibre: theory and experiment", IEEE J. Quant. Electron., Vol. 27, No. 4, 1991, pp. 908-913.
- [44] P. Urquhart, "Review of rare-earth-doped fibre lasers and amplifiers", IEE Proc., Part J, vol. 135, 1988, pp.385.
- [45] S. B. Poole, D. N. Payne, and M. E. Fermann, "Fabrication of low-loss optical fibres containing rare-earth ions", Electron. Lett., vol. 21, 1985, pp. 737-738.
- [47] D. N. Payne, "Active fibres and optical amplifiers", in fibre and Integrated Optics, vol. 11, 1992, pp. 191-219.
- [48] R. J. Mears, L. Reekie, and I. M. Jauncey, "High-power tunable erbium-doped fibre laser operating at $1.55\mu m$ ", Proc. CLEO '87, Optical Society of America Technical digest, vol. 14, 1987, p. 122
- [49] S. B. Poole, D. N. Payne, and M. E. Fermann, "Fabrication of low-loss optical fibres containing rare-earth ions", Electron. Lett., vol. 21, 1985, pp. 737
- [50] M. Nakazawa, Y. Kimura, and K. Suzuki, "Efficient Er^{3+} -doped optical fibre amplifier pumped by a $1.48\mu m$ InGaAsP laser diode", Appl. Phys. Lett., vol. 54, no. 4, 1989, pp. 295.
- [51] R. J. Mears, L. Reekie, I. M. Jauncey, and D. N. Payne, "Low noise erbium-doped fibre amplifier operating at $1.54\mu m$ ", Electron. Lett., vol. 23, no. 19, 1987, pp. 1026
- [52] E. Desurvire, J. R. Simpson, and P. C. Becker, "High-gain erbium-doped travelling-wave fibre amplifier", Opt. Lett., vol. 12, no. 11, 1987, pp. 888.
- [53] C. R. Giles, E. Desurvire, J. R. Talman, J. R. Simpson, and P.C. Becker," 2Gbit/s signal amplification at $1.53\mu m$ in an erbium-doped single-mode fibre

- amplifier”, J. Lightwave Technol., vol. 7, no. 4, 1989, pp.651
- [54] R. Olshansky, “Noise figure for erbium-doped optical fibre amplifiers”, Electron. Lett. vol. 24, no. 22, 1988, pp.1363.
- [55] E. Desurvire, C. R. Giles, J. R. Simpson, and J. L. Zyskind, “Efficient erbium-doped fibre amplifier at $\lambda = 1.53\mu\text{m}$ with high output saturation”, published in Opt. Lett, 1990,91,92
- [56] P. Blixt, J. Nilsson, T. Carlnas, and B. Jaskorzynska, “Concentration-dependent upconversion in Er^{3+} -doped fibre amplifiers: Experiments and modelling”, IEEE Trans. Photon. Technol. Lett., vol. 3, no. 11, 1991, pp. 996-998.
- [57] W. J. Miniscalco, “Erbium-doped glasses for fibre amplifiers at 1500nm” J. Light. Technol. vol. 9, no. 2, 1991, pp. 234-250.
- [58] M. Federighi, I. Massarek, and P. F. Trwoga, “Optical amplification in thin optical waveguides with high Er concentration”, IEEE Photon. Technol. Lett. , vol. 5, no. 2, 1993, pp. 227-229.
- [59] K. Arai, H. Namikawa, K. Kumata, and T. Honda, “Aluminium or phosphorous co-doping effects on the fluorescence and structural properties of neodymium-doped silica glass”, J. Appl. Phys., vol. 59, no. 10, 1986, pp. 3430-3436.
- [60] R. P. Tumminelli, B. C. Mccollum, and E. Snitzer, “Fabrication of high-concentration rare-earth doped optical fibres using chelates”, J. Light. Technol., vol. 8, no. 11, 1990, pp. 1680-1683.
- [61] C. Y. Chen, R. R. Petrin, D. C. Yeh, W. A. Sibley, and J. L. Adam, “Concentration-dependent energy-transfer processes in Er^{3+} - and Tm^{3+} - doped heavy-metal fluoride glass”, Optics Lett., vol. 14, no. 9, 1989, pp. 432-434.
- [62] J. Shmulovich, A. Wong, Y. H. Wong, P. C. Becker, A. J. Bruce, and R. Adar, “ Er^{3+} glass waveguide amplifier at $1.55\mu\text{m}$ on silicon”, Electron. Lett., vol. 28, no. 13, 1982, pp.1181-1182.
- [63] M.-W. Kim, W.-J. Cho, J.-C. Jo, and S. S. Choi, “ $1.55\mu\text{m}$ gain in a short Er^{3+} -doped Zirconium Fluoride glass fibre”, Japanese J. Appl. Phys., vol. 30A, 1991, pp. 2020.
- [64] E. Desurvire, “Study of the complex atomic susceptibility of erbium-doped fibre amplifiers”, J. Lightwave Technol., vol. 8, no. 10, 1990, 1517-1527.
- [65] R. H. Pantell, M. J. F. Digonnet, R. W. Sadowski, and H. J. Shaw, “Analysis of nonlinear optical switching in an erbium-doped fibre”, Jnl. of Light. Technol., vol. 11, no. 9, 1993, pp. 1416-1424.
- [66] F. Di Pasquale, M. Zoboli, M. Federighi, and I. Massarek, “Finite-element modelling of silica waveguide amplifiers with high erbium concentration”, IEEE J. Quant. Electron., vol. 30, no. 5, 1994, pp. 1277-1282.

- [67] P. L. Chu, and B. Wu, "Optical switching in twin-core erbium-doped fibres", *Optics Lett.*, vol. 17, no. 4, 1992, pp. 255-257.
- [68] R. H. Pantell, R. W. Sadowski, M. J. F. Dijonnet, and H. J. Shaw, "Laser-diode-pumped nonlinear switch in erbium-doped fibre", *Optics Lett.*, vol. 17, no. 14, pp.1026-1028, 1992.
- [69] H. G. Park, C. C. Pohalski, and B. Y. Kim, "Optical kerr switch using elliptical-core two-mode fibre", *Opt. Lett.*, vol. 13, no. 9, 1988, pp. 776-778.
- [70] T. H. Hoekstra, B. J. Offrein, P. V. Lambeck, and Th. J. A. Popma, "Nonlinear refractive index of erbium-doped Y_2O_3 integrated-optical waveguides", *Opt. Lett.*, vol. 18, no. 20, 1993, pp.1718-1720.
- [71] Cid B. de Araujo, A. S. L. Gomes, and R. Srivastava, "All-optical switching in rare-earth doped channel waveguide", *Appl. Phys. Lett.*, vol. 66, no. 4, 1995, pp. 413-415.
- [72] K. L. Hall, J. Mark, E. P. Ippen, and G. Eisenstein, *Appl. Phys. Lett.*, vol. 56, 1990, pp. 1740
- [73] G. Eisenstein, J. M. Wiesenfeld, M. Wegener, G. Sucha, D. S. Chemla, S. Weiss, G. Raybon, and U. Koren, *Appl. Phys. Lett.*, vol. 58, 1991, pp. 158
- [74] R. Frankenberger and R. Schimpe, *Appl. Phys. Lett.*, vol. 57, 1990, pp.2520.
- [75] L. F. Tiemeijer, *Appl. Phys. Lett.*, vol. 59, 1991, pp. 499
- [76] K. Kikuchi, M. Kakui, C. E. Zah, and T. P. Lee, *IEEE J. Quantum Electron.*, QE-28, 1992, pp. 151.
- [77] C. T. Hultgren and E. P. Ippen, *Appl. Phys. Lett.*, vol. 59, 1991, pp. 635.
- [78] C. T. Hultgren, D. J. Dougherty, and E. P. Ippen, *Appl. Phys. Lett.*, vol. 61, 1992, pp. 2767.
- [79] J. Manning, R. Olshansky, and C. B. Su, "The carrier-induced index change in AlGaAs and $1.3\mu\text{m}$ InGaAsP diode lasers", *IEEE J. Quant. Electron.*, vol. QE-19, no. 10, 1983, pp.1525.
- [80] K. L. Hall, A. M. Darwish, E. P. Ippen, U. Koren, and G. Raybon, "Femtosecond index nonlinearities in InGaAsP optical amplifiers", *Appl. Phys. Lett.*, vol. 62, no. 12, 1993, pp. 1320-1322.
- [81] S. A. Lyon, "Spectroscopy of hot carriers in semiconductors", *Jnl. of Luminescence*, vol. 35, 1986, pp.121-154.
- [82] H. Vach, C. T. Seaton, "Observation of intensity-dependent guided wave", *Optics Letter*, Vol. 9, No. 6, June 1984, pp. 238-240.
- [83] R. De La Fuente and A. Barthelemy, "Spatial soliton-induced guiding by cross-phase modulation, *IEEE J. Quant. Electron.*, vol. 28, no. 2, 1992, pp.547
- [84] R. De La Fuente, A. Barthelemy, and C. Froehly, "Spatial-soliton-induced guided

waves in a homogeneous nonlinear Kerr medium”, *Optics Lett.*, vol. 16, no. 11, 1991, pp. 793-795.

[85] M. A. Karpierz, T. R. Wolinski, and A. W. Domanski, “Liquid crystalline nonlinear directional couplers”, *SPIE* vol. 1895, 1992.

[86] R. DeSalvo, D. J. Hagan, M. Sheik-Bahae, G. Stegeman, and E. W. Van Stryland”, Self-focusing and defocusing by cascaded second-order effects in KTP”, *Opt Lett*, vol. 17, pp. 28-30, 1992

[87] C. Kelaidis, D. C. Hutchings, and J. M. Arnold, “Asymmetric two-step GaAlAs Quantum well for cascaded second-order processes”, *IEEE Trans on quant electronics*, vol 30, no. 12, 1994, pp. 2998-3005.

[88] M. L. Sundheimer, Ch Bosshard, E. M. W. Van Stryland, and G. Assanto, “Large nonlinear phase modulation in quasi-phase-matched KTP waveguides as a result of cascaded second-order processes”, *Opt Lett*, vol. 18, pp. 1397-1399, 1993

CHAPTER 2

SPATIAL AND TEMPORAL SOLITONS

2.1 INTRODUCTION

Solitons are pulses of light which travel unchanged for long distances. They were first discovered in water waves in 1838 by J. Scott Russell [1] and proposed for long distance fiber communications in 1973 by Hasegawa and Kodama [2].

Two main types of solitons exist: spatial and temporal. Spatial solitons are field shapes which maintain their shapes by balancing self-focusing with diffraction. They have future applications in construction of waveguideless components, eg. for switches, to carry light by light, to switch light using light, for lossless switching, and as scanners.

Temporal solitons (review in [3]) are pulses in time which maintain their shapes by balancing self-phase-modulation with dispersion. They can be used for pulse transmission for commercial long distance optical communications, in conjunction with erbium doped amplifiers.

Spatial and temporal solitons can be further classified into bright and dark solitons. Bright temporal solitons occur when the nonlinearity is positive and the group velocity dispersion negative (anomalous dispersion); dark temporal solitons occur when the nonlinearity is negative and the group velocity dispersion positive (normal dispersion).

The only material requirement for the propagation of bright *spatial* solitons is that the nonlinearity should be positive, and for dark solitons is that it should be negative. The sign of diffraction unfortunately cannot change unlike that of dispersion.

In this chapter the latest literature on spatial and temporal solitons is reviewed to set the background for later chapters.

2.2 SPATIAL SOLITONS

2.2.1 Bright spatial solitons

Fields which are not supported by waveguides broaden due to diffraction as they propagate. Bright solitons preserve their shapes in positive nonlinear media, by balancing the effects of self-focusing with diffraction. The self-focusing occurs because

the local intensity at the peak of the field induces a greater index change than the sides and is consequently slowed down with respect to the sides. A curved phase-front then results which focuses the field inwards. In the limit when the self-focusing balances with diffraction a bright soliton forms.

Bright spatial solitons are unstable in three-dimensional media[†] [4] because they are subjected to two transverse directions for diffraction. A calculation of the ‘critical’ power [4] needed for the existence of bright solitons in these media reveals that the critical power is a constant. This is clearly unstable, since if the power is increased slightly from the critical value, the soliton collapses uncontrollably, and if the power is reduced slightly from critical, the soliton diffracts uncontrollably. By limiting the diffraction to one transverse direction however [5], it is possible to form stable spatial solitons. In this case, the critical power is dependent on the width of the soliton. An increase of power causes the field to narrow due to self-focusing, and the narrowing continues until a width is reached where self-focusing balances with increased diffraction (the increased diffraction is because narrow fields diffract more- as in an aperture). Conversely if the power is reduced, the spatial soliton increases in width. The diffraction can be limited to one transverse direction by using a planar optical waveguide removing the diffraction from the other direction. Alternatively using highly elliptical beams makes it possible to excite spatial solitons in bulk media without the use of waveguides. In this case the diffraction is in one transverse direction, because it is negligible in the wider part of the beam.

Spatial solitons are particle-like waves. Two spatial solitons attract or repel each other depending on their relative phases. If the solitons are in phase, they attract. Each soliton provides an increasing index change away from the other soliton. Two out of phase solitons repel because each soliton provides a decreasing index change away from the other soliton. The repulsion between out of phase solitons can be exploited for constructing a tri-state switch [6] where a control soliton is applied to one or the other side of a signal soliton in order to send it to one direction or the other and be captured by a suitably placed waveguide.

Bright spatial solitons have been observed in photorefractive materials, liquid crystals, glasses, and $LiNbO_3$.

[†]Recently it has been shown theoretically [7-9] and experimentally [9] that bright spatial solitons can exist in *saturable* bulk three-dimensional materials.

2.2.2 Dark spatial solitons

A dark soliton is a depression in a constant field [4], and occurs in negative nonlinear

materials. Dark spatial solitons have an advantage over bright spatial solitons in that they are stable in three dimensions [10]. The fundamental dark soliton is a black soliton, which has a *zero* intensity minimum. To be a black soliton [4], the field must be zero at its minimum and there must be a step change in phase across the soliton (this phase shift can be induced by placing a glass slide to cover half the input beam).

Dark solitons can be generated experimentally by placing an object such as a notch or a thin wire to block parts of the beam [4].

2.2.3 Interaction between vector spatial solitons [16-17]

So far we have discussed scalar solitons with equal states of polarisation. The interaction of vector solitons which have different polarisations (or sometimes different wavelengths) produces other results [16]. The collision between vector solitons is inelastic. If two solitons with orthogonal linear polarisations collide, then after the collision each soliton picks up some energy from the other orthogonally polarised soliton, and their linear polarisations become elliptical, with the dominant part being the original polarisation. The collision is strongly dependent on the angle with which the solitons approach each other. If the angle is small, then the solitons merge. If the angle is large, then the solitons eventually separate after several rapid interactions. The advantage of orthogonally polarised *vector* solitons over scalar solitons is that the interaction is not dependent on phase [16]. Therefore parallel, orthogonally polarised vector solitons do not attract or repel each other as scalar solitons do. Vector solitons have been observed in photorefractive materials [18].

2.2.4 Light carrying light via cross-phase-modulation

It is possible for a high power pump soliton to form a waveguide so that a weaker power probe beam of a different wavelength can co-propagate by means of cross-phase-modulation [19]. This has been demonstrated experimentally using bright spatial solitons in liquid crystal CS_2 (with nonlinearity $n_2 = 3 \times 10^{-18} m^2/W$, and fast response time of $2 ps$) [20-21]. The wavelength ratio $(\lambda_2/\sqrt{n_{02}})/(\lambda_1/\sqrt{n_{01}})$ governs the amount of cross-phase-modulation [19]. The linear refractive indices $n_{01,2}$ are for λ_1 and λ_2 respectively. The ratio has to be less than or equal to $\sqrt{2}$ for the probe beam to be supported by the induced guide. If it is less, then the induced guide can support more than one mode. If the ratio is equal to $\sqrt{2}$, and the shapes and sizes of the probe and pump beams are equal (see also [22]) (irrespective of the intensities), the two beams maintain their widths as they propagate. In [20] the relevant wavelengths were $\lambda_1 = 1.06 \mu m$ and $\lambda_2 = 0.53 \mu m$, and the length of the liquid cell was $50 mm$. In [20-21, 23] elliptical beams were used to approximate quasi-two dimensional bright spatial

soliton in bulk materials.

For a nonlinear material where the nonlinearity originates from a molecular reorientational mechanism (like liquid crystals), if the polarisations of the pump and probe were parallel, then the pump carries the probe. However if the polarisations were orthogonal, the pump can split the probe beam [20] since the induced waveguide becomes antiguiding. This fact could be used to construct a polarisation beam splitter. In a true Kerr nonlinear material it is possible to self-focus two orthogonally polarised beams providing their shapes are similar [22].

Two bright spatial solitons which are orthogonally polarised have an interaction which is phase insensitive. In [20], it was shown how a weak signal beam could be captured by an orthogonally polarised strong pump soliton, by launching the two signals towards each other so that they collide at an angle. The capture was accompanied by radiation losses. Furthermore, the capture efficiency decreased with increasing angle. The experiment was performed in an AlGaAs waveguide, with photon energies just below the half-bandgap. The nonlinearity was $n_2 = 1.3 \times 10^{-17} \text{ m}^2/\text{W}$, and the power around 550W . The wavelength was $1.55\mu\text{m}$, and 670fs pulses at 76MHz were used.

It is also possible for dark solitons to form waveguides carrying other waves through cross-phase-modulation or photorefractive effect. These waveguides can be steered by applying a phase ramp across the soliton [24].

Two weak probe beams guided by dark spatial soliton guides placed in proximity can couple with each other [10,20].

2.2.5 Light carrying light using photorefractive materials

Photorefractive materials [25] use a combination of photoconductivity and the electrooptic effect to induce a refractive index change. The photoconductivity results in charge carriers being generated, migrating and becoming trapped at impurity sites. The trapped charges then produce internal electric fields which modify the refractive index through the electrooptic effect.

Spatial solitons have been observed in photorefractive (PR) materials recently [26-27] due to the balancing between self-scattering and diffraction. The sign and magnitude of the nonlinearity (due to self-scattering) in PR materials is determined by a dc field applied to the crystal. For high voltages, large amount of self-focusing occurs. When the voltage is reversed, the nonlinearity changes sign [26] (becomes diffracting). Dark solitons have been generated in $\text{Sr}_{0.6}\text{Ba}_{0.4}\text{Nb}_2\text{O}_6$ (SBN:60) using dc voltages of $\sim\pm 400\text{V}$ [28].

The properties of spatial solitons in photorefractive materials are much different to

those of Kerr solitons. They can be formed at very low powers since the efficiency of the self-scattering process is not dependent on the absolute light intensity [27] (eg. only $10\mu W$ was needed at $457nm$ wavelength in [26]). As a result, these solitons are not affected so much by losses and gains as Kerr solitons are. They retain their shapes even in the presence losses and gains. Bright spatial solitons are also stable in three dimensions in photorefractive materials in contrast with Kerr media [26].

The nonlinearity in PR materials is very slow. A nonlinear refractive index change can remain unaltered for many hours or even several days in the dark unless incoherent light is applied which erases the nonlinearity immediately.

The slowness of the nonlinearity and the independence of the magnitude of the nonlinearity on the soliton power, can be utilized to form temporary waveguides. One remarkable result is that a weak power (microwatts) soliton at one wavelength (eg $457nm$ [28]) can guide a much *higher* power probe beam (watts) at another wavelength where the material is photo-insensitive (eg. $633nm$).

Photorefractive spatial solitons can also be used to construct temporary and erasable directional couplers.

2.2.6 Spatial soliton x-junctions and couplers

By launching two pump solitons towards each other at an angle, spatial soliton x-junctions and couplers can be formed [29]. Two approaches are possible. Firstly, weak probe beams can be linearly coupled if they are copropagated with the pump solitons. Secondly, using materials with optical memory (so that the change in refractive index can be kept after the intense beam is switched off) recorded structures can be created and be used as linear couplers and x-junctions. Since the collision of (scalar) solitons is elastic (ie the solitons recover their original form after the collision with no associated radiation) these devices are also lossless. Another advantage is that the lengths of these devices are much shorter than those of standard couplers. For equal pump and probe wavelengths, bright soliton couplers transfer more light as the incident angle increases, while dark soliton couplers are remarkable due to the fact that they couple 100% of the light at all angles [30]. Coupling of spatial solitons, where the solitons reside in different planar waveguides has also been studied [31].

2.2.7 Optical vortex solitons

Optical vortices are circular beams possessing uniform amplitudes, but with 2π helical phase ramps centred about their dark cores [32-33]. The vortex soliton forms a three-dimensional dark graded index fiber within the bulk material. It can be launched [34] by introducing an optical vortex using the 'donut mode' [35] from the large intracavity

aperture of a laser. Vortex solitons have been demonstrated experimentally in PR materials [35].

2.2.8 Spiralling spatial solitons

Two in-phase bright solitons can be made to spiral [7] around each other in a three-dimensional material (using *saturable* nonlinearity) if they are released at skew angles relative to each other [7-8]. The principle is very similar to wave propagation in graded index fibres. In planar waveguides, the two solitons would periodically diverge and converge in planar fashion rather than spiralling.

Spiralling bright solitons have been demonstrated experimentally and numerically recently [9] in rubidium atomic vapour contained in a cylindrical Pyrex cell 200mm long. This was also the first demonstration of bright solitons in 3D saturable nonlinear materials.

2.3 TEMPORAL SOLITONS

Temporal solitons are pulses in time which use the nonlinearity of the material to overcome the effects of dispersion. The pulses preserve their shapes for several thousand kilometers and are very stable against perturbations [36-37]. They are in fact the only stable solution of the nonlinear Schrödinger equation. It can be shown that any pulse shape automatically reshapes itself into a temporal soliton as it propagates [38].

Bright temporal solitons [39] occur in the anomalous (negative) dispersion regime of the optical fibre, balancing the effects of dispersion with self-phase-modulation (SPM). The SPM introduces a frequency chirp on the pulse, which pushes the higher frequencies to the back and the lower frequencies to the front of the pulse. The frequency chirp occurs because the intensity in the steep edges of the temporal pulse is changing rapidly (in time) and induces a rapidly changing phase shift. Since rapidly varying phase-shifts are equivalent to frequency shifts, the result is that there is a positive frequency shift for the back of the pulse and a negative frequency shift for the front of the pulse. The frequency shift for the middle of the pulse is zero, since it corresponds with an intensity maxima (zero slope). Anomalous dispersion counteracts the frequency chirp by enabling the higher frequencies to travel faster than lower frequencies, to preserve the shape of the pulse.

Dark temporal solitons [40] are rapid intensity dips in an otherwise CW background. They occur in negative nonlinear materials, where the normal (positive) GVD balances with SPM. Experimentally, dark temporal solitons are generated by superimposing a rapid dip on a broad (but finite duration) bright pulse by means of a driving pulse.

The interaction between two bright temporal solitons is dependent on their relative phases ie two in-phase solitons attract, whereas two out-of-phase solitons repel each other. Two dark temporal solitons on the other hand always repel.

REFERENCES

- [1] J. S. Russell, in Reports of the Meetings of the British Association for the Advancement of Science, 1844, Liverpool Meeting, 1838.
- [2] A. Hasegawa and F. Tappert, "Transmission of stationary nonlinear optical pulses in dispersive dielectric fibers. I. Anomalous dispersion", Appl. Phys. Lett., vol. 23, 1973, pp. 142-144.
- [3] K. J. Blow and N. J. Doran, "Solitons in optical fibres", in Nonlinear waves in solid state physics, edited by A. D. Boardman et al., Plenum Press, New York, 1990, pp. 325-371.
- [4] Y. Silberberg, "Self-induced waveguides: spatial optical solitons", in Anisotropic and nonlinear Optical waveguides, edited by C. G. Someda and G. Stegeman, 1992 Elsevier Science Publishers, B. V.
- [5] J. S. Aitchison, Y. Silberberg, A. M. Weiner, D. E. Leaird, M. K. Oliver, J. L. Jackel, E. M. Vogel, and P. W. E. Smith, "Spatial optical solitons in planar glass waveguides", J. Opt. Soc. Am. B, Vol. 8, No.6, June 1991, pp. 238-240.
- [6] J-R Bian and A. K. Chan, "A nonlinear all-optical switch using spatial soliton interactions", Micr. Opt. Technol. Lett., vol. 4, no. 13, 1991, 575-580
- [7] L. Poladian, A. W. Snyder, and D. J. Mitchell, "Spiralling spatial solitons", Optics Commun., vol. 85, 1991, pp. 59-62
- [8] A. W. Snyder, D. J. Mitchell, L. Poladian, and F. Ladouceur, "Self-induced optical fibers: spatial solitary waves", Optics Letters, vol. 16, no. 1, 1991, pp. 21-21
- [9] V. Tikhonenko, J. Christou, and B. Luther-Daves, "Spiralling bright spatial solitons formed by the breakup of an optical vortex in a saturable self-focusing medium", J. Opt. Soc. Am. B, vol. 12, no. 11, pp.2046-2052, 1995.
- [10] A. A. Cruz-Cabrera and S. R. Skinner, "Coupling between parallel dark spatial soliton waveguides", Optics Lett., vol. 18, no. 17, pp. 1403-1405, 1993.
- [11] A. W. Snyder, D. J. Mitchell, and Y. Chen, "Spatial solitons of Maxwell's equations", Optics Lett., vol. 19, no. 8, 1994, pp. 524-526.
- [12] A. W. Snyder, D. J. Mitchell, and L. Poladian, "Linear approach for approximating spatial solitons and nonlinear guided modes", J. Opt. Soc. Am. B, vol. 8, no. 8, 1991, pp. 1618-1620.
- [14] A. W. Snyder, D. J. Mitchell, and B. Luther-Davies, "Dark spatial solitons constructed from modes of linear waveguides", J. Opt. Soc. Am. B, vol. 10, no. 12, 1993, pp.2341-2352.
- [15] L. Lerner, D.J. Mitchell, and A. W. Snyder, "Interacting gray solitons", Optics

Lett., vol. 19, no. 17, 1994, pp. 1302-1304.

[16] X. D. Cao and D. D. Meyerhofer, "All-optical switching by means of collisions of spatial vector solitons", *Optics Letters*, vol. 19, no. 21, 1994, pp. 1711-1713

[17] Y. Chen, "Variational principle for vector spatial solitons and nonlinear modes", *Optics Commun.*, vol. 84, no. 5,6, 1991, pp. 355-358

[18] M. Segev et. al., "Vector photorefractive spatial solitons", *Optics Lett.*, vol. 20, no. 17, 1995, pp.1764-1766

[19] R. De La Fuente, and A. Barthelemy, "Spatial solitons pairing by cross-phase modulation", *Optics Communications*, vol. 88, 1992, pp.419-423.

[20] R. De La Fuente and A. Barthelemy, "Spatial soliton-induced guiding by cross-phase modulation, *IEEE J. Quant. Electron.*, vol. 28, no. 2, 1992, pp.547

[21] R. De La Fuente, A. Barthelemy, and C. Froehly, "Spatial-soliton-induced guided waves in a homogeneous nonlinear Kerr medium", *Optics Lett.*, vol. 16, no. 11,1991, pp. 793-795

[22] A. M. Goncharenko, V. G. Kukushkin, Yu. A. Logvin, and A. M. Samson, "Self-focussing of two orthogonally polarised light beams in a nonlinear medium", *Opt. Quant. electron.*, vol. 25, 1993, pp. 97-104

[23] A. Barthelemy, S. Maneuf, and C. Froehly, "Propagation soliton et auto-confinement de faisceaux laser par nonlinearite optique de Kerr", *Opt. Commun*, vol. 55, no. 3, 1988, pp.193-198

[24] B. Luther-Davies, and X. Yang, "Steerable optical waveguides formed in self-defocussing media by using dark spatial solitons", *Optics Lett.*, vol. 17, no. 24, 1992, pp.1755-1757.

[25] M. Segev, A. Yariv, G. Salamo, G. Duree, J. Shultz, B. Crosiganai, P. Di Porto, and E. Sharp, "Photorefractive spatial solitons", *Optics and Photonics news*, 1993, pp.9

[26] G. C. Duree et. al., "Observation of self-trapping of an optical beam due to the photorefractive effect", *Phys. Rev. Lett.*, vol. 71, 1993, pp.533.

[27] M. Segev, B. Crosignani, A. Yariv, and B. Fischer, "Spatial solitons in photorefractive media",

[28] M. Morin, G. Duree, G. Salamo, M. Segev, "Waveguides formed by quasi-steady-state photorefractive spatial solitons", *Optics Lett.*, vol. 20, no. 20, 1995, pp. 2066-2069

[29] N. Akhmediev and A. Ankiewicz, "Spatial soliton X-junctions and couplers", *Opt. Comms.*, vol. 100, 1993, pp. 186-192

[30] A. P. Sheppard, "Devices written by colliding spatial solitons: a coupled mode theory approach", *Opt. Comms.*, vol. 102, 1993, pp.317-323.

- [31] A. D. Boardman, and K. Xie, "Spatial soliton dynamics in coupled planar waveguides", *Integrated Photonics Research*, 1993, pp.520-521.
- [32] G. Duree et. al., "Dark photorefractive spatial solitons and photorefractive vortex solitons", *Physical Rev. Letters*.
- [33] C. T. Law and G. A. Swartzlander, "Optical vortex solitons and the stability of dark soliton stripes", *Optics Letters*, vol. 18, no. 8, 1993, pp. 586-588.
- [34] G. A. Swartzlander, and C. T. Law, "Optical vortex soliton", *Optics and Photonics News*, 1993, p. 10
- [35] G. A. Swartzlander and C. T. Law, *Phys. Rev. Lett.*, vol. 69, 1992, p. 2503.
- [36] L. F. Mollenaur, J. P. Gordon, and S. G. Evangelides, "Multigigabit soliton transmissions traverse ultralong distances", *Laser Focus World*, 1991, pp. 159-170
- [37] K. J. Blow, and N. J. Doran, "Soliton phenomena in optical fibres", *Anisotropic and nonlinear optical waveguides*, edited by C. G. Someda and G. Stegeman, Elsevier Science Publishers, 1992, pp. 159-183.
- [38] A. Hasegawa and Y. Kodama, "Solitons in optical communications", *Oxford series in optical and imaging sciences*, 1995
- [39] H. A. Haus, "Optical fiber solitons, their properties and uses", *Proceedings of the IEEE*, vol. 81, no. 7, 1993, pp. 970-983.
- [40] Y. Kivshar, "IEEE J. Quant. Elect.", vol. 29, no. 1, 1993, pp. 250

CHAPTER 3

LINEAR STRONG COUPLED MODE THEORY

3.1 INTRODUCTION

The principles of linear strong coupled mode theory (SCMT) [1-4] are reviewed in this chapter. By using the word ‘strong’ it is meant that the theory is applicable to strongly coupled guides. However, the theory is not just limited to strong coupling. It is also more accurate and consistent in the weak coupling regime than prior weak coupled mode theories (WCMTs) (eg those of Yariv [5-6], and Kogelnik [7] etc). The difference between SCMT and WCMT lies in a coefficient called the ‘overlap integral’ which is normally neglected in WCMTs. The overlap integral is the integral of the product of distinct and separate modes, taken over all space. If the modes are assumed to be orthogonal, as in WCMTs, then these terms are neglected. However by ignoring the overlap integrals inconsistencies can develop, especially when the guides are asymmetrical. The problem is that WCMTs predict equal magnitudes for the coupling coefficients for these cases. However physical reasoning alone tells us that the coupling coefficients should be unequal. Also it can be shown that WCMTs predict inaccurate values for the coupling coefficients and coupling lengths in symmetrical couplers. In nonlinear couplers, the effect of the overlap integral would perhaps be even more important than in linear couplers, because there are a large number of nonlinear phenomena which involve interaction between different modes.

Hardy and Streifer (H-S) [1] were the first to point out that the overlap integral should not be neglected from the coupled mode equations. The paper was later subjected to much criticism (discussed in more detail in chapter 6, section 6.1). However these criticisms should be put in context, since the essence of H-S paper regarding the overlap integral was correct. Snyder and co-workers [8-10] criticised H-S paper for being over-convoluted, requiring radiation modes, and breaking power conservation. These short-comings were easily overcome in later papers with the aid of more elegant techniques than H-S method, ie using reciprocity (Chuang [11]), and variational methods (Chuang [2], Haus et. al. [3], and Huang [12]). The derivations using variational methods were especially elegant and simple, since all they involved was a derivation of a variational expression for the propagation coefficient which was then differentiated with respect to the mode amplitudes to obtain the coupled mode

equations. Snyder et. al. [8] had one further criticism where they questioned the accuracy of including the overlap integral in vector methods when using *TM* modes [1-3, 11-12] in the presence of abnormally strong guidance. They argued that scalar analysis was more accurate. This point was debatable (see chapter 6) and slightly academic [13] since it referred to the case of abnormally large index differences (core-cladding index ratio of $n_{co}/n_{cl} > 1.5$). From Snyder et al's graphs [8] it can be observed that for *TM* modes, the curve corresponding to a vector method [2-3, 11-12] was slightly more accurate than the one for the scalar method in normal guidance. Snyder and co-workers have subsequently used the overlap integral in their own work, renaming it the 'interaction coefficient' (see eg. [13] for linear couplers, and [3] for nonlinear couplers). In this thesis *TE* modes are used together with the assumption that the guidance is much less extreme than the case referred to by ref. 8. A vector method is also preferred, since it is more accurate for these cases.

There have been other (more recent) criticisms of strong coupled mode theory (eg [14]). However one should pay careful attention to the extreme numbers used and geometries discussed (see chapter 6 (section 6.1) for more details).

The overlap integral is also important for linear multiwaveguide couplers [4, 11,15-16]. It was mentioned by Hardy et al. [17] that when the guides are non-identical the effect of the overlap integral is important, even for weak coupling, otherwise large errors in the coupling length could arise.

3.2 LINEAR STRONG COUPLED MODE THEORY

The mode of a waveguide is defined as that field which propagates unaltered along the propagation axis of the waveguide. The mode must satisfy Maxwell's equations and all the boundary conditions imposed by that waveguide geometry. As a result of this definition, modes of the same waveguide, and modes of different waveguides must be orthogonal to each other. Modes cannot couple power with each other otherwise they would alter with propagation and could not be called 'modes'.

A mode satisfies Maxwell's equations and the boundary conditions for one specific waveguide geometry. If the geometry however were to be altered (or 'perturbed') in some way, then coupling between the fields would then occur. The modes of the unperturbed waveguide geometry would no longer remain as modes in an altered geometry, since they do not satisfy exactly the boundary conditions of the altered geometry. As they are no longer modes, they are no longer orthogonal with each other because of the definition of a 'mode' given above, and can therefore couple with each other.

If two waveguides are held a large distance away from each other, then the

geometry in the proximity of each waveguide is unaltered. The regions a long distance away are not so important because the guided field is negligible there. The modes of the isolated guides ('eigenmodes'[†]) propagate in this two guide system without changing or coupling to a great extent. However, if the waveguides are brought closer to each other, the refractive index in the proximity of each waveguide (where the field is non-negligible) is altered or 'perturbed' due to the presence of the other guide. Because of this perturbation, the eigenmodes no longer remain as 'modes' in the altered geometries. Therefore they no longer remain orthogonal with respect to each other and can couple with each other.

To replace the old 'eigenmodes' (which are now coupled), there now appears two new 'supermodes'[†] for the composite system. The supermodes are orthogonal and propagate undisturbed along the system at different speeds, periodically beating with each other. The beating appears to the observer as periodic power transfer (with propagation distance) between the eigenmodes. Half the beat length appears as complete power transfer from eigenmode 'p' to eigenmode 'q' and is called the 'coupling length'.

[†]Note: in this thesis the modes of a single guide are called 'eigenmodes' and the modes of a superstructure (two or more guides) are called 'supermodes'.

3.3 COUPLED MODE EQUATIONS

There are many ways to calculate the coupled mode equations, and as long as no terms are neglected, all these methods lead to the same equations. The main idea is this: an isolated waveguide labelled 'p' embedded in its surrounding medium is taken as the unperturbed system (see Fig. 3.1b below). The waveguide supports a single eigenmode (ie its guiding mode) which travels undisturbed along the guide and is orthogonal to eigenmodes belonging to other waveguides. This system is perturbed in such a way that another guide 'q' appears alongside the first guide. Coupling between the eigenmodes of guides 'p' and 'q' (Fig. 3.1a) occurs only because the permittivity of guide 'q' acts as a perturbation to guide 'p' (Fig. 3.1c). Due to the very presence of guide 'q', the permittivity of the surrounding medium to guide 'p' is increased. This increase in the permittivity (a 'perturbation') changes the conditions necessary for eigenmode 'p' to propagate unaltered (the unperturbed system was necessary for this). The result is that eigenmode 'p' no longer remains the mode and no longer remains orthogonal to eigenmode 'q'. In summary, the two guiding modes are now coupled together.

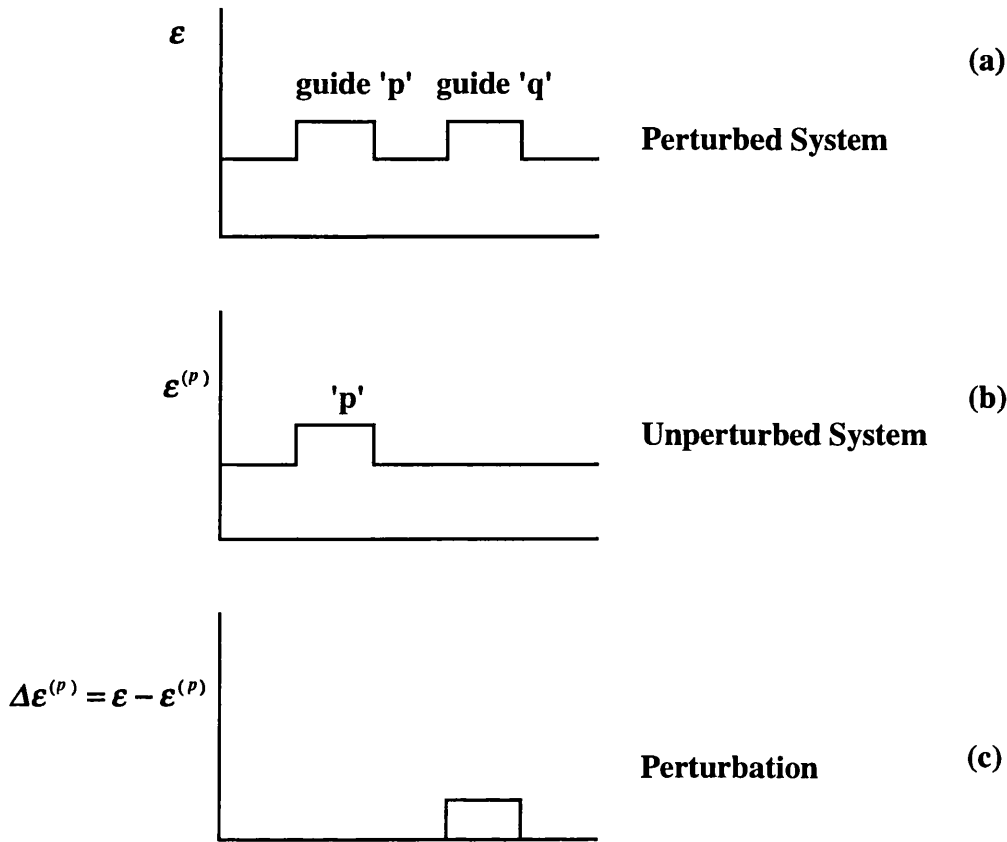


Fig. 3.1 a-c Illustrating the permittivity profiles for the unperturbed and perturbed systems, together with the perturbation which is responsible for the coupling between the waveguides

3.3.1 Strong coupled mode equations

One elegant way to calculate the coupled mode equations is to insert the fields for eigenmode 'p' (the unperturbed system) and the field for the composite system (guides 'p' and 'q'), together with the respective permittivity functions into Lorentz reciprocity theorem (see Appendix 4, eqn A4.9) and derive one coupled mode equation (see Chuang [2] for more details and chapter 6 for extension to nonlinear couplers). The same procedure can then be applied to guide 'q' to derive a second coupled mode equation (which mirrors the first derived equation).

The eigenmodes used to construct the total field for the composite system are assumed to each carry the full power in the coupler. To approximate the actual local field, the relevant eigenmode has to be scaled accordingly using a normalised amplitude. For example the field in the region of guide 'p' is approximately the eigenmode of guide 'p' multiplied by a (complex) scaling amplitude a_p , and the field in guide 'q' is approximately the eigenmode of guide 'q' multiplied by another scaling

amplitude a_q (the amplitudes are normalised such that $0 \leq |a_{p,q}| \leq 1$). The sum of these scaled eigenmodes approximates to the total field in the composite (perturbed) system.

In the end, the following coupled mode equations are derived irrespective of whether reciprocity [2], variational methods [2-3], H-S method [1] or weak coupled mode theories [5-7] are used (as long as terms are not neglected yet).

$$-j \frac{da_p}{dz} - jC_{pq} \frac{da_q}{dz} = (\beta_p + \bar{K}_{pp})a_p + (C_{pq}\beta_q + \bar{K}_{pq})a_q \quad (3.1)$$

$$-j \frac{da_q}{dz} - jC_{qp} \frac{da_p}{dz} = (\beta_q + \bar{K}_{qq})a_q + (C_{qp}\beta_p + \bar{K}_{qp})a_p \quad (3.2)$$

It is assumed that $e^{j(\beta z - \omega t)}$ convention is used for the fields. β_p and β_q are the propagation coefficients for the modes and are inversely proportional to the mode velocities. \bar{K}_{pq} and \bar{K}_{qp} are the coupling coefficients and describe the coupling between the fields. The arrow on top of the coupling coefficient implies the direction of power flow, ie from the scaled eigenmode associated with the right hand subscript to that associated with the left hand subscript. \bar{K}_{pp} and \bar{K}_{qq} are modification coefficients which increase the value of the (uncoupled) propagation coefficients. The overlap integrals are given as C_{pq} and C_{qp} and are symmetrical so that $C_{pq} = C_{qp}$. These terms are neglected in WCMTs and are the main difference between WCMTs and SCMTs, but since the eigenmodes are coupled, they cannot be zero. The definitions for the overlap integral [2] and the coupling coefficients are

$$C_{pq} = \frac{1}{4P} \iint_{-\infty}^{+\infty} (\underline{E}_t^{(p)} \times \underline{H}_t^{(q)} + \underline{E}_t^{(q)} \times \underline{H}_t^{(p)}) \cdot \hat{z} \, dx dy \quad (3.3)$$

$$\bar{K}_{qp} = \frac{\omega \epsilon_0}{4P} \iint_{-\infty}^{+\infty} ((\epsilon - \epsilon^{(p)}) \underline{E}_t^{(q)} \cdot \underline{E}_t^{(p)}) \, dx dy \quad (3.4)$$

where $(\underline{E}_t^{(p)}, \underline{H}_t^{(p)})$ and $(\underline{E}_t^{(q)}, \underline{H}_t^{(q)})$ are the transverse parts of the electric and magnetic fields for eigenmodes 'p' and 'q' respectively. ϵ is the total permittivity, $\epsilon^{(p)}$ the permittivity of guide 'p' embedded in its surrounding medium (see Fig. 3.1b), and ϵ_0 the permittivity of free space. It should be pointed out that the total permittivity is not the sum of $\epsilon^{(p)}$ and $\epsilon^{(q)}$, ie $\epsilon \neq \epsilon^{(p)} + \epsilon^{(q)}$, since $\epsilon^{(p)}$ and $\epsilon^{(q)}$ contain the permittivity of the surrounding medium in their definitions. The correct form for ϵ (for the two guide case) is $\epsilon = \epsilon^{(p)} + (\epsilon - \epsilon^{(p)})$ where $\epsilon^{(p)}$ is the unperturbed system, and $(\epsilon - \epsilon^{(p)})$ is the

perturbation.

Since the coupled 'eigenmodes' are no longer orthogonal to each other, there is a joint interaction between them, and this joint interaction can carry power. The overlap integral C_{pq} measures the degree of overlap between the eigenmodes, and can therefore be loosely described as a normalised Poynting theorem for spatially separated electric and magnetic fields. This is a similar situation to the electric and magnetic fields of an EM wave which carry power as a result of being coupled together (Poynting theorem). The overlap integral is a dimensionless quantity, normalised to 1 if the eigenmodes are overlapping completely, ie $C_{pp} = C_{qq} = 1$. In a single EM wave, the overlap integral is 1. If the electric and magnetic fields for this wave are now separated, the overlap between them would carry less power, and therefore the overlap integral would become less than 1. Eventually when the fields are well separated, almost no power is carried by the overlap, and then the overlap integral becomes zero.

It should also be noted that the overlap integral is an integral over all space, whereas the coupling coefficient is an integral over the perturbation region only.

The reason for the $4P$ normalisation in the denominator of the definition for C_{pq} (eqn. 3.3) can be seen by considering the total power P given by the Poynting theorem

$$P = \frac{1}{2} \iint_{-\infty}^{+\infty} (\underline{E}_i^{(p)} \times \underline{H}_i^{(p)}) \cdot \hat{z} dx dy = \frac{1}{2} \iint_{-\infty}^{+\infty} (\underline{E}_i^{(q)} \times \underline{H}_i^{(q)}) \cdot \hat{z} dx dy \quad (3.5)$$

If $p = q$ in the definition for C_{pq} (eqn. 3.3), the numerator becomes $2 \iint_{-\infty}^{+\infty} (\underline{E}_i^{(p)} \times \underline{H}_i^{(p)}) \cdot \hat{z} dx dy$ which is $4P$ (using the definition for P above). Therefore there is a $4P$ in the denominator of C_{pq} to cancel with the numerator, in order for $C_{pp} = C_{qq} = 1$ to be true.

3.3.2 Weak coupled mode equations

By neglecting the overlap integrals C_{pq} from eqn. 3.1 and 3.2 one arrives at the following (well-known) coupled mode equations.

$$-j \frac{da_p}{dz} = (\beta_p + \bar{K}_{pp}) a_p + \bar{K}_{pq} a_q \quad (3.6)$$

$$-j \frac{da_q}{dz} = (\beta_q + \bar{K}_{qq}) a_q + \bar{K}_{qp} a_p \quad (3.7)$$

However these equations are inaccurate and also inconsistent in certain cases. A

power conservation treatment of this equation reveals that the coupling coefficients must have equal magnitudes and be complex conjugates of each other (see section 3.8). But as explained in the following section, this cannot be the case if the guides are asymmetrical. Therefore eqns. 3.6 and 3.7 are inconsistent in this case.

3.4 PHYSICAL CONSEQUENCES OF THE OVERLAP INTEGRALS

Using reciprocity, it can be shown [2] that the quantity $\beta_p C_{pq} + \bar{K}_{pq}^+$ is symmetric.

$$\text{ie } \beta_p C_{pq} + \bar{K}_{qp} = C_{pq} \beta_q + \bar{K}_{pq} \quad (3.8)$$

This fact requires further attention. Eqn 3.8 can be rearranged to give

$$(\bar{K}_{pq} - \bar{K}_{qp}) = C_{pq} (\beta_p - \beta_q) \quad (3.9)$$

It can be seen from eqn 3.9 that the coupling coefficients are not equal to each other in general as thought by prior theories (eg. Kogelnik [7]). They are only equal if the guides are symmetrical (ie $\beta_p = \beta_q$) or if the guides are very weakly coupled, ie $C_{pq} \rightarrow 0$. The physical reasoning for this is as follows.

If the guides are identical (as in Fig. 3.2 below), then eigenmode 'p' overlaps waveguide 'q' by the same amount that eigenmode 'q' overlaps waveguide 'p'. Therefore the magnitude of the eigenmodes over the respective perturbations are the same, leading to equal coupling coefficients. However, if eigenmode 'p' is guided more strongly than eigenmode 'q' ($\beta_p > \beta_q$), as in Fig. 3.3 below, then eigenmode 'p' overlaps less with the perturbation than eigenmode 'q'. Therefore one *expects* the coupling coefficients to be different. More specifically, according to our earlier definition for \bar{K}_{pq} one expects $\bar{K}_{pq} > \bar{K}_{qp}$.

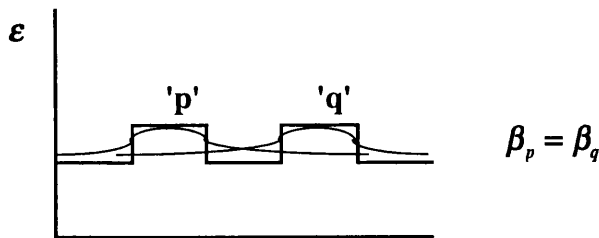


Fig. 3.2 Symmetrical guides

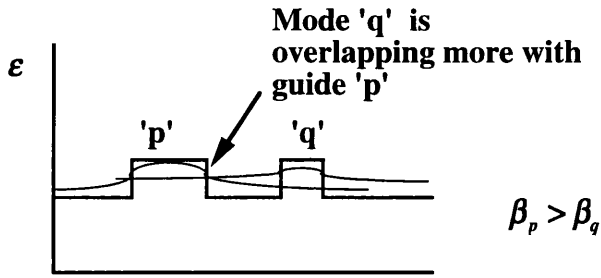


Fig. 3.3 Asymmetrical guides

In summary the asymmetry between the guides leads to unequal coupling coefficients. The inequality also depends on how strongly the guides are coupled. If the guides are very weakly coupled, then the overlap integral C_{pq} tends to zero, and as can be seen from eqn. 3.9 this leads to equal coupling coefficients, predicted by prior theories. In this case the fact that one eigenmode overlaps with its perturbation slightly more than the other eigenmode, does not make too much difference since the magnitude of each eigenmode over the perturbation region is small.

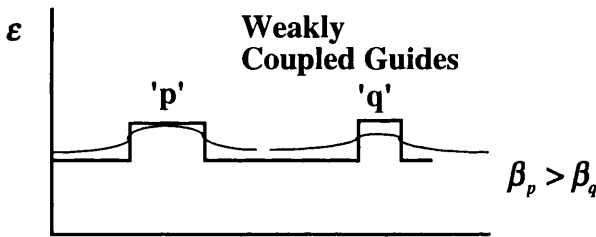


Fig. 3.4 Asymmetrical weakly coupled guides

3.5 MULTIWAVEGUIDE CASE

3.5.1 Comparison between different notations

After considerable manipulation much of which was unnecessary and conceptually in error according to Snyder et. al. [8-10] (see reply in [13]), Hardy and Streifer derived the following coupled mode equation [4,16].

$$-j \sum_{q=1}^N C_{pq} \frac{da_q}{dz} = \sum_{q=1}^N (\beta_p C_{pq} + \bar{L}_{pq}) a_q \quad \text{for } p = 1, \dots, N \quad (3.10)$$

where a_q is the (complex) amplitude of the eigenmode in guide 'q', and β_p is the propagation constant for eigenmode 'p'.

The coupling between the guiding modes is described by the coupling coefficient

[4,16] \vec{L}_{pq} . The arrow implies that power is being transferred from guide 'p' (the left subscript) to guide 'q' (the right subscript) due to the presence of guide 'q'. The perturbation is therefore removing power from guide 'p'. This is defined quantitatively as

$$\vec{L}_{pq} = \frac{\omega \epsilon_0}{4P} \iint_{-\infty}^{+\infty} \left((\epsilon - \epsilon^{(p)}) \underline{E}_i^{(p)} \cdot \underline{E}_i^{(q)} \right) dx dy \quad (3.11)$$

where ϵ is the total permittivity, $\epsilon^{(p)}$ the permittivity of guide 'p' embedded in its surrounding medium (see Fig. 3.1b), and ϵ_0 is the permittivity of free space.

Later Haus [3] using the variational principle, and Chuang [2,11] using both reciprocity and variational principle, derived the following equation

$$-j \sum_{q=1}^N C_{pq} \frac{da_q}{dz} = \sum_{q=1}^N (C_{pq} \beta_q + \vec{K}_{pq}) a_q \quad (3.12)$$

The definition for \vec{K}_{pq} was given in eqn. 3.4.

The differences between the two notations should be highlighted:

- 1- The definition of the coupling coefficient \vec{L}_{pq} (eqn 3.11) contains $(\epsilon - \epsilon^{(p)})$ which is the perturbation to eigenmode 'p', whereas that of \vec{K}_{pq} (eqn 3.4) contains $(\epsilon - \epsilon^{(q)})$.
- 2- The Hardy and Streifer coupled mode equations (eqn 3.10) contains the propagation coefficient β_p , whereas Haus' contains β_q .(eqn 3.12)

As explained by Hardy and Streifer [4], the two formulations are exactly the same. The following will attempt to explain the differences

\vec{L}_{pq} is defined as the transfer of power from eigenmode 'p' to eigenmode 'q' due to the perturbation resulting from the presence of guide 'q' (ie $(\epsilon - \epsilon^{(p)})$).

\vec{K}_{qp} (note the reversed subscripts) is defined exactly the same as \vec{L}_{pq} (ie the transfer of power from the eigenmode 'p' to eigenmode 'q' due to the perturbation resulting from the presence of guide 'q' (ie. $(\epsilon - \epsilon^{(p)})$). The perturbation is again removing power from eigenmode 'p'. Therefore \vec{L}_{pq} is the transpose of \vec{K}_{pq}

$$\text{ie} \quad \vec{L}_{pq} \equiv \vec{K}_{pq}^T \quad (3.13)$$

where the 'T' superscript implies transpose.

Starting from eqn 3.10, eqn 3.12 will now be derived. Substituting eqn 3.13 into eqn 3.10 gives

$$-j \sum_{q=1}^N C_{pq} \frac{da_q}{dz} = \sum_{q=1}^N (\beta_p C_{pq} + \vec{K}_{pq}^T) a_q \quad (3.14)$$

But as proved in several papers [2-4], and also in section 5.8.3, $\beta_p C_{pq} + \vec{K}_{pq}^T$ is symmetrical. Therefore eqn 3.14 becomes

$$-j \sum_{q=1}^N C_{pq} \frac{da_q}{dz} = \sum_{q=1}^N (C_{pq} \beta_q + K_{pq}) a_q \quad (3.15)$$

which is the form that Haus and Chuang derived (eqn 3.12). It can be noticed that we have dropped the arrow indicating the power transfer from K_{pq} , but it is implied that power is transferring from the eigenmode associated with the right-hand subscript to the left. If many waveguides [3,11] are considered (eg. N guides), then all of these terms could be put in matrix form,

$$\text{ie} \quad -jC \frac{d\underline{a}}{dz} = (\underline{C}\underline{\beta} + K)\underline{a} \quad (3.16)$$

where the notation of small letter underlined is used for column vectors, small letter double underlined for diagonal matrices, and capital letters for square matrices. The definitions are as follows

$$\underline{a} = \text{col}[a_1, a_2, \dots, a_N], \quad \underline{\underline{\beta}} = \text{diag}[\beta_1, \beta_2, \dots, \beta_N] \quad (3.18)$$

$$C = \begin{pmatrix} C_{11} & C_{12} & C_{13} & \cdots & C_{1N} \\ C_{21} & C_{22} & C_{23} & \cdots & \cdots \\ C_{31} & C_{32} & C_{33} & \cdots & \cdots \\ \cdots & \cdots & \cdots & \cdots & \cdots \\ C_{N1} & C_{N2} & C_{N3} & \cdots & C_{NN} \end{pmatrix} \quad K = \begin{pmatrix} K_{11} & K_{12} & K_{13} & \cdots & K_{1N} \\ K_{21} & K_{22} & K_{23} & \cdots & \cdots \\ K_{31} & K_{32} & K_{33} & \cdots & \cdots \\ \cdots & \cdots & \cdots & \cdots & \cdots \\ K_{N1} & K_{N2} & K_{N3} & \cdots & K_{NN} \end{pmatrix} \quad (3.18)$$

Hardy and Streifer's expression similarly becomes [11,15-16],

$$-jC \frac{d\underline{a}}{dz} = (\underline{\underline{\beta}}C + L)\underline{a} \quad (3.19)$$

Of the two coupled mode equations (eqns 3.16 and 3.19), we prefer Haus' notation (with the K matrix) since the differential equation can be solved more easily. For example, if we pre-multiply both sides of eqns 3.16 and 3.19 by C^{-1} , then we have

$$-j \frac{d\underline{a}}{dz} = (\underline{\underline{\beta}} + C^{-1}K)\underline{a} \quad (\text{Haus, Chuang}) \quad (3.20)$$

$$-j \frac{d\underline{a}}{dz} = (C^{-1}\underline{\underline{\beta}}C + C^{-1}L)\underline{a} \quad (\text{Hardy and Streifer}) \quad (3.21)$$

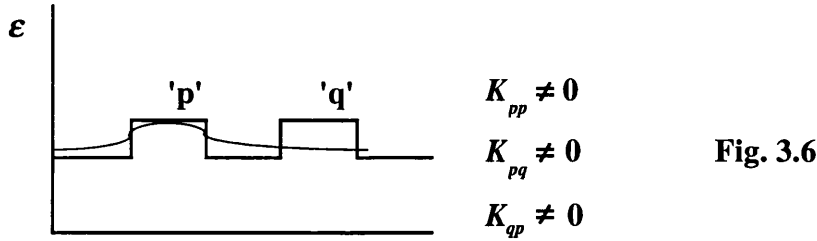
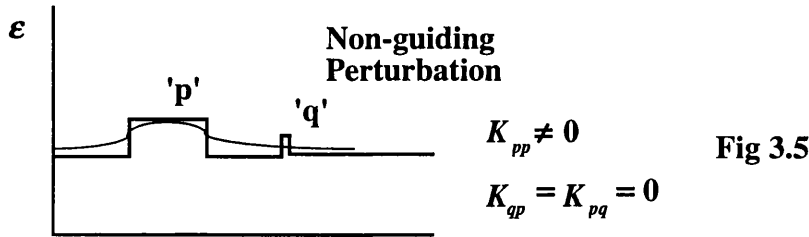
Clearly eqn 3.20 is much easier to work with. Therefore from now on, the K notation will be used.

3.6 THE 'MODIFICATION COEFFICIENT'

The diagonal elements of the K matrix (defined in the last section) have different physical origins from the off-diagonal elements. As explained above, the K_{pq} ($p \neq q$) terms are the coupling coefficients and lead to coupling between the eigenmodes. However the K_{pp} terms are 'modification coefficients' which modify the propagation coefficients of the eigenmodes. The modification is easily observed with the aid of an example using a non-guiding perturbation (see Fig. 3.5 below), since there are no coupling effects to complicate the issue. It can be seen that the evanescent tail of the otherwise unperturbed eigenmode travels through the high index perturbation which slows it down, and this retardation leads to an increase in the propagation coefficient of the eigenmode. For a waveguide perturbation (Fig. 3.6) exactly the same effect occurs but there is also some coupling.

We notice that in both notations, L_{pp} and K_{pp} are exactly the same,

$$L_{pp} = K_{pp} = \frac{\omega \epsilon_0}{4P} \iint_{-\infty}^{+\infty} \left((\epsilon - \epsilon^{(p)}) \underline{E}_t^{(p)} \cdot \underline{E}_t^{(p)} \right) dx dy \quad (3.22)$$



Figs 3.5 and 3.6 Illustrating the effect of the modification coefficient

3.5 RELATIVE MAGNITUDES OF K_{pp} AND K_{qp}

From the definition of the modification coefficient K_{pp} (eqn. 3.22), it is observed that the integral is evaluated over the perturbation region, which in Fig. 3.6 is guide 'q'. The modification coefficient K_{pp} is the product of the square of the eigenmode of guide 'p' multiplied by the perturbation situated in guide 'q' (a *different* guide). Since the magnitude of the eigenmode of one guide over the region of another guide is small (Figs 3.5 and 3.6), the modification coefficient K_{pp} is a small term.

The definition for the coupling coefficient K_{qp} however (eqn 3.22) contains the product of eigenmode 'q' with the perturbation situated in guide 'q' (the *same* guide). Consequently, the coupling coefficient K_{qp} is large compared with the modification coefficient K_{pp} . In summary $K_{qp} > K_{pp}$ where $q \neq p$.

3.8 LOSSLESS SYSTEM

The symmetry condition of eqn. 3.8 can be derived using reciprocity for a general case which could possibly include losses (see Chapter 5). However, for the case, where total power is conserved, a similar equation can be derived simply using power conservation. The coupled mode equation in matrix form (see eqn. 3.16) is given by

$$C \frac{da}{dz} = j(C\beta + K)a \tag{3.23}$$

Taking the adjoint operation (superscript $^+$) of eqn 3.23, noting that since C is a real symmetric matrix and $\underline{\underline{\beta}}$ a real diagonal matrix (lossless system), results in $C = C^+$ and $\underline{\underline{\beta}} = \underline{\underline{\beta}}^+$, we have

$$\frac{d\underline{\underline{a}}^+}{dz} C = -j\underline{\underline{a}}^+ (\underline{\underline{\beta}} C + K^+) \quad (3.24)$$

The total time averaged power as calculated in Appendix 6 is given by $\underline{\underline{a}}^+ C \underline{\underline{a}}$ (see comments following eqn A6.16). As the total power is conserved in a lossless system, its variation with propagation distance is zero [3], therefore

$$\frac{d(\underline{\underline{a}}^+ C \underline{\underline{a}})}{dz} = \frac{d\underline{\underline{a}}^+}{dz} C \underline{\underline{a}} + \underline{\underline{a}}^+ C \frac{d\underline{\underline{a}}}{dz} = 0 \quad (3.25)$$

Substituting eqns 3.23 and 3.24 into eqn 3.25, gives

$$\begin{aligned} \frac{d(\underline{\underline{a}}^+ C \underline{\underline{a}})}{dz} &= -j\underline{\underline{a}}^+ (\underline{\underline{\beta}} C + K^+) \underline{\underline{a}} + j\underline{\underline{a}}^+ (C \underline{\underline{\beta}} + K) \underline{\underline{a}} \\ &= j\underline{\underline{a}}^+ (C \underline{\underline{\beta}} - \underline{\underline{\beta}} C + (K - K^+)) \underline{\underline{a}} = 0 \end{aligned} \quad (3.26)$$

Rearranging the term in brackets on the RHS of eqn 3.26 gives

$$(K - K^+) = \underline{\underline{\beta}} C - C \underline{\underline{\beta}} \neq 0 \quad \text{unless } C \text{ is diagonal} \quad (3.27)$$

This is a similar equation to eqn 3.9 discussed before. In prior weak coupled mode theories [5-7] it was thought that the coupling coefficients were complex conjugates of each other, ie $K_{pq} = K_{qp}^*$ (or in matrix form $K = K^+$). But if C is not a diagonal matrix, (which it is not if the guides are strongly coupled), then $C \underline{\underline{\beta}} \neq \underline{\underline{\beta}} C$, so that $K \neq K^+$ results as seen from eqn 3.27. For weak coupling, the off-diagonal elements of C disappear to give

$$C = \begin{pmatrix} C_{11} & 0 & 0 & \dots & 0 \\ 0 & C_{22} & 0 & \dots & \dots \\ 0 & 0 & C_{33} & \dots & \dots \\ \dots & \dots & \dots & \dots & \dots \\ 0 & 0 & 0 & \dots & C_{NN} \end{pmatrix} = I \text{ (the identity matrix)} \quad (3.28)$$

where C becomes the identity matrix. In this case the coupling coefficients become complex conjugates of each other.

3.9 PRIOR WEAK COUPLED MODE THEORIES IN HINDSIGHT

The weak coupled mode equations of prior theories can now be re-examined with the benefit of hindsight, ie

$$-j(C)\frac{da}{dz} = ((C)\underline{\beta} + K)\underline{a} \quad \text{where } C = I \quad (3.29)$$

Therefore the overlap integrals are actually present in the ‘prior’ models but take the form of identity matrices. These equations are just the weak coupling limit of strong coupled mode theory.

3.10 SOLUTION OF COUPLED MODE EQUATIONS

The coupled mode equations (eqn. 3.20) can be solved very easily in terms of the mode amplitudes. For the two guide case eqn. 3.20 becomes

$$-j\frac{d}{dz}\begin{pmatrix} a_1 \\ a_2 \end{pmatrix} = \left[\begin{pmatrix} \beta_1 & 0 \\ 0 & \beta_2 \end{pmatrix} + \frac{1}{1-C_{12}^2} \begin{pmatrix} 1 & -C_{12} \\ -C_{21} & 1 \end{pmatrix} \begin{pmatrix} K_{11} & K_{12} \\ K_{21} & K_{22} \end{pmatrix} \right] \begin{pmatrix} a_1 \\ a_2 \end{pmatrix} \quad (3.30)$$

Eqn. 3.30 can now be expanded and expressed in the following forms

$$-j\frac{da_1(z)}{dz} = \beta_1^{mod} a_1(z) + K_{12}^{mod} a_2(z) \quad (3.31)$$

$$-j\frac{da_2(z)}{dz} = \beta_2^{mod} a_2(z) + K_{21}^{mod} a_1(z) \quad (3.32)$$

where the modified propagation coefficients β_1^{mod} and β_2^{mod} , and coupling coefficients K_{12}^{mod} and K_{21}^{mod} are defined as

$$\beta_1^{mod} = \beta_1 + \frac{1}{1-C_{12}^2}(K_{11} - C_{12}K_{21}) \quad , \quad \beta_2^{mod} = \beta_2 + \frac{1}{1-C_{12}^2}(K_{22} - C_{21}K_{12}) \quad (3.33)$$

$$K_{12}^{mod} = \frac{1}{1 - C_{12}^2} (K_{12} - C_{12} K_{22}) \quad , \quad K_{21}^{mod} = \frac{1}{1 - C_{12}^2} (K_{21} - C_{21} K_{11}) \quad (3.34)$$

It can be noticed from these definitions that the effect of the overlap integral is to modify the propagation coefficients and the coupling coefficients. To solve eqns. 3.31-3.32 for $a_1(z)$, a second order differential equation must be formed in terms of $a_1(z)$ only. The problem is that if eqn. 3.31 is differentiated wrt z , and eqn. 3.32 substituted, the resulting equation still contains $a_2(z)$, (ie the second order differential equation will not be in terms of $a_1(z)$ only). One way to eliminate this unwanted term is to initially make the following substitutions before forming the second order differential equation

$$a_1(z) = A_1(z) e^{j\beta_1^{mod} z} \quad a_2(z) = A_2(z) e^{j\beta_2^{mod} z} \quad (3.35)$$

where $A_1(z)$ and $A_2(z)$ are effectively slow varying amplitudes. Therefore eqns 3.31 and 3.32 become

$$-j \frac{dA_1(z)}{dz} = K_{12}^{mod} A_2(z) e^{2j\delta^{mod} z} \quad (3.36)$$

$$-j \frac{dA_2(z)}{dz} = K_{21}^{mod} A_1(z) e^{-2j\delta^{mod} z} \quad (3.37)$$

where $\delta^{mod} = \frac{\beta_2^{mod} - \beta_1^{mod}}{2}$ describes the asymmetry between the guides.

Differentiating eqn 3.36 wrt z , and substituting eqn 3.37 now gives

$$\frac{dA_1^2(z)}{dz^2} - 2j\delta^{mod} \frac{dA_1(z)}{dz} + K_{12}^{mod} K_{21}^{mod} A_1(z) = 0 \quad (3.38)$$

which can be solved easily using Laplace Transforms to give

$$\left\{ \begin{array}{l} s^2 \bar{A}_1(s) - sA_1(0) - A_1'(0) \\ -2j\delta^{mod} (s\bar{A}_1(s) - A_1(0)) \\ + K_{12}^{mod} K_{21}^{mod} \bar{A}_1(s) \end{array} \right\} = 0 \quad (3.39)$$

where $\bar{A}_1(s)$ is the Laplace Transform of $A_1(z)$. Rearranging eqn 3.39 in terms of $\bar{A}_1(s)$

leads to

$$\bar{A}_1(s) = \frac{(s - j\delta^{mod})A_1(0)}{(s - j\delta^{mod})^2 + p^{mod^2}} - \frac{j\delta^{mod}A_1(0)}{(s - j\delta^{mod})^2 + p^{mod^2}} + \frac{jK_{12}^{mod}A_2(0)}{(s - j\delta^{mod})^2 + p^{mod^2}} \quad (3.40)$$

where $p^{mod^2} = \delta^{mod^2} + K_{12}^{mod}K_{21}^{mod}$. Taking the inverse Laplace Transform of eqn. 3.40 and rearranging now gives

$$A_1(z) = \left\{ A_1(0) \left[\text{Cosp}^{mod} z - j \frac{\delta^{mod}}{p^{mod}} \text{Sinp}^{mod} z \right] + A_2(0) \left[j \frac{K_{12}^{mod}}{p^{mod}} \text{Sinp}^{mod} z \right] \right\} e^{j\delta^{mod} z} \quad (3.41)$$

$A_2(z)$ can be found either by symmetry, ie by replacing δ^{mod} with $-\delta^{mod}$ in eqn. 3.41 and switching around the 1 and 2 indices, or by differentiating $A_1(z)$ in eqn 3.41 wrt z and inserting it into eqn. 3.36 reaching

$$A_2(z) = \left\{ A_2(0) \left[\text{Cosp}^{mod} z + j \frac{\delta^{mod}}{p^{mod}} \text{Sinp}^{mod} z \right] + A_1(0) \left[j \frac{K_{21}^{mod}}{p^{mod}} \text{Sinp}^{mod} z \right] \right\} e^{-j\delta^{mod} z} \quad (3.42)$$

Substituting eqns 3.35 into eqns 3.41 and 3.42 allows us to express the solutions in terms of $a_1(z)$ and $a_2(z)$,

$$a_1(z) = \left\{ a_1(0) \left[\text{Cosp}^{mod} z - j \frac{\delta^{mod}}{p^{mod}} \text{Sinp}^{mod} z \right] + a_2(0) \left[j \frac{K_{12}^{mod}}{p^{mod}} \text{Sinp}^{mod} z \right] \right\} e^{\frac{j(\beta_1^{mod} + \beta_2^{mod})}{2} z} \quad (3.43)$$

$$a_2(z) = \left\{ a_2(0) \left[\text{Cosp}^{mod} z + j \frac{\delta^{mod}}{p^{mod}} \text{Sinp}^{mod} z \right] + a_1(0) \left[j \frac{K_{21}^{mod}}{p^{mod}} \text{Sinp}^{mod} z \right] \right\} e^{\frac{j(\beta_1^{mod} + \beta_2^{mod})}{2} z} \quad (3.44)$$

If guide 1 is initially excited, then $a_2(0) = 0$. Eqn. 3.44 therefore becomes

$$|a_2(z)|^2 = \frac{K_{21}^{mod^2}}{p^{mod^2}} |a_1(0)|^2 \text{Sin}^2 p^{mod} z \quad (3.45)$$

We note that $p^{mod} = \sqrt{\delta^{mod^2} + K_{12}^{mod}K_{21}^{mod}}$. Therefore for the symmetrical case (where $\delta^{mod} = 0$ and $K_{12}^{mod} = K_{21}^{mod}$) complete coupling occurs. In this case eqn. 3.45 becomes

$$|a_2(z)|^2 = |a_1(0)|^2 \text{Sin}^2 K_{12}^{mod} z \quad (3.46)$$

The coupling length can now be derived. Using eqn 3.46 complete coupling occurs when

$$z = L_c = \frac{\pi}{2K_{12}^{mod}} \quad (3.47)$$

From eqn 3.34 we see that for weak coupling, as $C_{12} \rightarrow 0$, $K_{12}^{mod} \rightarrow K_{12}$, therefore from eqn. 3.47 the coupling length becomes the well known $L_c = \pi/2K_{12}$. For the case of $C_{12} \neq 0$ then $K_{12}^{mod} > K_{12}$, and the effect of the overlap integral is to reduce the coupling length. For asymmetrical coupling, eqn. 3.45 becomes

$$|a_2(z)|^2 = \frac{K_{21}^{mod^2}}{\delta^{mod^2} + K_{12}^{mod} K_{21}^{mod}} |a_1(0)|^2 \text{Sin}^2 \sqrt{\delta^{mod^2} + K_{12}^{mod} K_{21}^{mod}} z \quad (3.48)$$

Which leads to incomplete coupling since $K_{21}^{mod^2} < \delta^{mod^2} + K_{12}^{mod} K_{21}^{mod}$.

3.11 CONCLUSIONS

In summary, the overlap integral measures the degree to which the two eigenmodes overlap each other. Assuming a two guide coupler for the moment, the total power is the sum of the power carried by the individual fields, plus the power carried by the overlap. If the power in the overlap is ignored, then in order to satisfy power conservation (for the lossless case), the coupling coefficients have to be complex conjugates of each other. Physically, if the power in the overlap does not exist, the power flowing out of the field of one guide must be equal the power flowing into the field of the other guide, otherwise power conservation is violated. Therefore the coupling coefficients have to be equal. With the overlap integral present, some of the power flowing out of one mode can flow into the overlap instead. Consequently the power flowing out of one mode does not necessarily have to equal the power flowing into the other mode, and so the coupling coefficients can be different. By including the overlap integral one has the freedom to make the coupling coefficients different for asymmetrical guides.

A more subtle effect of the overlap integral, as we saw was to modify the coupling coefficient, and thereby reduce the coupling length. Although this effect is minimal for linear couplers, it becomes important for nonlinear couplers even for symmetrical configurations.

Finally 100% coupling, albeit with shorter coupling lengths, is possible in strongly coupled waveguides so long as the guides are perfectly symmetrical ($\delta^{mod} = 0$) Otherwise incomplete coupling occurs.

REFERENCES

- [1] A. Hardy and W. Streifer, "Coupled mode theory of parallel waveguides", J. Light. Technol., vol LT-3, no. 5, 1985, pp. 1135-1146.
- [2] S-L Chuang, "A coupled mode formulation by reciprocity and a variational principle", J. Light. Technol., vol. LT-5, no. 1, 1987, pp. 5-15.
- [3] H. A. Haus, W. P. Huang, S. Kawakami, and N. A. Whitaker, "Coupled-mode theory of optical waveguides", J. Light. Technol. , vol. LT-5, no. 1, 1987, pp. 16-23
- [4] W. Streifer, M. Osinski, and A. Hardy, "Reformulation of the coupled-mode theory of multiwaveguide systems", J. Light. Technol., vol. LT-5, no. 1, 1987, pp. 1-4.
- [5] A. Yariv, "Coupled-Mode Theory for guided wave optics," IEEE J. Quantum Electron, Vol. QE-9, pp. 919-933, (1973)
- [6] H.F. Taylor and A. Yariv, "Guided wave optics", Proc. IEEE, Vol. 62, pp. 1044-1060 (1974)
- [7] H. Kogelnik, "Theory of dielectric waveguides", in Integrated Optics, 2nd ed., T. Tamir, Ed. New York: Springer-Verlag, 1979, Ch.2
- [8] A. W. Snyder, A. Ankiewicz, and A. Altintas, "Fundamental error of recent coupled mode formulations", Electron Lett, vol. 23, no. 20, 1987, pp. 1097-1098.
- [9] A. W. Snyder, and A. Ankiewicz, "Fibre couplers composed of unequal cores", Electron. Lett., vol. 22, no. 23, 1986, pp. 1237-1238.
- [10] A. W. Snyder and A. Ankiewicz, "Optical fiber couplers- optimum solution for unequal cores", J. Light. Technol., vol. 6, no. 3, 1988, pp. 463-474
- [11] S-L Chuang, "A coupled-mode theory for multiwaveguide systems satisfying the reciprocity and power conservations", J. Light. Technol. vol. LT-5, 1987, pp. 174-183.
- [12] W. Huang, "Variational coupled-mode theory of optical couplers", J. Light. Technol., vol. 8, no. 10, 1990, pp. 1565-1570.
- [13] W. Streifer, "Fundamental error of recent coupled mode formulations", Electronics Letters, vol. 24, no. 11, 1988, pp. 718-719.
- [14] K. Yasumoto, "Coupled-mode formulation of parallel dielectric waveguides using single perturbation technique", Microwave and optical Technol. Lett., vol. 4, no. 11, 1991, pp. 486-491

- [15] A. Hardy and W. Streifer, "Coupled modes of multiwaveguide systems and phased arrays", *J. Light. Technol.*, vol. LT-4, no. 1, 1986, pp. 90-99
- [16] A. Hardy and W. Streifer, "Coupled mode solutions of multiwaveguide systems", *IEEE J. Quant. Electron.*, vol. QE-22, no. 4, 1986, pp. 528-534.
- [17] A. Hardy, W. Streifer, and M. Osinski, "Weak coupling of parallel waveguides", *Optics Letters*, vol. 13, no. 2, 1988, pp. 161-163.

CHAPTER 4

THE NONLINEAR DIRECTIONAL COUPLER: REVIEW OF THE LITERATURE

4.1 INTRODUCTION

The nonlinear directional coupler (NLDC) will be an important component for future all-optical signal processing systems [1-2]. It will be used for many all-optical applications including all-optical switches [1], all-optical filters [3], pulse compressors [4], all-optical transistors [5], and all-optical logic functions [6-7].

Many aspects of the nonlinear directional coupler have been investigated in the recent literature. The purpose of this chapter is to review and summarize the main results. The topics reviewed include theoretical papers on the operation of the NLDC, the study of deleterious effects such as losses, saturation of the nonlinearity, and the slow response time of the nonlinearity; the improvement in switching obtained using asymmetric nonlinearities, asymmetric gains, and multiwaveguides; the pulsed operation of the NLDC, especially the important case of soliton pulse transmission, and pulse transmission in combination with the effects of gains, losses and saturation. Finally some issues regarding practical NLDCs are discussed.

4.2 THE NONLINEAR DIRECTIONAL COUPLER: THE BASICS AND GENERAL REVIEW OF THE LITERATURE

The NLDC [1] consists of two waveguides situated in close proximity embedded in a nonlinear material possessing an intensity dependent refractive index. Coupling between the guides occurs as a result of the evanescent overlap of the modes with neighbouring waveguides and the nonlinear media. At low powers the device behaves almost like a linear directional coupler. Assuming the length corresponds with one linear coupling length with one guide initially excited, full transfer of power from the feed guide to the second guide occurs. At very high input powers the guides become so mismatched that the power remains in the feed guide. There is an intermediate power called the 'critical' or 'switching' power where the power emerges equally from both guides. The critical power is unstable. Slightly below it and the power switches to the

second guide, and slightly above it and the power stays in the feed guide. This instability can be used for switching in a number of ways. If the feed guide is excited with a power just below critical, with an additional small signal inserted into either the feed or the second guide, then switching of the large power can be controlled by changing the amplitude and/or phase of the smaller signal [5]. As the phase of the small signal here is controlling the switching of a much larger power, the device is effectively an all-optical transistor. For fast nonlinearities, the nonlinearity is local in space and time, and several pulses propagate simultaneously and independently in the device in serial fashion [1]. Since the device processes all the pulses simultaneously, the switching time is limited only by the nonlinear response time, and not by the transit time.

The NLDC can be studied analytically using either the beam propagation method (BPM) [5] which is a numerical approach, or coupled mode theory, an analytical approach. Although BPM is an accurate method, the fact that it is numerical in nature means that it is not useful for identifying different physical mechanisms responsible for the coupling, or to study stability and chaos in a phase-space graphical approach.

The first coupled mode analysis of the NLDC was carried out by Jensen [1]. This was done by deriving two differential equations (coupled mode equations), and solving for the mode amplitudes in terms of elliptical functions. Formulae for the critical power and the coupling length were also derived. A much more elegant method was proposed in [8], where the mode amplitudes were formulated in terms of Stoke's parameters and inserted into the coupled mode equations. Two constants of motion were then derived (a Poincaré sphere and a parabola), and the intersection between the two resulted in the trajectories of motion depicting the evolution of the amplitudes and phases with distance. These trajectories were represented simultaneously (for all possible input conditions) on a Poincaré sphere. The trajectories resembled those encountered in nonlinear dynamics, where the centre of concentric circles is a stable point, and the col of a separatrix an unstable point. The authors also studied (in another paper [9]) the asymmetrical NLDC and showed that the asymmetrical NLDC is nonreciprocal, since if the power is inserted into the guide with the lower propagation coefficient, coupling is improved because the power reduces the mismatch, whereas if the power is inserted into the guide with the higher propagation coefficient, the coupling worsens because the power increases the mismatch.

There have been efforts to summarize the physics of the NLDC succinctly using graphical methods (phase-space portraits) [10-11]. Perhaps the most useful approach came from Snyder and co-workers [10]. The principle was based on the observation that the evolution of power in a nonlinear directional coupler is similar to that of a linear

coupler but with axial refractive index changes [12] (it was suggested by the same authors in another paper [12] that by freezing in these refractive index changes, the critical power can be reduced). It was then suggested that all the physics of nonlinear couplers could be understood by studying the coupling in linear asymmetric couplers. By superimposing the characteristics of the even and odd modes of linear asymmetric couplers together with the critical power characteristics on one portrait, defining stable and unstable regions, and establishing several rules for reading where power maxima or minima are situated (details in [10]), many of the operational characteristics of the nonlinear coupler can be read straight from the portrait, and several applications predicted [10, 13]. It was also shown that the portraits could be extended to non-Kerr materials including saturation.

There have been a series of papers aimed at improving the accuracy of coupled mode theory with respect to BPM. Fraile Pelaez and Assanto [14] first made the observation that Jensen's coupled mode equations were inconsistent. The equations incorporated some second order terms (nonlinear cross-coefficients) but did not include several others of the same magnitude. Fraile-Pelaez and Assanto showed that the inconsistency caused a big difference in the results. This inconsistency has also been pointed out for the three-guide NLDC [15]. Comparison between coupled mode theory and BPM still showed much difference, and some researchers at the time even doubted the applicability of coupled mode theory for NLDCs. The main reason for the difference was that the power dependency of the mode shapes had not been incorporated in coupled mode theory papers [eg. 8, 16-18] until that period. This point was briefly mentioned in [19] in the context of the sign of the nonlinearity, and later in detail by Meng and Okamoto [20]. However, the coupled mode equations were still not accurate for strongly coupled nonlinear couplers. Ankiewicz and Peng [21] incorporated the power dependence, and in an effort to allow the equations to be applicable for strong coupling included the overlap integral (or 'interaction coefficient') but did not include nonlinear cross-coefficient terms. This was inconsistent and lead to serious errors in their results. As the overlap integral and the nonlinear cross-coefficients are interdependent, great care was needed when including the overlap integral for strongly coupled nonlinear couplers (more so in fact than in weak coupling or linear couplers). The overlap integral and the nonlinear cross-coefficients must either be present or absent together.

The critical power in a symmetric nonlinear directional coupler has been calculated using nonlinear supermodes [22]. In that paper it was claimed that the supermode approach was more accurate than the eigenmode approach. Unfortunately however,

although only a very weakly coupled device was chosen (where all methods would in principle have lead to similar results) their results were highly inaccurate. In addition, it was found in a recent paper [23] that the (power dependent) nonlinear even mode is unstable [23] above a certain bifurcation power, and the odd mode absent above another higher power, so it is not certain whether this approach can work.

4.3 PULSED OPERATION OF NONLINEAR DIRECTIONAL COUPLERS

The pulsed operation of the NLDC has also been studied. In ideal nonlinear materials, eg. glasses, the response time of the nonlinearity is almost instantaneous. Therefore if the pulse shape is much longer than the response time of the nonlinearity, each part of the pulse travels through the NLDC as though it were a CW case. This means that for gaussian pulses, for example, the pulse undergoes break-up. The peak of the pulse remains in the first guide, and the low intensity sides are coupled into the second guide. This pulse break-up could be exploited for pulse compression [4], but overall is undesirable since it prevents the cascading of such devices. One way to ensure that pulse break-up does not occur is to use square pulses [24]. But this approach has its drawbacks since it requires a relatively complex pulse-shaping process, leading to severe dispersive distortion of the steep pulse edges for ultrashort pulses. Another approach is to use temporal solitons. It has been found that temporal solitons switch through nonlinear couplers without break-up, ie as a single entity (this was shown numerically in [25] and analytically using a variational method [26]). Solitons do not break up since they possess a uniform nonlinear phase-shift across the whole pulse [27] (the single phase-shift is evident in the basic formula for the soliton derived from the nonlinear Schrödinger equation [eg. 28]), therefore virtually complete coupling can be achieved [25]. As the soliton pulse couples from one guide to the other, its amplitude decreases and the pulse becomes wider, whereas the amplitude of the pulse in the other guide increases and the pulse becomes narrower. The switching transition is as sharp as the CW case.

Two different modes of operation for the pulsed NLDC exist [29-30]. The first is known as self-switching. By changing the power of the input soliton itself, the soliton can be switched from one output guide to the other. The second method involves the signal soliton acting as a pump in one input guide, and a much weaker pulse [31] (or even CW beam) enabling the switching depending on the phase. All optical switching of pulses due to variation of the phase of a seeded input has been shown experimentally in fibre rocking filters [32]. Here, the input is a soliton pulse of one polarisation, and a fraction of the power is used as seed for the other polarisation. By varying the phase of

the seed pulse all-optical switching was achieved. The critical power was $750W$ and $30ps$ pulses were used. The coupling length was around $1.27m$.

4.4 INCORPORATION OF OTHER EFFECTS

The effects of gains, losses, saturation of nonlinearity, and asymmetry of nonlinearity have been studied for the CW and pulse cases.

4.4.1 Diffusion

The effect of diffusion of the nonlinearity on the operation of the NLDC was studied in [33] using BPM. It was found that the effect of diffusion was to homogenize the nonlinear refractive index profile over distances of the order of the diffusion length resulting in a reduction in the peak refractive index. It was found that the longer the diffusion length, the more the switching deteriorated (since the nonlinearly induced mismatch between the propagation constants of the two guides was reduced), and eventually resulted in the coupling becoming linear.

4.4.2 Saturation

Saturation deteriorates the switching characteristics of nonlinear couplers [34-38]. At very high powers, the refractive indices of the guides reach their maximum values and the NLDC behaves as a linear coupler.

4.4.3 Asymmetric nonlinearities/waveguides

The effect of asymmetrical nonlinearities in NLDCs has been studied using a supermode approach [39] (but the analysis did not include power dependence of the mode shapes). It was found that NLDCs with asymmetrical nonlinearity have lower critical powers providing that the nonlinearity in the output guide is greater than that in the feed guide [39-40]. The asymmetric coupler has also been studied using the eigenmode approach incorporating the overlap integral [41]. It was found that inclusion of the overlap lead to a reduction in the critical power. The results of this paper are however rather dubious since apart from not including power dependent fields, it was inconsistent in including the overlap integral but ignoring the nonlinear cross-coefficients, the same error as was made in [16].

The case of one guide linear and the other nonlinear has been studied [38]. It was found that the switching was sharper for when the feed guide was nonlinear. The saturable nonlinearity caused reduced transfer of power. For weak saturation it was found that linear guide excitation was preferable, but for large saturations nonlinear

guide excitation was preferable. However, the analysis did not include either power dependent fields or the overlap integral, and so applied for the weakly coupled case only. Also only the specific combination of a linear and a nonlinear guide was studied, and the analysis was not extended to other cases. The asymmetric nonlinearity using CW, as well as picosecond and femtosecond solitons was studied in [6]. It was shown that ultrafast logic gates such as NOT, AND, OR, and XOR could be implemented by appropriate choice of parameters.

It was shown by Farjady and Wilson [3] that asymmetric guides can also be used to construct all-optical filters. This was achieved by employing different guide widths in order to introduce waveguide dispersion. The nonlinear filter was tunable using the intensity of the light, and the bandwidth narrowed with intensity (an intensity dependent filter has also been experimentally demonstrated in birefringent fiber rocking filters [67], but the integrated optic filter [3] has the added advantage that it can also be intensity tuned with the bandwidth remaining constant).

4.4.4 Incorporation of gains and losses

Strategically placed gains and losses can lead to improvement in the switching characteristics. Gains are useful in any case because they can be used to overcome the degradation due to inevitable losses in the system.

The effect of introducing gain into the NLDC was studied in [42-43]. An empirical formula for the switching power was derived in [42], which agreed well with numerical simulations, for different coupling lengths. It was observed that for the CW case, gain reduced the switching power and resulted in the switching being much sharper. However, for large gains the switching characteristics were deteriorated. One solution to overcome the degradation was to use gain in the feed core, and loss in the second core [44]. It was found that as the magnitude of the loss/gain (imaginary parts of the propagation coefficient) reached values comparable to the coupling coefficient the critical power reduced significantly. The reduction in critical power was also accompanied by an increase in device length. However, this increase happened to be less than would have occurred for a lossless NLDC, assuming the same reduction in critical power. It was also found that the critical power can be reduced by a further factor of 2.5 times if the gain medium has a positive nonlinearity, and the loss medium a negative nonlinearity. It was mentioned that the coupler with gain in one guide and equal amount of loss in the other was acutely sensitive to the difference in the real parts of the refractive index between the guides.

The use of losses to improve the switching characteristics was avoided in [42] by

using solitons. Soliton switching resulted in better switching characteristics for high gains. The calculations initially assumed that the gain bandwidth was pseudo-infinite, but a limited bandwidth was subsequently taken into account. Finally, the device was modelled using the irregular bandwidth of erbium-doped fibre, resulting in a degradation in the switching characteristics.

In [43] it was suggested that the presence of *different* gains in the waveguides can improve the switching characteristics and the tolerance towards degradation due to saturation (saturation is inevitable when high nonlinearities are present, and affects active couplers more than passive couplers). The oscillations in the switching characteristics at low powers (below switching power) can be improved [43] using saturation in the input guide and no saturation in the second guide, eg with input guide nonlinear and output guide linear. The oscillations above the switching power can be reduced by allowing the nonlinear saturation in the two guides to be as similar as possible.

4.4.5 Multiwaveguide nonlinear directional couplers

Multiwaveguide nonlinear couplers have been studied using coupled mode theory and BPM. It has been suggested that the use of multiple waveguides could result in sharper switching between the *outer* waveguides (the intermediate guides are parasitic in this case) [45]. The improved switching is at the expense of slightly larger critical powers, and slightly longer lengths ($L = \sqrt{(N-1)}L_c$, where L_c is the coupling length for the two guide linear coupler, and N the number of guides). Increasing the length in the two guide coupler though results in large oscillations in the low input power region of the switching characteristics.

Attempts have been made to derive analytical solutions for the coupled mode equations of the three guide nonlinear coupler. Two constants of motion can be extracted (which are the total power and the Hamiltonian) [46-48]. The exact solution for the centre waveguide excitation case was calculated in [47]. The solution for the side-excitation case is considerably more difficult to derive, and has not been derived so far. However a power-portrait approach [49] has been used to study phase-controlled switching [49].

The pulsed operation of three-guide nonlinear couplers was studied in [23]. The effect of gain in three-guide nonlinear couplers was studied in [50]. It was shown that gain allowed full switching between all three ports, but strategically positioned gains and losses did not improve the switching as in two-guide couplers.

Finally, Chaos has been shown to occur in three-guide nonlinear couplers [47,51].

4.4.6 Nonparallel nonlinear directional couplers

The NLDCs considered so far have all involved parallel guides. Nonparallel guides are of practical interest since they are easier to fabricate. In contrast to parallel couplers they do not have strict requirements on their lengths. One example is the nonlinear bent coupler [52-53], which consists of two fibre cores with a separation which starts off as large, reduces to a minimum distance, and increases again. The switching in this type of coupler is asymptotic. As with the parallel NLDC, varying the phase of a seed signal in one input guide can enable the switching of a much larger power in the other guide.

4.5 PRACTICAL NONLINEAR DIRECTIONAL COUPLERS

Practical NLDCs have been constructed using a variety of materials, but the most successful so far have been in semiconductors and glasses. The nonlinearity in semiconductors is very large due to resonance enhancement. NLDCs have been constructed in GaAs/AlGaAs MQWs using the nonlinearity near the bandedge [54-57] exploiting the excitonic enhancement [58]. However these devices were very lossy. NLDCs have also been constructed in the low absorption region just below the half-bandgap [59]. Other materials have been considered as well. For example parallel [60-61] and nonparallel [62] nonlinear directional couplers based on the photorefractive effect of $LiNbO_3$ ('optical damage').

There are several approaches [29] to implementing the NLDC in fibres. The physics for all of them is identical [63]. The first method, perhaps the most obvious one, is to switch, using the evanescent overlap of the modes, between the cores of a twin-core fibre [64]. The second approach is to make use of a single-core birefringent fibre [65], with coupling occurring between the circular polarisations. A right-handed circular polarisation is switched to left-handed circular below the critical power, but not above. At the critical power the output is linearly polarised (equal amounts of left-hand and right-hand polarisations present).

The third approach employs a polarisation-rocking rotator/filter [65-66]. In this device the principal axes of the fibre are periodically twisted by a small angle and twisted back after a short distance. By using the correct length for each twisted section, it is possible to rotate the linear polarisation by an angle which is twice the angle of the twist. By using several of these sections in succession, a linearly polarised light can be made to rotate over 90 degrees. Thus the device can be used as a polarisation rotator, and in combination with a polariser, as a filter. The nonlinear filter can also be used as a switch, since if the power is just above critical, the polarisation is unchanged, whereas if it is just below the polarisation is rotated by 90 degrees.

REFERENCES

- [1] S. M. Jensen, "The nonlinear coherent coupler", *IEEE Transactions on Microwave Theory and Techniques*, MTT-30, no. 10, 1982, pp. 1568-1571.
- [2] A. A. Maier, "Self-switching of light in a directional coupler", *Sov. J. Quant. Electron.*, vol. 14, no. 1, 1984, pp. 1011-1014.
- [3] F. Farjady and M.G. F. Wilson, "New application for the nonlinear directional coupler- intensity controlled tunable optical filter", *Electron. Lett.*, vol. 27, no. 24, 1991, pp. 2218-2219.
- [4] K-I Kitayama and S. Wang, "Optical pulse compression by nonlinear coupling", *Appl. Phys. Lett.*, vol. 43, no. 1, 1983, pp. 17-19.
- [5] S. Wabnitz, E. M. Wright, C. T. Seaton, and G. I. Stegeman, "Instabilities and all-optical phase-controlled switching in a nonlinear directional coherent coupler", *Appl. Phys. Lett.*, vol. 49, no. 14, 1986, pp. 838- 840.
- [6] C-C Yang and A. J. S. Wang, "Asymmetric nonlinear coupling and its applications to logic functions", *IEEE J. Quant. Electron.*, vol. 28, no. 2, 1992, pp. 479-487.
- [7] C. G. Krautschik, G. I. Stegeman, and R. H. Stolen, "Asymmetric response of nonlinear coupled-mode devices: all-optical logic gates with a rocking-filter fiber", *Optics Letters*, vol. 18, no. 13, 1993, pp. 1050-1052.
- [8] B. Daino, G. Gregori, and S. Wabnitz, "Stability analysis of nonlinear coherent coupling", *J. Appl. Phys.*, vol. 58, no. 12, 1985, pp. 4512-4514.
- [9] S. Trillo and S. Wabnitz, "Nonlinear nonreciprocity in a coherent mismatched coupler", *Appl. Phys. Lett.*, vol. 49, no. 13, 1986, pp. 752-754.
- [10] A. W. Snyder, D. J. Mitchell, L. Poladian, D. R. Rowland, and Y. Chen, "Physics of nonlinear fibre couplers", *J. Opt. Soc. Am. B*, vol. 8, no. 10, 1991, pp. 2102-2118.
- [11] A. T. Pham, and L. N. Binh, "All-optical modulation and switching using a nonlinear-optical directional coupler", *J. Opt. Soc. Am. B*, vol. 8, no. 9, 1991, pp. 1914-1931.
- [12] A. W. Snyder, and Y. Chen, "Nonlinear fibre couplers: switches and polarisation beam splitters", *Optics Letters*, vol. 14, no. 10, 1989, pp. 517-519.
- [13] D. R. Rowland, "All-optical devices using nonlinear fibre couplers", *J. Light. Technol.*, vol. 9, no. 9, 1991, pp. 1074-1083.
- [14] F. J. Fraile-Pelaez and G. Assanto, "Coupled-mode equations for nonlinear directional couplers", *Applied Optics*, vol. 29, no. 15, 1990, pp. 2216-2217.
- [15] C. Mapalagama and R. T. Deck, "Modified theory of three-channel kerr-type

- nonlinear directional coupler”, J. Opt. Soc. Am. B, vol. 9, no. 12, 1992, pp. 2258-2264.
- [16] A. Ankiewicz, “Novel effects in non-linear coupling”, Opt. Quant. Electron. , vol. 20, 1988, pp. 329-337.
- [17] A. Ankiewicz, “Interaction coefficient in detuned nonlinear couplers”, Optics Communications, vol. 66, no. 5,6, 1988, pp. 311-314.
- [18] Y. Chen, “Solution to full coupled wave equations of nonlinear coupled systems”, IEEE J. Quant. Elect., vol. 25, no. 10, 1989, pp. 2149-2153.
- [19] F. J. Fraile-Pelaéz, G. Assanto, and D. R. Heatley, “Sign-dependent response of nonlinear directional couplers”, Optics Commun., vol. 77, no. 5,6, 1990, pp. 402-406.
- [20] X. J. Meng, and N. Okamoto, “Improved coupled-mode theory for nonlinear directional couplers”, IEEE J. Quant. Electron., vol. 27, no. 5, 1991, 1175-1181.
- [21] A. Ankiewicz and G-D Peng, J. Opt. Soc. Am. B, vol. 9, 1992, pp. 1341
- [22] F. Dios, X. Nogués, and F. Canal, “Critical power in a symmetric nonlinear directional coupler”, Opt. Quant. Electron., vol. 24, 1992, pp. 1191-1201.
- [23] A. D. Capobianco, and G. F. Nalesso, “Determination and stability analysis of the supermodes in nonlinear directional couplers through a variational approach”, Optical and Quant. Electron., vol. 27, 1995, pp. 1015-1026.
- [24] A. M. Weiner et. al., “Use of femtosecond square pulses to avoid pulse breakup in all-optical switching”, IEEE J. Quant. Electron., vol. 25, no. 12, 1989, pp. 2648-2655.
- [25] S. Trillo, S. Wabnitz, E. M. Wright, and G. I. Stegeman, “Soliton switching in fibre nonlinear directional couplers”, Optics Letters, vol. 13, no. 8, 1988, pp. 672-674.
- [26] P. L. Chu, B. A. Malomed, and G. D. Peng, “Soliton switching and propagation in nonlinear fibre couplers: analytical results”, J. Opt. Soc. Am. B, vol. 10, no. 8, pp.1379-1385, 1993.
- [27] K. J. Blow, and N. J. Doran, “Soliton phenomena in optical fibres”, Anisotropic and nonlinear optical waveguides, edited by C. G. Someda And G. Stegeman, Elsevier Science Publishers, 1992, pp. 159-183.
- [28] A. Hasegawa and Y. Kodama, “Solitons in optical communications”, Oxford series in optical and imaging sciences, 1995; K. J. Blow, and N. J. Doran, “Soliton phenomena in optical fibres”, Anisotropic and nonlinear optical waveguides, edited by C. G. SOMEDA and G. STEGEMAN, Elsevier Science Publishers, 1992, pp. 159-183.
- [29] M. Romagnoli, S. Trillo, and S. Wabnitz, “Soliton switching in nonlinear

- couplers”, *Optical and quantum Electron.*, vol. 24, 1992, S1237-S1267
- [30] S. Trillo, and S. Wabnitz, ”Nonlinear dynamics and instabilities of coupled waves and solitons in optical fibres”, *Anisotropic and Nonlinear optical waveguides*, Edited by C. G. Someda, and G. Stegeman, 1992, Elsevier Science Publishers B. V.
- [31] S. Trillo and S. Wabnitz, “Weak-pulse-activated coherent soliton switching in nonlinear couplers”, *Optics Lett.*, vol. 16, no. 1, 1991, pp.1-3
- [32] C. G. Krautschik, G. I. Stegeman, and R. H. Stolen, “Phase controlled all-optical switching in rocking filter fibres”, *Appl. Phys. Lett.*, vol. 61, no. 15, 1992, pp. 1751-1753.
- [33] D. R. Heatley, E. M. Wright, J. Ehrlich, and G. I. Stegeman, “Nonlinear directional coupler with diffusive Kerr-type nonlinearity”, *Optics Lett.*, vol. 13, no. 5, 1988, pp. 419-421.
- [34] E. Caglioti, S. Trillo, S. Wabnitz, B. Daino, and G. I. Stegeman, “Power-dependent switching in a coherent nonlinear directional coupler in the presence of saturation”, *Appl. Phys. Lett.*, vol. 51, no. 4, 1987, pp. 293-295.
- [35] G. I. Stegeman, C. T. Seaton, C. N. Ironside, T. Cullen, and A. C. Walker, “Effects of saturation and loss on nonlinear directional couplers”, *Appl. Phys. Lett.*, vol. 50, no. 16, 1987, pp. 1035-1037.
- [36] L. Thylen, E. M. Wright and G. I. Stegeman, “Numerical analysis of nonlinear coherent couplers exhibiting saturable index changes”, *J. Opt. Soc. Am. B*, vol. 5, no. 2, 1988, pp. 467-471
- [37] G. I. Stegeman, E. Caglioti, S. Trillo, and S. Wabnitz, “Parameter trade-offs in nonlinear directional couplers: two level saturable nonlinear media”, *Optics Comms.*, vol. 63, no. 5, 1987, pp. 281-284.
- [38] M. Bertolotti, M. Monaco, and C. Sibilia: "Role of the asymmetry in a third-order nonlinear directional coupler", *Optics Communications*, Vol. 116, 1995, pp. 405-410
- [39] M. A. Karpierz, “Nonlinear directional couplers with asymmetrical distribution of nonlinearity”, *Optics Commun.*, vol. 90, 1992, pp. 241-244.
- [40] M. A. Karpierz, D. F. Clark, I. Andonovic, and B. Culshaw: "Nonsymmetrical nonlinear directional coupler", *SPIE Vol. 1085 Optical fibres and Their applications* (1989), pp. 397-402
- [41] A. Ankiewicz, "Interaction coefficient in detuned nonlinear couplers", *Optics Communications*, Vol 66, No. 5,6, may 1988, pp. 311-314
- [42] J. Wilson, G. I. Stegeman, and E. M. Wright, “All-optical switching of solitons in an active nonlinear directional coupler”, *Opt. Quant. Electron.*, vol. 24, 1992, S1325-1336.

- [43] J. Atai and Y. Chen, "Nonlinear mismatches between two cores of saturable nonlinear couplers", *IEEE J. Quant. Electron.*, vol. 29, no. 1, 1993, pp. 242-249.
- [44] Y. Chen, A. W. Snyder, and D.N. Payne, "Twin core nonlinear couplers with gain and loss", *IEEE J. Quant. Electron.*, vol. 28, no. 1, 1992, 239-245.
- [45] Y. Chen, A. W. Snyder, and D. J. Mitchell, "Ideal optical switching by nonlinear multiple (parasitic) core couplers", *Electron. Lett.*, vol. 26, no. 1, pp. 77-78, 1990.
- [46] C. Schmidt-Hattenberger, R. Muschall, U. Trutschel, and F. Lederer, "Nonlinear eigenmodes of a three-core fibre coupler", *Opt. Quant. Electron.*, vol. 24, 1992, pp. 691-701.
- [47] L. J. Bernstein, "The three-waveguide nonlinear directional coupler: the center waveguide excitation", *Opt. Comms.*, vol. 94, 1992, pp. 406-416.
- [48] C. Schmidt-Hattenberger, U. Trutschel, and F. Lederer, "Nonlinear switching in multiple-core couplers", *Optics Lett.*, vol. 16, no. 5, 1991, pp. 294, 296.
- [49] C. Schmidt-Hattenberger, R. Muschall, F. Lederer, and U. Trutschel, "Phase-controlled switching in nonlinear multiport fibre couplers", *J. Opt. Soc. Am. B*, vol. 10, no. 9, 1993, pp. 1592-1599.
- [50] F. Di Pasquale, H. E. Hernandez Figueroa, 'Improved all optical switching in a three slab nonlinear directional coupler with gain', *IEEE J. Quant. Elect.*, May 1994, Vol. 30, No. 5, pp. 1254-1258.
- [51] N. Finlayson and G. I. Stegeman, "Spatial switching, instabilities, and chaos in a three-waveguide nonlinear directional coupler", *Appl. Phys. Lett.*, vol. 56, no. 23, 1990, pp. 2276-2278.
- [52] V. Leutheuser, U. Langbein, and F. Lederer, "Optical response of a nonlinear bent directional coupler", *Optics. Comm.*, vol. 75, no. 3,4, 1990, pp. 251-255.
- [53] Z. Jakubczyk, R. Tremblay, and R. Vallee, "Nonlinear curved fibre coupler", *J. Appl. Phys.*, vol. 66, no. 10, 1989, pp. 5113-5115.
- [54] P. Li Kam Wa, J. E. Stitch, N. J. Mason, J. S. Roberts, and P. N. Robson, "All optical multiple-quantum well waveguide switch", *Electron. Lett.*, vol. 21, 1985, pp. 26-27
- [55] P. Li Kam Wa, J. H. Marsh, P. N. Robson, J. S. Roberts, and N. J. Mason, "Nonlinear propagation in GAAs/GaAlAs multiple quantum well waveguides", *SPIE*, vol. 578, Boston, MA, 1985
- [56] P. Li Kam Wa, P. N. Robson, J. P. R. David, G. Hill, P. Mistry, M. A. Pate, and J. S. Roberts, "All-optical switching effects in a passive GaAs/GAAlAs multiple quantum well waveguide resonator", *Electron. Lett.*, vol. 22, pp.1129-1130, 1986
- [57] P. Li Kam Wa, and P. N. Robson, "Nonlinear multiple quantum well waveguide devices", *Proc. SPIE*, vol. 800, Novel Optoelectron. Devices, 1987, pp. 43-49.

- [58] R. Jin, C. L. Chuang, H. M. Gibbs, S. W. Koch, J. N. Polky, and G. A. Pubanz "Picosecond all-optical switching in single-mode GaAs/AlGaAs strip-loaded nonlinear directional couplers", Appl. Phys. Lett., Vol. 53, No.19, November 1988, pp. 1791-1793.
- [59] H. K. Tsang, R. S. Grant, R. V. Penty, I. H. White, J. B. D. Soole, E. Colas, H. P. Leblanc, N. C. Andreadakis, M. S. Kim, and W. Sibbett, "GaAs/GaAlAs Multiquantum well waveguides for all-optical switching at $1.55\mu m$ ", Electron. Lett., Vol. 27, no.22, October 1991, pp. 1993-1995.
- [60] G. T. Harvey, G. Astfalk, A. Y. Feldblum and B. Kassahun, IEEE J. Quant. Electron., vol. 22, 1986, pp. 239
- [61] C. T. Mueller And E. Garmire, Appl. Opt., vol. 23, 1984, pp. 4348.
- [62] S-J Hwang, W-Y Lee, and H-M Wang, "The characteristics of a nonlinear directional coupler with nonparallel waveguides", Opt. Quant. Electron., vol. 25, 1993, pp. 207-213.
- [63] A. W. Snyder, Y. Chen, D. Rowland, and D. J. Mitchell, "Unification of nonlinear-optical fibre devices", Optics Letters, vol. 15, no. 3, 1990, pp. 171-173.
- [64] S. R. Friberg, Y. Silberberg, M. K. Oliver, M. J. Andrejco, M. A. Saifi, and P. W. Smith, "Ultrafast all-optical switching in a dual-core fibre nonlinear coupler", Appl. Phys. Lett., Vol. 51, No.15, October 1987, pp. 1135-1137.
- [65] G. I. Stegeman, E. M. Wright, N. Finlayson, G. Assanto, W. C. Banyai, S. Trillo, S. Wabnitz, and R. H. Stolen, "All-optical polarisation switching in fibres", SPIE vol. 1085, Optical fibres and Their applications V, 1989, pp. 137-157.
- [66] R. H. Stolen, A. Ashkin, W. Pleibel, and J. M. Dziedzic, "In-line fibre-polarisation-rocking rotator and filter", optics Lett., vol. 9, no. 7, 1984, pp. 300-302.
- [67] S. Trillo, S. Wabnitz, W. C. Banyai, N. Finlayson, C. T. Seaton, G. I. Stegeman, and R. H. Stolen, "Observation of ultrafast nonlinear polarisation switching induced by polarisation instability in a birefringent fiber rocking filter", IEEE J. Quant. Electron., vol. 25, no. 1, 1989, pp. 104-112

CHAPTER 5

NEW FORMALISM AND IDENTITIES FOR THE NONLINEAR COUPLED MODE EQUATIONS

5.1 INTRODUCTION

We start off the work in this thesis, by studying in detail the nonlinear directional coupler (NLDC). In this chapter the nonlinear coefficients appearing in the nonlinear coupled mode equations are reformulated, and some new identities derived. The purpose of the reformulation is in order to structure the full coupled mode equations for the NLDC which in the literature often look very complicated (much more complicated than linear coupled mode equations). This is expected because in nonlinear media the polarisation response of the medium becomes a nonlinear function of the electric field, and the expansion of the nonlinear polarisation (which is proportional to the triple product of the sum of eigenmodes) leads to an enormous number of additional nonlinear terms (see chapter 6). The number of terms is large even for the two guide [1-2] and three guide [3] cases. Since the nonlinear coefficients are not defined in a systematic way in the literature, it is very difficult to keep track of all the terms, and quite cumbersome to manipulate the equations even for the simple two guide case. The best option is to reformulate the equations into a matrix formalism just as can be done for the linear coupled mode equations [4-5], so that one can immediately assign the origins of each term to a particular matrix. In this chapter, the nonlinear coefficients are first reformulated more systematically so that the nonlinear interactions are then represented in a form which can be compared more directly to the linear coupling and modification coefficients. Using only three definitions, all the nonlinear interactions in the multiwaveguide nonlinear coupler are then represented. These coefficients are used in the derivation of the multiwaveguide nonlinear equations in chapter 6.

Later in the chapter two new identities are derived for the nonlinear directional coupler, which together with a well-known identity for the linear coupler [7], form a complete set of identities. The three identities are exact so long as power dependent mode shapes are used in their derivations. In the low power/nonlinearity regime each identity is derivable from the other two. These identities can be used to show clearly the physical relationships between different nonlinear mechanisms, and enable quick proofs of various parameters. For example they can be used to calculate the nonlinear

propagation coefficient, to check orders of magnitude between nonlinear coefficients, and to check numerical accuracies of coefficients in computer programs. We also show in chapter 6 that the identities can be used to relate the coupled mode equations of Fraile-Pelaez and Assanto [2] and Meng and Okamoto [1], which were each derived using different unperturbed systems.

5.2 DEFINITION OF THE NONLINEAR COEFFICIENTS

As explained above, the nonlinear coefficients found in the literature are defined in a non-systematic way which does not allow them to be easily related to each other. For example, Jensen [8] used Q_1, Q_2, Q_3, Q_4 formalism. Mapalagama and Deck [3] used $k_n, k_{n,n\pm 1}, Q_n, Q_{n,n\pm 1}, R_{n,n\pm 1}, T_{n\pm 1,n}, S_{n,n\pm 1,n-1}$ which is even more complicated, and Meng and Okamoto [1] chose Q_1, Q_2, k_s, k_c, k_r , which although an improvement, is still not systematic enough.

Before explaining our approach we first discuss the definition for the nonlinearity. The nonlinearity is usually defined in terms of the nonlinear (intensity dependent) refractive index n_2 with units of m^2/W , so that $n = n_0 + n_2 I$ (where n is the total refractive index, n_0 the linear refractive index, and I the intensity). It is often convenient, as is here, to use another version for the nonlinearity in terms of the nonlinear permittivity $\alpha(x, y)$ (units of m^2/V^2) defined as

$$\varepsilon(x, y, z) = \varepsilon_{lin}(x, y) + \alpha(x, y) |\underline{E}(x, y, z)|^2 \quad (5.1)$$

where (x, y) are the transverse coordinates, and z is the direction of propagation. $\varepsilon_{lin}(x, y)$ describes the linear permittivity for the whole system, $\underline{E}(x, y, z)$ specifies the total field for the system, and $\alpha(x, y)$ the nonlinearity. The nonlinearity can have any magnitude, sign, or distribution in the cross-section of the system.

It can be shown (see Appendix 1) that the nonlinear refractive index n_2 , the nonlinear permittivity α , and the third order susceptibility $\chi^{(3)}$ can be related as follows

$$\alpha = \varepsilon_0 n_0^2 c n_2 = \frac{3}{4} \chi^{(3)} \quad (5.2)$$

where ε_0 is the permittivity of free space, n_0 the linear refractive index, and c the speed of light.

In order to redefine the coefficients, we first note that the definition for all the nonlinear coefficients found in papers in the literature (eg eqns 3b-3d in [2], and eqns 10-15 in [1]) involve the interaction of four fields. Using a similar idea to an

explanation given in four wave mixing papers [6] where two frequencies beat to produce an index grating, which causes diffraction of a third field, it can be argued that two of the fields contribute to the nonlinear refractive index change, which causes coupling between the other two.

The nonlinear coefficients can therefore be written down in the form of $Q_{pq}^{(a)}$ and the K_{pq}^{NL} formalism as follows

$$Q_{pq}^{(a)} = \frac{\omega \epsilon_0}{4P} \iint_{-\infty}^{+\infty} \left[\alpha E_t^{(a)^2} \right] \underline{E}_t^{(p)} \cdot \underline{E}_t^{(q)} dx dy \quad (5.3)$$

$$K_{pq}^{NL} = \frac{\omega \epsilon_0}{4P} \iint_{-\infty}^{+\infty} \left[(\alpha - \alpha^{(q)}) E_t^{(q)^2} \right] \underline{E}_t^{(q)} \cdot \underline{E}_t^{(p)} dx dy \quad (5.4)$$

where α is the nonlinearity for the whole system and $\alpha^{(q)}$ the nonlinearity of waveguide 'q'. The terms in the square brackets are the nonlinear perturbations. $Q_{pq}^{(a)}$ formalism is such that the superscript of $Q_{pq}^{(a)}$ refers to the field which induces the nonlinear permittivity across the whole system ($E_t^{(a)^2}$ in this case), and the 'p' and 'q' subscripts refer to the fields which are coupled by this perturbation. The formalism for the K_{pq}^{NL} is similar to $Q_{pq}^{(a)}$ except the nonlinear perturbation is assumed to occur everywhere except in guide 'q'. Since the eigenmode 'q' induces the nonlinear perturbation, and the perturbation is outside guide 'q', K_{pq}^{NL} is a smaller term than $Q_{pq}^{(a)}$. The reason why the two formalisms above simplify the analysis is that for both cases, the subscripts of $Q_{pq}^{(a)}$ and K_{pq}^{NL} are similar to the subscripts of the linear coupling and modification coefficients. For example $Q_{ab}^{(a)}$, and K_{ab}^{NL} both belong to the same family as the coupling coefficient K_{ab} , and $Q_{aa}^{(a)}$, $Q_{aa}^{(b)}$, K_{aa}^{NL} all have a similar effect to the modification coefficient K_{aa} .

We should note the symmetry of the subscripts in $Q_{pq}^{(a)}$. The 'p' and 'q' subscripts can be interchanged without affecting the integral, but we also note that this symmetry does not apply to the relationship between the superscript and one of the subscripts.

$$\text{ie } Q_{pq}^{(a)} = Q_{qp}^{(a)} \neq Q_{pq}^{(b)} = Q_{qp}^{(b)}$$

The magnitude of the different nonlinear coefficients depend on the induced nonlinear perturbation as well as the magnitude of the fields interacting with the perturbation.

The individual nonlinear coefficients are now discussed, assuming for now that the waveguides are identical and the nonlinearities are situated within the film regions.

(i) $Q_{aa}^{(a)}$ is the largest nonlinear coefficient. From eqn. 5.3 $Q_{aa}^{(a)}$ is defined as

$$Q_{aa}^{(a)} = \frac{\omega \mathcal{E}_0}{4P} \iint_{-\infty}^{+\infty} \left(\alpha E_t^{(a)^2} \right) \underline{E}_t^{(a)} \cdot \underline{E}_t^{(a)} dx dy \quad (5.5)$$

Since its effect is to increase the propagation constant, it has a similar role as the linear modification coefficient. The term is large because both the nonlinear perturbation $\alpha E_t^{(a)^2}$ and the fields which interact with this perturbation $E_t^{(a)^2}$ belong to the guide 'a'. Meng and Okamoto called $Q_{aa}^{(a)}$ the 'self-phase-modulation' term, but more accurately the self-phase-modulation term is given by $Q_{aa}^{(a)} - K_{aa}^{NL}$.

(ii) $Q_{ab}^{(a)}$ ($a \neq b$) is the next most important term (ignored completely by Jensen). From eqn. 5.3 $Q_{ab}^{(a)}$ is defined as

$$Q_{ab}^{(a)} = \frac{\omega \mathcal{E}_0}{4P} \iint_{-\infty}^{+\infty} \left(\alpha E_t^{(a)^2} \right) \underline{E}_t^{(a)} \cdot \underline{E}_t^{(b)} dx dy \quad (5.6)$$

Frailé Pelaez and Assanto [2] stated that this term is of the same order as $Q_{bb}^{(a)}$ term, but evidently it is larger in magnitude than $Q_{bb}^{(a)}$ (for weak coupling), because one of the fields is the eigenmode of guide 'a' which interacts with the large nonlinear perturbation in the vicinity of guide 'a'. Since $Q_{ab}^{(a)}$ describes the nonlinear coupling between the fields $\underline{E}_t^{(a)}$ and $\underline{E}_t^{(b)}$ due to the nonlinear perturbation inside guide 'a', it is related to the coupling coefficient. For convenience this term is called the 'larger cross-phase-modulation' term in this thesis.

(iii) $Q_{bb}^{(a)}$ ($a \neq b$) is related to the modification coefficient K_{aa} , but is widely known as 'the cross-phase-modulation' term [1, 8]. From eqn. 5.3 $Q_{bb}^{(a)}$ is defined as

$$Q_{bb}^{(a)} = \frac{\omega \mathcal{E}_0}{4P} \iint_{-\infty}^{+\infty} \left(\alpha E_t^{(a)^2} \right) \underline{E}_t^{(b)} \cdot \underline{E}_t^{(b)} dx dy \quad (5.7)$$

Jensen (among others) gave it far too much emphasis. It is actually a small term (in weak coupling), because it involves the interaction of the small tail of eigenmode 'b' overlapping the nonlinear perturbation situated in a different guide 'a'.

(iv) $Q_{bc}^{(a)}$ ($a \neq b \neq c$) terms are extremely small, and defined as

$$Q_{bc}^{(a)} = \frac{\omega \mathcal{E}_0}{4P} \iint_{-\infty}^{+\infty} \left(\alpha E_t^{(a)^2} \right) \underline{E}_t^{(b)} \cdot \underline{E}_t^{(c)} dx dy \quad (5.8)$$

They are small because the small tails of different eigenmodes $\underline{E}_t^{(b)}$ and $\underline{E}_t^{(c)}$ are interacting with the nonlinear perturbation (which occurs in the vicinity of a different guide 'a'). For convenience this term is henceforth called the four wave mixing (FWM) term.

(v) K_{ba}^{NL} is a coupling coefficient, and has a similar role to K_{ba} and $Q_{ba}^{(b)}$. From eqn. 5.4 K_{ba}^{NL} is defined as

$$K_{ba}^{NL} = \frac{\omega \mathcal{E}_0}{4P} \iint_{-\infty}^{+\infty} \left(\alpha - \alpha^{(a)} \right) E_t^{(a)^2} \underline{E}_t^{(a)} \cdot \underline{E}_t^{(b)} dx dy \quad (5.9)$$

and causes nonlinear coupling between guide 'a' and guide 'b', due to the nonlinear perturbation situated in guide 'b' induced by the tail of $\underline{E}_t^{(a)}$. This term is a much smaller term than K_{ba} , because the perturbation is induced nonlinearly rather than linearly. The nonlinear perturbation is also very small (compared to linear perturbations) since it is induced by the small 'tail' of eigenmode 'a' rather than its main part. This term is henceforth called the 'nonlinear coupling coefficient'.

(vi) K_{aa}^{NL} is another coefficient which is the nonlinear analogue of the 'modification coefficient'. From eqn. 5.4 K_{aa}^{NL} is defined as,

$$K_{aa}^{NL} = \frac{\omega \mathcal{E}_0}{4P} \iint_{-\infty}^{+\infty} \left(\alpha - \alpha^{(a)} \right) E_t^{(a)^2} \underline{E}_t^{(a)} \cdot \underline{E}_t^{(a)} dx dy \quad (5.10)$$

This term can be called the 'nonlinear modification coefficient'. K_{aa}^{NL} involves the interaction of the small tails of $\underline{E}_t^{(a)}$ and $\underline{E}_t^{(a)}$ fields with the nonlinear perturbation caused by the small tail of $E_t^{(a)^2}$. Therefore it is even smaller than the K_{ba}^{NL} term (at least the latter contains the main body of the $\underline{E}_t^{(b)}$ field in the region of the perturbation).

Finally it should be noted that although $Q_{pq}^{(a)} = Q_{qp}^{(a)} \neq Q_{pq}^{(b)} = Q_{qp}^{(b)}$, the subscripts for the nonlinear coupling coefficients cannot be interchanged, ie $K_{pq}^{NL} \neq K_{qp}^{NL}$.

5.3 POWER DEPENDENT COEFFICIENTS

So far, it has been assumed that the shapes of the eigenmodes are independent of power. However, this assumption is only accurate for low powers or low nonlinearities. For higher powers, the field shapes are power dependent, and the integrals of these fields (ie all the linear and nonlinear coefficients) are also power dependent [1]. If coupled mode theory is to be accurate it is necessary to include this power dependency [1,9]. As shown by Meng and Okamoto [1], this power dependency is the most important parameter in the accuracy of the coupled mode equations.

The effect of the power dependence on the field is different depending on the location of the nonlinearity. If the nonlinearity is positive and located in the film region (as in Fig. 5.1), the field narrows and focuses within the film, leading to less overlap with the other guide and reduced magnitude of coupling coefficient. If the nonlinearity is in the middle coupling region however, the effect is for the field to be skewed towards that region (as in Fig. 5.2), leading to an increase in the overlap and the coupling coefficients.

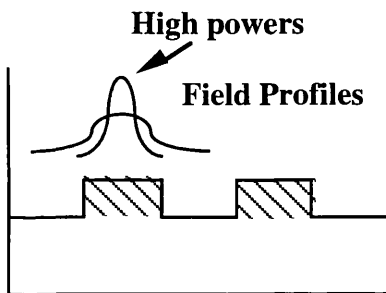


Fig. 5.1

Nonlinear film region

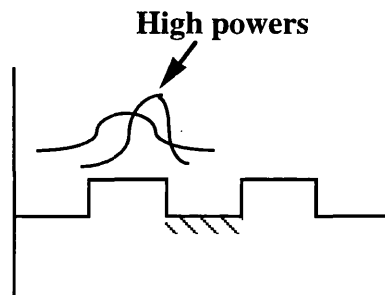


Fig. 5.2

Nonlinear coupling region

Fig. 5.1, 5.2 Power dependent mode shapes

5.4 DERIVATION OF NEW IDENTITIES

In linear strong coupled mode theory, it is well-known that a simple identity exists which shows the relationship between the asymmetrical coupling coefficients (see chapter 3). This derivation has been carried out using power conservation for the lossless case, and Lorentz' reciprocity theorem for the general case. As shown in this chapter, similar identities are derivable for the nonlinear case.

5.4.1 Lorentz reciprocity theorem

Lorentz' reciprocity theorem is frequently used in derivations involving linear reciprocal

media [4,7]. The theorem (in its right form) is also applicable for non-reciprocal media such as the grating coupler (see Griffel and Hardy [10]) and the nonlinear directional coupler (Meng and Okamoto [1]). The theorem is defined as follows: if $\underline{E}^{(1)}$, $\underline{H}^{(1)}$ and $\underline{E}^{(2)}$, $\underline{H}^{(2)}$ are two sets of fields which satisfy Maxwell's equations and all the boundary conditions for their respective systems (ie are the modes of their respective systems), then they satisfy the following Lorentz equation exactly (full derivation of Lorentz equation is in Appendix 4)

Lorentz' Reciprocity Theorem

$$\frac{\partial}{\partial z} \iint_{-\infty}^{+\infty} (\underline{E}_t^{(1)} \times \underline{H}_t^{(2)} - \underline{E}_t^{(2)} \times \underline{H}_t^{(1)}) \cdot \hat{z} \, dx dy = j\omega\epsilon_0 \iint_{-\infty}^{+\infty} (\epsilon^{(2)} - \epsilon^{(1)}) \underline{E}^{(1)} \cdot \underline{E}^{(2)} \, dx dy \quad (5.11)$$

The theorem, in the form above, is applicable for nonreciprocal media because the $\partial/\partial z$ derivative in the LHS of the equation implies that in the derivation of this equation, the volume of integration is taken as an infinitesimally thin thickness Δz of an infinitely large radius cylinder surrounding the waveguide (see Appendix 4). Since the section is so thin, the permittivity is approximately z-invariant within that section, and the system behaves similarly to a reciprocal medium within that section.

Meng and Okamoto [1] were the first to use the reciprocity theorem for the two-guide nonlinear directional coupler. However their conjugated form of the reciprocity formula only applied to the lossless case. The version in eqn. 5.11 is the non-conjugated form and therefore applies for the general lossy case also. Another difference between the reciprocity formula in [1] and eqn. 5.11 is that the RHS of the formula in [1] is in terms of the polarisation response, whereas ours (and Chuang's [7]) is in terms of permittivities. The two versions are identical in other respects.

5.4.2 Derivation of new identities

As mentioned in the previous section, the reciprocity theorem is satisfied exactly as long as the fields $\underline{E}^{(1)}$, $\underline{H}^{(1)}$ and $\underline{E}^{(2)}$, $\underline{H}^{(2)}$ are the modes of the respective systems (ie satisfy the boundary conditions and Maxwell's equations exactly for their respective systems). If the guides in systems <1> and <2> are nonlinear, then in order for the fields to satisfy Maxwell's equations and the boundary conditions exactly, their shapes must be dependent on power.

In the next few sections we will derive three identities for the nonlinear directional

coupler. These identities will be exact as long as power dependent mode shapes are used in their derivations. Throughout, real TE fields are assumed, and $e^{j(\beta z - \omega t)}$ convention used for forward travelling fields.

5.4.2.1 'Nonlinear-nonlinear' identity

The first identity to be derived shows the relationship between the fields of two nonlinear waveguides. One nonlinear waveguide is perturbed in such a way that the waveguide disappears and another is formed at a different location. The approach is similar to the linear coupled mode theory derivation, but in this case, the 'perturbed system' is exact, since single waveguides are used where it is possible to find the exact power dependent field. Coupled mode theory however is not exact, since the perturbed system consists of two guides, and the total field is *approximated* by the scaled sum of the eigenmodes (ie is not exact).

To calculate the identity two nonlinear systems are considered (which are illustrated in Fig. 5.3). The nonlinear guide 'p' is taken as the unperturbed system. The perturbation causes it to disappear and a nonlinear guide 'q' forms at a different location. The perturbed system is therefore the nonlinear guide 'q'.

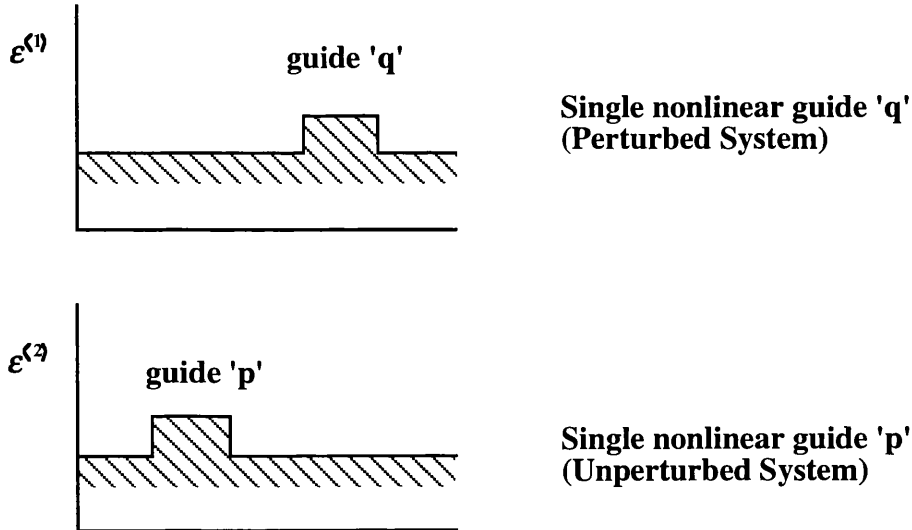


Fig. 5.3 Perturbing a nonlinear guide to form another nonlinear guide

The first set of solutions refers to a forward travelling wave in guide 'q'

$$\epsilon^{(1)} = \epsilon^{(q)}(x, y) + \alpha^{(q)} |E^{(1)}|^2 \tag{5.12}$$

$$\underline{E}^{(1)} = \underline{E}_i^{(q)} e^{j\beta_q z} \quad \underline{H}^{(1)} = (\underline{H}_i^{(q)} + \underline{H}_z^{(q)}) e^{j\beta_q z} \quad (5.13)$$

where $\varepsilon^{(q)}$ describes the linear permittivity of guide 'q' embedded in its linear surrounding medium, $\alpha^{(q)}$ is the nonlinearity inside guide 'q' only. It should also be noted that $\underline{E}_i^{(q)}$, $\underline{H}_i^{(q)}$, and $\underline{H}_z^{(q)}$ are all power dependent.

The second set of solutions is for a wave travelling in the backward direction in guide 'p'. Z-reversal symmetry (eqns 5.14-5.15 below) is used to transform the -z travelling transverse and longitudinal fields into +z travelling fields. Therefore the following transformations are made (see Appendix 3 for full details)

$$\beta_p^- \rightarrow -\beta_p \quad (5.14)$$

$$E_i^{(p)-} \rightarrow E_i^{(p)} \quad H_i^{(p)-} \rightarrow -H_i^{(p)} \quad H_z^{(p)-} \rightarrow -H_z^{(p)} \quad (5.15)$$

Using eqns 5.14 and 5.15, the second set of solutions then becomes

$$\varepsilon^{(2)} = \varepsilon^{(p)}(x, y) + \alpha^{(p)} |\underline{E}^{(2)}|^2 \quad (5.16)$$

$$\underline{E}^{(2)} = \underline{E}_i^{(p)} e^{-j\beta_p z} \quad \underline{H}^{(2)} = (-\underline{H}_i^{(p)} + \underline{H}_z^{(p)}) e^{-j\beta_p z} \quad (5.17)$$

where $\underline{E}_i^{(p)}$, $\underline{H}_i^{(p)}$, and $\underline{H}_z^{(p)}$ are power dependent, and $\alpha^{(p)}$ is the nonlinearity inside guide 'p'. It must be noted that β_p and β_q are the nonlinear propagation constants for the isolated guides. Substituting the two sets of solutions (ie eqns. 5.12-5.13 and 5.16-5.17) into Lorentz' equation (eqn 5.11), making use of the definition for C_{pq} (eqn 3.3) results in

$$(\beta_p - \beta_q) C_{pq} = \frac{\omega \varepsilon_0}{4P} \iint_{-\infty}^{+\infty} \left[(\varepsilon^{(p)} - \varepsilon^{(q)}) + (\alpha^{(p)} |\underline{E}_i^{(p)}|^2 - \alpha^{(q)} |\underline{E}_i^{(q)}|^2) \right] \underline{E}_i^{(q)} \cdot \underline{E}_i^{(p)} dx dy \quad (5.18)$$

Recalling the definitions for K_{pq} , $Q_{pq}^{(q)}$, and K_{pq}^{NL} (eqns. 3.4, 5.3, and 5.4 respectively) and noting that all these coefficients together with C_{pq} are power dependent since they all include power dependent eigenmodes, eqn 5.18 reduces to

$$(\beta_p - \beta_q) C_{pq} = (K_{pq} - K_{qp}) + (K_{pq}^{NL} - K_{qp}^{NL}) + (Q_{pq}^{(p)} - Q_{qp}^{(q)}) \quad (5.19)$$

which can be re-arranged to give the ‘nonlinear-nonlinear’ identity

Nonlinear-nonlinear identity

$$\beta_p C_{pq} + K_{qp} + K_{qp}^{NL} - Q_{pq}^{(p)} = C_{pq} \beta_q + K_{pq} + K_{pq}^{NL} - Q_{pq}^{(q)} \quad (5.20)$$

which is an identity relating the field of nonlinear guide ‘p’ to a nonlinear guide ‘q’. It should be noted that this identity is exact as long as power dependent fields are used .

5.4.2.2 The ‘linear-nonlinear’ identity

In a similar approach to section 5.8.2 a linear guide ‘p’ can be perturbed to form a nonlinear guide ‘q’. This time only one set of fields is power dependent: that belonging to guide ‘q’.

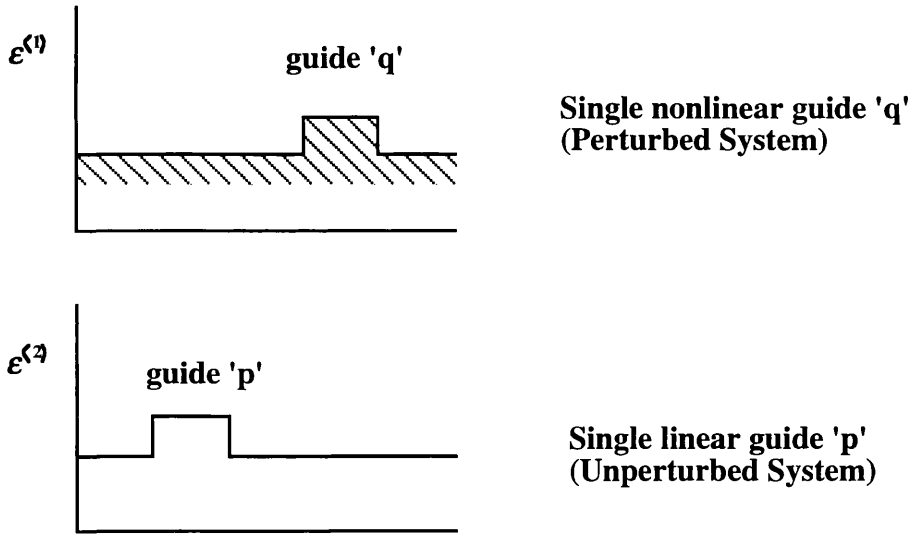


Fig. 5.4 Illustrating the unperturbed and the perturbed systems

The perturbed system, system <1> is defined as follows

$$\epsilon^{(1)} = \epsilon^{(q)}(x, y) + \alpha^{(q)} |\underline{E}^{(1)}|^2 \quad (5.21)$$

$$\underline{E}^{(1)} = \underline{E}_t^{(q)} e^{j\beta_q z} \quad \underline{H}^{(1)} = (\underline{H}_t^{(q)} + \underline{H}_z^{(q)}) e^{j\beta_q z} \quad (5.22)$$

where $\underline{E}_t^{(q)}$, $\underline{H}_t^{(q)}$, and $\underline{H}_z^{(q)}$ are power dependent, and β_q is the nonlinear propagation

coefficient for guide 'q'.

The unperturbed system, system <2> is as follows:

$$\varepsilon^{(2)} = \varepsilon^{(p)}(x, y) \quad (5.23)$$

$$\underline{E}^{(2)} = \overline{\underline{E}_t^{(p)}} e^{-j\overline{\beta}_p z} \quad \underline{H}^{(2)} = \left(-\overline{\underline{H}_t^{(p)}} + \overline{\underline{H}_z^{(p)}} \right) e^{-j\overline{\beta}_p z} \quad (5.24)$$

The overhead bars refer to linearity. Thus $\overline{\beta}_p$ is the linear propagation coefficient for eigenmode 'p', and β_q is the nonlinear propagation coefficient for eigenmode 'q'. Substituting these two sets of solutions into Lorentz' equation gives

$$(\beta_q - \overline{\beta}_p) C_{pq}^- = \frac{\omega \varepsilon_0}{4P} \iint_{-\infty}^{+\infty} \left[-(\varepsilon^{(p)} - \varepsilon^{(q)}) + (\alpha^{(q)} |\underline{E}_t^{(q)}|^2) \right] \overline{\underline{E}_t^{(q)}} \cdot \overline{\underline{E}_t^{(p)}} dx dy \quad (5.25)$$

The linear and nonlinear coefficients this time include one set of power dependent eigenmodes 'q', and one set of power independent eigenmodes 'p'. The coefficients are defined as

$$C_{pq}^- = \frac{1}{4P} \iint_{-\infty}^{+\infty} \left(\overline{\underline{E}_t^{(p)}} \times \underline{H}_t^{(q)} + \underline{E}_t^{(q)} \times \overline{\underline{H}_t^{(p)}} \right) \cdot \hat{z} dx dy \quad (5.26)$$

$$K_{pq}^- = \frac{\omega \varepsilon_0}{4P} \iint_{-\infty}^{+\infty} (\varepsilon - \varepsilon^{(q)}) \overline{\underline{E}_t^{(p)}} \cdot \underline{E}_t^{(q)} dx dy \quad (5.27)$$

$$K_{pq}^{NL} = \frac{\omega \varepsilon_0}{4P} \iint_{-\infty}^{+\infty} (\alpha - \alpha^{(q)}) \overline{\underline{E}_t^{(p)}} \cdot \underline{E}_t^{(q)} dx dy \quad (5.28)$$

$$Q_{pq}^{(q)} = \frac{\omega \varepsilon_0}{4P} \iint_{-\infty}^{+\infty} (\alpha \overline{\underline{E}_t^{(p)}}) \cdot \underline{E}_t^{(q)} dx dy \quad (5.29)$$

where C_{pq}^- , K_{pq}^- , K_{pq}^{NL} . and $Q_{pq}^{(q)}$ are all power dependent as they all involve the 'q'th eigenmode which is power dependent.

Now incorporating eqns 5.26-5.29 into eqn 5.25, eqn 5.25 reduces to the 'linear-nonlinear' identity.

Linear-nonlinear identity

$$C_{pq}^- \beta_q + K_{pq}^- + K_{pq}^{NL} - Q_{pq}^{(q)} = \overline{\beta}_p C_{pq}^- + K_{qp}^- \quad (5.30)$$

This identity is used in section 5.4.2.4 to derive the nonlinear propagation coefficient and to prove that the overlap integral and the nonlinear cross-coefficients are related.

5.4.2.3 'Linear-linear' identity

Finally the derivation of a well-known identity for the linear coupler [7] is derived. Reciprocity is used here for the derivation, but power conservation could also have been used (but then it would then have only applied for the lossless case). Therefore this time two linear systems are considered (see Fig. 5.5). System <2> is taken as the initial 'unperturbed state', and consists of the permittivity of waveguide 'p' together with its surrounding medium $\epsilon^{(2)}$. By perturbing this system ($\epsilon^{(1)} - \epsilon^{(2)}$), system <2> can be transformed to system <1> with permittivity profile $\epsilon^{(1)}$. Both systems <1> and <2> are linear. Therefore the fields for both systems are the linear eigenmodes, and independent of power.

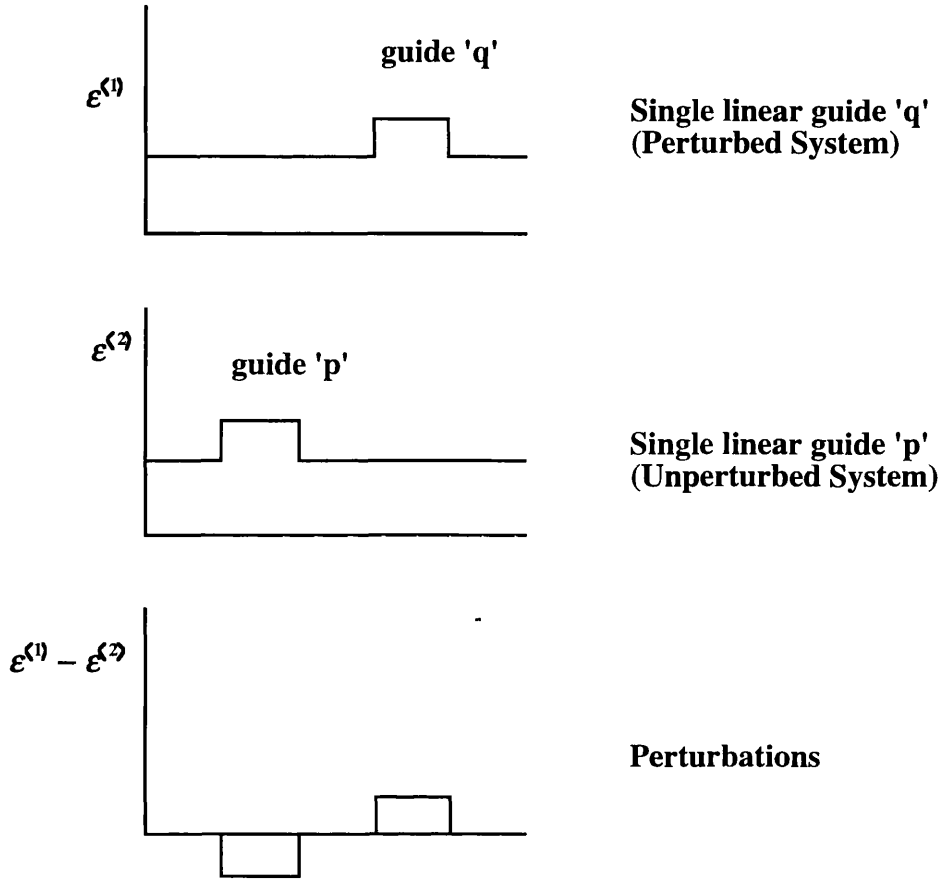


Fig. 5.5 Perturbing one linear waveguide to form another

The permittivity and the fields for system <1> are defined as follows

$$\epsilon^{(1)} = \epsilon^{(q)}(x, y) \tag{5.31}$$

$$\underline{E}^{(1)} = \underline{E}_t^{(q)} e^{j\bar{\beta}_q z} \quad \underline{H}^{(1)} = \left(\overline{H}_t^{(q)} + \overline{H}_z^{(q)} \right) e^{j\bar{\beta}_q z} \tag{5.32}$$

The permittivity and fields for the second system are defined as follows:

$$\epsilon^{(2)} = \epsilon^{(p)}(x, y) \tag{5.33}$$

$$\underline{E}^{(2)} = \underline{E}_t^{(p)} e^{-j\bar{\beta}_p z} \quad \underline{H}^{(2)} = \left(-\overline{H}_t^{(p)} + \overline{H}_z^{(p)} \right) e^{-j\bar{\beta}_p z} \tag{5.34}$$

where $\bar{\beta}_p$ and $\bar{\beta}_q$ are the *linear* propagation constants for eigenmodes 'p' and 'q'. All

the fields are assumed to be power independent (linear). Substituting these two sets of solutions into Lorentz' equation results in the following identity

$$(\overline{\beta}_p - \overline{\beta}_q) C_{pq}^- = (K_{pq}^- - K_{qp}^-) \quad (5.35)$$

where C_{pq}^- and K_{pq}^- are also power independent (linear). This equation is well-known and a physical explanation is given in detail in chapter 3. It effectively shows that the linear coupling coefficients are not equal for asymmetrical guides. Equality is achieved only if the two guides are identical $\overline{\beta}_p = \overline{\beta}_q$ or are very weakly coupled (ie $C_{pq}^- \rightarrow 0$). C_{pq}^- and K_{pq}^- are defined as follows

$$C_{pq}^- = \frac{1}{4P} \iint_{-\infty}^{+\infty} \left(\overline{E}_t^{(p)} \times \overline{H}_t^{(q)} + \overline{E}_t^{(q)} \times \overline{H}_t^{(p)} \right) \cdot \hat{z} \, dx dy \quad (5.36)$$

$$K_{pq}^- = \frac{\omega \epsilon_0}{4P} \iint_{-\infty}^{+\infty} \left(\epsilon - \epsilon^{(q)} \right) \overline{E}_t^{(p)} \cdot \overline{E}_t^{(q)} \, dx dy \quad (5.37)$$

5.4.2.4 Applications of the identities

The linear-nonlinear identity (eqn. 5.30) can be used to calculate the power dependent nonlinear propagation coefficient. Substituting 'q' for 'p' in the linear-nonlinear identity leads to

$$\beta_q = \overline{\beta}_q + \frac{Q_{qq}^{(q)} - K_{qq}^{NL}}{C_{qq}^-} \quad (5.38)$$

which is a formula for the nonlinear propagation constant taking into account the dependence of the field shapes on intensity. If the low power limit is assumed so that the mode shapes are approximately linear, eqn. 5.38 approximates as

$$\beta_q = \overline{\beta}_q + Q_{qq}^{(q)} - K_{qq}^{NL} \quad (5.39)$$

where $Q_{qq}^{(q)} - K_{qq}^{NL}$ is the 'self-phase modulation term'. We note that the overhead bars are removed from the fields because there is very little difference between the mode

shapes of the linear and nonlinear fields. Inserting the definitions given in eqns 5.5 and eqn 5.10 into $Q_{qq}^{(q)} - K_{qq}^{NL}$ results in

$$Q_{qq}^{(q)} - K_{qq}^{NL} = \frac{\omega \epsilon_0}{4P} \iint_{-\infty}^{+\infty} \left[\alpha^{(q)} E_r^{(q)4} \right] dx dy \quad (5.40)$$

and eqn. 5.39 becomes $\beta_q = \bar{\beta}_q + \Delta\beta^{NL}(P)P$ (5.41)

Using eqns. 5.39-5.41, $\Delta\beta^{NL}(P)$ can be written down as

$$\Delta\beta^{NL}(P) = \frac{Q_{qq}^{(q)} - K_{qq}^{NL}}{P} = \frac{\omega \epsilon_0}{4P^2} \iint_{-\infty}^{+\infty} \left[\alpha^{(q)} E_r^{(q)4} \right] dx dy \quad (5.42)$$

which compares well with that derived using a different technique by Stegeman et al (eqn. 3 in [11]). Continuing with the low power limit assumption, and rearranging the linear-nonlinear identity (eqn. 5.30) in terms of β_q , results in an alternative formula for the propagation coefficient as follows

$$\beta_q = \bar{\beta}_p + \frac{(K_{qp} - K_{pq})}{C_{pq}} - \frac{K_{pq}^{NL}}{C_{pq}} + \frac{Q_{pq}^{(q)}}{C_{pq}} \quad (5.43)$$

The linear-linear identity from eqn. 5.35 is given by

$$\bar{\beta}_q - \bar{\beta}_p = \frac{(K_{qp} - K_{pq})}{C_{pq}} \quad (5.44)$$

which when inserted into eqn. 5.43 leads to

$$\beta_q = \bar{\beta}_q - \frac{K_{pq}^{NL}}{C_{pq}} + \frac{Q_{pq}^{(q)}}{C_{pq}} \quad (5.45)$$

which compares with the formula for β_q obtained in eqn 5.39. Equating these two equations results in

$$Q_{pq}^{(q)} - K_{pq}^{NL} = C_{pq} (Q_{qq}^{(q)} - K_{qq}^{NL}) \quad (5.46)$$

The resemblance between this equation and the linear-linear identity (eqn. 5.35) is enlightening. The left-hand side of the equation is the difference between nonlinear coupling coefficients, and the right-hand-side is the difference between coefficients which are related to the propagation coefficient. From this equation one can observe clearly that if the nonlinear coupling coefficients $Q_{pq}^{(q)}$ and K_{pq}^{NL} are ignored from the left hand side of the equation, the overlap integral C_{pq} must be zero, otherwise an inconsistency occurs.

5.4.2.5 Relationship between the three identities

In the low power regime, it can be shown that the three identities derived in the previous section are inter-related. For example, transposing the linear-nonlinear identity (eqn. 5.30), subtracting the result from the linear-nonlinear identity (eqn. 5.30), and substituting the linear-linear identity (eqn. 5.35) into the result, leads to the nonlinear-nonlinear identity (eqn. 5.20). Hence only two of the identities are needed to derive the third.

5.5 CONCLUSIONS

The main nonlinear coefficients were explained, and two new identities derived. In the low power regime it was shown that the three identities were inter-derivable. These identities were used to calculate the nonlinear propagation coefficient, and to prove that the overlap integral and the nonlinear cross-coefficients are related. In chapter 6 it will also be shown that the identities can relate the coupled mode equations of Meng and Okamoto [1] and Fraile-Pelaez and Assanto [2].

REFERENCES

- [1] X. Meng and N. Okamoto, "Improved coupled-mode theory for Nonlinear Directional Couplers", IEEE J. Quant. Electron., Vol 27, No.5, May 1991, pp. 1175-1181
- [2] F. J. Fraile-Pelaez and G. Assanto, "Coupled-mode equations for nonlinear directional couplers", Applied Optics, vol. 29, no. 15, 1990, pp. 2216-2217.
- [3] C. Mapalagama and R. T. Deck, "Modified theory of three-channel Kerr-type nonlinear directional coupler", J. Opt. Soc. Am. B, Vol. 9, No. 12, pp. 2258-2264, Dec 1992.
- [4] S-L Chuang, "A coupled-mode theory for multiwaveguide systems satisfying the reciprocity and power conservations", J. Light. Technol. vol. LT-5, 1987, pp. 174-183.
- [5] W. Streifer, M. Osinski, and A. Hardy, "Reformulation of the coupled-mode theory of multiwaveguide systems", J. Light. Technol., vol. LT-5, no. 1, 1987, pp. 1-4.
- [6] G. P. Agrawal, "Population pulsations and nondegenerate four wave mixing in semiconductor lasers and amplifiers", vol. 5, no. 1, J. Opt. Soc. Am. B, pp. 147-159, 1988.
- [7] S. L. Chuang, "A coupled mode formulation by reciprocity and a variational principle", J. Lightwave Technol, Vol. LT-5, No.1, pp. 5-15, 1987
- [8] S. M. Jensen, "The nonlinear coherent coupler", IEEE Transactions on Microwave Theory and Techniques, MTT-30, no. 10, 1982, pp. 1568-1571.
- [9] A. Ankiewicz and G-D Peng, J. Opt. Soc. Am. B, vol. 9, 1992, pp. 1341
- [10] G. Griffel, M. Itzkovich, and Amos A. Hardy, "Coupled Mode formulation for Directional Couplers with longitudinal perturbation", J. Quantum Electronics, Vol. 27, No.4, April 1991, pp.985-994.
- [11] G. I. Stegeman, E. M. Wright, N. Finlayson, R. Zanoni, and C. T. Seaton, "Third order nonlinear integrated optics", J. Lightwave Technol., vol. 6, no. 6, 1988, pp. 953-968

CHAPTER 6

STRONG COUPLED MODE THEORY FOR THE MULTIWAVEGUIDE NONLINEAR DIRECTIONAL COUPLER

This chapter discusses for the first time to our knowledge strong coupling in multiwaveguide nonlinear directional couplers. The complete coupled mode equations with all the terms kept in the equations are derived (see sections 6.2 and 6.3). The two guide case is compared with some papers in the literature (section 6.4). The all guide interaction case is studied in section 6.7.

6.1 INTRODUCTION

The case of strong coupling in nonlinear couplers has not been studied satisfactorily in the literature even for the simple two guide case. Many papers cut out terms from the nonlinear coupled mode equations for mathematical convenience. However the most correct and accurate form of the equations is with all the terms included. Terms are often ignored from the equations without careful consideration of the implications, and this sometimes leads to inconsistencies. For example, Jensen [1] kept some terms in his equations but ignored others of greater magnitude (as pointed out by Fraile-Pelaez and Assanto (FP-A) [2]). Also the overlap integral and the nonlinear cross-coefficients do not always appear (or disappear) together in coupled mode equations, whereas they should because they are linked (this was also briefly mentioned in FP-A [2]). For example Ankiewicz and Peng [3], and Ankiewicz [4-5] incorporated the overlap integral, but ignored many terms which depended on the cross-interaction between different fields. In the case of the first paper [3], as shown in chapter 12, the consequences were rather dire since the inclusion of the overlap integral not only did not improve their results, it actually worsened them from the simple case where the overlap integral was not present (therefore not achieving the objective of that paper). A less severe inconsistency is to include the nonlinear cross-coefficients but to ignore the overlap integral eg as in Meng and Okamoto [7] (however since a weakly coupled geometry was considered- where the nonlinear cross-coefficients and the overlap integral were small in magnitude-the accuracy of the results did not suffer too much).

Meng and Okamoto (M-O) [7] were the first to incorporate power dependent mode shapes in their equations. This power dependency happens to be the most important parameter in the accuracy of the coupled mode equations, especially for small guide separations, and has naturally not been incorporated in many important papers before M-O (eg Chen [8]).

Many of the works on three guide nonlinear couplers are also inaccurate for the same reasons as for two guide couplers. The equations are usually inconsistent, because sometimes the cross-phase-modulation term (see eqn 5.7) is included without the inclusion of the larger-cross-phase-modulation terms (see eqn 5.6) (Schmidt-Hattenberger et. al. [9]). Usually the overlap integral is ignored although the nonlinear cross-coefficients are present [9-10]. It was mentioned by Hardy et. al. [11] that the overlap integral cannot be neglected in the analysis of *linear* multiwaveguide couplers even in very weak coupling (one should note that the overlap integral affects nonlinear couplers to a greater extent than linear couplers). The power dependence of the fields is also often not incorporated [9-10] and practical values for the coefficients relating to real geometries are sometimes not used [9].

In addition, papers on three guide nonlinear couplers usually do not consider linear and nonlinear interactions between non-adjacent guides [9-10]. In the aligned geometries of the guides (see Fig. 6.1) it is easily possible for non-adjacent guides to interact. For example later on, in chapter 12, the case of two guides with $0.5\mu\text{m}$ film thickness separated by $1.5\mu\text{m}$ is studied. It is shown there that the critical power is sensitive to variation of guide separation ranging up to $8.0\mu\text{m}$. Therefore over this distance at least 5 such waveguides with separations of $1.5\mu\text{m}$ would all be able to interact linearly and nonlinearly with each other. It is not sufficient to just assume interaction between adjacent guides in this case. In non-aligned geometries (Fig 6.1) it is also easily possible for all the guides to interact with each other.

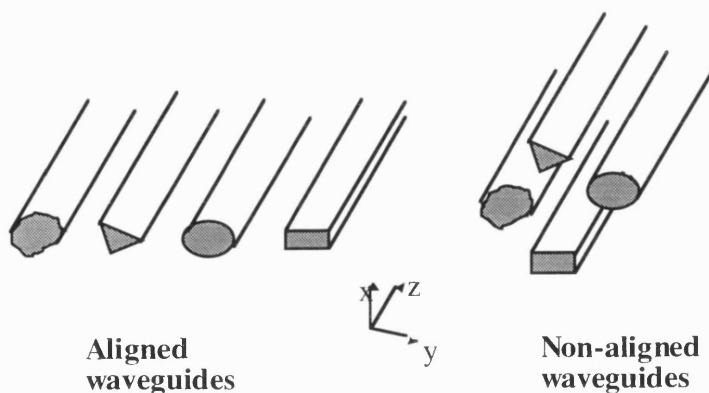


Fig. 6.1 illustrating the aligned and non-aligned waveguide geometries.

In this chapter the general coupled mode equations for the multiwaveguide nonlinear coupler are derived. The multiwaveguide case is studied here in order to generalise the equations for an arbitrary set of parallel waveguides, instead of tailoring for specific geometries. In addition, the equations are derived in their unmodified forms with all the terms present, including the overlap integral. This ensures that the equations are free from inconsistencies, and apply for strong coupling. The derivation uses an approach where the total field of the coupler is constructed from the scaled sum of the power dependent eigenmodes. Furthermore maximum generality is maintained by allowing the guides to be unequal (unlike the usual adjacent guide assumptions in papers in the literature on three guide couplers), and the nonlinearity can be situated anywhere in the cross-section of the system. In addition the equations apply to lossy cases as well as the lossless cases of [7,12].

In the second part of this chapter, and for the first time to our knowledge, all the guides are allowed to interact linearly and nonlinearly with each other for a general formation of the guides. In chapter 7 the equations are re-packaged and reduced to a one-line matrix equation.

There has been some debate regarding the accuracy of linear strong coupled mode theory in the past decade, and some of these should be addressed before applying the theory to nonlinear couplers. Hardy and Streifer (H-S) [13] pointed out that the overlap integral which occurs in the derivation of the linear coupled mode equations should be kept in the equations in order to avoid the inconsistencies which appeared in prior theories regarding the coupling coefficients. H-S theory was later criticised by Snyder et. al. [14-15]. Their main criticism was however rather academic since unrealistic numbers and geometries were used. For example Snyder et al [14] mentioned that the theory is fundamentally in error for *TM* modes when vector methods such as H-S theory are used in the case of abnormally large refractive index changes for the guides (core-cladding index ratios of $n_{co}/n_{cl} > 1.5$). On the other hand the graphs of Snyder et. al. (and later Haus et. al.) [14, 16] showed that for less extreme guidance cases the vector methods of [13, 17-18] were in fact slightly more accurate than scalar methods [15]. Other criticisms concerning H-S theory by the same authors [14-15] (regarding power conservation, and radiation modes) were easily dealt with in other papers soon after (Chuang [17], and Haus et. al. [18]). Vassallo [19] later compared carefully the different formulations and found that vector theories were more accurate than scalar theories for moderate guidance. He also found that although the accuracy of vector methods becomes less with increasing guidance, it does not break down as dramatically as claimed by Snyder et. al. [14]. Streifer [20] also later showed that the actual values

of the propagation coefficients of the supermodes using the H-S theory were in fact more accurate than those of prior theories, even for the large guidance of $n_{co}/n_{cl} > 1.5$. Only the difference in the propagation coefficients of the prior theories happened to be accurate for these cases. Haus et. al. [16] finally showed that the vector theories can be adjusted for very strong guidance by correcting for polarisation effects.

The debate above is irrelevant to the work in this thesis, since real TE fields are used throughout here, and the index differences are assumed to be much less than the extreme cases referred to in [14] where discrepancies might arise. Moreover a vector approach is used in this thesis since there seems to be general agreement that they are more accurate than scalar methods for moderate guidance geometries.

There have been other papers recently claiming inaccuracy of the strong coupled mode theory in strong coupling [21], and corrections have been proposed using the singular perturbation technique [21-23]. However these papers are not very convincing, since in [22] where numerical proof was actually given, it can be seen that strong coupled mode theory [13,18] diverges from exact only for an extreme (academic) case of small guide separation ($0.2\mu m$) and guide thickness ($0.1\mu m$). It should be noted that there is a certain minimum separation that is possible anyway in nonlinear coupled mode theory using nonlinear eigenmode approach. The guide separations cannot be too small, otherwise the nonlinearity of the adjacent guide would cause the isolated guide eigenmode shape approximation to be inaccurate.

To determine the accuracy, applicability, and range of applicability of strong coupled mode theory in the case of nonlinear couplers, it is not sufficient to use theoretical arguments only because these could be vague, subjective, and may only apply to extreme cases. It is necessary to check the accuracy of the equations numerically for different geometries and different parameters against independent and accurate methods such as BPM. Unfortunately this has not been done in many papers for nonlinear couplers, eg. Ankiewicz and Peng [3], Meng and Okamoto [7], and Chen [8]. Comparisons with BPM have been carried out only in two papers to our knowledge [12,24] and in both cases very weakly coupled geometries were studied.

Finally, an alternative method to the eigenmode approach is to employ power dependent supermodes (note that using *linear* supermodes would not be accurate because the field shapes in actual couplers are power dependent not linear), thus avoiding the approximation of constructing the total field from the eigenmodes. However this analysis has been tried in [24], and the results were inaccurate compared with BPM (as evident from their Fig 4). This was for the case of very weak coupling where one would expect all methods to give approximately the same results. Moreover in a recent paper [25] it was found that the even supermode is unstable above a

bifurcation power, and the odd supermode unstable above a certain power above that, so there are still question marks regarding this approach.

6.2 DERIVATION OF THE NONLINEAR COUPLED MODE EQUATIONS

To derive the nonlinear coupled mode equations, we start from an isolated guide (unperturbed system), and add perturbations to transform it into the nonlinear multiwaveguide (perturbed) system. The isolated guide (unperturbed system) can be chosen as linear or nonlinear (see Fig. 6.2) and the choice is purely a matter of convenience. Fraile-Pelaez and Assanto (FP-A) [2] used the linear guide, and Meng and Okamoto (M-O) [7] used the nonlinear guide as the unperturbed system. It seems that if power dependent mode shapes are used, as in M-O [7], it is more convenient to use the nonlinear waveguide as the unperturbed system, because then all the fields in the coefficients will be power dependent, instead of there being a mixture of power dependent and power independent fields. If power dependence is not at issue then it may be more convenient to start from the linear guide as the unperturbed system as in FP-A [2]. Starting with a linear isolated guide leads to equations which include the linear propagation constant, whereas starting from the nonlinear guide leads to equations involving the nonlinear propagation constant. At low powers, the resulting coupled mode equations can be related via the identities derived in chapter 5, as shown in section 6.4.2 below.

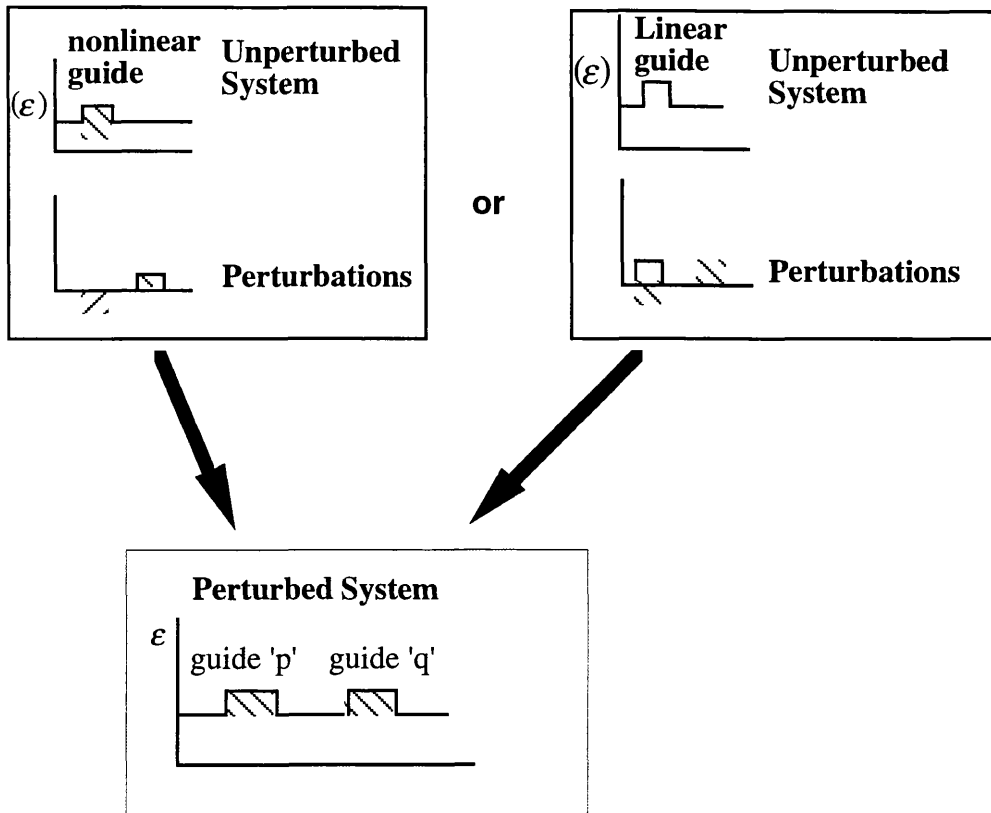


Fig. 6.2 Constructing the perturbed system from the choice of either a linear or nonlinear isolated waveguide for the unperturbed system.

6.3 DESCRIPTION OF THE MULTIWAVEGUIDE SYSTEM UNDER CONSIDERATION

The multiwaveguide system under consideration consists of N parallel waveguides embedded in their surrounding media (see Fig. 6.3). The waveguides are positioned in an aligned or quasi-aligned formation so that only adjacent guides are interacting (this constraint will be removed in section 6.6 so that all the guides will be able to interact with each other). The nonlinearity can be located anywhere in the cross-sectional plane of the system. For example, it could be situated in one or more film regions and/or their surrounding media. The whole system is invariant in the z -direction, and the waveguides can be unequal, and with arbitrary shapes (therefore applies to fibres as well as planar guides).

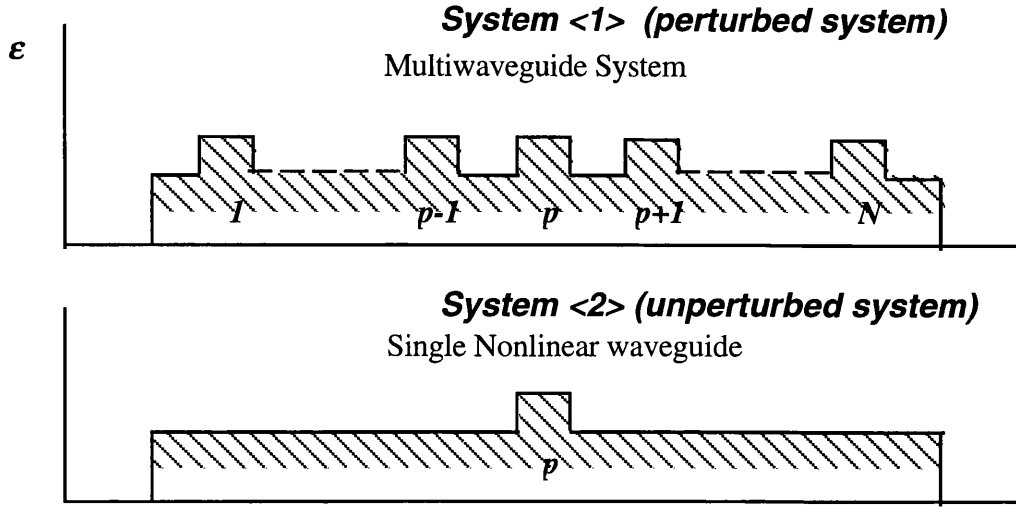


Fig. 6.3 Showing the perturbed and the unperturbed systems

The permittivity for system <1> (the perturbed system) is given by

$$\epsilon^{(1)} = \epsilon(x, y, z) = \epsilon^{(p)}(x, y) + \Delta\epsilon^{(p)}(x, y) + \alpha|\underline{E}^{(1)}|^2 \quad (6.1)$$

where $\epsilon^{(1)}$ is the permittivity for the whole system, (which includes all the nonlinear/linear waveguides, as well as their nonlinear/linear surroundings), $\epsilon^{(p)}(x, y)$ the linear permittivity for guide 'p' together with its (linear) surrounding medium. $\Delta\epsilon^{(p)}(x, y)$ includes the linear perturbations to guide 'p': ie the linear perturbation due to the other waveguides. $\alpha|\underline{E}^{(1)}|^2$ is the nonlinear permittivity change for the system (where $\alpha(x, y)$ describes the nonlinearity of the whole system). $\underline{E}^{(1)}$ and $\underline{H}^{(1)}$ are the total fields for the system, constructed from the scaled sum of the power dependent eigenmodes of the individual nonlinear waveguides ie

$$\underline{E}^{(1)} = \sum_{q=1}^N a_q(z) \underline{E}_t^{(q)} \quad \underline{H}^{(1)} = \sum_{q=1}^N a_q(z) (\underline{H}_t^{(q)} + \underline{H}_z^{(q)}) \quad (6.2)$$

The second system consists of a single nonlinear waveguide 'p'.

$$\epsilon^{(2)} = \epsilon^{(p)}(x, y) + \alpha^{(p)}|\underline{E}^{(2)}|^2 \quad (6.3)$$

where $\alpha^{(p)}$ is the nonlinearity of guide 'p'. $\alpha^{(p)}|\underline{E}^{(2)}|^2$ is the nonlinear permittivity caused by the eigenmode of guide 'p'. $\underline{E}^{(2)}$ and $\underline{H}^{(2)}$ correspond with the exact

nonlinear (power dependent) eigenmode of the isolated waveguide 'p':

$$\underline{E}^{(2)} = \underline{E}_t^{(p)} e^{-j\beta_p z} \quad \underline{H}^{(2)} = (-\underline{H}_t^{(p)} + \underline{H}_z^{(p)}) e^{-j\beta_p z} \quad (6.4)$$

β_p is the nonlinear propagation coefficient of the isolated nonlinear guide 'p'.

Inserting eqns. 6.1-6.4 into Lorentz' reciprocity (eqn 5.11) gives

$$-j \sum_{q=1}^N C_{pq} \frac{\partial a_q}{\partial z} = \sum_{q=1}^N (K_{qp} + \beta_p C_{pq}) a_q + \frac{\omega \epsilon_0}{4P e^{-j\beta_p z}} \iint_{-\infty}^{+\infty} \left(\alpha |\underline{E}^{(1)}|^2 \underline{E}^{(1)} \cdot \underline{E}^{(2)} - \alpha^{(p)} |\underline{E}^{(2)}|^2 \underline{E}^{(2)} \cdot \underline{E}^{(1)} \right) \quad (6.5)$$

where C_{pq} and K_{pq} are defined in chapter 3 (eqns. 3.3 and 3.4 respectively) and P is the total power. Inserting eqns 6.1-6.4 into the nonlinear part of eqn 6.5 and expanding, results in eqn 6.6 below (see Appendix 5 for further explanations). We note that the complex conjugates of the transverse fields in eqn 6.6 are specifically shown in the equations for the moment (even though the fields are known to be real).

$$-j \sum_{q=1}^N C_{pq} \frac{\partial a_q}{\partial z} = \sum_{q=1}^N (K_{qp} + \beta_p C_{pq}) a_q \quad (6.6a)$$

$$+ \frac{\omega \epsilon_0}{4P} \iint_{-\infty}^{+\infty} \left(\alpha \sum_{\ell} a_{\ell} |a_{\ell}|^2 |\underline{E}_t^{(\ell)}|^2 \underline{E}_t^{(\ell)} \underline{E}_t^{(p)} \right) dx dy \quad (6.6b)$$

$$+ 2 \times \frac{\omega \epsilon_0}{4P} \iint_{-\infty}^{+\infty} \left(\alpha \sum_{\ell} a_{\ell} \underline{E}_t^{(\ell)} \sum_m |a_m|^2 |\underline{E}_t^{(m)}|^2 \underline{E}_t^{(p)} (1 - \delta_{\ell m}) \right) dx dy \quad (6.6c)$$

$$+ \frac{\omega \epsilon_0}{4P} \iint_{-\infty}^{+\infty} \left(\alpha \sum_{\ell} a_{\ell}^* \underline{E}_t^{(\ell)*} \sum_m a_m a_n \underline{E}_t^{(m)} \underline{E}_t^{(n)} \underline{E}_t^{(p)} (1 - \delta_{\ell m})(1 - \delta_{\ell n})(1 - \delta_{mn}) \right) dx dy \quad (6.6d)$$

$$+ \frac{\omega \epsilon_0}{4P} \iint_{-\infty}^{+\infty} \left(\alpha \sum_{\ell} a_{\ell}^2 \underline{E}_t^{(\ell)2} \sum_m a_m^* \underline{E}_t^{(m)*} \underline{E}_t^{(p)} (1 - \delta_{\ell m}) \right) dx dy \quad (6.6e)$$

$$- \frac{\omega \epsilon_0}{4P} \iint_{-\infty}^{+\infty} \left(\alpha^{(p)} |\underline{E}_t^{(p)}|^2 \underline{E}_t^{(p)} \sum_m a_m \underline{E}_t^{(m)} \right) dx dy \quad (6.6f)$$

where $\ell = 1, \dots, N$ and $m = 1, \dots, N$. It should be noted that had a linear waveguide 'p' been chosen as the unperturbed system, the final line 6.6f would have disappeared

from the equations. Also, if the multiwaveguide system were linear instead of nonlinear, then lines 6.6b-6.6f would have disappeared leaving only the first line 6.6a.

An approximation is now made. It is assumed that coupling only occurs between adjacent guides (all the multiwaveguide NLDC papers [eg. 9] make this assumption, but this constraint will be removed in section 6.6 of this chapter). Therefore expanding over $\ell = p + 1, p, p - 1$, and $m = p + 1, p, p - 1$, and substituting eqns. 5.3 and 5.4 (ie definitions for $Q_{pq}^{(a)}$ and K_{pq}^{NL} respectively) into eqn 6.6a-f leads to

$$\begin{aligned}
 -j \frac{\partial a_p}{\partial z} - j \sum_{r=p-1, p+1} C_{pr} \frac{\partial a_r}{\partial z} &= \sum_{r=p-1, p, p+1} [\beta_p C_{pr} + K_{rp} + K_{rp}^{NL} + |a_r|^2 Q_{pr}^{(r)} - Q_{pr}^{(p)}] a_r \\
 + \sum_{r=p-1, p+1} (2a_p |a_r|^2 + a_r^2 a_p^*) Q_{pp}^{(q)} &+ \sum_{r=p-1, p+1} (2a_r |a_p|^2 + a_p^2 a_r^*) Q_{pr}^{(p)} + \sum_{r=p-1, p+1} (2a_{2p-r} |a_r|^2 + a_r^2 a_{2p-r}^*) Q_{2p-r, p}^{(r)} \\
 + 2(a_{p+1}^* a_p a_{p-1} + a_{p-1}^* a_{p+1} a_p + a_p^* a_{p+1} a_{p-1}) &Q_{p+1, p-1}^{(p)}
 \end{aligned} \tag{6.7}$$

where $\sum_{r=p-1, p+1}$ notation implies summing over $r = p + 1$ and $p - 1$ (and not p)

Using eqn. 5.20 and replacing subscript ‘ q ’ with ‘ r ’, the nonlinear-nonlinear relationship becomes

$$\beta_p C_{pr} + K_{rp} + K_{rp}^{NL} - Q_{pr}^{(p)} = C_{pr} \beta_r + K_{pr} + K_{pr}^{NL} - Q_{pr}^{(r)} \tag{6.8}$$

and substituting this identity into eqn 6.7 leads to

$$\begin{aligned}
 -j \frac{\partial a_p}{\partial z} - j \sum_{r=p-1, p+1} C_{pr} \frac{\partial a_r}{\partial z} &= \sum_{r=p-1, p, p+1} [C_{pr} \beta_r + K_{pr} + K_{pr}^{NL} + |a_r|^2 Q_{pr}^{(r)} - Q_{pr}^{(r)}] a_r \\
 + \sum_{r=p-1, p+1} (2a_p |a_r|^2 + a_r^2 a_p^*) Q_{rr}^{(p)} &+ (2a_r |a_p|^2 + a_p^2 a_r^*) Q_{rp}^{(p)} + (2a_{2p-r} |a_r|^2 + a_r^2 a_{2p-r}^*) Q_{2p-r, p}^{(r)} \\
 + 2(a_{p+1}^* a_p a_{p-1} + a_{p-1}^* a_{p+1} a_p + a_p^* a_{p+1} a_{p-1}) &Q_{p+1, p-1}^{(p)}
 \end{aligned} \tag{6.9}$$

which is one of N differential equations for the N -guide coupler. Each differential equation is signified by a value for p which is a number between 1 to N . The beautiful symmetry in eqn. 6.9 should be examined. It seems likely that some kind of matrix formulation must be possible (see chapter 7).

6.4 THE TWO GUIDE CASE

The equation above (eqn. 6.9) is now expanded for the two guide case, and compared with the coupled mode equations derived in the literature. In particular M-O [7] used an approach similar to the one here, ie a nonlinear isolated guide as the unperturbed system, whereas FP-A [2] used the isolated linear guide as the unperturbed system. The two sets of equations look different at first sight, so it is important to compare them with each other, as well as with our equations. Using eqn. 6.9 and expanding for the two guide case

$p = 1$ case becomes

$$\begin{aligned}
 -jC_{11} \frac{da_1}{dz} - jC_{12} \frac{da_2}{dz} &= (C_{11}\beta_1 + K_{11} + K_{11}^{NL} + |a_1|^2 Q_{11}^{(1)} - Q_{11}^{(1)})a_1 \\
 &+ (C_{12}\beta_2 + K_{12} + K_{12}^{NL} + |a_2|^2 Q_{12}^{(2)} - Q_{12}^{(1)})a_2 + (2a_1|a_2|^2 + a_2^2 a_1^*)Q_{22}^{(1)} + (2a_2|a_1|^2 + a_1^2 a_2^*)Q_{21}^{(1)}
 \end{aligned} \tag{6.10}$$

and $p = 2$ becomes

$$\begin{aligned}
 -jC_{22} \frac{da_2}{dz} - jC_{21} \frac{da_1}{dz} &= (C_{21}\beta_1 + K_{21} + K_{21}^{NL} + |a_1|^2 Q_{21}^{(1)} - Q_{21}^{(2)})a_1 \\
 &+ (C_{22}\beta_2 + K_{22} + K_{22}^{NL} + |a_2|^2 Q_{22}^{(2)} - Q_{22}^{(2)})a_2 + (2a_2|a_1|^2 + a_1^2 a_2^*)Q_{22}^{(1)} + (2a_1|a_2|^2 + a_2^2 a_1^*)Q_{12}^{(2)}
 \end{aligned} \tag{6.11}$$

6.4.1 Comparison with Meng And Okamoto (M-O)

Our formulation is more accurate and general than those of M-O [7]. In this section it is shown that eqns 6.10 and 6.11 can compare with those of M-O for the lossless case.

Considering $p = 1$ case, ie using eqn. 6.10 and rearranging it results in

$$-j \frac{\partial a_1}{\partial z} - jC_{12} \frac{\partial a_2}{\partial z} = (\beta_1 + K_{11} + K_{11}^{NL})a_1 + (K_{12} + C_{12}\beta_2 + K_{12}^{NL})a_2 \tag{6.12a}$$

$$+ [(a_1 a_2^* + a_2 a_1^*)Q_{22}^{(1)} + |a_2|^2 (Q_{21}^{(2)} - Q_{12}^{(1)}) - Q_{12}^{(1)} C_{12} (a_1 a_2^* + a_2 a_1^*)] a_2 \tag{6.12b}$$

$$+ [|a_2|^2 (Q_{22}^{(1)} - Q_{11}^{(1)}) + (a_1 a_2^* + a_2 a_1^*)Q_{12}^{(1)} - Q_{11}^{(1)} C_{12} (a_1 a_2^* + a_2 a_1^*)] a_1 \tag{6.12c}$$

which can be compared to M-O's equation by substituting their notation, ie

$$Q_1 \equiv K_{11} + K_{11}^{NL} = K_{22} + K_{22}^{NL} \quad (6.13a)$$

$$Q_2 \equiv K_{12} + K_{12}^{NL} = K_{21} + K_{21}^{NL} \quad (6.13b)$$

$$k_s \equiv Q_{11}^{(1)} = Q_{22}^{(2)} \quad k_c \equiv Q_{22}^{(1)} = Q_{11}^{(2)} \quad (6.13c)$$

$$k_t \equiv Q_{12}^{(1)} = Q_{12}^{(2)} \quad (6.13d)$$

$$P_{ab} \equiv C_{12} = C_{21} \quad (6.13e)$$

There are several differences between our equation (eqn. 6.12) and M-O's (their eqns. 7a and 7b). Firstly, it is noticed that the overlap integral is only present on the left hand side of their equations. Terms which are multiplied by this overlap integral in lines 6.12b and 6.12c are therefore neglected from their equations. It may be argued that $Q_{12}^{(1)}C_{12}$ in line 6.12b is negligible anyway, but the same cannot be said of $Q_{11}^{(1)}C_{12}$ in line 6.12c since it is of the same order as $Q_{12}^{(1)}$ and should not be neglected as M-O have done. Therefore M-O's equations really only apply for very weakly coupled geometries which they studied. Secondly, the power conservation formula $|a_1|^2 + |a_2|^2 = 1$ is used in their equations, whereas if the overlap integral is present it should be $P = |a_1|^2 + |a_2|^2 + C_{12}(a_1^*a_2 + a_2^*a_1) = 1$ (see eqn. A6.17). Furthermore the $|a_2|^2(Q_{21}^{(2)} - Q_{12}^{(1)})$ term is neglected from their equations. $Q_{21}^{(2)} = Q_{12}^{(1)}$ occurs only if the nonlinearities in the two guides are exactly equal. If they are different, then $Q_{21}^{(2)} \neq Q_{12}^{(1)}$. For example if $\alpha^{(2)}$ is positive and the nonlinearities in the two guides are equal in magnitude, but opposite in sign, then the $|a_2|^2(Q_{21}^{(2)} - Q_{12}^{(1)})$ term becomes the not so negligible $2|a_2|^2 Q_{21}^{(2)}$.

6.4.2 Comparison with Fraile-Pelaez (FP-A)

Our equations (eg. eqn. 6.10) are similar to those of M-O (eg. eqn 6.12) because the isolated *nonlinear* guide was chosen as the unperturbed system. However FP-A [2] chose the isolated linear guide as the unperturbed system instead. The two sets of equations could in theory be shown to be similar using a rigorous proof. However, here we show using a simple method, by considering the low power limit where the field shapes are approximately linear, that the two sets of equations can be related via

the identities derived in chapter 5. By applying the nonlinear-nonlinear identity (eqn 5.20 with 'q' replaced by 'r') to eqn. 6.9 followed by the linear-nonlinear identity (eqn 5.30 with 'q' replaced by 'r', and the 'p' and 'r' indices interchanged) eqn. 6.9 becomes

$$\begin{aligned}
-j \frac{\partial a_p}{\partial z} - j \sum_{r=p-1, p+1} C_{pr} \frac{\partial a_r}{\partial z} &= \sum_{r=p-1, p, p+1} \left[C_{pr} \bar{\beta}_r + K_{pr} + |a_r|^2 Q_{pr}^{(r)} \right] a_r \\
+ \sum_{r=p-1, p+1} \left(2a_p |a_r|^2 + a_r^2 a_p^* \right) Q_{rr}^{(p)} &+ \left(2a_r |a_p|^2 + a_p^2 a_r^* \right) Q_{rp}^{(p)} + \left(2a_{2p-r} |a_r|^2 + a_r^2 a_{2p-r}^* \right) Q_{2p-r, p}^{(r)} \\
+ 2 \left(a_{p+1}^* a_p a_{p-1} + a_{p-1}^* a_{p+1} a_p + a_p^* a_{p+1} a_{p-1} \right) &Q_{p+1, p-1}^{(p)} \tag{6.14}
\end{aligned}$$

Equation 6.14 can now be used to derive the equations for the two guide case.

When $p = 1$, eqn. 6.14 becomes

$$\begin{aligned}
-j C_{11} \frac{da_1}{dz} - j C_{12} \frac{da_2}{dz} &= \left(C_{11} \bar{\beta}_1 + K_{11} + |a_1|^2 Q_{11}^{(1)} \right) a_1 + \left(C_{12} \bar{\beta}_2 + K_{12} + |a_2|^2 Q_{12}^{(2)} \right) a_2 \\
+ \left(2a_1 |a_2|^2 + a_2^2 a_1^* \right) Q_{22}^{(1)} &+ \left(2a_2 |a_1|^2 + a_1^2 a_2^* \right) Q_{21}^{(1)} \tag{6.15}
\end{aligned}$$

when $p = 2$

$$\begin{aligned}
-j C_{22} \frac{da_2}{dz} - j C_{21} \frac{da_1}{dz} &= \left(C_{22} \bar{\beta}_2 + K_{22} + |a_2|^2 Q_{22}^{(2)} \right) a_2 + \left(C_{21} \bar{\beta}_1 + K_{21} + |a_1|^2 Q_{21}^{(1)} \right) a_1 \\
+ \left(2a_2 |a_1|^2 + a_1^2 a_2^* \right) Q_{22}^{(1)} &+ \left(2a_1 |a_2|^2 + a_2^2 a_1^* \right) Q_{12}^{(2)} \tag{6.16}
\end{aligned}$$

According to FP-A, Jensen [1] made several inconsistencies here. In the $p = 1$ case above (eqn. 6.15) for example, Jensen kept only the self-phase-modulation $Q_{11}^{(1)}$ and the cross-phase-modulation terms $Q_{22}^{(1)}$, but did not include the larger-cross-phase-modulation terms $Q_{21}^{(1)}$ and $Q_{12}^{(2)}$. Furthermore Jensen neglected the $a_2^2 a_1^*$ terms but kept the $2a_1 |a_2|^2$ terms even though both were multiplied by the same coefficient $Q_{22}^{(1)}$. Eqns. 6.15 and 6.16 can be converted into FP-A's notation, by assuming that the overlap integrals disappear (ie $C_{12} \rightarrow 0$), and substituting the following coefficients

$$Q_5 \equiv Q_{21}^{(2)} = Q_{21}^{(1)} = Q_{12}^{(2)} = Q_{21}^{(1)} \quad (6.17a)$$

$$Q_3 \equiv Q_{11}^{(1)} = Q_{22}^{(2)} \quad (6.17b)$$

$$Q_4 \equiv Q_{11}^{(2)} = Q_{22}^{(1)} \quad (6.17c)$$

$$a \equiv a_1 \quad b \equiv a_2 \quad (6.17d)$$

However, the cross-phase-modulation terms $Q_{22}^{(1)}$, $Q_{12}^{(1)}$, and $Q_{12}^{(2)}$ should not have appeared in FP-A's equations either, since they disappear also with C_{12} , as $C_{12} \rightarrow 0$. Therefore at weak coupling the nonlinear coupling equations should become

$$-j \frac{da_1}{dz} = (\bar{\beta}_1 + K_{11} + |a_1|^2 Q_{11}^{(1)})a_1 + K_{12}a_2 \quad (6.18a)$$

$$-j \frac{da_2}{dz} = K_{21}a_1 + (\bar{\beta}_2 + K_{22} + |a_2|^2 Q_{22}^{(2)})a_2 \quad (6.18b)$$

6.5 THREE WAVEGUIDES

The coupled mode equations for the three-guide coupler can be written down using eqn. 6.9.

For $p = 1$

$$\begin{aligned} -j \frac{da_1}{dz} - jC_{12} \frac{da_2}{dz} = & (C_{11}\beta_1 + K_{11} + K_{11}^{NL} + |a_1|^2 Q_{11}^{(1)} - Q_{11}^{(1)})a_1 + (C_{12}\beta_2 + K_{12} + K_{12}^{NL} + |a_2|^2 Q_{12}^{(2)} - Q_{12}^{(2)})a_2 \\ & + (2a_1|a_2|^2 + a_2^2 a_1^*)Q_{22}^{(1)} + (2a_2|a_1|^2 + a_1^2 a_2^*)Q_{21}^{(2)} \end{aligned} \quad (6.19)$$

$p = 2$ becomes

$$\begin{aligned} -j \frac{da_2}{dz} - jC_{21} \frac{da_1}{dz} - jC_{23} \frac{da_3}{dz} = & (C_{21}\beta_1 + K_{21} + K_{21}^{NL} + |a_1|^2 Q_{21}^{(1)} - Q_{21}^{(1)})a_1 \\ & + (C_{22}\beta_2 + K_{22} + K_{22}^{NL} + |a_2|^2 Q_{22}^{(2)} - Q_{22}^{(2)})a_2 + (C_{23}\beta_3 + K_{23} + K_{23}^{NL} + |a_3|^2 Q_{23}^{(3)} - Q_{23}^{(3)})a_3 \\ & + (2a_2|a_1|^2 + a_1^2 a_2^*)Q_{11}^{(2)} + (2a_2|a_3|^2 + a_3^2 a_2^*)Q_{33}^{(2)} + (2a_1|a_2|^2 + a_2^2 a_1^*)Q_{12}^{(2)} \end{aligned}$$

$$+(2a_3|a_2|^2 + a_2^2 a_3^*)Q_{32}^{(2)} + (2a_3|a_1|^2 + a_1^2 a_3^*)Q_{32}^{(1)} + (2a_1|a_3|^2 + a_3^2 a_1^*)Q_{12}^{(3)} + 2(a_3^* a_2 a_1 + a_1^* a_3 a_2 + a_2^* a_3 a_1)Q_{31}^{(2)} \quad (6.20)$$

and $p = 3$ becomes

$$-j \frac{da_3}{dz} - jC_{32} \frac{da_2}{dz} = (C_{32}\beta_2 + K_{32} + K_{32}^{NL} + |a_2|^2 Q_{32}^{(2)} - Q_{32}^{(2)})a_2 + (C_{33}\beta_3 + K_{33} + K_{33}^{NL} + |a_3|^2 Q_{33}^{(3)} - Q_{33}^{(3)})a_3 + (2a_3|a_2|^2 + a_2^2 a_3^*)Q_{22}^{(3)} + (2a_2|a_3|^2 + a_3^2 a_2^*)Q_{23}^{(3)} \quad (6.21)$$

Equations 6.19-6.21 should be compared with eqns 7.29-7.31 which assumes interactions between all the waveguides.

6.6 $N > 3$ GUIDES (4-GUIDE COUPLER FOR EXAMPLE)

The coupled mode equation for the 4-guide coupler (third waveguide) can be written down using eqn 6.9, as follows:

$$p = 3$$

$$-j \frac{da_3}{dz} - jC_{32} \frac{da_2}{dz} - jC_{34} \frac{da_4}{dz} = (C_{32}\beta_2 + K_{32} + K_{32}^{NL} + |a_2|^2 Q_{32}^{(2)} - Q_{32}^{(2)})a_2 + (C_{33}\beta_3 + K_{33} + K_{33}^{NL} + |a_3|^2 Q_{33}^{(3)} - Q_{33}^{(3)})a_3 + (C_{34}\beta_4 + K_{34} + K_{34}^{NL} + |a_4|^2 Q_{34}^{(4)} - Q_{34}^{(4)})a_4 + (2a_3|a_2|^2 + a_2^2 a_3^*)Q_{22}^{(3)} + (2a_3|a_4|^2 + a_4^2 a_3^*)Q_{44}^{(3)} + (2a_2|a_3|^2 + a_3^2 a_2^*)Q_{23}^{(3)} + (2a_4|a_3|^2 + a_3^2 a_4^*)Q_{43}^{(3)} + (2a_4|a_2|^2 + a_2^2 a_4^*)Q_{42}^{(3)} + 2(a_4^* a_3 a_2 + a_2^* a_4 a_3 + a_3^* a_4 a_2)Q_{42}^{(3)} \quad (6.22)$$

6.7 ASSUMING INTERACTION BETWEEN ALL THE WAVEGUIDES

The adjacent guide interaction case which was assumed in the previous section, really applies to a set of weakly-coupled guides positioned in an aligned geometry. If the guides are non-aligned (as in multi-core fibres), or closely spaced, then interaction between many guides is possible.

For the derivation of all-guide interactions, we follow the same model, and procedure up to eqn. 6.6. This time, instead of expanding over $p-1, p,$ and $p+1$, as was done in eqn. 6.7, the following coefficients are substituted directly.

$$Q_{pq}^{(a)} = \frac{\omega \epsilon_0}{4P} \iint_{-\infty}^{+\infty} \left(\alpha E_t^{(a)^2} \right) \underline{E}_t^{(p)} \cdot \underline{E}_t^{(q)} dx dy \quad (6.23a)$$

$$K_{pq}^{NL} = \frac{\omega \epsilon_0}{4P} \iint_{-\infty}^{+\infty} \left(\alpha - \alpha^{(q)} \right) E_t^{(q)^2} \underline{E}_t^{(p)} \cdot \underline{E}_t^{(q)} dx dy \quad (6.23b)$$

$$S_{\ell mn}^{(p)} = \frac{\omega \epsilon_0}{4P} \iint_{-\infty}^{+\infty} \left(\alpha \underline{E}_t^{(\ell)} \cdot \underline{E}_t^{(m)} \underline{E}_t^{(n)} \cdot \underline{E}_t^{(p)} \right) dx dy \quad \ell \neq m \neq n \quad (6.23c)$$

$S_{\ell mn}^{(p)}$ are very small terms, even smaller than the $Q_{bc}^{(a)}$ term of eqn 5.8, because at least $Q_{bc}^{(a)}$ contained $E_t^{(a)^2}$.

The nonlinear-nonlinear identity of eqn 5.20 is now applied to derive the following coupled mode equations for the all-guide interaction case

All-guide interaction case

$$\begin{aligned} -j \sum_q C_{pq} \frac{\partial a_q}{\partial z} = & \sum_q \left[C_{pq} \beta_q + K_{pq} + K_{pq}^{NL} - Q_{pq}^{(q)} \right] a_q + 2 \sum_\ell a_\ell \sum_m |a_m|^2 Q_{\ell p}^{(m)} (1 - \delta_{\ell m}) \\ & + \sum_\ell a_\ell^2 \sum_m a_m^* Q_{mp}^{(\ell)} (1 - \delta_{\ell m}) + \sum_\ell a_\ell^* \sum_m a_m \sum_n a_n S_{\ell mn}^{(p)} (1 - \delta_{\ell m}) (1 - \delta_{\ell n}) (1 - \delta_{mn}) \end{aligned} \quad (6.24)$$

which describes all-guide interaction between any number of guides. Eqn. 6.24 is one of N differential equations. These equations are reformulated into a single line matrix equation in chapter 7 (section 7.3).

6.8 CONCLUSIONS

In this chapter we derived (for the first time to our knowledge) the full coupled mode equations for the multiwaveguide nonlinear directional coupler. Initially it was assumed that the interaction was between adjacent guides, but later on all-guide interaction was considered. The equations were expanded out for several cases. The two guide case was compared and contrasted with those in papers in the literature.

REFERENCES

-
- [1] S. M. Jensen, "The nonlinear coherent coupler", IEEE Transactions on Microwave Theory and Techniques, MTT-30, no. 10, 1982, pp. 1568-1571.
- [2] F. J. Fraile-Pelaez and G. Assanto, "Coupled-mode equations for nonlinear directional couplers", Applied Optics, vol. 29, no. 15, 1990, pp. 2216-2217.
- [3] A. Ankiewicz and G-D Peng, J. Opt. Soc. Am. B, vol. 9, 1992, pp. 1341.
- [4] A. Ankiewicz, "Interaction coefficient in detuned nonlinear couplers", Optics Commun., vol. 66, no. 5,6, 1988, pp. 311-314.
- [5] A. Ankiewicz, "Novel effects in non-linear coupling", Optics and Quant Electron., vol. 20, 1988, pp. 329-337.
- [7] X. Meng and N. Okamoto, "Improved coupled-mode theory for Nonlinear Directional Couplers", IEEE J. Quant. Electron., Vol 27, No.5, May 1991, pp. 1175-1181
- [8] Y. Chen, "Solution to full coupled wave equations of nonlinear coupled systems", IEEE J. Quant. Elect., vol. 25, no. 10, 1989, pp. 2149-2153.
- [9] C. Schmidt-Hattenberger, U. Trutschel, and F. Lederer, "Nonlinear switching in multiple-core couplers", Optics Letters, vol. 16, no. 5, 1991, pp. 294-296.
- [10] C. Mapalagama and R. T. Deck, J. Opt. Soc. Am. B, vol. 9, no. 12, 1992, pp. 2258.
- [11] A. Hardy, W. Streifer, and M. Osinski, "Weak coupling of parallel waveguides", Optics Letters, vol. 13, no. 2, pp. 161-163, 1988.
- [12] F. J. Fraile-Pelaéz, G. Assanto, and D. R. Heatley, "Sign-dependent response of nonlinear directional couplers", Optics Comm., vol. 77, no. 5,6, 1990, pp. 402-406.
- [13] A. Hardy, and W. Streifer, "Coupled mode theory of parallel waveguides", J. Light. Technol., vol. LT-3, no. 5, 1985, pp. 1135-1146.
- [14] A. W. Snyder, A. Ankiewicz, and A. Altintas, "Fundamental error of recent coupled mode formulations", Electron. Lett., vol. 23, no. 20, 1987, pp. 1097-1098.
- [15] A. W. Snyder, and A. Ankiewicz, "Optical fiber couplers-optimum solution for unequal cores", J. Light. Technol., vol. 6, no. 3, Mar 1988, pp. 463-474.
- [16] H. A. Haus, W. P. Huang, A. W. Snyder, "Coupled-mode formulations", Optics Letters, vol. 14, no. 21, Nov. 1989, pp. 1222-1224.
- [17] S-L Chuang, "A coupled mode formulation by reciprocity and a variational principle", J. Light. Technol., vol. LT-5, no. 1, 1987, pp. 5-15.
- [18] H. Haus, W. P. Huang, S. Kawakami, and N. A. Whitaker, "Coupled-mode theory of optical waveguides", J. Light. Technol., vol. LT-5, no. 1, 1987, pp. 16-23.

- [19] C. Vassallo, "About coupled-mode theories for dielectric waveguides", *J. Light. Technol.*, vol. 6, no. 2, Feb 1988, pp. 294-303.
- [20] W. Streifer, "Comment-fundamental error of recent coupled mode equations", *Electron. Lett.*, vol. 24, no. 11, May 1988, pp. 718-719.
- [21] Z. H. Wang and S. R. Seshadri, "Asymptotic theory of guided waves in two parallel, identical dielectric waveguides", *J. Opt. Soc. Am. A*, vol. 5, no. 6, 1988, pp. 782-792.
- [22] K. Yasumoto, "Coupled-mode formulation of parallel dielectric waveguides using singular perturbation technique", *Micr. and Opt. Tech. Lett.*, vol. 4, no. 11, 1991, pp. 486-491.
- [23] K. Yasumoto, "Coupled-mode formulation of parallel dielectric waveguides", *Optics Lett.*, vol. 18, no. 7, 1993, pp. 503-504.
- [24] F. Dios, X. Nogués, and F. Canal, "Critical power in a symmetric nonlinear directional coupler", *Opt. Quant. Electron.*, vol. 24, 1992, pp. 1191-1201.
- [25] A. D. Capobianco, and G. F. Nalesso, "Determination and stability analysis of the supermodes in nonlinear directional couplers through a variational approach", *Optical and Quant. Electron.*, vol. 27, 1995, pp. 1015-1026.

CHAPTER 7

IN MATRIX FORM

7.1 INTRODUCTION

In this chapter, the coupled mode equations derived in chapter 6 are transformed into matrices. This type of matrix representation is new for multiwaveguide nonlinear couplers in the literature, although the linear versions are well-known [1-3].

In section 7.2 the adjacent guide interactions case is examined, and in section 7.3 the all-guide interaction case is studied. The resulting single-line matrix equation is used in section 7.4 to check power conservation for the lossless case. It is found that the inconsistencies inherent in many coupled mode equations in the literature sometimes lead to violation of conservation of power.

7.2 ADJACENT GUIDE INTERACTIONS

7.2.1 The formulation

The matrix form for the adjacent guide interaction case is derived in this section. The nonlinear coupled mode equations for this case was derived in chapter 6 (eqn. 6.9), and is repeated here

$$\begin{aligned} -j \frac{\partial a_p}{\partial z} - j \sum_{r=p-1, p+1} C_{pr} \frac{\partial a_r}{\partial z} &= \sum_{r=p-1, p, p+1} [K_{pr} + K_{pr}^{NL} + C_{pr} \beta_r + |a_r|^2 Q_{pr}^{(r)} - Q_{pr}^{(p)}] a_r \\ + \sum_{r=p-1, p+1} (2a_p |a_r|^2 + a_r^2 a_p^*) Q_{rr}^{(p)} &+ (2a_r |a_p|^2 + a_p^2 a_r^*) Q_{rp}^{(p)} + (2a_{2p-r} |a_r|^2 + a_r^2 a_{2p-r}^*) Q_{2p-r, p}^{(r)} \\ + 2(a_{p+1}^* a_p a_{p-1} + a_{p-1}^* a_{p+1} a_p + a_p^* a_{p+1} a_{p-1}) &Q_{p+1, p-1}^{(p)} \end{aligned} \quad (7.1)$$

This equation can be written in matrix form almost by inspection. For the ' p 'th guide it becomes the following

Adjacent guide interactions- matrix form

$$-j\underline{C}^{(p)} \frac{d\underline{a}^{(p)}}{dz} = \left(\begin{array}{c} \underline{K}^{(p)} + \underline{K}_{NL}^{(p)} + \underline{C}^{(p)} \underline{\beta}^{(p)} + \underline{Q}^{(p)} |\underline{a}^{(p)}|^2 - \underline{Q}^{(p)T} + \\ 2\underline{a}^{(p)T} \underline{X}^{(p)} \underline{a}^{(p)*} + \underline{a}^{(p)+} \underline{X}^{(p)} \underline{a}^{(p)} + \underline{a}^{(p)+} \underline{A}^{(p)} \end{array} \right) \underline{a}^{(p)} \quad (7.2)$$

where $+$ and T are the adjoint and transpose operators respectively. The matrix definitions are given in eqns. 7.5-7.16 below, and the notation for the vectors and matrices is the same as in chapter 3 (see comments which follow eqn 3.16).

The derivation of the first five terms on the RHS of eqn 7.2 is fairly straightforward. The derivation of the last three terms seem slightly more complicated, but in fact not so if one recalls the following rule for representing quadratic forms in terms of matrices (eg see [4]).

$$\text{ie.} \quad a_1^2 x_{11} + a_1 a_2 x_{12} + a_2 a_1 x_{21} + a_2^2 x_{22} \equiv (a_1 \quad a_2) \begin{pmatrix} x_{11} & x_{12} \\ x_{21} & x_{22} \end{pmatrix} \begin{pmatrix} a_1 \\ a_2 \end{pmatrix} \quad (7.3)$$

We note that for a linear coupler, all the nonlinear terms in eqn 7.2 disappear to give

$$-j\underline{C}^{(p)} \frac{d\underline{a}^{(p)}}{dz} = \left(\underline{K}^{(p)} + \underline{C}^{(p)} \underline{\beta}^{(p)} \right) \underline{a}^{(p)} \quad (7.4)$$

The definitions of the matrices for the inner waveguides are slightly different to the outer waveguides, because the inner guides are adjacent to two waveguides, whereas the outer guides are adjacent to one guide only.

Inner Waveguides $p \neq 1$ or N

The definitions for the matrices are

$$|\underline{a}^{(p)}|^2 = \underline{a}^{(p)} \underline{a}^{(p)*} \quad \underline{a}^{(p)} = \begin{pmatrix} a_{p-1} \\ a_p \\ a_{p+1} \end{pmatrix} \quad \underline{\underline{a}}^{(p)} = \begin{pmatrix} a_{p-1} & 0 & 0 \\ 0 & a_p & 0 \\ 0 & 0 & a_{p+1} \end{pmatrix} \quad (7.5)$$

$$\underline{K}^{(p)} = \begin{pmatrix} K_{p,p-1} & K_{p,p} & K_{p,p+1} \end{pmatrix} \quad \underline{K}_{NL}^{(p)} = \begin{pmatrix} K_{p,p-1}^{NL} & K_{p,p}^{NL} & K_{p,p+1}^{NL} \end{pmatrix} \quad (7.6)$$

$$\underline{Q}^{(p)} = \begin{pmatrix} Q_{p,p-1}^{(p-1)} & Q_{p,p}^{(p)} & Q_{p,p+1}^{(p+1)} \end{pmatrix} \quad \underline{C}^{(p)} = \begin{pmatrix} C_{p,p-1} & C_{p,p} & C_{p,p+1} \end{pmatrix} \quad (7.7)$$

$\underline{\beta}^{(p)}$ is the diagonal matrix

$$\underline{\beta}^{(p)} = \begin{pmatrix} \beta_{p-1} & 0 & 0 \\ 0 & \beta_p & 0 \\ 0 & 0 & \beta_{p+1} \end{pmatrix} \quad X^{(p)} = \begin{pmatrix} 0 & Q_{p-1,p}^{(p)} & Q_{p-1,p}^{(p+1)} \\ Q_{p-1,p-1}^{(p)} & 0 & Q_{p+1,p+1}^{(p)} \\ Q_{p+1,p}^{(p-1)} & Q_{p+1,p}^{(p)} & 0 \end{pmatrix} \quad (7.8)$$

$$\underline{A}^{(p)} = \begin{pmatrix} 0 & a_{p+1} & a_p \\ a_{p+1} & 0 & a_{p-1} \\ a_p & a_{p-1} & 0 \end{pmatrix} Q_{p+1,p-1}^{(p)} \quad (\text{note } A^{(1)} = A^{(N)} = 0) \quad (7.9)$$

The $A^{(p)}$ terms are very small, because they contain the tiny terms $Q_{p+1,p-1}^{(p)}$

For outer waveguides ($p=1$ or N)

The derivation for the outer waveguides follow directly from those of the inner guides. For example the definition for $\underline{K}^{(p)}$ above is $\underline{K}^{(p)} = \begin{pmatrix} K_{p,p-1} & K_{p,p} & K_{p,p+1} \end{pmatrix}$. If the guide under consideration is an outer guide, eg. if $p = 1$, then the $K_{p,p-1}$ term does not exist since the $(p - 1)$ 'th eigenmode (referred to in the subscript of $K_{p,p-1}$) does not exist. Therefore $\underline{K}^{(p)}$ becomes $\underline{K}^{(p)} = \begin{pmatrix} K_{p,p} & K_{p,p+1} \end{pmatrix}$. Similar argument can be also applied to the other definitions.

$$\underline{a}^{(1)} = \begin{pmatrix} a_1 \\ a_2 \end{pmatrix} \quad \underline{a}^{(N)} = \begin{pmatrix} a_{N-1} \\ a_N \end{pmatrix} \quad (7.10)$$

$$X^{(1)} = \begin{pmatrix} 0 & Q_{22}^{(1)} \\ Q_{21}^{(1)} & 0 \end{pmatrix} \quad X^{(N)} = \begin{pmatrix} 0 & Q_{N-1,N}^{(N)} \\ Q_{N-1,N-1}^{(N)} & 0 \end{pmatrix} \quad (7.11)$$

$$\underline{\beta}^{(1)} = \begin{pmatrix} \beta_1 & 0 \\ 0 & \beta_2 \end{pmatrix} \quad \underline{\beta}^{(N)} = \begin{pmatrix} \beta_{N-1} & 0 \\ 0 & \beta_N \end{pmatrix} \quad (7.12)$$

$$\underline{Q}^{(1)} = \begin{pmatrix} Q_{11}^{(1)} & Q_{12}^{(2)} \end{pmatrix} \quad \underline{Q}^{(N)} = \begin{pmatrix} Q_{N,N-1}^{(N-1)} & Q_{NN}^{(N)} \end{pmatrix} \quad (7.13)$$

$$\underline{C}^{(1)} = \begin{pmatrix} C_{11} & C_{12} \end{pmatrix} \quad \underline{C}^{(N)} = \begin{pmatrix} C_{N,N-1} & C_{NN} \end{pmatrix} \quad (7.14)$$

$$\underline{K}^{(1)} = \begin{pmatrix} K_{11} & K_{12} \end{pmatrix} \quad \underline{K}^{(N)} = \begin{pmatrix} K_{N,N-1} & K_{NN} \end{pmatrix} \quad (7.15)$$

$$\underline{K}_{NL}^{(1)} = \begin{pmatrix} K_{11}^{NL} & K_{12}^{NL} \end{pmatrix} \quad \underline{K}_{NL}^{(N)} = \begin{pmatrix} K_{N,N-1}^{NL} & K_{NN}^{NL} \end{pmatrix} \quad (7.16)$$

7.3 MATRIX FORM ASSUMING INTERACTION BETWEEN ALL THE GUIDES

Using the same procedure as in section 7.2.1, the following one line matrix formulation can be written down almost by inspection of eqn 6.24.

$$-jC \frac{da}{dz} = \left(C\underline{\underline{\beta}} + K + K^{NL} + Q|\underline{a}|^2 - Q^T + 2\underline{a}^T \underline{X} \underline{a}^* + \underline{a}^+ \underline{X} \underline{a} + \underline{a}^+ \underline{A} \right) \underline{a} \quad (7.17)$$

All-guide interaction- matrix form

Where the matrix definitions are

$$|\underline{a}|^2 = \underline{a} \underline{a}^* \quad \underline{a} = \begin{pmatrix} a_1 \\ a_2 \\ a_3 \\ \vdots \\ a_N \end{pmatrix} \quad \underline{\underline{a}} = \begin{pmatrix} a_1 & 0 & 0 & \dots & 0 \\ 0 & a_2 & 0 & \dots & 0 \\ 0 & 0 & a_3 & \dots & 0 \\ \dots & \dots & \dots & \dots & 0 \\ 0 & 0 & 0 & 0 & a_N \end{pmatrix} \quad (7.18)$$

$$\underline{X} = \begin{pmatrix} X^{(1)} \\ X^{(2)} \\ X^{(3)} \\ \vdots \\ X^{(N)} \end{pmatrix} \quad X^{(p)} = \begin{pmatrix} 0 & Q_{p1}^{(2)} & Q_{p1}^{(3)} & Q_{p1}^{(4)} & \dots & Q_{p1}^{(N)} \\ Q_{p2}^{(1)} & 0 & Q_{p2}^{(3)} & Q_{p2}^{(4)} & \dots & Q_{p2}^{(N)} \\ Q_{p3}^{(1)} & Q_{p3}^{(2)} & 0 & Q_{p3}^{(4)} & \dots & Q_{p3}^{(N)} \\ \dots & \dots & \dots & 0 & \dots & \dots \\ \dots & \dots & \dots & \dots & \dots & \dots \\ Q_{pN}^{(1)} & Q_{pN}^{(2)} & Q_{pN}^{(3)} & Q_{pN}^{(4)} & \dots & 0 \end{pmatrix} \quad (7.19)$$

$$K = \begin{pmatrix} K_{11} & K_{12} & K_{13} & \dots & K_{1N} \\ K_{21} & K_{22} & K_{23} & \dots & \dots \\ K_{31} & K_{32} & K_{33} & \dots & \dots \\ \dots & \dots & \dots & \dots & \dots \\ K_{N1} & K_{N2} & K_{N3} & \dots & K_{NN} \end{pmatrix} \quad Q = \begin{pmatrix} Q_{11}^{(1)} & Q_{12}^{(2)} & Q_{13}^{(3)} & \dots & Q_{1N}^{(N)} \\ Q_{21}^{(1)} & Q_{22}^{(2)} & Q_{23}^{(3)} & \dots & \dots \\ Q_{31}^{(1)} & Q_{32}^{(2)} & Q_{33}^{(3)} & \dots & \dots \\ \dots & \dots & \dots & \dots & \dots \\ Q_{N1}^{(1)} & Q_{N2}^{(2)} & Q_{N3}^{(3)} & \dots & Q_{NN}^{(N)} \end{pmatrix} \quad (7.20)$$

$$K^{NL} = \begin{pmatrix} K_{11}^{NL} & K_{12}^{NL} & K_{13}^{NL} & \cdots & K_{1N}^{NL} \\ K_{21}^{NL} & K_{22}^{NL} & K_{23}^{NL} & \cdots & \cdots \\ K_{31}^{NL} & K_{32}^{NL} & K_{33}^{NL} & \cdots & \cdots \\ \cdots & \cdots & \cdots & \cdots & \cdots \\ K_{N1}^{NL} & K_{N2}^{NL} & K_{N3}^{NL} & \cdots & K_{NN}^{NL} \end{pmatrix} \quad (7.21)$$

$$\underline{\underline{\beta}} = \begin{pmatrix} \beta_1 & 0 & 0 & \cdots & 0 \\ 0 & \beta_2 & 0 & \cdots & 0 \\ 0 & 0 & \beta_3 & \cdots & 0 \\ \cdots & \cdots & \cdots & \cdots & 0 \\ 0 & 0 & 0 & 0 & \beta_N \end{pmatrix} \quad C = \begin{pmatrix} C_{11} & C_{12} & C_{13} & \cdots & C_{1N} \\ C_{21} & C_{22} & C_{23} & \cdots & \cdots \\ C_{31} & C_{32} & C_{33} & \cdots & \cdots \\ \cdots & \cdots & \cdots & \cdots & \cdots \\ C_{N1} & C_{N2} & C_{N3} & \cdots & C_{NN} \end{pmatrix} \quad (7.22)$$

$$\underline{A} = \begin{pmatrix} A^{(1)} \\ A^{(2)} \\ A^{(3)} \\ \vdots \\ A^{(N)} \end{pmatrix} \quad A^{(p)} = \begin{pmatrix} 0 & A_{12}^{(p)} & A_{13}^{(p)} & \cdots & A_{1N}^{(p)} \\ A_{21}^{(p)} & 0 & A_{23}^{(p)} & \cdots & \cdots \\ A_{31}^{(p)} & A_{32}^{(p)} & 0 & \cdots & \cdots \\ \cdots & \cdots & \cdots & \cdots & \cdots \\ A_{N1}^{(p)} & A_{N2}^{(p)} & A_{N3}^{(p)} & \cdots & 0 \end{pmatrix} \quad (7.23)$$

$$A_{\ell m}^{(p)} = \sum_n S_{\ell mn}^{(p)} a_n (1 - \delta_{\ell n})(1 - \delta_{mn})(1 - \delta_{\ell m}) \quad (7.24)$$

The \underline{A} vector is very small (because it depends on the $S_{\ell mn}^{(p)}$ terms) and can be neglected. The definitions for \underline{A} (eqn. 7.23) and \underline{X} (eqn. 7.19) require further explanation. \underline{A} and \underline{X} are column vectors, where each element of the vector is an $N \times N$ matrix. The terms $2\underline{a}^T \underline{X} \underline{a}^* \underline{a}$, $\underline{a}^+ \underline{X} \underline{a} \underline{a}$, and $\underline{a}^+ \underline{A} \underline{a}$ in eqn. 7.17 must be expanded out with care: one should note that the \underline{a} and \underline{a}^* type matrices are treated as scalars by the \underline{X} and \underline{A} vectors (ie the whole vectors \underline{a} and matrices \underline{a} matrix multiply each element of \underline{X} and \underline{A}). Thus the first element of $2\underline{a}^T \underline{X} \underline{a}^* \underline{a}$ in eqn. 7.17 is $2\underline{a}^T X^{(1)} \underline{a}^* \underline{a}$, and the rest of the elements are

$$2\underline{a}^T \underline{X} \underline{a}^* \underline{a} = 2\underline{a}^T \begin{bmatrix} X^{(1)} \\ X^{(2)} \\ \vdots \\ X^{(N)} \end{bmatrix} \underline{a}^* \underline{a} = \begin{bmatrix} 2\underline{a}^T X^{(1)} \underline{a}^* \underline{a} \\ 2\underline{a}^T X^{(2)} \underline{a}^* \underline{a} \\ \vdots \\ 2\underline{a}^T X^{(N)} \underline{a}^* \underline{a} \end{bmatrix} \quad (7.25)$$

Eqn 7.25 is dimensionally correct since the result (the RHS) gives an $N \times 1$ column vector- referring to N coupled mode equations. Therefore dimensionally, the pre-

multiplied and the post-multiplied parts of eqn 7.25 become

$$(1 \times N) \begin{bmatrix} N \times N \\ N \times N \\ \vdots \\ N \times N \end{bmatrix} (N \times N)(N \times 1) = \begin{bmatrix} (1 \times N) \times N \times N \times (N \times N)(N \times 1) \\ (1 \times N) \times N \times N \times (N \times N)(N \times 1) \\ \vdots \\ (1 \times N) \times N \times N \times (N \times N)(N \times 1) \end{bmatrix} = [N \times 1] \quad (7.26)$$

7.3.1 Two guide coupler

The two guide case can now be written down by substituting $p = 1$ and $p = 2$ into eqn. 7.17.

When $p = 1$

$$\begin{aligned} -j \frac{da_1}{dz} - jC_{12} \frac{da_2}{dz} &= (C_{11}\beta_1 + K_{11} + K_{11}^{NL} + |a_1|^2 Q_{11}^{(1)} - Q_{11}^{(1)})a_1 \\ &+ (C_{12}\beta_2 + K_{12} + K_{12}^{NL} + |a_2|^2 Q_{12}^{(2)} - Q_{12}^{(1)})a_2 + (2a_1|a_2|^2 + a_2^2 a_1^*)Q_{11}^{(2)} + (2a_2|a_1|^2 + a_1^2 a_2^*)Q_{12}^{(1)} \end{aligned} \quad (7.27)$$

when $p = 2$

$$\begin{aligned} -j \frac{da_2}{dz} - jC_{21} \frac{da_1}{dz} &= (C_{21}\beta_1 + K_{21} + K_{21}^{NL} + |a_1|^2 Q_{21}^{(1)} - Q_{21}^{(2)})a_1 \\ &+ (C_{22}\beta_2 + K_{22} + K_{22}^{NL} + |a_2|^2 Q_{22}^{(2)} - Q_{22}^{(2)})a_2 + (2a_2|a_1|^2 + a_1^2 a_2^*)Q_{22}^{(1)} + (2a_1|a_2|^2 + a_2^2 a_1^*)Q_{21}^{(2)} \end{aligned} \quad (7.28)$$

Note that $Q_{11}^{(2)} \equiv Q_{22}^{(1)}$ in eqns. 7.27 and 7.28. These two equations can be compared with those derived in chapter 6 (ie eqns 6.10 and 6.11).

7.3.2 The three guide coupler

Similarly the three guide coupler can be written as (where no term has been neglected)

$$-jC_{11} \frac{da_1}{dz} - jC_{12} \frac{da_2}{dz} - jC_{13} \frac{da_3}{dz} = (C_{11}\beta_1 + K_{11} + K_{11}^{NL} + |a_1|^2 Q_{11}^{(1)} - Q_{11}^{(1)})a_1$$

$$\begin{aligned}
& + \left(C_{12}\beta_2 + K_{12} + K_{12}^{NL} + |a_2|^2 Q_{12}^{(2)} - Q_{12}^{(1)} \right) a_2 + \left(C_{13}\beta_3 + K_{13} + K_{13}^{NL} + |a_3|^2 Q_{13}^{(3)} - Q_{13}^{(1)} \right) a_3 \\
& + \left(2a_1|a_2|^2 + a_2^2 a_1^* \right) Q_{11}^{(2)} + \left(2a_1|a_3|^2 + a_3^2 a_1^* \right) Q_{11}^{(3)} + \left(2a_2|a_1|^2 + a_1^2 a_2^* \right) Q_{12}^{(1)} \\
& + \left(2a_2|a_3|^2 + a_3^2 a_2^* \right) Q_{12}^{(3)} + \left(2a_3|a_1|^2 + a_1^2 a_3^* \right) Q_{13}^{(1)} + \left(2a_3|a_2|^2 + a_2^2 a_3^* \right) Q_{13}^{(2)} + 2(a_1^* a_2 a_3 + a_2^* a_1 a_3 + a_3^* a_1 a_2) S_{123}^{(1)}
\end{aligned} \tag{7.29}$$

$$\begin{aligned}
& -jC_{21} \frac{da_1}{dz} - jC_{22} \frac{da_2}{dz} - jC_{23} \frac{da_3}{dz} = \left(C_{21}\beta_1 + K_{21} + K_{21}^{NL} + |a_1|^2 Q_{21}^{(1)} - Q_{21}^{(2)} \right) a_1 \\
& + \left(C_{22}\beta_2 + K_{22} + K_{22}^{NL} + |a_2|^2 Q_{22}^{(2)} - Q_{22}^{(1)} \right) a_2 + \left(C_{23}\beta_3 + K_{23} + K_{23}^{NL} + |a_3|^2 Q_{23}^{(3)} - Q_{23}^{(2)} \right) a_3 \\
& + \left(2a_1|a_2|^2 + a_2^2 a_1^* \right) Q_{22}^{(2)} + \left(2a_2|a_1|^2 + a_1^2 a_2^* \right) Q_{22}^{(1)} + \left(2a_3|a_1|^2 + a_1^2 a_3^* \right) Q_{23}^{(1)} \\
& + \left(2a_1|a_3|^2 + a_3^2 a_1^* \right) Q_{21}^{(3)} + \left(2a_2|a_3|^2 + a_3^2 a_2^* \right) Q_{22}^{(3)} + \left(2a_3|a_2|^2 + a_2^2 a_3^* \right) Q_{23}^{(2)} + 2(a_1^* a_2 a_3 + a_2^* a_1 a_3 + a_3^* a_1 a_2) S_{123}^{(2)}
\end{aligned} \tag{7.30}$$

$$\begin{aligned}
& -jC_{31} \frac{da_1}{dz} - jC_{32} \frac{da_2}{dz} - jC_{33} \frac{da_3}{dz} = \left(C_{31}\beta_1 + K_{31} + K_{31}^{NL} + |a_1|^2 Q_{31}^{(1)} - Q_{31}^{(3)} \right) a_1 \\
& + \left(C_{32}\beta_2 + K_{32} + K_{32}^{NL} + |a_2|^2 Q_{32}^{(2)} - Q_{32}^{(3)} \right) a_2 + \left(C_{33}\beta_3 + K_{33} + K_{33}^{NL} + |a_3|^2 Q_{33}^{(3)} - Q_{33}^{(1)} \right) a_3 \\
& + \left(2a_1|a_2|^2 + a_2^2 a_1^* \right) Q_{31}^{(2)} + \left(2a_2|a_1|^2 + a_1^2 a_2^* \right) Q_{32}^{(1)} + \left(2a_3|a_1|^2 + a_1^2 a_3^* \right) Q_{33}^{(1)} \\
& + \left(2a_1|a_3|^2 + a_3^2 a_1^* \right) Q_{31}^{(3)} + \left(2a_2|a_3|^2 + a_3^2 a_2^* \right) Q_{32}^{(3)} + \left(2a_3|a_2|^2 + a_2^2 a_3^* \right) Q_{33}^{(2)} + 2(a_1^* a_2 a_3 + a_2^* a_1 a_3 + a_3^* a_1 a_2) S_{123}^{(3)}
\end{aligned} \tag{7.31}$$

These equations can be compared with the adjacent guide interaction case of eqns 6.19-6.21.

7.4 LOSSLESS CASE: VIOLATION OF CONSERVATION OF POWER IN KEY PAPERS

In chapter 5 it was shown using reciprocity that the overlap integral must be removed from the equations in cases where the nonlinear coupling coefficients are not present (see explanations following eqn. 5.46). In this section we show that the equations of some key papers [5-12] which include this inconsistency may be breaking conservation

of power in the lossless case.

The proof is as follows. For a lossless coupler, the total time-averaged power is constant with distance (and proportional to $\underline{a}^+ C \underline{a}$) (see Appendix 6, and [13-14]) .

Therefore differentiating $\underline{a}^+ C \underline{a}$ with distance gives

$$\frac{\partial}{\partial z} (\underline{a}^+ C \underline{a}) = \frac{\partial \underline{a}^+}{\partial z} C \underline{a} + \underline{a}^+ C \frac{\partial \underline{a}}{\partial z} = 0 \quad (7.32)$$

Eqn 7.17 can be written down as

$$C \frac{d \underline{a}}{dz} = j \left[\left(C \underline{\underline{\beta}} + K + K^{NL} + Q |\underline{a}|^2 - Q^T \right) \underline{a} + 2 \underline{\underline{\ell}} + \underline{\underline{m}} + \underline{\underline{n}} \right] \quad (7.33)$$

where $\underline{\underline{\ell}}$, $\underline{\underline{m}}$, and $\underline{\underline{n}}$ are column vectors such that

$$\underline{\underline{\ell}} = \begin{bmatrix} \underline{a}^T X^{(1)} \underline{a}^* \underline{a} \\ \underline{a}^T X^{(2)} \underline{a}^* \underline{a} \\ \vdots \\ \underline{a}^T X^{(N)} \underline{a}^* \underline{a} \end{bmatrix} \quad \underline{\underline{m}} = \begin{bmatrix} \underline{a}^+ X^{(1)} \underline{a} \underline{a} \\ \underline{a}^+ X^{(2)} \underline{a} \underline{a} \\ \vdots \\ \underline{a}^+ X^{(N)} \underline{a} \underline{a} \end{bmatrix} \quad \underline{\underline{n}} = \begin{bmatrix} \underline{a}^+ A^{(1)} \underline{a} \\ \underline{a}^+ A^{(2)} \underline{a} \\ \vdots \\ \underline{a}^+ A^{(N)} \underline{a} \end{bmatrix} \quad (7.34)$$

It should be noted that the elements of $\underline{\underline{\ell}}$, $\underline{\underline{m}}$, and $\underline{\underline{n}}$ are scalars.

Taking the adjoint operation of eqn. 7.33 gives

$$\frac{d \underline{a}^+}{dz} C = -j \left[\underline{a}^+ \left(\underline{\underline{\beta}} C + K^+ + K^{NL^*} + |\underline{a}|^2 Q^+ - Q \right) + 2 \underline{\underline{\ell}}^+ + \underline{\underline{m}}^+ + \underline{\underline{n}}^+ \right] \quad (7.35)$$

Substituting eqns 7.33 and 7.35 into eqn 7.32 gives

$$\frac{\partial}{\partial z} (\underline{a}^+ C \underline{a}) = \frac{\partial \underline{a}^+}{\partial z} C \underline{a} + \underline{a}^+ C \frac{\partial \underline{a}}{\partial z} = 0 \quad (7.36)$$

$$= j \underline{a}^+ \left[\left(C \underline{\underline{\beta}} - \underline{\underline{\beta}} C \right) + (K - K^+) + (K^{NL} - K^{NL^*}) + \left(Q |\underline{a}|^2 - |\underline{a}|^2 Q^+ \right) + (Q - Q^T) \right] \underline{a} \quad (7.37)$$

$$+ 2j \left[\underline{a}^+ \underline{\underline{\ell}} - \underline{\underline{\ell}}^+ \underline{a} \right] + j \left[\underline{a}^+ \underline{\underline{m}} - \underline{\underline{m}}^+ \underline{a} \right] + j \left[\underline{a}^+ \underline{\underline{n}} - \underline{\underline{n}}^+ \underline{a} \right] \quad (7.38)$$

For weak coupling $C \underline{\underline{\beta}} = \underline{\underline{\beta}} C$, ie C must be a diagonal matrix (the identity matrix). In eqn. 7.37 $Q |\underline{a}|^2 = |\underline{a}|^2 Q^+$ occurs only as $Q \rightarrow \underline{\underline{Q}}$. Therefore this proves that the off-

diagonal elements of the Q matrix also disappear when the overlap integral is not present. In other words the nonlinear cross-phase-modulation terms (non-diagonal elements of Q) and the overlap integral are linked. To conserve power, the following can also be observed from lines 7.36-7.38.

$$K = K^+ \quad K^{NL} = K^{NL+} \quad (7.39)$$

$$Q \rightarrow \underline{\underline{Q}}_s \quad (7.40)$$

where
$$\underline{\underline{Q}}_s = \text{diag}[Q_{11}^{(1)}, Q_{22}^{(2)}, Q_{33}^{(3)}, \dots, Q_{NN}^{(N)}] \quad (7.41)$$

$$\underline{a}^+ \underline{\ell} = \underline{\ell}^+ \underline{a} \quad \underline{a}^+ \underline{n} = \underline{n}^+ \underline{a} \quad \underline{a}^+ \underline{m} = \underline{m}^+ \underline{a} \quad (7.42)$$

From line 7.42, it can be seen that $\underline{a}^+ \underline{\ell}$, $\underline{a}^+ \underline{m}$, and $\underline{a}^+ \underline{n}$ must be real, which proves that \underline{X} and $\underline{A}^{(p)}$ must be zero. The proof for the last sentence is as follows: For example, noting the definition for $\underline{\ell}$ from line 7.34, we observe that $\underline{a}^+ \underline{\ell}$ is a scalar (since \underline{a}^+ is a row vector, and $\underline{\ell}$ is a column vector containing scalar elements). Therefore the first element of $\underline{a}^+ \underline{\ell}$ becomes

$$a_1^+ \ell_1 = a_1^+ \underline{a}^T X^{(1)} \underline{\underline{a}}^* \underline{a} \quad (7.43)$$

$a_1^+ \ell_1 = \ell_1^+ a_1$ can be written as

$$a_1^+ \underline{a}^T X^{(1)} \underline{\underline{a}}^* \underline{a} = \underline{a}^+ \underline{\underline{a}} X^{(1)+} \underline{\underline{a}}^* a_1 \quad (7.44)$$

But $\underline{\underline{a}}^* \underline{a}$ on the LHS of eqn. 7.44 can be written as $\underline{\underline{a}} \underline{\underline{a}}^*$, and $\underline{a}^+ \underline{a}$ on the RHS as $\underline{a}^T \underline{\underline{a}}^*$. Therefore eqn 7.44 becomes

$$a_1^+ \underline{a}^T X^{(1)} \underline{\underline{a}} \underline{\underline{a}}^* = \underline{a}^T \underline{\underline{a}}^* X^{(1)+} \underline{\underline{a}}^* a_1 \quad (7.45)$$

Both sides are post-multiplied (ignoring scalars for the moment) by $\underline{\underline{a}}^*$, and pre-multiplied by \underline{a}^T . Therefore ignoring these, eqn. 7.45 becomes

$$a_1^+ X^{(1)} \underline{\underline{a}} = \underline{\underline{a}}^* X^{(1)+} a_1 \quad (7.46)$$

For eqn 7.46 to be true, a minimum prerequisite would be for $X^{(1)}$ to be diagonal, but

from the definition for $X^{(1)}$ (in section 7.3), we see that the diagonal elements are zero. Therefore $X^{(1)}$ must be zero. Similarly $X^{(2)}$, $X^{(3)}$, $\dots X^{(N)}$ and $A^{(1)}$, $A^{(2)}$, $\dots A^{(N)}$ should also be zero.

Therefore the coupled mode equation, eqn. 7.33 for weak coupling becomes

$$-j \frac{da}{dz} = \left(\underline{\beta} + K + K^{NL} + \underline{Q}_s |a|^2 - \underline{Q}_s \right) a \quad (7.47)$$

Papers which insist on including the other nonlinear terms in weak coupled mode theory are breaking power conservation.

7.5 CONCLUSIONS

The coupled mode equations derived in chapter 6 were reformulated in matrix form in this chapter. Both the all-guide and adjacent guide interaction cases were presented. It was also shown using power conservation arguments that it is inconsistent to include the nonlinear cross-coefficients without the overlap integral (and vice-versa).

REFERENCES

- [1] S-L Chuang, "A coupled-mode theory for multiwaveguide systems satisfying the reciprocity theorem and power conversation", *J. Light. Technol.*, vol. LT-5, no. 1, 1987, pp. 174-183.
- [2] A. Hardy and W. Streifer, "Coupled mode solutions of multiwaveguide systems", *IEEE J. Quant. Electron.*, vol. QE-22, no. 4, 1986, pp. 528-534.
- [3] A. Hardy and W. Streifer, "Coupled modes of multiwaveguide systems and phased arrays", *J. Light. Technol.*, vol. LT-4, no. 1, 1986, pp. 90-99.
- [4] L. Bostock, S. Chandler, and C. Rourke, "Further pure mathematics", Stanley Thornes (Publishers) Ltd, 1985
- [5] S. M. Jensen, "The nonlinear coherent coupler", *IEEE Transactions on Microwave Theory and Techniques*, MTT-30, no. 10, 1982, pp. 1568-1571.
- [6] F. J. Fraile-Pelaez and G. Assanto, "Coupled-mode equations for nonlinear directional couplers", *Applied Optics*, vol. 29, no. 15, 1990, pp. 2216-2217.
- [7] A. Ankiewicz and G-D Peng, *J. Opt. Soc. Am. B*, vol. 9, 1992, pp. 1341.
- [8] A. Ankiewicz, "Interaction coefficient in detuned nonlinear couplers", *Optics Commun.*, vol. 66, no. 5,6, 1988, pp. 311-314.
- [9] A. Ankiewicz, "Novel effects in non-linear coupling", *Optics and Quant Electron.*, vol. 20, 1988, pp. 329-337.
- [10] X. Meng and N. Okamoto, "Improved coupled-mode theory for Nonlinear Directional Couplers", *IEEE J. Quant. Electron.*, Vol 27, No.5, May 1991, pp. 1175-1181
- [11] C. Schmidt-Hattenberger, U. Trutschel, and F. Lederer, "Nonlinear switching in multiple-core couplers", *Optics Letters*, vol. 16, no. 5, 1991, pp. 294-296.
- [12] C. Mapalagama and R. T. Deck, *J. Opt. Soc. Am. B*, vol. 9, no. 12, 1992, pp. 2258.
- [13] H. A. Haus and W. Huang, "Coupled mode theory", *Proc. IEEE*, vol. 79, no. 10, 1991, pp. 1505-1518.
- [14] H. Haus, W. P. Huang, S. Kawakami, and N. A. Whitaker, "Coupled-mode theory of optical waveguides", *J. Light. Technol.*, vol. LT-5, no. 1, 1987, pp. 16-23.

CHAPTER 8

BEAM PROPAGATION METHOD AND COUPLED MODE THEORY PROGRAMS

8.1 INTRODUCTION

In this chapter the numerical methods used in the rest of the thesis are discussed. In particular the beam propagation method (BPM) algorithm is explained in section 8.2. BPM will be used to check the accuracy of the nonlinear coupled mode equations (developed in chapters 6 and 7), as well to study the stability of nonlinear guided waves in chapter 10, and soliton emission and couplers in chapter 13. In section 8.3 the full form of the two guide nonlinear coupled mode equations are prepared in a form which allows them to be numerically solved using Runge-Kutta integration.

8.2 BEAM PROPAGATION METHOD ALGORITHM

8.2.1 Introduction

The beam propagation method (BPM) [1-6] is a numerical tool used to study wave propagation in optical devices. In addition to being very accurate, it is also convenient because it aids the visualisation of wave propagation in complicated structures without resorting to involved mathematics. BPM was first proposed by Feit and Fleck [1-5,7], and later applied to nonlinear directional couplers (NLDCs) by Thylén [8-10]. It is used in this thesis mainly to check the accuracy of the nonlinear coupled mode equations. Useful reviews of BPM can be found in [6,9,11-12].

The idea behind BPM is as follows: a beam of light propagating through an optical structure (eg a waveguide) is subject to two effects. The first is due to diffraction which occurs because of the wave nature of light. The second is focusing and is due to parts of the field propagating through high index media (eg film regions of waveguides). These parts of the field become phase-shifted with respect to the other parts. A curved phase-front then develops across the field in the high index regions, leading to focusing of the field in those regions. High index regions therefore act as local lenses for the field. The two effects of diffraction and focusing should, in practical devices, act simultaneously and continuously on the field throughout the propagation. However, in order to model the real case in a computer simulation, it is necessary to separate the effects and apply them sequentially. The device is therefore divided (computationally) into many longitudinal sections. Throughout each section the field propagates as though

diffraction were the only effect occurring. The lens effect is only introduced at one point in the middle of each section (as an infinitely thin sheet). This procedure is repeated for all the other sections sequentially. If the section lengths are reduced to small values, the diffraction and lens effects appear to occur continuously throughout the length of the device just as in real life.

Mathematically, the wave equation is numerically integrated in such a way that the diffraction and lens effects are integrated separately. One approach is the Feit and Fleck method [1-5,7], which is more accurate than paraxial methods [1,13]. In both cases the diffraction step can be calculated using the fast fourier transform (FFT). Finite difference (FD) methods are slightly less accurate than FFT but much faster (with parallel processing the calculations can be speeded up even further [14-16]).

In this thesis the Feit and Fleck method is chosen because of its ease of implementation, high speed, and reasonably good accuracy.

8.2.2 The beam propagation method algorithm

The method used in this section follows that of Feit and Fleck [7]. The wave equation, assuming no variation of the field in the y-direction is

$$\frac{\partial^2 E}{\partial x^2} + \frac{\partial^2 E}{\partial z^2} + \frac{\omega^2}{c^2} n^2 E = 0 \quad (8.1)$$

where n is the refractive index, and E the electric field. The equation can be simplified by using the operators P and Q [7,14] defined as

$$P = \frac{\partial}{\partial z} \text{ and } Q = \left(\nabla_{\perp}^2 + \frac{\omega^2}{c^2} n^2 \right)^{1/2} \quad (8.2)$$

where $\nabla_{\perp}^2 = \frac{\partial^2}{\partial x^2}$. Therefore eqn. 8.1 can be shortened to $(P^2 + Q^2)E = 0$, which can be factorised in the following way [14]

$$[(P + jQ)(P - jQ) + j(PQ - QP)]E = 0 \quad (8.3)$$

Provided that there are no sudden variations in the refractive index along the z-direction, one can assume that $PQ = QP$ in eqn. 8.3 [7]. Substituting the definition for P from eqn. 8.2 and solving eqn. 8.3 gives

$$E(x, \Delta z) = e^{\pm j \left(\nabla_{\perp}^2 + \frac{\omega^2}{c^2} n^2 \right)^{1/2} \Delta z} E(x, 0) \quad (8.4)$$

In eqn 8.4 the exponential term is an operator acting on the input field $E(x, 0)$ to a section (of length Δz), to transform it into the output field $E(x, \Delta z)$. It carries the information regarding the diffraction and lens effects. To split the two effects, the exponent of the operator can be rearranged with the aid of the following exact identity [17]

$$(1 + \mu)^{1/2} = 1 + \frac{\mu}{1 + (1 + \mu)^{1/2}} \quad (8.5)$$

which when used in eqn 8.4 leads to

$$E(x, \Delta z) = e^{\pm j \Delta z \left(\frac{\omega n}{c} + \frac{\nabla_{\perp}^2}{\frac{\omega n}{c} + \left(\frac{\omega^2 n^2}{c^2} + \nabla_{\perp}^2 \right)^{1/2}} \right)} E(x, 0) \quad (8.6)$$

The first term in the exponent of the exponential in eqn. 8.6 includes only the refractive index, and so describes the lens action. The second term contains ∇_{\perp}^2 and refers to diffraction. To keep this second term as entirely diffractive, the material is assumed to be homogeneous. Therefore n is replaced with a constant ('background') refractive index n_0 (ie. the refractive index of the cladding at negligible intensity). It should also be noted that paraxial methods diverge here from Feit and Fleck method by neglecting ∇_{\perp}^2 from the denominator of this second term. The first term in the exponent in eqn. 8.6 can be expressed as $\omega n/c = k + k(n/n_0 - 1)$, where $k = \omega n_0/c$. Therefore eqn. 8.6 becomes

$$E(x, \Delta z) = e^{\pm j \Delta z \left[k + k \left(\frac{n}{n_0} - 1 \right) + \frac{\nabla_{\perp}^2}{k + (k^2 + \nabla_{\perp}^2)^{1/2}} \right]} E(x, 0) \quad (8.7)$$

which is in a form where the lens and diffraction effects are separated. The exponent can now be simplified still further. The first term in the exponent (ie. k) can be removed by substituting $E(x, \Delta z) = \mathcal{E}(x, \Delta z) e^{jk\Delta z}$, and the second term condensed to χ where $\chi = k(n/n_0 - 1)$. Moreover if forward travelling waves are considered only (ie. '+' sign), eqn. 8.7 then becomes

$$\mathcal{E}(x, \Delta z) = e^{j\Delta z \left[\chi + \frac{\nabla_{\perp}^2}{k + (k^2 + \nabla_{\perp}^2)^{1/2}} \right]} \mathcal{E}(x, 0) \quad (8.8)$$

Eqn. 8.8 can be written in the symmetrised split-operator form to second order in Δz [2,8]

$$\mathcal{E}(x, \Delta z) = \exp \left\{ j \frac{\Delta z}{2} \left[\frac{\nabla_{\perp}^2}{k + (k^2 + \nabla_{\perp}^2)^{1/2}} \right] \right\} \exp(j\Delta z \chi) \exp \left\{ j \frac{\Delta z}{2} \left[\frac{\nabla_{\perp}^2}{k + (k^2 + \nabla_{\perp}^2)^{1/2}} \right] \right\} \mathcal{E}(x, 0) \quad (8.9)$$

In conclusion the single exponential operator of eqn. 8.8 has been split here into three operators. The operators act from right to left on $\mathcal{E}(x, 0)$. The input field is taken through a diffraction step for half a section $\Delta z/2$. The lens effect (the middle operator) is then inserted as a single sheet. The lens sheet incorporates information regarding the waveguides and the nonlinearities. Finally the field is taken through another half-section diffraction step (the left hand operator in eqn 8.9).

Computational implementation of the lens step is straightforward- it is just a multiplication term. However, the diffraction steps contain the ∇_{\perp}^2 operator, and are therefore not yet in a computable form. Ignoring the lens step in eqn. 8.9 for now, the diffraction for a length $\Delta z/2$ is

$$\mathcal{E} \left(x, \frac{\Delta z}{2} \right) = \exp \left\{ j \frac{\Delta z}{2} \left[\frac{\nabla_{\perp}^2}{k + (k^2 + \nabla_{\perp}^2)^{1/2}} \right] \right\} \mathcal{E}(x, 0) \quad (8.10)$$

where $\mathcal{E}(x, 0)$ is the input field to the half section, and $\mathcal{E} \left(x, \frac{\Delta z}{2} \right)$ the output field from the half-section. To allow the ∇_{\perp}^2 operator to be computable one can work in the fourier domain. Therefore substituting

$$\mathcal{E}(x, z) = \sum_{m=-N/2+1}^{N/2} \mathcal{E}_m(z) \exp[j\mathcal{K}_m x] \quad (8.11)$$

where $\mathcal{E}_m(z)$ is the field amplitude in the fourier domain, and N the number of points, with \mathcal{K}_m defined as $\mathcal{K}_m = 2\pi m/L_x$ where L_x is the length of the window in the transverse x -direction. Eqn. 8.10 becomes

$$\mathcal{E}_m\left(\frac{\Delta z}{2}\right) = \exp\left\{-j\frac{\Delta z}{2}\left[\frac{\mathcal{K}_m^2}{k + (k^2 - \mathcal{K}_m^2)^{1/2}}\right]\right\}\mathcal{E}_m(0) \quad (8.12)$$

This equation can now be used to calculate the output field.

8.2.3 The computer model

The BPM program was written in Fortran. The calculation part of the program is outlined in Fig. 8.1. As can be seen from the figure, the optical structure is divided into many longitudinal sections of length Δz (shown here to be separated by vertical dotted lines). In the middle of each section the lens effect due to the waveguides and nonlinearities is inserted (shown by the vertical solid lines). When two sections meet back to back, it can be seen that two half-section diffraction steps join together to form a full-section diffraction step. Therefore the half-step diffraction sections in eqn. 8.9 are more important in theory than in practice. Only the first and last diffraction steps are needed to be half-sections. The other steps are in practice full-sections.

A window size of length L_x is chosen. The input field is discretised in the x -direction into N sections. To propagate the field for the first half-section diffraction step, eqn. 8.12 is used. The input field is first transformed to the Fourier domain, using FFT. It is then multiplied by the exponential in eqn. 8.12 (care must be taken in the definition of \mathcal{K}_m since the FFT transformation (NAG routine C06FCF) rearranges the field in the Fourier domain). Finally an inverse FFT reverts the output field back into the spatial domain. The lens action is next applied using the $\exp(j\Delta z\chi)$ operator (noting that the refractive index is intensity dependent in χ). This procedure is repeated for all the sections, with the full-section diffraction steps, using Δz instead of $\Delta z/2$ in eqn. 8.12.

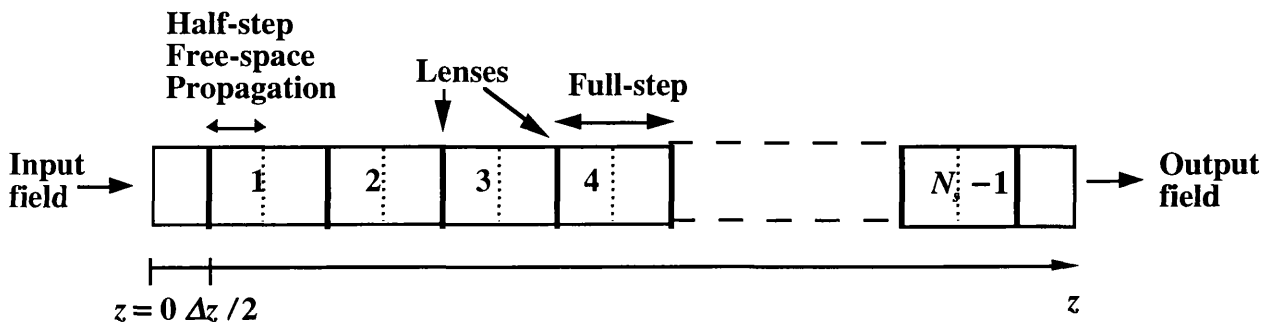


Fig. 8.1 Illustrating the BPM algorithm

8.2.4 Optimising the BPM program

The window size is first optimised. The window should be large enough to allow room for all the interactions to occur, ie the window edges should be situated where the field is negligible. However the window size cannot be too large because the reduced density of the nodes would lead to a reduced accuracy. Increasing the number of nodes at this point to restore the density, would slow the computation time down. In our program we chose a window size consisting of the length of the structure in the x -direction plus $8.0\mu\text{m}$ leeway on either side.

The number of nodes N is chosen such that the results are not altered when N is changed (note that N has to be a power of 2 for the FFT routine to be efficient). It was found by experimentation that for a window size of around $25\mu\text{m}$, $N = 256, 512, 1024, 2048$ etc gave similar results independent of the value for N . Below 256 points, the results could not be trusted because they depended on the value of N . $N = 1024$ was chosen as a safe measure.

The longitudinal section lengths (step size) was found in a similar way. The correct step size should be in the range such that the results are not altered by changing the step size. For a directional coupler, step sizes below $1.0\mu\text{m}$ gave similar results, whereas in the case of soliton generation smaller section lengths, eg $0.1\mu\text{m}$, were necessary.

The program runs reasonably fast. One run of 20000 sections takes approximately 14 minutes on our computer.

8.2.5 The input field to NLDC

In order to use the BPM program to study the coupling mechanism in the NLDC, any change in the field shape must be due to the coupling, and not due to its non-modal nature. Therefore it is necessary to excite the NLDC with the exact nonlinear (intensity dependent) eigenmode. To generate the nonlinear eigenmode two choices seem available. One is to calculate the nonlinear mode analytically using the method of chapter 10. Another is to connect a lead-in guide to the NLDC and excite it with a linear TE_0 mode (see chapter 9). The idea is for the lead-in guide to convert the linear mode to a nonlinear mode before it reaches the NLDC.

The feasibility of the lead-in guide approach for mode generation was tested first of all. A linear TE_0 mode was used to excite a nonlinear waveguide composed of a linear film and nonlinear cladding on one side. However, a stable and stationary mode did not arise even after large propagation distances (see Fig. 8.2). The field wobbled as it propagated, even at low powers.

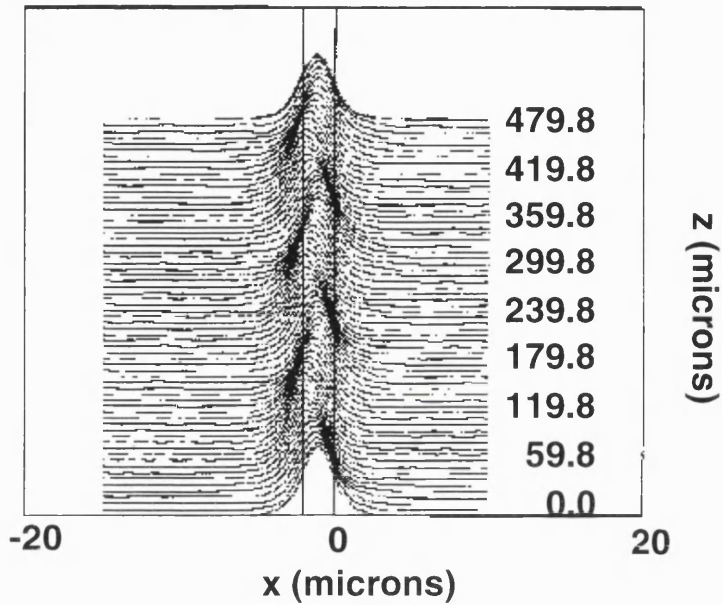


Fig. 8.2. Exciting the guide with a non-modal field shape (linear TE mode) (input power=70 Watts/m).

As the power was increased we observed that solitons were generated from the film into the nonlinear cladding (see Fig. 8.3).

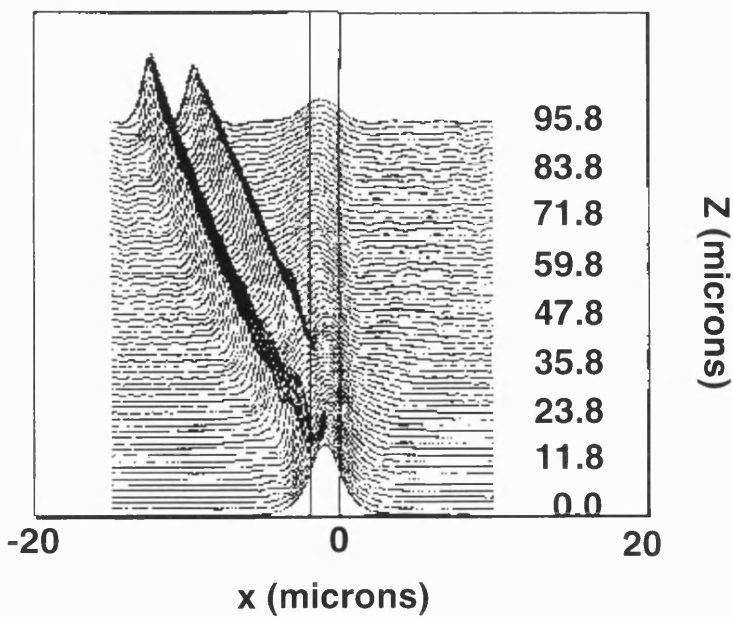


Fig. 8.3 Multisoliton generation occurs at high powers(300 Watts/m)

In conclusion a stable and stationary nonlinear eigenmode could not be generated for the NLDC by using a lead-in guide (unless the lead-in guide has *graded* nonlinearity-see chapter 13). Using the method outlined in chapter 10, we calculated the exact nonlinear eigenmode and used it to excite the isolated guide. We observed that the field remained steady and there were no wobbles or soliton generation, even at high input powers. (see Fig. 8.4)

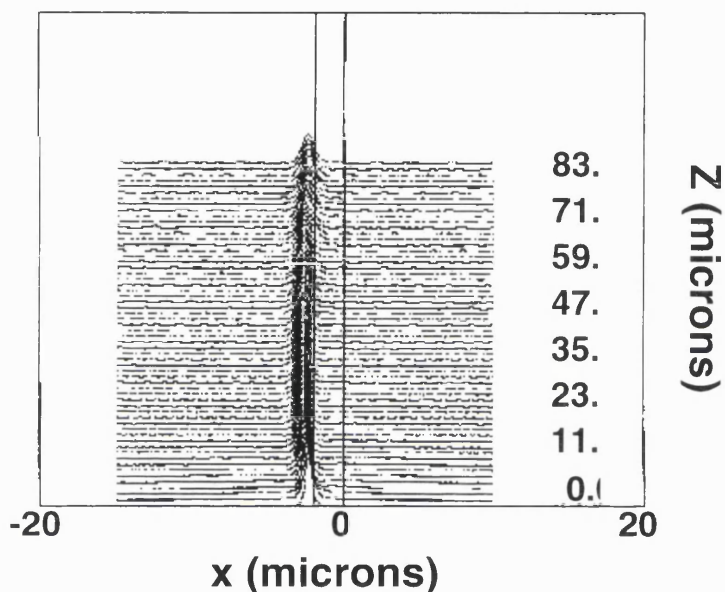


Fig. 8.4 Exciting the guide with the correct nonlinear TE mode (input power= 300 Watts/m)

8.2.6 Absorbing edges

At high powers there might be some radiated energy formed which then travel to the edges of the windows. There, instead of moving out of the window edges, as would occur in real life, these radiation are either reflected from the window edges or move out of one window edge, only to appear from the other window edge. These radiation then accumulate within the window boundaries and start to interfere with the propagating wave. Similar problems occur when solitons are generated. One way to avoid the problem (see Marcuse [12]), is to insert thin absorbing layers on the edges of the windows, so that waves reaching the windows would not be able to reenter the region within the window boundaries. The absorbing layers can be implemented by adding a small positive imaginary part to the refractive index in these regions. The exact value for this imaginary part is important and was found by trial and error. We found

that if the absorption was too high, then there was no improvement and the soliton was reflected from the absorption layer. If the value for the absorption was too small however, the soliton was not attenuated enough, and still reflected from the side of the window. By trial and error, we found that the value for the imaginary refractive index was around $3.5 \times 10^{-2} j$.

8.3 RUNGE-KUTTA SOLUTION OF COUPLED MODE EQUATIONS

8.3.1 Introduction

The coupled mode equations of chapter 7, can either be solved analytically or numerically. The analytical solution is considerably more difficult than the numerical solution especially if the overlap integral is included (see chapter 11). In order to solve the equations numerically, a similar approach to the BPM approach can be taken. Here the NLDC is divided into short longitudinal sections (we found 300 was adequate). The material is assumed to be linear in each section, so that the linear coupled mode equations can be solved using Runge-Kutta. The nonlinearity is introduced between the sections, and the propagation and coupling coefficients adjusted accordingly. The coupled mode equations first need to be transformed into a form which can be solved via Runge-Kutta. Studying eqn. 7.17, it can be seen that one problem is the overlap integral on the LHS of the equation making things difficult. Therefore pre-multiplying both sides of eqn. 7.17 by C^{-1} and expanding out for the two waveguide case, using the matrix definitions in eqns 7.18-7.24.

$$\begin{aligned}
 -j \frac{d}{dz} \begin{pmatrix} a_1 \\ a_2 \end{pmatrix} &= \begin{pmatrix} \beta_1 & 0 \\ 0 & \beta_2 \end{pmatrix} + \\
 &\frac{1}{1-C_{12}^2} \begin{pmatrix} 1 & -C_{12} \\ -C_{21} & 1 \end{pmatrix} \begin{pmatrix} K_{11} & K_{12} \\ K_{21} & K_{22} \end{pmatrix} + \\
 &\frac{1}{1-C_{12}^2} \begin{pmatrix} 1 & -C_{12} \\ -C_{21} & 1 \end{pmatrix} \begin{pmatrix} K_{11}^{NL} & K_{12}^{NL} \\ K_{21}^{NL} & K_{22}^{NL} \end{pmatrix} + \\
 &\frac{1}{1-C_{12}^2} \begin{pmatrix} 1 & -C_{12} \\ -C_{21} & 1 \end{pmatrix} \begin{pmatrix} Q_{11}^{(1)} & Q_{12}^{(2)} \\ Q_{21}^{(1)} & Q_{22}^{(2)} \end{pmatrix} \begin{pmatrix} |a_1|^2 & 0 \\ 0 & |a_2|^2 \end{pmatrix} + \\
 &\frac{-1}{1-C_{12}^2} \begin{pmatrix} 1 & -C_{12} \\ -C_{21} & 1 \end{pmatrix} \begin{pmatrix} Q_{11}^{(1)} & Q_{21}^{(1)} \\ Q_{12}^{(2)} & Q_{22}^{(2)} \end{pmatrix} + \\
 \Rightarrow &\frac{2}{1-C_{12}^2} \begin{pmatrix} 1 & -C_{12} \\ -C_{21} & 1 \end{pmatrix} \begin{pmatrix} a_1 & a_2 \\ a_1 & a_2 \end{pmatrix} \begin{pmatrix} 0 & Q_{11}^{(2)} \\ Q_{12}^{(1)} & 0 \end{pmatrix} \begin{pmatrix} a_1^* & 0 \\ 0 & a_2^* \end{pmatrix} + \\
 &\frac{1}{1-C_{12}^2} \begin{pmatrix} 1 & -C_{12} \\ -C_{21} & 1 \end{pmatrix} \begin{pmatrix} a_1^* & a_2^* \\ a_1^* & a_2^* \end{pmatrix} \begin{pmatrix} 0 & Q_{11}^{(2)} \\ Q_{12}^{(1)} & 0 \end{pmatrix} \begin{pmatrix} a_1 & 0 \\ 0 & a_2 \end{pmatrix} \\
 &\begin{pmatrix} 0 & Q_{21}^{(2)} \\ Q_{21}^{(1)} & 0 \end{pmatrix} \begin{pmatrix} a_1^* & 0 \\ 0 & a_2^* \end{pmatrix} + \\
 &\begin{pmatrix} 0 & Q_{21}^{(2)} \\ Q_{21}^{(1)} & 0 \end{pmatrix} \begin{pmatrix} a_1 & 0 \\ 0 & a_2 \end{pmatrix} \end{pmatrix} \begin{pmatrix} a_1 \\ a_2 \end{pmatrix} \quad (8.13)
 \end{aligned}$$

Multiplying out the matrices now gives

$$\Rightarrow -j \frac{d}{dz} \begin{pmatrix} a_1 \\ a_2 \end{pmatrix} = \begin{pmatrix} \left(\beta_1 & 0 \\ 0 & \beta_2 \right) + \frac{1}{1-C_{12}^2} \begin{pmatrix} K_{11} - C_{12}K_{21} & K_{12} - C_{12}K_{22} \\ K_{21} - C_{21}K_{11} & K_{22} - C_{21}K_{12} \end{pmatrix} + \frac{1}{1-C_{12}^2} \begin{pmatrix} K_{11}^{NL} - C_{12}K_{21}^{NL} & K_{12}^{NL} - C_{12}K_{22}^{NL} \\ K_{21}^{NL} - C_{21}K_{11}^{NL} & K_{22}^{NL} - C_{21}K_{12}^{NL} \end{pmatrix} + \frac{-1}{1-C_{12}^2} \begin{pmatrix} Q_{11}^{(1)} - C_{12}Q_{12}^{(2)} & Q_{21}^{(1)} - C_{12}Q_{22}^{(2)} \\ Q_{12}^{(2)} - C_{21}Q_{11}^{(1)} & Q_{22}^{(2)} - C_{21}Q_{21}^{(1)} \end{pmatrix} + \frac{1}{1-C_{12}^2} \begin{pmatrix} |a_1|^2(Q_{11}^{(1)} - C_{12}Q_{21}^{(1)}) & |a_2|^2(Q_{12}^{(2)} - C_{12}Q_{22}^{(2)}) \\ |a_1|^2(Q_{21}^{(1)} - C_{21}Q_{11}^{(1)}) & |a_2|^2(Q_{22}^{(2)} - C_{21}Q_{12}^{(2)}) \end{pmatrix} + \frac{2}{1-C_{12}^2} \begin{pmatrix} a_1^* a_2 (Q_{12}^{(1)} - C_{12}Q_{22}^{(1)}) & a_1 a_2^* (Q_{11}^{(2)} - C_{12}Q_{21}^{(2)}) \\ a_1^* a_2 (Q_{22}^{(1)} - C_{21}Q_{12}^{(1)}) & a_1 a_2^* (Q_{21}^{(2)} - C_{21}Q_{11}^{(2)}) \end{pmatrix} + \frac{1}{1-C_{12}^2} \begin{pmatrix} a_1 a_2^* (Q_{12}^{(1)} - C_{12}Q_{22}^{(1)}) & a_1^* a_2 (Q_{11}^{(2)} - C_{12}Q_{21}^{(2)}) \\ a_1 a_2^* (Q_{22}^{(1)} - C_{21}Q_{12}^{(1)}) & a_1^* a_2 (Q_{21}^{(2)} - C_{21}Q_{11}^{(2)}) \end{pmatrix} \end{pmatrix} \begin{pmatrix} a_1 \\ a_2 \end{pmatrix} \quad (8.14)$$

It can be seen from eqn 8.14 that the terms in the leading diagonal contribute to the nonlinear propagation coefficient (β^{NL}), and the off-diagonal elements contribute to the nonlinear coupling coefficient (K_{pq}^{NL}). So, the coupled mode equations can be expressed as

$$-j \frac{da_1(z)}{dz} = \beta_1^{NL}(z)a_1(z) + K_{12}^{NL}(z)a_2(z) \quad (8.15)$$

$$-j \frac{da_2(z)}{dz} = \beta_2^{NL}(z)a_2(z) + K_{21}^{NL}(z)a_1(z) \quad (8.16)$$

where β_1^{NL} , β_2^{NL} , K_{12}^{NL} , and K_{21}^{NL} are defined as

$$\beta_1^{NL} = \beta_1 + \frac{1}{1-C_{12}C_{21}}(K_{11} - C_{12}K_{21}) + \frac{1}{1-C_{12}C_{21}}(K_{11}^{NL} - C_{12}K_{21}^{NL}) + \frac{|a_1|^2}{1-C_{12}C_{21}}(Q_{11}^{(1)} - C_{12}Q_{21}^{(1)})$$

$$\frac{-1}{1-C_{12}C_{21}}(Q_{11}^{(1)} - C_{12}Q_{12}^{(2)}) + \frac{2a_1^* a_2}{1-C_{12}C_{21}}(Q_{12}^{(1)} - C_{12}Q_{22}^{(1)}) + \frac{a_1 a_2^*}{1-C_{12}C_{21}}(Q_{12}^{(1)} - C_{12}Q_{22}^{(1)}) \quad (8.17)$$

$$\beta_2^{NL} = \beta_2 + \frac{1}{1 - C_{12}C_{21}}(K_{22} - C_{21}K_{12}) + \frac{1}{1 - C_{12}C_{21}}(K_{22}^{NL} - C_{21}K_{12}^{NL}) + \frac{|a_2|^2}{1 - C_{12}C_{21}}(Q_{22}^{(2)} - C_{21}Q_{12}^{(2)}) +$$

$$\frac{-1}{1 - C_{12}C_{21}}(Q_{22}^{(2)} - C_{21}Q_{21}^{(1)}) + \frac{2a_1a_2^*}{1 - C_{12}C_{21}}(Q_{21}^{(2)} - C_{21}Q_{11}^{(2)}) + \frac{a_1^*a_2}{1 - C_{12}C_{21}}(Q_{21}^{(2)} - C_{21}Q_{11}^{(2)})$$
(8.18)

$$K_{12}^{NL} = \frac{1}{1 - C_{12}C_{21}}(K_{12} - C_{12}K_{22}) + \frac{1}{1 - C_{12}C_{21}}(K_{12}^{NL} - C_{12}K_{22}^{NL}) + \frac{|a_2|^2}{1 - C_{12}C_{21}}(Q_{12}^{(2)} - C_{12}Q_{22}^{(2)}) +$$

$$-\frac{1}{1 - C_{12}C_{21}}(Q_{21}^{(1)} - C_{12}Q_{22}^{(2)}) + \frac{2a_1a_2^*}{1 - C_{12}C_{21}}(Q_{11}^{(2)} - C_{12}Q_{21}^{(2)}) + \frac{a_1^*a_2}{1 - C_{12}C_{21}}(Q_{11}^{(2)} - C_{12}Q_{21}^{(2)})$$
(8.19)

$$K_{21}^{NL} = \frac{1}{1 - C_{12}C_{21}}(K_{21} - C_{21}K_{11}) + \frac{1}{1 - C_{12}C_{21}}(K_{21}^{NL} - C_{21}K_{11}^{NL}) + \frac{|a_1|^2}{1 - C_{12}C_{21}}(Q_{21}^{(1)} - C_{21}Q_{11}^{(1)}) +$$

$$-\frac{1}{1 - C_{12}C_{21}}(Q_{12}^{(2)} - C_{21}Q_{11}^{(1)}) + \frac{2a_1^*a_2}{1 - C_{12}C_{21}}(Q_{22}^{(1)} - C_{21}Q_{12}^{(1)}) + \frac{a_1a_2^*}{1 - C_{12}C_{21}}(Q_{22}^{(1)} - C_{21}Q_{12}^{(1)})$$
(8.20)

noting that β_1 and β_2 refer to the nonlinear propagation coefficients for the isolated guides. It is interesting to note here that although the nonlinear propagation coefficients (eqns. 8.17 and 8.18) are complex quantities, the two differential equations (8.15 and 8.17) still satisfy power conservation (see chapter 7).

To solve eqns. 8.15 and 8.16 using Runge-Kutta, we have to first eliminate $\beta_1^{NL}a_1$ and $\beta_2^{NL}a_2$ terms (to decouple the equations), ie substitute $a_1(z) = A_1(z)e^{j\beta_1^{NL}(z)z}$, and $a_2(z) = A_2(z)e^{j\beta_2^{NL}(z)z}$, where $A_1(z)$ and $A_2(z)$ are complex amplitudes.

In addition the Runge-Kutta (R-K) method (NAG routine D02BBF) requires everything to be in terms of real functions. Therefore $A_1(z)$ and $A_2(z)$ can be split into real modulus and phase form as follows

$$A_1(z) = A_{1r}(z)e^{j\varphi_1(z)} \quad A_2(z) = A_{2r}(z)e^{j\varphi_2(z)} \quad (8.21)$$

where $A_{1r}(z)$, $A_{2r}(z)$, $\varphi_1(z)$, and $\varphi_2(z)$ are all real quantities. Substituting $a_1(z) = A_{1r}(z)e^{j(\varphi_1(z) + \beta_1^{NL}(z)z)}$, and $a_2(z) = A_{2r}(z)e^{j(\varphi_2(z) + \beta_2^{NL}(z)z)}$ into eqns. 8.15 and 8.16

and simplifying gives

$$-j \frac{dA_{1r}(z)}{dz} + A_{1r}(z) \left(\frac{d\varphi_1(z)}{dz} + z \frac{d\beta_1^{NL}(z)}{dz} \right) = K_{12}^{NL}(z) A_{2r}(z) e^{j[\varphi_2(z) - \varphi_1(z) + (\beta_2^{NL}(z) - \beta_1^{NL}(z))z]} \quad (8.22)$$

and

$$-j \frac{dA_{2r}(z)}{dz} + A_{2r}(z) \left(\frac{d\varphi_2(z)}{dz} + z \frac{d\beta_2^{NL}(z)}{dz} \right) = K_{21}^{NL}(z) A_{1r}(z) e^{j[\varphi_1(z) - \varphi_2(z) + (\beta_1^{NL}(z) - \beta_2^{NL}(z))z]} \quad (8.23)$$

Eqns. 8.22 and 8.23 still contain complex terms. Therefore taking the real and imaginary parts, results in four equations, which can be solved using R-K method.

$$\begin{aligned} \frac{d\varphi_1(z)}{dz} &= -z \operatorname{Re} \left(\frac{d\beta_1^{NL}(z)}{dz} \right) + \operatorname{Re} \left(K_{12}^{NL}(z) \right) \frac{A_{2r}(z)}{A_{1r}(z)} \operatorname{Re} \left[e^{j[\varphi_2(z) - \varphi_1(z) + (\beta_2^{NL}(z) - \beta_1^{NL}(z))z]} \right] - \\ &\operatorname{Im} \left(K_{12}^{NL}(z) \right) \frac{A_{2r}(z)}{A_{1r}(z)} \operatorname{Im} \left[e^{j[\varphi_2(z) - \varphi_1(z) + (\beta_2^{NL}(z) - \beta_1^{NL}(z))z]} \right] \end{aligned} \quad (8.24)$$

$$\begin{aligned} \frac{dA_{1r}(z)}{dz} &= z A_{1r}(z) \operatorname{Im} \left(\frac{d\beta_1^{NL}(z)}{dz} \right) - \operatorname{Re} \left(K_{12}^{NL}(z) \right) A_{2r}(z) \operatorname{Im} \left[e^{j[\varphi_2(z) - \varphi_1(z) + (\beta_2^{NL}(z) - \beta_1^{NL}(z))z]} \right] - \\ &\operatorname{Im} \left(K_{12}^{NL}(z) \right) A_{2r}(z) \operatorname{Re} \left[e^{j[\varphi_2(z) - \varphi_1(z) + (\beta_2^{NL}(z) - \beta_1^{NL}(z))z]} \right] \end{aligned} \quad (8.25)$$

$$\begin{aligned} \frac{d\varphi_2(z)}{dz} &= -z \operatorname{Re} \left(\frac{d\beta_2^{NL}(z)}{dz} \right) + \operatorname{Re} \left(K_{21}^{NL}(z) \right) \frac{A_{1r}(z)}{A_{2r}(z)} \operatorname{Re} \left[e^{j[\varphi_1(z) - \varphi_2(z) + (\beta_1^{NL}(z) - \beta_2^{NL}(z))z]} \right] - \\ &\operatorname{Im} \left(K_{21}^{NL}(z) \right) \frac{A_{1r}(z)}{A_{2r}(z)} \operatorname{Im} \left[e^{j[\varphi_1(z) - \varphi_2(z) + (\beta_1^{NL}(z) - \beta_2^{NL}(z))z]} \right] \end{aligned} \quad (8.26)$$

$$\begin{aligned} \frac{dA_{2r}(z)}{dz} &= z A_{2r}(z) \operatorname{Im} \left(\frac{d\beta_2^{NL}(z)}{dz} \right) - \operatorname{Re} \left(K_{21}^{NL}(z) \right) A_{1r}(z) \operatorname{Im} \left[e^{j[\varphi_1(z) - \varphi_2(z) + (\beta_1^{NL}(z) - \beta_2^{NL}(z))z]} \right] - \\ &\operatorname{Im} \left(K_{21}^{NL}(z) \right) A_{1r}(z) \operatorname{Re} \left[e^{j[\varphi_1(z) - \varphi_2(z) + (\beta_1^{NL}(z) - \beta_2^{NL}(z))z]} \right] \end{aligned} \quad (8.27)$$

Eqns 8.24-8.27 were solved using NAG, Runge Kutta (fourth order). At the end of

each section, the propagation coefficients, and coupling coefficients were adjusted using eqns 8.17-8.20. For guide 1 excitation initial values for the parameters were $\varphi_1(0) = 0.0$, $\varphi_2(0) = 0.0$, $A_{1r}(0) = 1.0$, and $A_{2r}(0) = 0.0$

REFERENCES

- [1] J. A. Fleck, J. R. Morris, and M.D. Feit, "Time-dependent propagation of high energy laser beams through the atmosphere", *Appl. Phys.* 10, 1976, pp. 129-160.
- [2] M. D. Feit, and J. A. Fleck JR., "Light propagation in graded-index optical fibers", *Applied Optics*, Vol 17, No. 24, December 1978, pp. 3990-3998.
- [3] M. D. Feit, and J. A. Fleck JR., "Calculation of dispersion in graded-index multimode fibers by a propagating-beam method", *Applied Optics*, Vol 18, No. 16, August 1979, pp. 2843-2851.
- [4] M. D. Feit, and J. A. Fleck JR., "Computation of mode eigenfunctions in graded-index optical fibers by the propagating beam method", *Applied Optics*, Vol 19, No. 13, July 1980, 2240-2246.
- [5] M. D. Feit, and J. A. Fleck JR., "Propagating beam theory of optical fiber cross-coupling", *J. Opt. Soc. Am.*, Vol 71, No. 11, November 1981, 1361-1372.
- [6] J. Van Roey, J. Van Der Donk, and P. E. Lagasse, "Beam-propagation method: analysis and assessment", *J. Opt. Soc. Am.*, Vol 71, No. 7, July 1981, 803-810.
- [7] M. D. Feit, and J. A. Fleck JR., "Beam nonparaxiality, filament formation, and beam breakup in the self-focusing of optical beams", *J. Opt. Soc. Am. B*, Vol 5, No. 3, March 1988, 633-640.
- [8] L. Thylen, and D. Yevick, "Beam propagation method in anisotropic media", *Applied Optics*, Vol 21, No. 15, August 1982, 2751-2754.
- [9] L. Thylen, "The beam propagation method: an analysis of its applicability", *Optical and Quantum Electronics*, Vol 15, 1983, 433-439.
- [10] L. Thylen, E. M. Wright, G. I. Stegeman, C. T. Seaton, and J. V. Moloney, "Beam-propagation method analysis of a nonlinear directional coupler", *Optics Letters*, Vol 11, No. 11, Nov 1986, pp. 739-741
- [11] A. C. Newell, and J. V. Moloney, "Nonlinear optics", Addison-Wesley Publishing Company, 1992.
- [12] D. Marcuse, "Theory of dielectric optical waveguides", Academic Press, 1991
- [13] G. P. Agrawal, "Fast-Fourier-transform based beam-propagation model for stripe-geometry semiconductor lasers: Inclusion of axial effects", *J. Appl. Phys.*, Vol 56, No. 11, December 1984, pp. 3100-3109.
- [14] H. M. Masoudi and J. M. Arnold, "Parallel beam propagation methods", *IEEE Photonics Technology Letters*, vol. 6, no. 7, 1994, pp. 848- 850.
- [15] H. M. Masoudi and J. M. Arnold, "Parallel beam propagation method for the analysis of second harmonic generation", *IEEE Photonics Technology Letters*, vol 7,

no 4, 1995, pp. 400-402.

[16] H. M. Masoudi and J. M. Arnold, "Modelling second-order nonlinear effects in optical waveguides using a parallel-processing beam propagation method", IEEE J. Quant. Electron., vol. 31, no. 12, 1995, 2106-2113.

[17] D. J. Thomson and N. R. Chapman, "A wide-angle split-step algorithm for the parabolic equation", J. Acoust. Soc. Am. , Vol 74, No. 6, December 1983, pp. 1848-1854.

CHAPTER 9

POWER INDEPENDENT COEFFICIENTS

9.1 INTRODUCTION

In this chapter, the linear and nonlinear coefficients which appeared in the nonlinear coupled mode equations of chapters 6-8 are calculated. It is assumed that the mode shapes are power independent. In practice however, the local intensity of the field in the nonlinear medium alters the local refractive index, and so alters the refractive index cross-section defining the waveguide. This means that the linear TE_0 mode ceases to remain the mode of the nonlinear waveguide at high powers. Nonlinear (power dependent) modes therefore have to be used (see chapter 10). The results of this chapter will be used to compare against those of chapter 10.

9.2 THE SLAB WAVEGUIDE

The mode of an isolated planar waveguide is first calculated. The structure under consideration [1] is illustrated in Fig. 9.1. The film region has a refractive index n_2 , thickness d and is deposited on a substrate with refractive index n_3 . The region above the film has a refractive index n_1 . If $n_1 = n_3$, the structure is considered symmetric, and if $n_1 \neq n_3$, asymmetric. The planar waveguide is extended to infinity in the y -direction. There are two boundaries at $x = 0$, and $x = -d$. To find the fields, the wave equation has to be solved in each of the regions. It must be ensured that the transverse components of the electric and magnetic fields in neighbouring regions match at the boundaries.

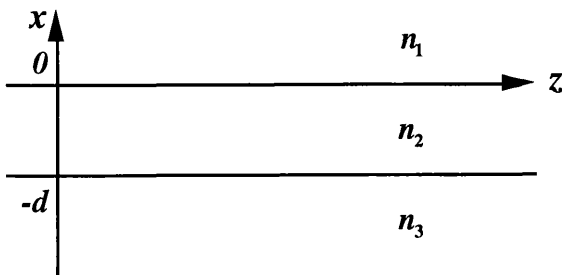


Fig. 9.1 The slab waveguide arrangement

Using Maxwell's equations, and assuming TE propagation $\underline{E} = (0, E_y, 0)$, and $\underline{H} = (H_x, 0, H_z)$, the following wave equation can be derived (see eqn. A2.4).

$$\frac{\partial^2 E_y}{\partial x^2} = -(k_0^2 \epsilon - \beta^2) E_y \quad (9.1)$$

where $k_0^2 = \omega^2 \mu_0 \epsilon_0$ and assuming that E_y has $e^{j\beta z}$ dependence (where β is the propagation coefficient), so that $\partial^2 E_y / \partial z^2$ becomes $-\beta^2 E_y$. Eqn. 9.1 is a second order differential equation which has to be solved for each of the three regions. The solutions then involve four unknown, three of which can be eliminated by matching the transverse electric and magnetic fields (E_y and H_z respectively) at the two boundaries $x = 0$, and $x = -d$. The field solutions are

$$E_y = A e^{-\delta x} \quad x \geq 0 \quad (9.2)$$

$$= A \left(\cos \kappa x - \frac{\delta}{\kappa} \sin \kappa x \right) \quad -d \leq x \leq 0 \quad (9.3)$$

$$= A \left(\cos \kappa d + \frac{\delta}{\kappa} \sin \kappa d \right) e^{\gamma(x+d)} \quad x \leq -d \quad (9.4)$$

These solutions involve the amplitude coefficient A , which will be related to power in section 9.4.

9.2.1 Eigenvalue equation

The boundary conditions also lead [1] to the asymmetrical and symmetrical forms of the eigenvalue equation

$$\tan \kappa d = \frac{\kappa(\gamma + \delta)}{\kappa^2 - \gamma\delta} \quad (\text{and } \tan \kappa d = \frac{2\kappa\delta}{\kappa^2 - \delta^2} \text{ for symmetric}) \quad (9.5)$$

where κ is the cut-off coefficient, and γ and δ are the decay coefficients. The definitions for κ , δ , and γ are,

$$\kappa^2 = n_2^2 k_0^2 - \beta^2, \quad \delta^2 = \beta^2 - n_1^2 k_0^2 = (n_2^2 - n_1^2) k_0^2 - \kappa^2 \quad (9.6)$$

$$\gamma^2 = \beta^2 - n_3^2 k_0^2 = (n_2^2 - n_3^2) k_0^2 - \kappa^2 \quad (9.7)$$

9.3 CALCULATING THE PROPAGATION COEFFICIENT

The eigenvalue equation for the symmetrical structure (eqn. 9.5) can be used to calculate κ , δ , and γ in eqns. 9.2-9.4 [1], as well as the propagation coefficient β . Using the double angle formula for tangents, eqn. 9.5 becomes $\tan \kappa d/2 = \delta/\kappa$, which can be solved for β . For example substituting $u = \kappa d$, and inserting the definition for δ in terms of κ (see eqn. 9.6) gives

$$\tan u/2 = \left[(n_2^2 - n_1^2) \frac{k_0^2 d^2}{u^2} - 1 \right]^{1/2} \quad (9.8)$$

Solving eqn. 9.8 for u results in determination of the values for κ , δ and β (with the aid of eqns. 9.6-9.7). The usual approach is to plot the functions of both sides of eqn. 9.8 and find the intersection [1].

9.4 RELATING A TO TOTAL POWER [1]

The amplitude coefficient A in eqns. 9.2-9.4, is the only unknown and is related to the total power carried by the field. The time-averaged power per unit area (or intensity or irradiance) is given by the Poynting vector. The total power P can be determined by integrating the Poynting vector over infinite cross-sectional area (in the x-y plane) (see eqn. A6.14)

$$P = \frac{1}{2} \operatorname{Re} \iint_{-\infty}^{+\infty} (\underline{E}_t \times \underline{H}_t^*) \cdot \underline{\hat{z}} \, dx dy \quad (9.9)$$

where \underline{E}_t and \underline{H}_t are the transverse components of the electric and magnetic fields respectively. For a *TE* mode, E_y can be substituted for \underline{E}_t , and H_x for \underline{H}_t . One of the integrals in eqn. 9.9 can be neglected (over y) since a slab guide is being considered and the fields are uniform in the y -direction. Therefore dealing in terms of power per unit length (in the y -direction) \mathcal{P} , instead of the total power P , eqn. 9.9 becomes

$$\frac{\beta}{|\beta|} \mathcal{P} = \frac{\beta}{2\omega\mu_0} \int_{-\infty}^{+\infty} |E_y|^2 \, dx \quad (9.10)$$

Note that $\beta/|\beta|$ is used in eqn. 9.10 so that the sign of the propagation coefficient specifies the direction of the power flow. Substituting eqns. 9.2-9.4 into eqn. 9.10 and integrating results in

$$\frac{\beta}{|\beta|} \mathcal{P} = \frac{\beta}{2\omega\mu_0} \left[\begin{aligned} &A^2 \left(\frac{1}{2\delta} + \frac{1}{2\gamma} + \frac{d}{2} + \frac{\delta^2 d}{2\kappa^2} \right) \\ &+ A^2 \text{Sin}\kappa d \text{Cos}\kappa d \left(\frac{1}{2\kappa} - \frac{\delta^2}{2\kappa^3} + \frac{\delta}{\gamma\kappa} \right) \\ &+ A^2 \text{Sin}^2 \kappa d \left(\frac{1}{2\gamma} \left(\frac{\delta^2}{\kappa^2} - 1 \right) + \frac{\delta}{\kappa^2} \right) \end{aligned} \right] \quad (9.11)$$

Substituting for $\text{Sin}\kappa d$ and $\text{Cos}\kappa d$ from eqns. A2.5 into eqn. 9.11 and after lengthy manipulations we arrive at

$$A^2 = \frac{4\kappa^2 \omega\mu_0 \mathcal{P}}{|\beta|(\kappa^2 + \delta^2) \left(d + \frac{1}{\gamma} + \frac{1}{\delta} \right)} \quad (\text{and } A^2 = \frac{4\kappa^2 \omega\mu_0 \mathcal{P}}{|\beta|(\kappa^2 + \delta^2) \left(d + \frac{2}{\delta} \right)} \text{ for the symmetric case}) \quad (9.12)$$

Eqns 9.12 relate the amplitude A to the power per unit length \mathcal{P} . It can be seen that A is directly proportional to the full power P . The formula for A can now used in the field definitions (eqns. 9.2-9.4).

9.5 TWO WAVEGUIDES

Now that the linear mode profile for one waveguide is calculated, it is a simple matter to calculate the mode profile for a second waveguide placed a distance w away. The first waveguide is labelled 'p', and the second waveguide 'q' (see Fig. 9.2)

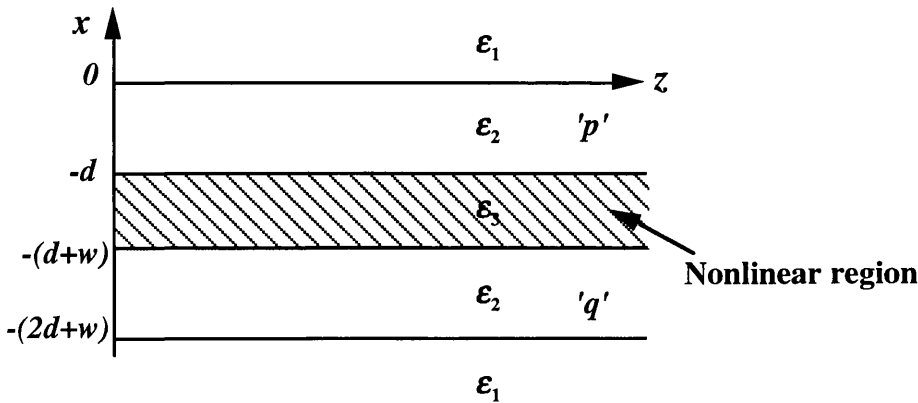


Fig. 9.2 Parallel slab directional coupler

The field for guide 'p' can be written down as (see eqns. 9.2-9.4)

$$E_y^{(p)} = Ae^{-\delta x} \quad x \geq 0 \quad (9.13)$$

$$= A \left(\text{Cos} \kappa x - \frac{\delta}{\kappa} \text{Sin} \kappa x \right) \quad -d \leq x \leq 0 \quad (9.14)$$

$$= A \left(\text{Cos} \kappa d + \frac{\delta}{\kappa} \text{Sin} \kappa d \right) e^{\gamma(x+d)} \quad x \leq -d \quad (9.15)$$

Exchanging δ for γ in eqns. 9.13-9.15 and shifting x by $(d+w)$ gives eigenmode 'q'

$$E_y^{(q)} = Ae^{-\gamma(x+(d+w))} \quad x \geq -(d+w) \quad (9.16)$$

$$= A \left(\text{Cos} \kappa(x+(d+w)) - \frac{\gamma}{\kappa} \text{Sin} \kappa(x+(d+w)) \right) \quad -(2d+w) \leq x \leq -(d+w) \quad (9.17)$$

$$= A \left(\text{Cos} \kappa d + \frac{\gamma}{\kappa} \text{Sin} \kappa d \right) e^{\delta(x+2d+w)} \quad x \leq -(2d+w) \quad (9.18)$$

We note that the fields in guides 'p' and 'q' have amplitude A (note also that A should not be confused with a_1 , a_2 , A_1 , A_2 in eg. section 3.10, which are normalised scaling amplitudes).

9.6 CALCULATING THE LINEAR COEFFICIENTS

Now that the equations for the modes of the two guides are calculated, it is possible to calculate analytical solutions for the linear and nonlinear coefficients.

9.6.1 Overlap integral

The overlap integral was defined in eqn. 3.3. Relating H_x and E_y via eqn. A2.2 the overlap integral becomes

$$C_{pq} = \frac{\beta}{2\omega\mu_0\mathcal{P}} \int_{-\infty}^{+\infty} E_y^{(p)} E_y^{(q)} dx \quad (9.19)$$

Inserting the fields from eqns. 9.13-9.18, integrating and substituting for A^2 from eqn. 9.12, followed by much rearrangement, a solution for the overlap integral can be derived.

$$C_{pq} = \frac{2\kappa^2\beta e^{-\delta w}}{|\beta|(\kappa^2 + \delta^2)\left(d + \frac{2}{\delta}\right)} \left[\begin{aligned} & \frac{1}{2\delta} e^{-\delta d} \\ & + \frac{1}{\kappa} \text{Sin}\kappa d \\ & + w \left(\text{Cos}\kappa d + \frac{\delta}{\kappa} \text{Sin}\kappa d \right) \\ & + \left(\text{Cos}\kappa d + \frac{\delta}{\kappa} \text{Sin}\kappa d \right) \frac{2\delta\kappa(1 - e^{-\delta d} \text{Cos}\kappa d) + (\kappa^2 - \delta^2)e^{-\delta d} \text{Sin}\kappa d}{\kappa(\delta^2 + \kappa^2)} \\ & + \frac{\left(\text{Cos}\kappa d + \frac{\delta}{\kappa} \text{Sin}\kappa d \right)^2}{2\delta} e^{-\delta d} \end{aligned} \right] \quad (9.20)$$

The variation of the overlap integral with guide separation (using eqn. 9.20) is shown in Fig. 9.3 for various guide thicknesses. We used the NLDC structure studied by Meng and Okamoto (M-O) [2] and Seaton et. al. [3] ie $n_1 = n_3 = n_5 = 1.55$, $n_2 = n_4 = 1.57$, $\lambda = 1.064\mu\text{m}$. It can be observed from Fig. 9.3 that the overlap integral is a function of both guide separation and guide thickness. The overlap integral increases with reduction in guide thickness d because the modes spread out more and overlap to a greater extent. The overlap integral also increases with reduction in guide separation, because the modes are brought physically closer together (and overlap more). From Fig. 9.3 it can be observed that the overlap integral for $d = 2\mu\text{m}$, $w = 2.4\mu\text{m}$ is around 0.0577. This tells us that the structure studied by M-O [2] was very weakly coupled. In chapter 12, a thinner guide is considered ($d = 0.5\mu\text{m}$), which leads to a much larger value for the overlap integral (of around 0.58 for the same separation- ie a $10 \times$ increase in the strength of the coupling).

We stress that the overlap integrals calculated here only incorporate linear (power-independent) modes. The variation of the overlap integral with guide thickness and separation would be different with nonlinear modes (see chapter 10).

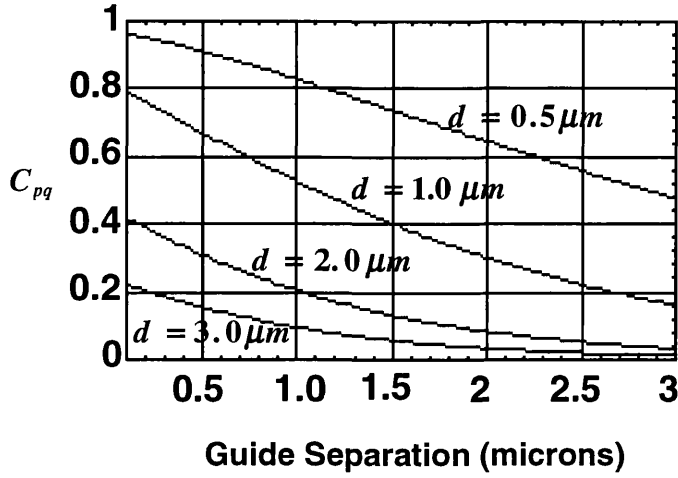


Fig. 9.3 Variation of the overlap integral with guide width d and separation w
 $n_1 = n_3 = n_5 = 1.55$, $n_2 = n_4 = 1.57$, $n_{3NL} = 10^{-9} m^2 / W$

9.6.2 The coupling coefficient

The coupling coefficient was defined in eqn. 3.4. Since the perturbation is over guide 'p', the integral is also taken over that region. Therefore

$$K_{pq} = \frac{\omega \epsilon_0}{4P} \int_{-d}^0 (\epsilon_2 - \epsilon_3) E_y^{(p)} E_y^{(q)} dx \quad (9.21)$$

If the modes of the two guides (eqn. 9.14 and 9.16) are inserted into eqn. 9.21 and the integral solved (substituting for A^2 from eqn. 9.12) we have

$$K_{pq} = \frac{\kappa^2 k_0^2 (\epsilon_2 - \epsilon_3) e^{-\gamma(d+w)}}{|\beta| (\kappa^2 + \delta^2) \left(d + \frac{1}{\gamma} + \frac{1}{\delta} \right)} \left(\frac{1 / \kappa (\kappa^2 + \gamma \delta) e^{\gamma d} \text{Sin} \kappa d + (\gamma - \delta) (e^{\gamma d} \text{Cos} \kappa d - 1)}{(\kappa^2 + \gamma^2)} \right) \quad (9.22)$$

For symmetrical geometries (where $\gamma = \delta$), eqn. 9.22 reduces to

$$K_{pq} = \frac{\kappa k_0^2 (\epsilon_2 - \epsilon_3) e^{-\delta w}}{|\beta| (\kappa^2 + \delta^2) \left(d + \frac{2}{\delta} \right)} \text{Sin} \kappa d \quad (9.23)$$

Eqn. 9.23 shows that there is an exponential decrease ($e^{-\delta w}$) of the coupling coefficient with guide separation w . This can be observed in Fig. 9.4.

9.6.3 The modification coefficient

The modification coefficient was defined in eqn. 3.22. Integrating over the perturbation region (over guide 'q').

$$K_{pp} = \frac{\omega \epsilon_0}{4P} \int_{-(2d+w)}^{-(d+w)} (\epsilon_2 - \epsilon_3) E_y^{(p)^2} dx \quad (9.24)$$

Inserting for $E_y^{(p)}$ from eqn. 9.17, and substituting for A^2 from eqn. 9.12 gives

$$K_{pp} = \frac{k_0^2 \kappa^2 (\epsilon_2 - \epsilon_3) e^{-2\delta w}}{2\delta |\beta| (\kappa^2 + \delta^2) \left(d + \frac{2}{\delta}\right)} \left(\cos \kappa d + \frac{\delta}{\kappa} \sin \kappa d\right)^2 (1 - e^{-2\delta d}) \quad (9.37)$$

We can see that this time that there is a much sharper exponential decrease ($e^{-2\delta w}$) than for the coupling coefficient in eqn. 9.23 ($e^{-\delta w}$).

The variation of the coupling and modification coefficients is drawn in Fig. 9.4.

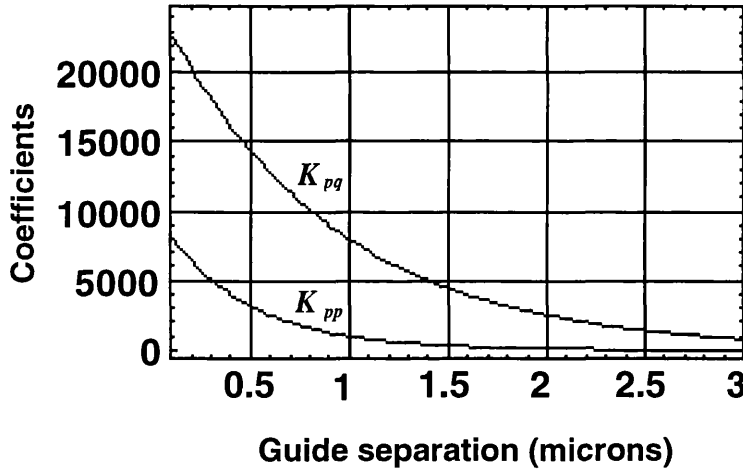


Fig. 9.4 Variation of the coupling and modification coefficient with guide separation. $n_1 = n_3 = n_5 = 1.55$, $n_2 = n_4 = 1.57$, $n_{3NL} = 10^{-9} m^2 / W$

9.7 CALCULATING THE NONLINEAR COEFFICIENTS

9.7.1 The self-phase-modulation (SPM)

The self-phase-modulation term, being the largest nonlinear coefficient, is calculated first. We use eqn. 5.5 and integrate over the nonlinear region.

$$Q_{pp}^{(p)} = \frac{\omega \epsilon_0}{4P} \iint_{-\infty}^{+\infty} \left[\alpha_3 E_i^{(p)^2} \right] \underline{E}_i^{(p)} \cdot \underline{E}_i^{(p)} dx dy = \frac{\omega \epsilon_0}{4P} \int_{-(d+w)}^{-d} \left[\alpha_3 E_y^{(p)^4} \right] dx \quad (9.25)$$

Using eqn. 9.15 for $E_y^{(p)}$ and integrating, and substituting for A^4 from eqn. 9.12

$$Q_{pp}^{(p)} = \frac{k_0^4 \alpha_3 \kappa^4 \mathcal{P} (\text{Cos} \kappa d + \delta / \kappa \text{Sin} \kappa d)^4}{\omega \epsilon_0 \delta |\beta|^2 (\kappa^2 + \delta^2)^2 (d + (2 / \delta))^2} [1 - e^{-4 \delta w}] \quad (9.26)$$

It is noticed from eqn. 9.26 that $Q_{pp}^{(p)}$ is directly proportional to power \mathcal{P} . It can also be noticed that for zero separation $w = 0$, $Q_{pp}^{(p)} = 0$. This is expected because there is no nonlinearity for zero separation, and hence no $Q_{pp}^{(p)}$. As the separation increases, $Q_{pp}^{(p)}$ also increases, until at large separations $e^{-4 \delta w} \rightarrow 0$, and $Q_{pp}^{(p)}$ reaches a maximum. For large separations the field is so small that any increase in separation would not increase $Q_{pp}^{(p)}$ significantly.

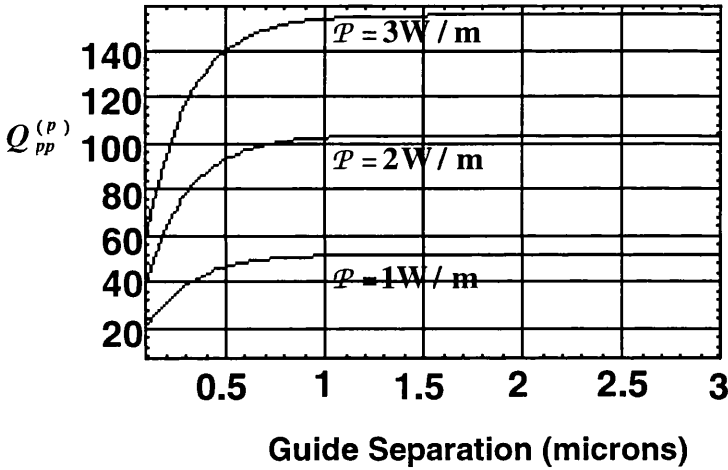


Fig. 9.5 The variation of $Q_{pp}^{(p)}$ with increasing guide separation for different input powers ($\mathcal{P} = 1, 2$, and 3 W/m) $n_1 = n_3 = n_5 = 1.55$, $n_2 = n_4 = 1.57$, $n_{3NL} = 10^{-9} \text{ m}^2 / \text{W}$

9.7.2 The larger-cross-phase-modulation (larger-XPM) coefficient

The larger-XPM term is the next coefficient to be determined. Since a symmetrical structure is being assumed, the bracketed indices can be interchanged, ie. $Q_{pq}^{(p)} = Q_{pq}^{(q)}$. (Naturally the non-bracketed indices 'p' and 'q' can be interchanged regardless). From eqn 5.6

$$Q_{pq}^{(p)} = \frac{\omega \epsilon_0}{4 \mathcal{P}} \iint_{-\infty}^{+\infty} [\alpha_3 E_t^{(p)2}] \underline{E}_t^{(p)} \cdot \underline{E}_t^{(q)} dx dy = \frac{\omega \epsilon_0}{4 \mathcal{P}} \int_{-(d+w)}^{-d} [\alpha_3 E_y^{(p)3} E_y^{(q)}] dx \quad (9.27)$$

Once again, substituting the fields from eqns 9.13-9.18, and A^4 from eqn. 9.12

$$Q_{pq}^{(p)} = \frac{2k_0^4 \alpha_3 \kappa^4 \mathcal{P} (\cos \kappa d + \delta / \kappa \sin \kappa d)^3 e^{-\delta w}}{\omega \epsilon_0 \delta |\beta|^2 (\kappa^2 + \delta^2)^2 (d + (2/\delta))^2} [1 - e^{-2\delta w}] \quad (9.28)$$

This equation should be compared with eqn. 9.26. We notice that there is an $e^{-\delta w} (1 - e^{-2\delta w})$ factor. This means that for zero separation $Q_{pq}^{(p)}$ is zero. This is expected because at zero separation, there is no nonlinearity, and hence no $Q_{pq}^{(p)}$. As the separation is increased, there is more nonlinearity, and $Q_{pq}^{(p)}$ increases because $(1 - e^{-2\delta w})$ factor increases. For large separations, the modes overlap less, leading to a decrease in $Q_{pq}^{(p)}$. We can observe this in eqn. 9.28, where $e^{-\delta w}$ factor dominates for large w . We also notice that $Q_{pq}^{(p)}$ is directly proportional to power \mathcal{P} as was the case for $Q_{pp}^{(p)}$.

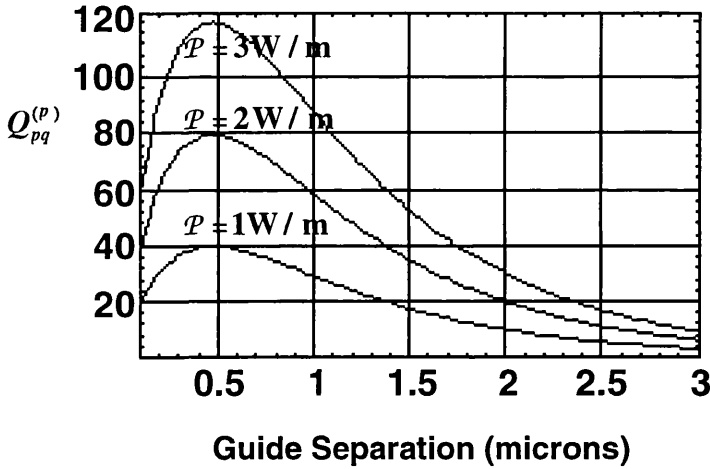


Fig. 9.6 The variation of $Q_{pq}^{(p)}$ with increasing guide separation for different input powers ($\mathcal{P} = 1, 2, \text{ and } 3 \text{ W/m}$). $n_1 = n_3 = n_5 = 1.55$, $n_2 = n_4 = 1.57$, $n_{3NL} = 10^{-9} \text{ m}^2/\text{W}$

9.7.3 The cross-phase-modulation term (XPM)

We used the definition of eqn. 5.7, and integrated it over the nonlinear separation region.

$$Q_{pp}^{(q)} = \frac{\omega \epsilon_0}{4\mathcal{P}} \iint_{-\infty}^{+\infty} [\alpha_3 E_t^{(q)^2}] \underline{E}_t^{(p)} \cdot \underline{E}_t^{(p)} dx dy = \frac{\omega \epsilon_0}{4\mathcal{P}} \int_{-(d+w)}^{-d} [\alpha_3 E_y^{(q)^2}] E_y^{(p)^2} dx \quad (9.29)$$

Making use of eqns. 9.16 and 9.17 for the fields in eqn. 9.29, substituting for A^4 from eqn. 9.12 gives

$$Q_{pp}^{(q)} = \frac{4k_0^4 \alpha_3 \kappa^4 \mathcal{P} (\cos \kappa d + \delta / \kappa \sin \kappa d)^2 w e^{-2\delta w}}{\omega \epsilon_0 |\beta|^2 (\kappa^2 + \delta^2)^2 (d + (2/\delta))^2} \quad (9.30)$$

Here we notice that there is a $w e^{-2\delta w}$ factor in $Q_{pp}^{(q)}$. Therefore for small separations $Q_{pp}^{(q)}$ is directly proportional to the guide separation since w is dominating. As w is increased the $e^{-2\delta w}$ takes over, and $Q_{pp}^{(q)}$ starts to decrease. As with $Q_{pp}^{(p)}$ and $Q_{pq}^{(p)}$, $Q_{pp}^{(q)}$ is directly proportional to input power \mathcal{P} . Eqn. 9.30 is plotted for different guide separations, and input powers.

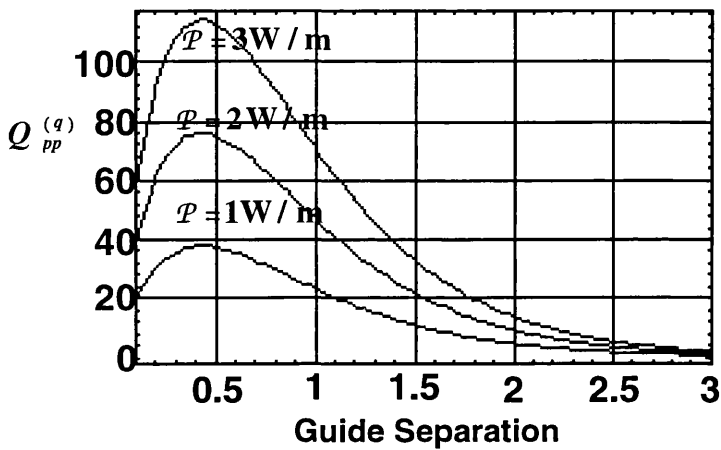


Fig. 9.7 The variation of $Q_{pp}^{(q)}$ with guide separation for different input powers ($\mathcal{P} = 1, 2,$ and 3 W/m)

9.8 COMPARISON BETWEEN THE NONLINEAR COEFFICIENTS

It is interesting to compare the three coefficients on one graph to observe the relative magnitudes (see Fig. 9.8). It can be seen that for large guide separations, the SPM term ($Q_{pp}^{(p)}$) dominates. As the guide separation is reduced, the two XPM terms ($Q_{pq}^{(p)}$, and $Q_{pp}^{(q)}$) increase and become comparable to the SPM curve. The two XPM curves are similar in magnitude for all separations. At very small guide separations, all three coefficients become exactly the same.

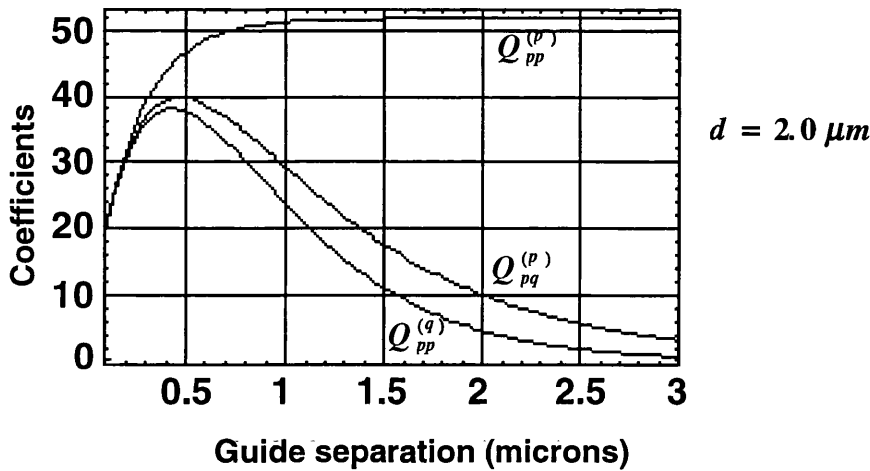


Fig. 9.8 The variation of $Q_{pp}^{(p)}$, $Q_{pq}^{(p)}$, and $Q_{pp}^{(q)}$ with increasing guide separation, with $\mathcal{P} = 1.0W/m$, and $d = 2.0\mu m$, $n_1 = n_3 = n_5 = 1.55$, $n_2 = n_4 = 1.57$, $n_{3NL} = 10^{-9}m^2/W$

In the next graph, the guide thicknesses are reduced to $1.0\mu m$. We observe that as a result of the reduction in guide thickness, the XPM terms have become larger. The SPM coefficient is also larger because the mode is extended to a greater extent into the nonlinear region.

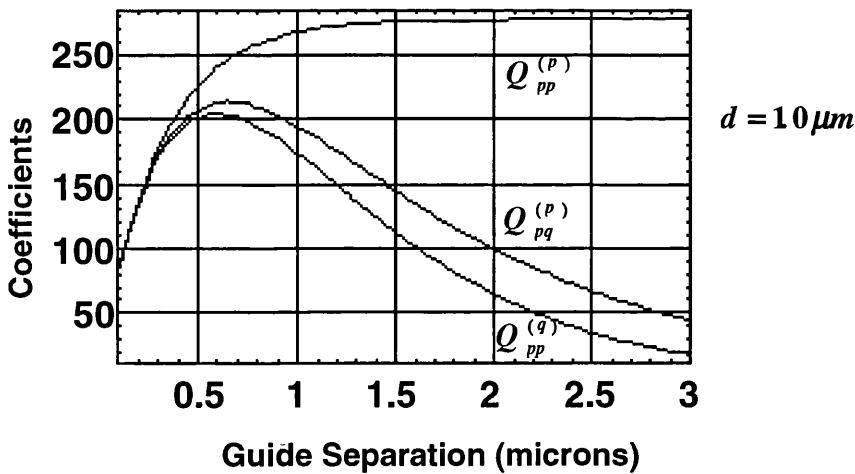


Fig. 9.9 The variation of $Q_{pp}^{(p)}$, $Q_{pq}^{(p)}$, and $Q_{pp}^{(q)}$ with increasing guide separation, with $\mathcal{P} = 1.0W/m$, and $d = 1.0\mu m$, $n_1 = n_3 = n_5 = 1.55$, $n_2 = n_4 = 1.57$, $n_{3NL} = 10^{-9}m^2/W$

In the next graph, the coefficients are plotted against total input power \mathcal{P} .

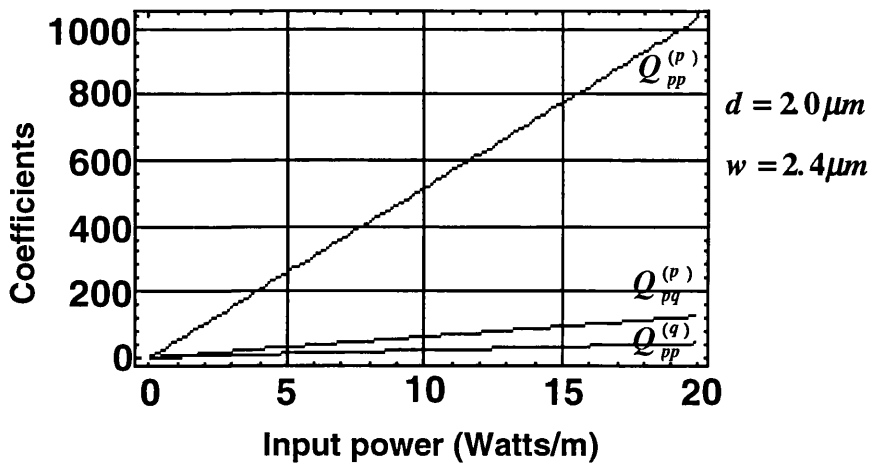


Fig. 9.10 The variation of $Q_{pp}^{(p)}$, $Q_{pq}^{(p)}$, and $Q_{pp}^{(q)}$ with total input power \mathcal{P} , $n_1 = n_3 = n_5 = 1.55$, $n_2 = n_4 = 1.57$, $n_{3NL} = 10^{-9} m^2 / W$

It can be seen that all three coefficients are linearly proportional to \mathcal{P} , as expected from eqns. 9.26, 9.28, and 9.30.

9.9 CONCLUSIONS

The linear and nonlinear coefficients were calculated in this chapter, assuming power independent mode shapes. Some numerical results for the variation of these coefficients with different parameters were given.

REFERENCES

- [1] D. Marcuse, "Theory of Dielectric Optical Waveguides", Academic Press, 1991.
- [2] X. J. Meng, and N. Okamoto, "Improved coupled-mode theory for nonlinear directional couplers", IEEE J. Quant. Electron., May 1991, pp. 1175-1181
- [3] C. T. Seaton et. al., "Calculations of nonlinear TE waves guided by thin dielectric films bounded by nonlinear media", IEEE J. Quant. Electron., vol. QE-21, no. 7, 1985, pp. 774-783.

CHAPTER 10

COEFFICIENTS INCORPORATING NONLINEAR TE MODES

10.1 INTRODUCTION

In this chapter the nonlinear modes used to excite the nonlinear directional coupler (NLDC) are calculated. Nonlinear modes have power dependent shapes, unlike linear modes. Since nonlinear modes satisfy Maxwell's equations and the boundary conditions they are true modes, and therefore do not change with propagation distance (assuming the structure is z-invariant). Nonlinear modes are often called nonlinear guided waves (NLGWs) in the literature.

In the first part of this chapter, the literature on NLGWs is surveyed. The nonlinear modes of planar guides with nonlinear cladding(s) are next calculated. In the latter part of the chapter, some new results are presented on the variation of the nonlinear coefficients with power, guide width and separation.

10.2 NONLINEAR GUIDED WAVES- LITERATURE SURVEY

Theoretical work on NLGWs started with the single nonlinear interface [1-3] (good reviews can be found in [4-6]), which is an interface between a linear and a nonlinear medium. This type of interface supports a guided wave provided that at least one of the media has a positive (self-focusing) nonlinearity, and the power of the wave is above a minimum threshold. The work on nonlinear interfaces led naturally to the study of NLGWs in nonlinear waveguides. Initially, waveguides with one [7-8], and both claddings nonlinear [9-11], were studied. Later, nonlinear films [12-15] were investigated. Nonlinear films are more complicated to analyse than claddings, because they support standing waves. In the linear regime, this means that the field solutions are in terms of sines and cosines. In the nonlinear regime however the solutions are in terms of the *elliptical* sine and cosine functions. Most papers on NLGWs concentrate on positive (self-focusing) nonlinearities because they appear to give more interesting results, however negative (self-defocusing) nonlinearities in waveguides have also been looked at (eg. ref. 8).

The stability of NLGWs has been examined both numerically [16-20] and analytically [4,21-22]. The numerical investigation has been mainly with the aid of the beam propagation method (BPM). The stability is determined by studying the propagation of the field: if it stays attached to the waveguide and does not oscillate laterally (wobble) within the waveguide, then the field is termed as stable; if it does not remain attached to the guide, then it is termed unstable. Sometimes a field may appear stable over short distances, but in fact is weakly unstable and the instability starts to appear later on. Therefore care must be taken to ensure that the propagation distance is long enough in studying the instability.

Stability of nonlinear guided waves has also been studied analytically. Kolokolov [23] suggested that on a dispersion diagram, where input power (\mathcal{P}) is drawn against propagation coefficient (β), the regions where the slope is positive (ie. $d\mathcal{P}/d\beta > 0$) correspond with stable modes, and those where the slope is negative with unstable modes. This argument applies only for *TE* waves supported by guides with *one* nonlinear cladding. For example, it was shown in [17] that for the case of a linear film with equal nonlinear claddings on both sides, $d\beta/d\mathcal{P} > 0$ is not necessarily the condition for a stable mode.

The symmetrical nonlinearity case (equal nonlinearities on both sides of the linear film) has been studied theoretically [16, 24-25]. In [16] it was found that in this case the dispersion curve bifurcates into two surface wave branches, where the lower one is stable for $d\mathcal{P}/d\beta > 0$, and the upper one unstable. The modes on this unstable level can be shown in a BPM simulation to be two surface modes emerging symmetrically from the film region into the cladding regions. As these modes are unstable, after a certain propagation distance the spatial symmetry breaks down, and only one surface mode remains, corresponding with the lower level on the dispersion curve.

For asymmetrical nonlinearities the dispersion curves become even more complex [16], with three power levels being present. Positive slopes on the bottom two levels correspond with stable modes. The top level is unstable regardless of the sign of the slope. On a BPM diagram one can see that solitons are emitted into the cladding with the larger nonlinearity.

So far the nonlinear claddings have been assumed to be spatially semi-infinite in extent. The dispersion characteristics for a linear waveguide with limited width of nonlinear-bounding layers have been examined recently [26]. It was found that the device exhibited hysteresis characteristics similar to those of the nonlinear Fabry-Pérot etalon. As the thickness of the bounding layers increased both the critical power (at which point the peak of the field emerges into the cladding) and the hysteresis were

reduced.

An elegant method to determine the stability of the branches of a dispersion diagram for a particular geometry has been described by Mitchell and Snyder [27]. The dispersion curve is first subdivided into different branches using bifurcation points. A known stable branch on the dispersion diagram is found using the basic physical parameters of the waveguide under study, and this branch is numbered 0. The immediately adjacent branch is then numbered according to its stability. The numbering is according to whether the next branch continues from the previous branch or whether, it separates from or converges to a fork type bifurcation point. The positive slope curves are temporarily labelled 'possibly stable'. The numbering strategy is such that if the next branch is 'possibly stable' then the branch is numbered one point above the previous neighbouring branch and if unstable one point less. When all of the branches have been numbered, the branches labelled zero are known for certain to be stable. This is because they can be related to the initial branch which was also numbered zero and known to be stable.

10.2.1 Miscellaneous NLGWs

In addition to *TE* NLGWs, *TM* NLGWs [4,28-30] have also been studied. These modes are more complicated to calculate than *TE* modes because two fields are involved. However, they exhibit essentially the same phenomena as *TE* modes. Mixed *TE-TM* modes have also been studied [4,31], and these have no counterparts in linear optics. These fields are neither *TE* nor *TM*. One polarisation is able to provide a channel for the other polarisation.

The nonlinear supermodes for slab and channel nonlinear couplers have been calculated from a variational approach [32]. It was found that the symmetric supermodes were stable only if the power was less than a bifurcation power. Above this power until a second higher power, the asymmetric mode is stable, but the symmetric mode collapses. The device can therefore be used as a switch, since if a small amount of the asymmetric mode (eg. 1%) is added to the symmetric mode in this regime, then the symmetric mode transfers all its energy into either guide, depending on the phase of the asymmetric mode. Above the second power, both the symmetric and asymmetric modes are unstable.

10.2.2 Practical NLGWS

10.2.2.1 Launching requirements

Practical requirements for launching a nonlinear mode are not too strict. For example, if the nonlinear waveguide is excited with a field which corresponds approximately to the

nonlinear mode (eg. a gaussian field [33-35] with approximately the right width, and centre position), then it will evolve into the nonlinear field after a short distance.

10.2.2.2 Effect of losses, saturation, and diffusion

So far the nonlinearity has been assumed to be local (ie not diffusive) and lossless. The effect of diffusive nonlinearities on NLGWs was studied in [36], and losses in [35, 37-39]. It was found that attenuation becomes a function of power in NLGWs [37]. For example as the power was increased the TE_0 field shifted towards the cladding, and consequently travelled through more loss. The ‘dispersion characteristics’ for the variation of the absorption with power [37] are very similar to the dispersion characteristics for the propagation coefficient with power. For example at low powers, where film-guided modes exist (ie. the peak of the field is inside the film), the attenuation is power independent.

The effect of absorption on NLGWs [38] is also dependent upon whether the absorption is greater in the film or the cladding. If the cladding is more absorbing, the NLGW tends to become focused in the film, since the part propagating through the cladding dissipates away due to absorption. If the film is more absorbing however, the field shifts towards the cladding and may even be emitted as a soliton.

Experimentally, nonlinear guided waves have been observed using liquid crystal MBBA as the nonlinear cladding [35]. The losses were so great that only 1% transmission was observed. Both TE_0 and TE_1 modes were examined. There was an associated saturation of the transmitted power observed at high powers for both modes. The TE_1 mode also exhibited this saturation. In addition, the transmitted power/input power curve for the TE_1 mode showed hysteresis behaviour between increasing the input power, and then reducing it. This has obvious applications in bistability.

10.2.2.3 Nonlinear mode along a curved interface

Nonlinear wave propagation along a curved or angled interface was studied in ref. 40. It was found that surface waves cannot propagate along a single nonlinear interface bent toward the nonlinear medium.

10.2.3 Soliton interaction with nonlinear interfaces and waveguides

The interaction of a soliton with a nonlinear interface is a useful case to study, because it helps to explain some interesting phenomena associated with soliton emission from nonlinear waveguides later on.

The behaviour of a soliton as it approaches the interface between two different nonlinear media can be studied analytically using equivalent particle theory (EPT) [41-43]. One example is the case where the soliton crosses the interface from a lower nonlinearity to a higher nonlinearity medium. In EPT the soliton is treated as a particle, and the interface as a potential barrier. The soliton crosses the interface depending on its power as well as the incident angle relative to the interface. At glancing angles to the interface, the soliton is reflected. As the angle is increased, the soliton penetrates further into the interface each time before being reflected, analogous to a Goos-Hänchen shift. At larger angles, the soliton penetrates completely through the interface and refracts. The refraction follows a nonlinear version of Snell's law because it depends on the soliton power as well as the incident angle. The greater the power, the less the soliton deviates from its original course. Once the soliton crosses the interface, it changes shape to become a soliton of the new medium. In general, transmission through the interface can occur if the mismatch in the nonlinearity at the interface is small, less than around 40% change. In this worst-case scenario there is around 11% radiation, but for smaller mismatches, there is only a very small amount of radiation. The power dependent refraction of the soliton can give rise to an all-optical spatial scanner [44], where the soliton refracts through different angles depending on the input power.

Finally the case of an $N > 1$ † soliton crossing the interface has also been considered [41-43]. In this case the soliton breaks up into several fundamental solitons and some radiation results.

† an $N > 1$ soliton has the same shape as the fundamental soliton, except with N times the amplitude.

10.2.4 Soliton emission from nonlinear waveguides

The linear core/one nonlinear cladding waveguide can lead to soliton emission [24, 45] providing the power is higher than a certain threshold. The waveguide emits solitons when it no longer can carry all the power, and has to shed the extra energy. Therefore these nonlinear waveguides can be used as soliton generators [45]. The threshold power required for soliton generation suggests that nonlinear waveguides could be used as optical limiters [45]. As the input power is increased further, multisoliton emission is possible [45]. The released soliton(s) can be captured by another waveguide situated close by. This suggests a further application as a soliton coupler [46].

The emission of spatial solitons from linear waveguides with nonlinearity on one side can be viewed as an unbalanced force on the linear *TE* mode, which accelerates the

field towards the nonlinear region [47]. A soliton then breaks off from the waveguide, and launches into the cladding, leaving behind some residual power in the waveguide. The angle of emission of the soliton is dependent on the input power. This is because the unbalanced lateral force on the *TE* mode is dependent on the input power. The higher the power becomes, the greater the lateral momentum before the soliton is launched, and the larger the angle of emission. The power dependent angle of emission of the soliton suggests a potential use of such nonlinear waveguides as optical scanners [45].

As the input power is increased past the threshold, more and more residual power is left behind in the waveguide, until the residual power becomes high enough for another soliton to be emitted. Another way to view this is that if the input power is much higher than that of the threshold soliton, multisoliton emission occurs because this case is similar to the case of the multi-order soliton crossing a nonlinear interface [47]: ie. the soliton breaks up. The behaviour is strongly dependent on the width of the waveguide and the wavelength. For the case where the width is equal to the wavelength, a potential energy diagram (potential energy vs. position of centre of gravity of the beam in terms of lateral distance away from waveguide centre) shows a minima where the stable mode occurs. There is a potential barrier to prevent it from going into the cladding. As the power is increased the potential barrier reduces so that the soliton is eventually released into the cladding. For the case of the guide width equalling twice the wavelength, the potential barrier is much less, and soliton emission occurs much more readily above a threshold power.

10.2.5 Spatial soliton emission from tapered waveguides

The effect of tapering the guide has been investigated [48]. At very low powers, the tapering causes the TE_0 field to evolve adiabatically from initially that of thick film to that of the thin film. At higher powers, as the tapered guide narrows, the guided mode suddenly becomes a surface wave radiating some energy in the process. At much higher powers, the tapered guide loses the excess energy in the form of a soliton. If both sides of the tapered guide are nonlinear, the direction in which the soliton is emitted can be controlled by adding a small amount of TE_1 mode at the input and varying its phase.

10.2.6 Gain

The effect of gain on soliton emission from the linear film with symmetrical nonlinearities has been observed [49]. It was found that for low gains, the reshaping of

the field was adiabatic, but where the power reached above the peak of the N-shaped dispersion curve (see Fig. 10.4), multiple spatial solitons were emitted periodically from both sides of the film.

10.3 THE NONLINEAR SLAB WAVEGUIDE

To model the nonlinear directional coupler (NLDC) consisting of two linear film regions separated by a nonlinear medium, the modes of the isolated nonlinear guides are calculated in this section.

Since symmetry is assumed, the mode shapes of the two guides are mirror images of each other. Therefore once one of the modes is determined, the other can be found very easily by taking the mirror image.

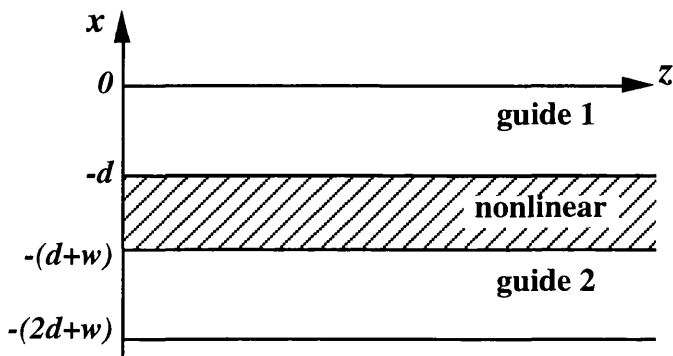


Fig. 10.1 The nonlinear directional coupler

Each guide is taken in isolation, where it consists of a linear film, with semi-infinite linear cladding region on one side and semi-infinite nonlinear cladding on the other.

The mode satisfies Maxwell's equation in each of the three regions of the waveguides as well as the boundary conditions at the interfaces. Initially it is assumed that both claddings are nonlinear. Therefore the field shape of a homogeneous nonlinear medium is first calculated using Maxwell's equations, and these field shapes are joined at the interfaces to the field shape of the linear film region such that boundary conditions are satisfied. Finally, one of the claddings then becomes linear, resulting in the desired mode shape.

10.3.1 Nonlinear waves in a self-focusing nonlinear medium

Using Maxwell's equations, the following wave equation for *TE* propagation can be derived (see eqn. A2.4).

$$\frac{\partial^2 E_y}{\partial x^2} = (\beta^2 - k_0^2 \varepsilon) E_y \quad (10.1)$$

where k_0 is the free-space wave-vector, β the propagation coefficient, ε the permittivity (nonlinear in this chapter), such that $\varepsilon = \bar{\varepsilon} + \alpha |E_y|^2$, where $\bar{\varepsilon}$ is the linear permittivity of the material. E_y the complex electric field, and α the nonlinearity (which is local in space and time- nonlocality implies processes such as diffusion). Self-focusing nonlinearities are assumed so that $\alpha \geq 0$. Also δ is defined such that $\delta^2 = \beta^2 - k_0^2 \bar{\varepsilon}$. Substituting for ε and β into eqn 10.1 gives

$$\frac{\partial^2 E_y}{\partial x^2} - \delta^2 E_y + k_0^2 \alpha |E_y|^2 E_y = 0 \quad (10.2)$$

Since E_y is complex, it can be split it into a modulus (E), and phase (ϕ) notation [4], where E , and ϕ are real, ie $E_y = E(\beta, \omega, x) e^{j\phi(\beta, \omega, x)}$. Therefore the real part of eqn 10.2 becomes

$$\frac{\partial^2 E}{\partial x^2} + k_0^2 \alpha E^3 - \delta^2 E - \left(\frac{\partial \phi}{\partial x} \right)^2 E = 0 \quad (10.3)$$

and the imaginary part becomes

$$\frac{\partial^2 \phi}{\partial x^2} E + 2 \frac{\partial E}{\partial x} \frac{\partial \phi}{\partial x} = 0 \quad (10.4)$$

Equation 10.4 can be integrated to give

$$\frac{\partial \phi}{\partial x} = \frac{K}{E^2} \quad (10.5)$$

where K is a constant of integration. Substituting eqn. 10.5 into eqn. 10.3 and assuming the field becomes very small at large distances from the waveguide, so that one can say that as $x \rightarrow \pm\infty$, $E \rightarrow 0$ [10], causes $K = 0$. Therefore

$$\frac{\partial^2 E}{\partial x^2} + k_0^2 \alpha E^3 - \delta^2 E = 0 \quad (10.6)$$

which after integrating and factorising becomes

$$\left[\left(\frac{\partial E}{\partial x} \right) - E \sqrt{\delta^2 - \frac{k_0^2 \alpha}{2} E^2} \right] \left[\left(\frac{\partial E}{\partial x} \right) + E \sqrt{\delta^2 - \frac{k_0^2 \alpha}{2} E^2} \right] = 0 \quad (10.7)$$

Eqn 10.7 can be solved to give

$$E = \frac{\delta}{k_0} \sqrt{\frac{2}{\alpha}} \operatorname{sech} \delta(x - x_0) \quad (10.8)$$

We note that had the nonlinearity been self-defocusing $\alpha < 0$, the solution would have been Sinh^{-1} instead of Sech (ie Cosh^{-1}) [8,10]. Also x_0 is a constant of integration [10], giving the location of the field maximum. One can prove this as follows: the field maximum (E_{max}) occurs when $(\partial E/\partial x) = 0$. Therefore inserting this substitution into eqn. 10.7, and solving for E results in

$$E_{max} = \frac{\delta}{k_0} \sqrt{\frac{2}{\alpha}} \quad (10.9)$$

Now exactly the same result for E_{max} can be derived from eqn. 10.8 by inserting $x = x_0$. Therefore $x = x_0$ must be the location of the field maximum in the nonlinear medium.

10.3.2 Linear core with nonlinear cladding on both sides

The field solution for the nonlinear medium can now be incorporated into the nonlinear region of the waveguides.

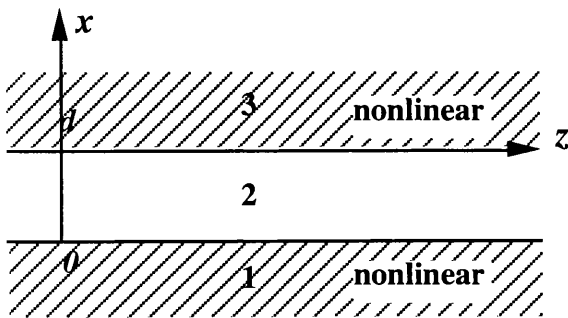


Fig. 10.2 Illustrating linear core with nonlinear claddings.

We consider a general asymmetric waveguide composed of a linear core with asymmetric cladding (ie. different linear and nonlinear indices on either side) (see Fig. 10.2).

To write down the fields for the three regions, we make use of eqn. 10.8 for regions 1 and 3, and assume oscillatory fields for the linear core (region 2). Therefore the fields in the three regions can be written down as [10]

$$E_1(x) = \sqrt{\frac{2}{\alpha_1}} \frac{\delta_1 c}{\omega} [\text{Cosh} \delta_1 (x - x_{01})]^{-1} \quad x < 0 \quad (10.10)$$

$$E_2(x) = A \exp(j\kappa x) + B \exp(-j\kappa x) \quad 0 \leq x < d \quad (10.11)$$

$$E_3(x) = \sqrt{\frac{2}{\alpha_3}} \frac{\delta_3 c}{\omega} [\text{Cosh} \delta_3 (x - d - x_{03})]^{-1} \quad x \geq d \quad (10.12)$$

where x_{01} and x_{03} are the positions of the field maxima in regions 1 and 3 respectively. If either x_{01} or x_{03} are situated within their respective nonlinear regions (1 and 3 respectively), then the field maximum is situated in that region (the field would then be defined as a surface mode). If neither x_{01} nor x_{03} are in their respective regions, then the field maximum is in the linear core, and only the tails are in the nonlinear regions. For example if $x_{03} > d$ (see Fig. 10.2), then there is a field maximum inside region 3 (at $x = x_{03}$), followed by an exponential decay as x is increased to infinity. If $x_{03} < d$ then the field maximum does not appear in region 3 and only the exponential decay does. If region 3 were linear then x_{03} would be at minus infinity. The same type of argument could be applied to x_{01} and region 1. $\delta_{1,3}$ and κ are defined as (cf. eqns. 9.6 and 9.7)

$$\delta_{1,3} = (\beta^2 - k_0^2 \bar{\epsilon}_{1,3})^{1/2} \quad \kappa = (k_0^2 \bar{\epsilon}_2 - \beta^2)^{1/2} \quad (10.13)$$

Matching the transverse electric field E at $x = 0$ (eqns. 10.10 and 10.11) and at $x = d$ (eqns. 10.11 and 10.12) results in

$$A + B = \sqrt{\frac{2}{\alpha_1}} \frac{\delta_1 c}{\omega} [\text{Cosh} \delta_1 x_{01}]^{-1} \quad (10.14)$$

$$A \exp(j\kappa d) + B \exp(-j\kappa d) = \sqrt{\frac{2}{\alpha_3}} \frac{\delta_3 c}{\omega} [\text{Cosh} \delta_3 x_{03}]^{-1} \quad (10.15)$$

Now matching the transverse component of the magnetic field H_z at the two boundaries. Therefore matching H_z (proportional to dE/dx -see eqn. A6.2) at $x=0$ (using eqns. 10.10 and 10.11), and at $x=d$ (using eqns. A6.2, 10.11, and 10.12) gives

$$j\kappa(A - B) = \sqrt{\frac{2}{\alpha_1}} \frac{\delta_1^2 c}{\omega} \text{Sech}\delta_1 x_{01} \text{Tanh}\delta_1 x_{01} \quad (10.16)$$

$$j\kappa(Ae^{j\kappa d} - Be^{-j\kappa d}) = \sqrt{\frac{2}{\alpha_3}} \frac{\delta_3^2 c}{\omega} \text{Sech}\delta_3 x_{03} \text{Tanh}\delta_3 x_{03} \quad (10.17)$$

Eqns. 10.14-10.17 are four equations which can be used to solve for A , B , $\text{Sech}\delta_3 x_{03}$, and $\text{Sech}\delta_1 x_{01}$. Using eqns. 10.14 and 10.16, we first determine A and B ,

$$A = \left(\frac{\delta_1 c}{\omega} \sqrt{\frac{1}{2\alpha_1}} \text{Sech}\delta_1 x_{01} \right) \left(1 - j \frac{\delta_1}{\kappa} \text{Tanh}\delta_1 x_{01} \right) \quad (10.18)$$

$$B = \left(\frac{\delta_1 c}{\omega} \sqrt{\frac{1}{2\alpha_1}} \text{Sech}\delta_1 x_{01} \right) \left(1 + j \frac{\delta_1}{\kappa} \text{Tanh}\delta_1 x_{01} \right) \quad (10.19)$$

Substituting for A and B from eqns. 10.18 and 10.19 into eqns 10.15 gives

$$\sqrt{\frac{2}{\alpha_3}} \delta_3 \text{Sech}\delta_3 x_{03} = \left(\delta_1 \sqrt{\frac{2}{\alpha_1}} \text{Sech}\delta_1 x_{01} \right) \left(\text{Cos}\kappa d + \frac{\delta_1}{\kappa} \text{Tanh}\delta_1 x_{01} \text{Sin}\kappa d \right) \quad (10.20)$$

Substituting for A and B (eqns. 10.18 and 10.19) into eqns 10.17 gives

$$\sqrt{\frac{2}{\alpha_3}} \frac{\delta_3^2}{\kappa} \text{Sech}\delta_3 x_{03} \text{Tanh}\delta_3 x_{03} = \left(\delta_1 \sqrt{\frac{2}{\alpha_1}} \text{Sech}\delta_1 x_{01} \right) \left(\frac{\delta_1}{\kappa} \text{Tanh}\delta_1 x_{01} \text{Cos}\kappa d - \text{Sin}\kappa d \right) \quad (10.21)$$

It is useful to introduce the following parameters [10]

$$E_0(\beta, x_{01}) = E_1(x)|_{x=0} = \sqrt{\frac{2}{\alpha_1}} \frac{\delta_1 c}{\omega} \text{Sech}\delta_1 x_{01} \quad (10.22)$$

$$E_d(\beta, x_{03}) = E_3(x)|_{x=d} = \sqrt{\frac{2}{\alpha_3}} \frac{\delta_3 c}{\omega} \text{Sech} \delta_3 x_{03} \quad (10.23)$$

where E_0 is the field amplitude at $x = 0$, E_d is the field amplitude at $x = d$.
Substituting E_0 and E_d into eqns. 10.20 and 10.21 respectively gives

$$E_d = E_0 \left(\text{Cos} \kappa d + \frac{\delta_1}{\kappa} \text{Tanh} \delta_1 x_{01} \text{Sin} \kappa d \right) \quad (10.24)$$

$$\frac{\delta_3}{\kappa} E_d \text{Tanh} \delta_3 x_{03} = E_0 \left(\frac{\delta_1}{\kappa} \text{Tanh} \delta_1 x_{01} \text{Cos} \kappa d - \text{Sin} \kappa d \right) \quad (10.25)$$

Eliminating E_0 and E_d from eqns. 10.24 and 10.25 leads to the nonlinear eigenvalue equation [3,10,17]

$$\text{Tan} \kappa d = \frac{\kappa (\delta_1 \text{Tanh} \delta_1 x_{01} - \delta_3 \text{Tanh} \delta_3 x_{03})}{\kappa^2 + \delta_1 \delta_3 \text{Tanh} \alpha_1 x_{01} \text{Tanh} \delta_3 x_{03}} \quad (10.26)$$

This equation is the nonlinear version of eqn. 9.5 (see chapter 9) which was for the linear case. We note that here we have $\delta_1 \text{Tanh} \delta_1 x_{01}$ and $-\delta_3 \text{Tanh} \delta_3 x_{03}$ in place of δ and γ of eqn. 9.5. It is encouraging to note that eqn. 9.5 can be derived exactly using eqn. 10.26 if we let $x_{01} \rightarrow \infty$, and $x_{03} \rightarrow -\infty$ (ie. when both claddings are linear),

$$\text{Tan} \kappa d = \frac{\kappa (\delta_1 + \delta_3)}{\kappa^2 - \delta_1 \delta_3} \quad (10.27)$$

Substituting for A and B from eqns. 10.18 and 10.19 and E_0 from eqn. 10.22 into eqns 10.10-10.12 and re-arranging gives,

$$E_1(x) = E_0 [\text{Cosh} \delta_1 x - \text{Sinh} \delta_1 x \text{Tanh} \delta_1 x_{01}]^{-1} \quad x < 0 \quad (10.28)$$

$$E_2(x) = E_0 \left(\text{Cos} \kappa x + \frac{\delta_1}{\kappa} \text{Sin} \kappa x \text{Tanh} \delta_1 x_{01} \right) \quad 0 \leq x < d \quad (10.29)$$

$$E_3(x) = E_0 \left(\text{Cos} \kappa d + \frac{\delta_1}{\kappa} \text{Sin} \delta_2 d \text{Tanh} \delta_1 x_{01} \right) \left[\text{Cosh} \delta_3 (x-d) - \text{Sinh} \delta_3 (x-d) \text{Tanh} \delta_3 x_{03} \right]^{-1} \quad x \geq d \quad (10.30)$$

These equations are the nonlinear versions of eqns 9.2-9.4.

10.3.4 Linear core with nonlinear cladding on one side

To model the nonlinear directional coupler with the nonlinearity in the separation region [51], one cladding (region 3) is allowed to become linear, but the other cladding remains as nonlinear [10] (see Fig. 10.3)

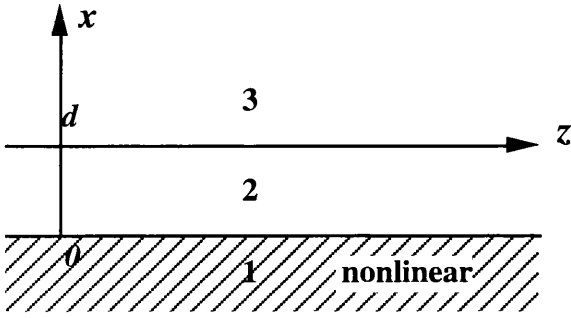


Fig. 10.3 illustrating linear core, and nonlinearity in region 1 only.

Therefore as $x_{03} \rightarrow -\infty$, the eigenvalue equation (eqn. 10.26) becomes

$$\text{Tan} \kappa d = \frac{\kappa (\delta_1 \text{Tanh} \delta_1 x_{01} + \delta_3)}{\kappa^2 - \delta_1 \delta_3 \text{Tanh} \delta_1 x_{01}} \quad (10.31)$$

Also as $x_{03} \rightarrow -\infty$, the fields become (using eqns. 10.28-10.30)

$$E_1(x) = E_0 \left[\text{Cosh} \delta_1 x - \text{Sinh} \delta_1 x \text{Tanh} \delta_1 x_{01} \right]^{-1} \quad x < 0 \quad (10.32)$$

$$E_2(x) = E_0 \left(\text{Cos} \kappa x + \frac{\delta_1}{\kappa} \text{Sin} \kappa x \text{Tanh} \delta_1 x_{01} \right) \quad 0 \leq x < d \quad (10.33)$$

$$E_3(x) = E_0 \left(\text{Cos} \kappa d + \frac{\delta_1}{\kappa} \text{Sin} \kappa d \text{Tanh} \delta_1 x_{01} \right) e^{-\delta_3 (x-d)} \quad x \geq d \quad (10.34)$$

10.3.5 Calculating the total power

In this section, Poynting's theorem is used to calculate the total power \mathcal{P} carried by the nonlinear waveguide. The motive is to relate the power-dependent propagation coefficient β to the total power \mathcal{P} [4,8]. Time-averaged intensity I_{av} can be calculated using eqn. A6.12. Power per unit length can be derived by integrating the intensity over total cross-section.

$$\mathcal{P} = \int_{-\infty}^{+\infty} I_{av} dx = \frac{\beta}{2\omega\mu_0} \int_{-\infty}^{+\infty} E^2 dx \quad (10.35)$$

Substituting the field (eqns. 10.32-10.34) into eqn. 10.35 and integrating gives

$$\mathcal{P} = \frac{\beta\delta_1^2(1 - \text{Tanh}^2\delta_1x_{01})}{k_0^2\omega\mu_0\alpha_1} \left[\begin{aligned} & \frac{1}{\delta_1[1 + \text{Tanh}\delta_1x_{01}]} + \\ & \frac{d}{2} \left[1 + \frac{\delta_1^2}{\kappa^2} \text{Tanh}^2\delta_1x_{01} \right] + \\ & \frac{\text{Sin}2\kappa d}{4\kappa} \left[1 - \frac{\delta_1^2}{\kappa^2} \text{Tanh}^2\delta_1x_{01} \right] + \\ & \frac{\delta_1}{\kappa^2} \text{Tanh}\delta_1x_{01} \text{Sin}^2\kappa d + \\ & \frac{1}{2\delta_3} \left(\text{Cos}\kappa d + \frac{\delta_1}{\kappa} \text{Tanh}\delta_1x_{01} \text{Sin}\kappa d \right)^2 \end{aligned} \right] \quad (10.36)$$

This equation relates the total power \mathcal{P} to the propagation coefficient β . We therefore note that κ , δ_1 , and δ_3 can be related to β via eqns. 10.13, and $\text{Tanh}\delta_1x_{01}$ can be calculated by rearranging the eigenvalue equation (eqn. 10.31). ie.

$$\text{Tanh}\delta_1x_{01} = \frac{\kappa(\kappa \text{Tan}\kappa d - \delta_3)}{\delta_1(\kappa + \delta_3 \text{Tan}\kappa d)} \quad (10.37)$$

The relationships between the power \mathcal{P} and the mode index (β/k_0) (commonly referred to as the dispersion curves [eg. 16]) are plotted in Fig. 10.4 using eqn. 10.36 for various guide thicknesses. When plotting the curves it is useful to note that the power \mathcal{P} in eqn. 10.36 is always real, even if κ is driven imaginary. This is because $\text{Cos}\kappa d$ becomes $\text{Cosh}|\kappa|d$ for imaginary κ and hence is real, and $\text{Sin}\kappa d/\kappa$ becomes $\text{Sinh}|\kappa|d/|\kappa|$ and is also real. Furthermore a close examination of eqn. 10.37 reveals that $\text{Tanh}\delta_1x_{01}$ must be real even if κ is imaginary, therefore \mathcal{P} is always real.

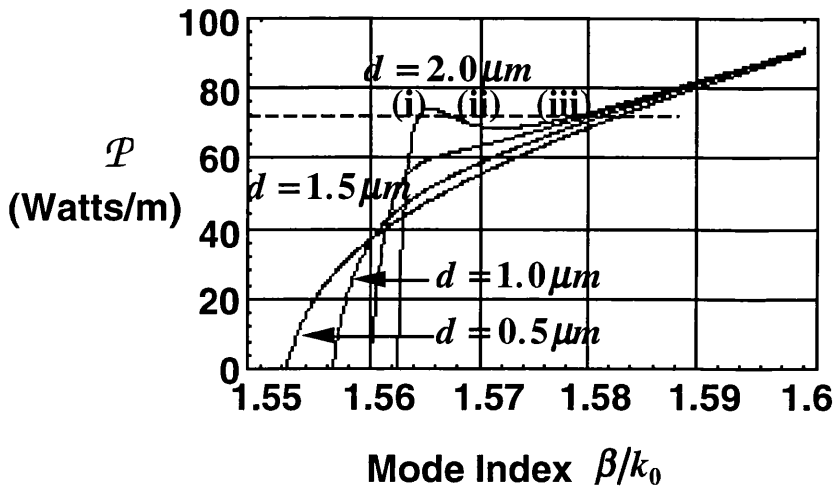


Fig. 10.4 Relationship between power/unit length \mathcal{P} and mode index for various guide thicknesses. $\bar{\epsilon}_1 = \bar{\epsilon}_3 = (1.55)^2$, and $\bar{\epsilon}_2 = (1.57)^2$, $\alpha_1 = 6.377 \times 10^{-12} \text{ m}^2/\text{V}^2$, $\lambda = 1.064 \mu\text{m}$ [11,51]

From Fig. 10.4, it is observed that at low powers (eg. zero power), the mode index is larger for the thicker guides. This is because the field is contained mostly within the high index core in these guides, and so the index of the mode happens to be large.

As the input power is increased, the mode indices of the thinner guides increase more rapidly than the thicker guides. In this case the modes of thin guides are spread more outside the film region and therefore have a larger proportion in the nonlinear cladding region. Any slight increase in the power is likely to increase the refractive index in the cladding by an appreciable amount and this causes the mode index to be increased.

The curve for the $d = 2.0 \mu\text{m}$ guide is interesting in that it peaks suddenly at $\mathcal{P} \cong 74 \text{ W/m}$, then decreases and then follows the other curves. The peak is due to the mode transitioning from a virtually power-independent film-guided mode to a power-dependent surface mode. For thick guides ($d = 2.0 \mu\text{m}$), the mode is concentrated in the film region and has only a small fraction in the nonlinear region. Consequently quite large powers are needed to cause the mode to become power dependent.

Once the power is large enough, the subsequent transition from linear *TE* mode to surface mode is rapid (for the thick guides). Also once the surface modes have been formed for different thickness guides, they become similar to one another and independent of the guides they originate from. This is the reason why the $d = 2.0 \mu\text{m}$ curve decreases at first before joining the other curves at larger mode indices.

The $d = 2.0\mu\text{m}$ curve shown in Fig. 10.4 looks different to that in [8], and [11]. The peak (threshold power) here reaches around 74 W/m whereas theirs reaches a much higher power. There are two reasons why we believe our curve is more correct than the one in ref. 11. Firstly, 74 W/m corresponds with the 'maximum power' observed by Meng and Okamoto [51]. Secondly, we found that the mode index (β/k_0) at $\mathcal{P} = 0$ here corresponds with that calculated using the linear eigenvalue equation (which is around 1.56229), whereas [8,11] gives around 1.567.

Between 70 and 74 W/m , with $d = 2.0\mu\text{m}$, there are three values for the mode index (labelled (i), (ii), and (iii) in Fig. 10.4), for every value of \mathcal{P} . According to Kolokolov [23], the modes which lie on the positive slope (eg. (i) and (iii) in Fig. 10.4) correspond with stable modes, and the ones lying on the negative slope with the unstable mode. If the guide is excited with one of the stable modes, then the field stays stationary with propagation distance, but if the unstable mode is chosen, the mode wobbles between the two stationary mode. The variation of the field with distance when the nonlinear guide is excited in turn with modes corresponding to points (i), (ii) and (iii) on Fig. 10.4 are shown in a BPM diagram (see Figs. 10.5-10.7 respectively). Using a power of 72 Watts/m Figs. 10.5, and 10.7 correspond with the stable modes (points (i) and (iii)), whereas Fig. 10.6 (point (ii)) corresponds with an unstable mode. It is noticed, that the field 'wobbles' sideways periodically as it propagates.

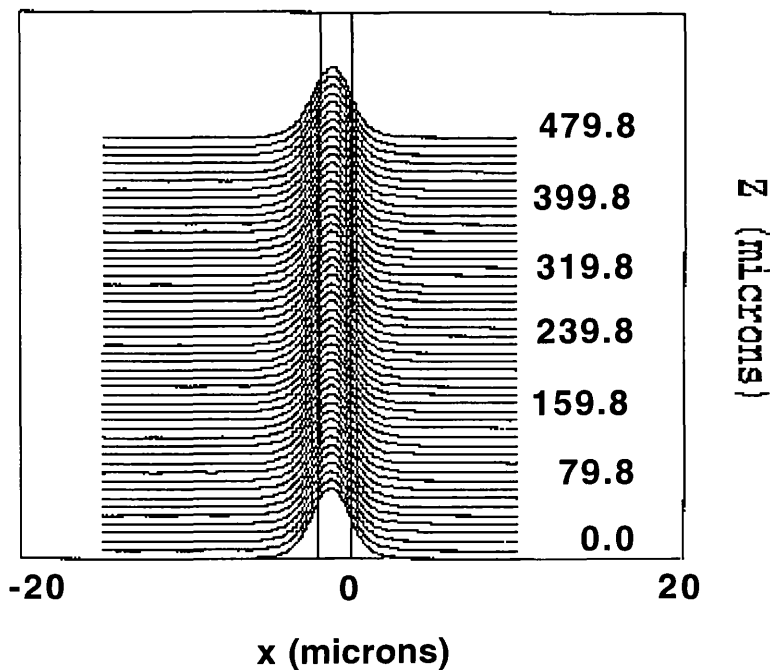


Fig. 10.5 BPM simulation. Power= 72 Watts/m . Relating to state (i) in Fig. 10.4

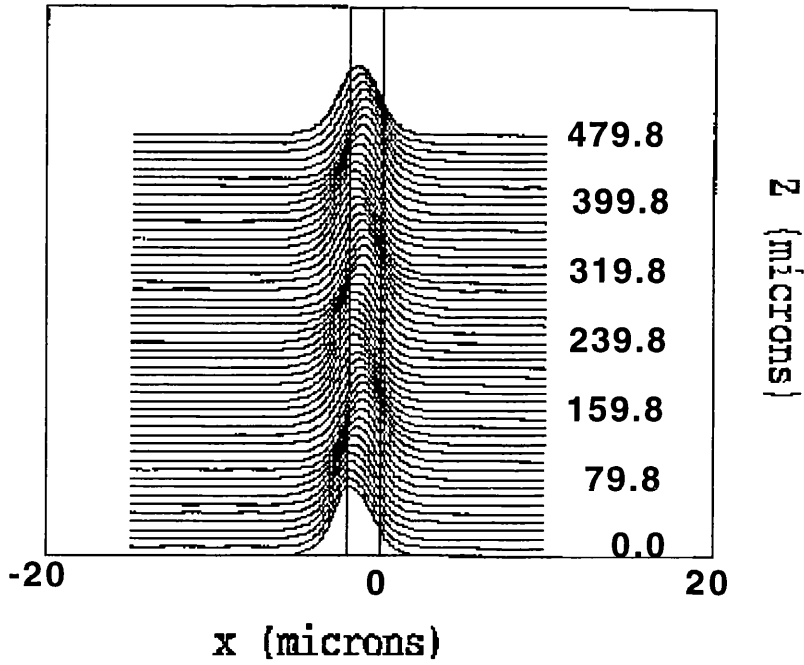


Fig. 10.6 BPM simulation. Nonlinearity in the left hand cladding. Power=72 Watts/m, state (ii) in Fig. 10.4

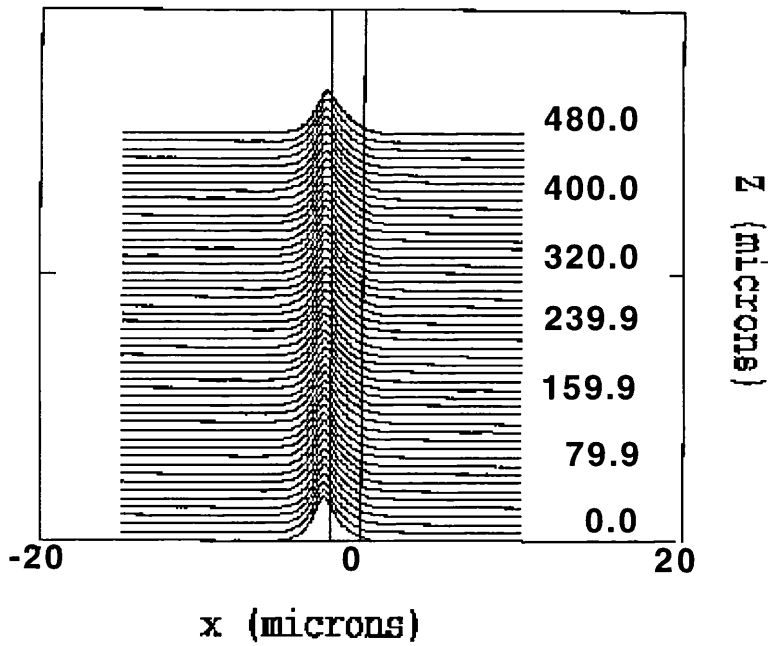


Fig. 10.7 BPM simulation. Nonlinearity in the left hand cladding. Power=72 Watts/m, state (iii) in Fig. 10.4

Therefore we need to use either points (i) or (iii) in Fig. 10.4 for input to the BPM program. The relationships between power \mathcal{P} , and x_{01} are shown in Figs. 10.8 and 10.9 for two guide thicknesses $d = 2.0\mu\text{m}$, and $d = 1.0\mu\text{m}$ respectively. We note that $x < 0$ refers to the nonlinear cladding and $0 \leq x \leq d$ the linear film.

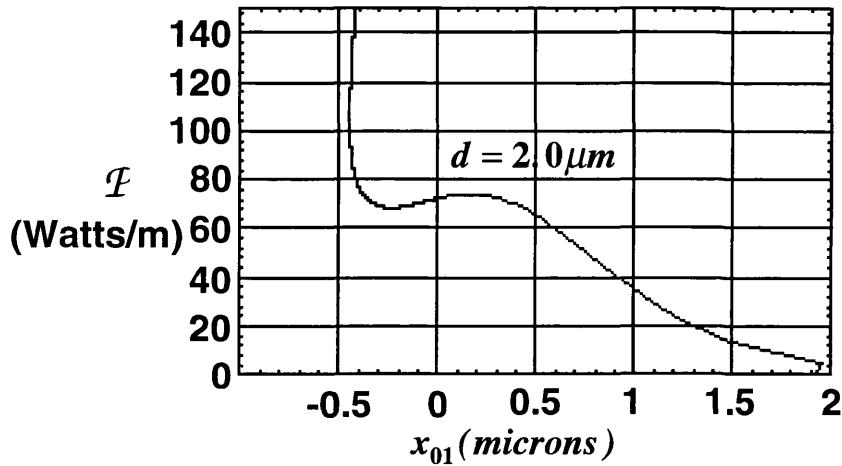


Fig. 10.8 Illustrating total power/unit length against x_{01} for $d = 2.0\mu\text{m}$

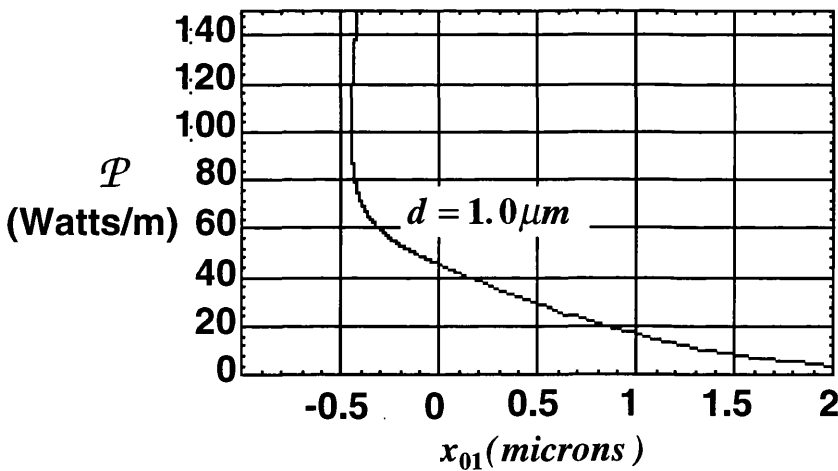


Fig. 10.9 Illustrating power/unit length against x_{01} for $d = 1.0\mu\text{m}$

At low input powers, the nonlinear cladding is approximately linear. Therefore x_{01} is large and positive in Figs. 10.8 and 10.9 (cf Fig. 10.3). As the input power increases, x_{01} decreases, and shifts towards the nonlinear region. Once x_{01} reaches zero, the field becomes a surface mode. A further increase in the power causes the field maximum to enter the nonlinear region. x_{01} keeps decreasing until it reaches around $-0.4\mu\text{m}$, where it stops decreasing. At this point the field starts to narrow.

We notice that once the mode becomes a surface wave ($\mathcal{P} = 74 \text{ W/m}$) the curves for the two thicknesses (Figs. 10.8 and 10.9) become similar. This is expected, because once a mode becomes self-guiding, it is independent of its original guide.

10.3.6 Comparing the field amplitude with that calculated in chapter 9

To check whether the formulation in this chapter matches the one in chapter 9, the linear limit of E_0 can be calculated. This should result in eqn. 9.12.

To calculate E_0 for linear guides, we cannot use eqn. 10.14 and simply say $x_{01} \rightarrow \infty$. There is an α_1 in the denominator which tends to zero for linear guides. Another approach is to use the relationship between \mathcal{P} and E_0 derived in eqn. 10.36 and let $x_{01} \rightarrow \infty$. Therefore eqn. 10.36 becomes (after a little rearranging),

$$\mathcal{P} = \frac{\beta E_0^2}{2\omega\mu_0} \left[\begin{aligned} &\frac{1}{2\delta_1} + \frac{1}{2\delta_3} + \frac{d}{2} + \frac{\delta_1^2 d}{2\kappa^2} \\ &+ \text{Sin} \kappa d \text{Cos} \kappa d \left(\frac{1}{2\kappa} - \frac{\delta_1^2}{2\kappa^3} + \frac{\delta_1}{\delta_3 \kappa} \right) \\ &+ \text{Sin}^2 \kappa d \left(\frac{1}{2\delta_3} \left(\frac{\delta_1^2}{\kappa^2} - 1 \right) + \frac{\delta_1}{\kappa^2} \right) \end{aligned} \right] \quad (10.38)$$

After much manipulations, eqn. 10.38 becomes

$$E_0^2 = \frac{4\kappa^2 \omega \mu_0 \mathcal{P}}{\beta (\kappa^2 + \delta_1^2) \left(d + \frac{2}{\delta_1} \right)} \quad (10.39)$$

which reassuringly compares exactly with that calculated for linear guides in chapter 9 (see eqn. 9.12).

10.4 THE NONLINEAR DIRECTIONAL COUPLER

In nonlinear directional couplers (NLDCs), the situation is a little more complex. Since the power of the mode determines its shape, the problem is determining what power to use. One can either consider the fractional power carried by each mode at a particular propagation distance [53], or use the full power in the NLDC for the individual modes. The latter approach was the one taken by Meng and Okamoto [51]. As seen in chapter 12, this gives accurate results. We also propose in chapter 12 that because some of the power is stored in the overlap integral, this should not be included in the total power for

Chapter 10 Coefficients incorporating nonlinear *TE* modes

calculating the mode shapes.

We assume the guides are identical. Shifting the fields (eqns. 10.40-10.42) by $-d$ gives the equation for guide '1'.

$$E_1 = E_0 \left[\text{Cos} \kappa d + \frac{\delta_1}{\kappa} \text{Sin} \kappa d \text{Tanh} \delta_1 x_{01} \right] e^{-\delta_3 x} \quad x \geq 0 \quad (10.40)$$

$$E_1 = E_0 \left[\text{Cos} \kappa (x + d) + \frac{\delta_1}{\kappa} \text{Sin} \kappa (x + d) \text{Tanh} \delta_1 x_{01} \right] \quad -d < x \leq 0 \quad (10.41)$$

$$E_1 = E_0 \left[\text{Cosh} \delta_1 (x + d) - \text{Sinh} \delta_1 (x + d) \text{Tanh} \delta_1 x_{01} \right]^{-1} \quad x \leq -d \quad (10.42)$$

Therefore, $E_1(-d) = E_0$, and $E_1(0) = E_d$

For the second guide, we reverse the fields (eqns. 10.40-10.42), and shift by $-(2d + w)$ to give

$$E_2 = E_0 \left[\text{Cosh} \delta_1 (x + d + w) + \text{Sinh} \delta_1 (x + d + w) \text{Tanh} \delta_1 x_{01} \right]^{-1} \quad x \geq -(d + w) \quad (10.43)$$

$$E_2 = E_0 \left[\text{Cos} \kappa (x + d + w) - \frac{\delta_1}{\kappa} \text{Sin} \kappa (x + d + w) \text{Tanh} \delta_1 x_{01} \right] \quad -(2d + w) \leq x \leq -(d + w) \quad (10.44)$$

$$E_2 = E_0 \left[\text{Cos} \kappa d + \frac{\delta_1}{\kappa} \text{Sin} \kappa d \text{Tanh} \delta_1 x_{01} \right] e^{\delta_3 (x + 2d + w)} \quad x \leq -(2d + w) \quad (10.45)$$

Therefore $E_2(-(d + w)) = E_0$, and $E_2(-(2d + w)) = E_d$

To draw the field for each guide, we use the values for δ_1 , κ , E_0 and x_{01} as calculated from eqns. 10.36 and 10.37 for a particular power \mathcal{P} . It should be noted that the fields E_1 , and E_2 are real, even if κ is driven imaginary at high powers for the same reasons as given after eqn. 10.37.

Eqns. 10.40-10.45 are used to draw the modes of the two guides for different input powers (see Figs. 10.10). The vertical lines show the guide edges. We can observe that at high powers

(chained curves), the modes penetrate into the separation region, and increase their overlap. At even higher powers (solid curves) we notice that the fields narrow and reduce their overlap.

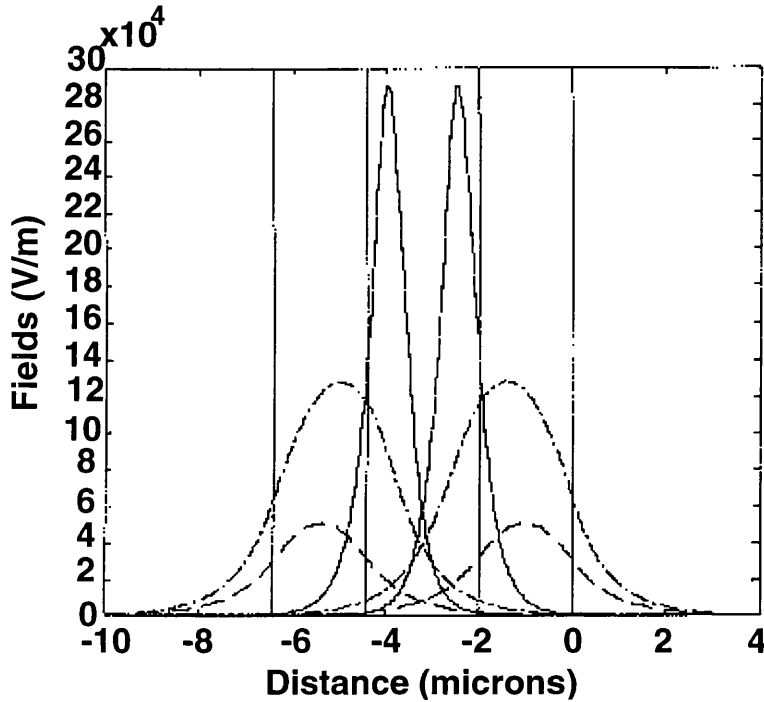


Fig. 10.10 Mode shapes for three powers $\mathcal{P} = 10 \text{ W/m}$ (dashed), 40 W/m (chained), 100 W/m (solid) ($d = 2.0 \mu\text{m}$, $w = 2.4 \mu\text{m}$, $n_1 = n_3 = n_5 = 1.55$, $n_2 = n_4 = 1.57$)

In the next section, the properties of all the linear and nonlinear coefficients are investigated. It is rather difficult to derive analytical solutions in view of the fact that the equations for the fields are more complicated here than for the linear case in Chapter 7. Therefore the integrations are performed numerically using NAG integration package D01GAF, which uses third-order finite difference formulae (according to a method by Gill and Miller [52])

10.5 VARIATION OF COEFFICIENTS WITH INPUT POWER

In this section a study of the characteristics of all the coefficients appearing in the two guide coupled mode equations is made. The guide parameters are the same as Meng and Okamoto [51], ie two guides (thickness d) separated by a nonlinear medium of width w . We assume that the refractive indices are $n_1 = n_3 = 1.55$, $n_2 = 1.57$, and $n_{3NL} = 10^{-9} \text{ m}^2/\text{W}$.

For simplicity we use the same notation as in chapter 9, ie. Q_1 , Q_2 , Q_3 notation for the nonlinear coefficients, and assume perfect symmetry such that $Q_1 = Q_{11}^{(1)} = Q_{22}^{(2)}$, $Q_2 = Q_{12}^{(1)} = Q_{12}^{(2)}$, $Q_3 = Q_{11}^{(2)} = Q_{22}^{(1)}$. We also note that $K_{11} = K_{22}$ and $K_{12} = K_{21}$.

10.5.1 Overlap integrals

In chapter 9 we studied the variation of the overlap integral with guide separation w for various guide thicknesses d (see Fig. 9.3). At that stage we assumed that the field shapes were power independent (linear). We observed that the overlap integral increased with reduction in the guide separation. The variation of the overlap integral with input power is now investigated in Fig 10.11 for various guide separations. A thickness of $d = 2.0\mu\text{m}$ is assumed for both guides. It can be seen that using power dependent field shapes causes the overlap integral to become a nonlinear function of input power. The power independent (linear) case is shown for comparison (see horizontal dotted line in Fig. 10.11).

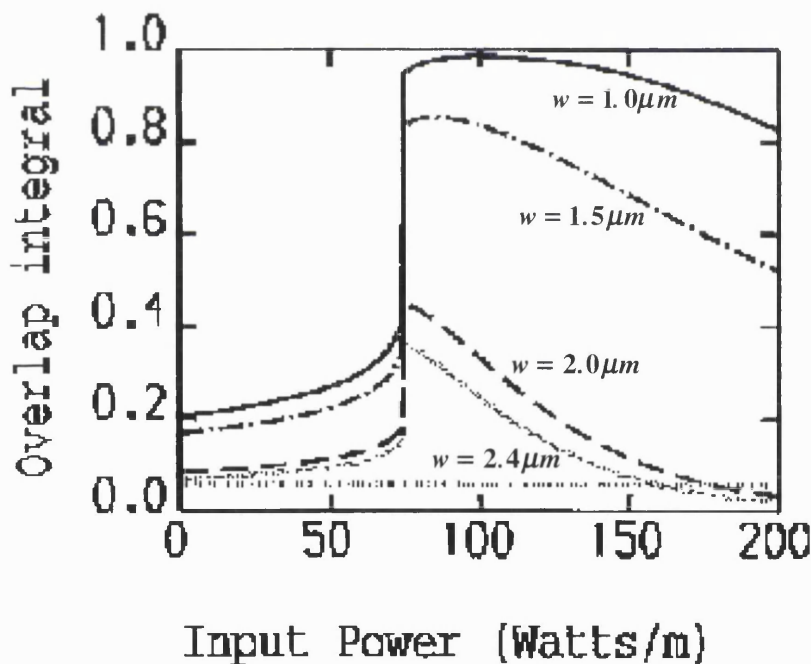


Fig. 10.11 Variation of overlap integral with input power $d = 2.0\mu\text{m}$, (i) $w = 1.0\mu\text{m}$ (solid), (ii) $w = 1.5\mu\text{m}$ (chained), (iii) $w = 2.0\mu\text{m}$ (chained), (iv) $w = 2.4\mu\text{m}$ (dotted) (power dependent curve), (v) $w = 2.4\mu\text{m}$ (power independent curve)

The solid curve in Fig. 10.11 refers to the case when the guides are closest together ($w = 1.0\mu\text{m}$). It can be observed that at low powers the overlap integral increases with

input power. As the input power increases, the fields are attracted towards the nonlinear separation region, and overlap each other more as a result. The increase in the overlap integral with input power is slow at first, but then gradually becomes more rapid, and asymptotic at threshold power (around 74 W/m). Physically the threshold power is the power where the guided mode suddenly becomes a surface mode. At this power, the overlap integral jumps from 0.4 to 0.95. Above this power, the overlap integral increases gradually with input power until it reaches a value close to 1. As before, the increase occurs because the modes slant towards each other as the power is increased. At a certain power, the modes stop shifting further into the cladding (see Fig. 10.8), and instead start to narrow because of self-focusing (see Fig. 10.10). Consequently the overlap between the modes starts to reduce (see Fig. 10.11), and the overlap integral decreases. Although the initial increase in the overlap integral with input power has been mentioned before [51], we are the first to mention this decrease in the overlap integral with input power.

The effect of the decrease in overlap integral due to field narrowing becomes important for larger separations. Above threshold power, the overlap integral reduces at a rate which is greater for larger guide separations. At very large separations (eg. $w = 6.0 \mu\text{m}$ not shown in Fig. 10.11), the overlap integral just drops discontinuously to a lower value at threshold power.

The $d = 0.5 \mu\text{m}$ case was also investigated (graphs not included here). The modes for this case are wider spread than the $d = 2.0 \mu\text{m}$ case. Consequently these modes are affected more by the nonlinearity in the cladding, and are more sensitive to changes in input powers. The variation of the overlap integral with input power is continuous here and occurs over all powers, in contrast to the $d = 2.0 \mu\text{m}$ case where the overlap integral changes significantly only near the threshold power. The discontinuity seen in the $d = 2.0 \mu\text{m}$ case is not observed here, but the variation is otherwise similar. As in the $d = 2.0 \mu\text{m}$ case, at low powers the overlap integral increases because the modes overlap more, and at high powers reduces because of self-focusing. At an intermediate power the overlap integral peaks. The peak tends to move to lower input powers as the guide separation is increased. This is because field narrowing effects are more important for large guide separations.

10.5.2 Coupling coefficient

The variation of the coupling coefficient with input power and guide separation was investigated next. We observed that the relationships were similar to those found for the overlap integral. The variation with guide separation was exactly the same as with the

overlap integral. The coupling coefficient decreased because the modes were physically more apart. The variation with input power was slightly different to that of the overlap integral, because whereas the overlap integral is an integral over all space and depends on the physical overlap between the modes, the coupling coefficient is an integral over one of the guide regions, and is therefore dependent on the field strength in that region. Therefore even if the overlap between the modes increases with input power, this does not necessarily mean the coupling coefficient increases, because it is the field strength over the perturbation region which matters. We found that the coupling coefficient did not generally increase as much as the overlap integral at lower powers, but started to reduce at higher powers due to self-focusing of the field.

We varied the film thickness to investigate the variation of the coupling coefficient with input power. We found discontinuities at threshold power for the $d = 2.0\mu\text{m}$ case, similar to those for the overlap integral above. Above threshold we found that the coupling coefficient decreased sharply until at very high powers it reached zero.

For the smaller thicknesses the coupling coefficient varied continuously with input power, just as was observed for the overlap integral. We saw that the peak shifted to lower input powers as the guide thickness was decreased.

The effect of the overlap integral on the coupling coefficient (ie. K_{pq}^m) was examined next. As indicated in previous chapters (also see eqn. 11.11), the overlap integral modifies the value of each coefficient, and it is the modified value, ie K_{pq}^m and not the actual coefficient K_{pq} which determine the critical power. This can be seen clearly in the critical power formula (CPF) (see eqn. 11.42) derived in chapter 11. It can be seen that the modified form of the coefficients rather than the actual coefficients appear in formula.

For the thick guide ($d = 2.0\mu\text{m}$) where the overlap integral is negligible, the value for K_{pq}^m was exactly the same as K_{pq} at all powers. However for the $d = 0.5\mu\text{m}$ case where the overlap integral is large (see Fig. 10.12) we saw that K_{pq}^m was larger than K_{pq} for the lower powers. At higher powers the curves are similar.

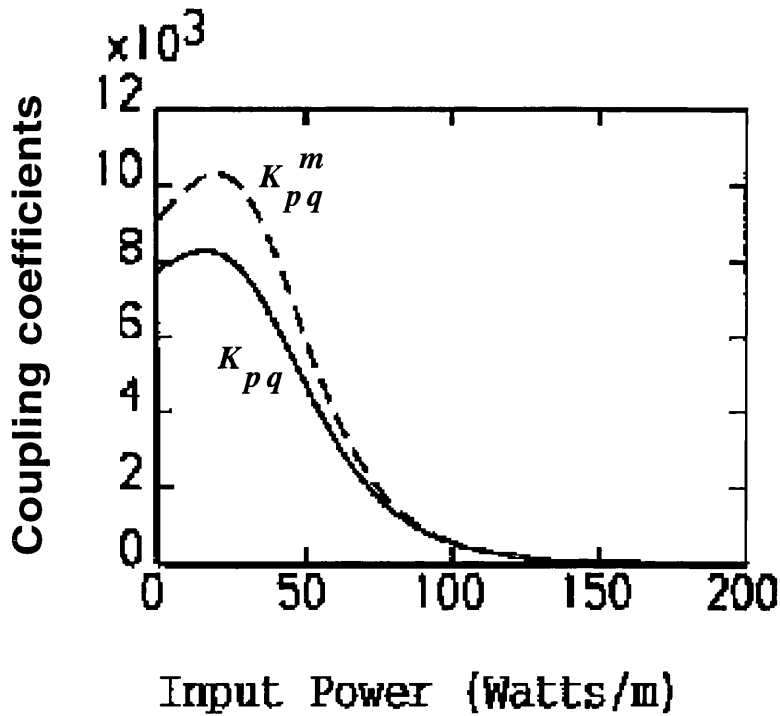


Fig. 10.12 Variation of coupling coefficients with input power for $d = 0.5\mu\text{m}$, $w = 2.0\mu\text{m}$ (i) K_{pq} (solid curve), (ii) K_{pq}^m (dashed curve)

10.5.3 Nonlinear modification coefficient (NLMC)

Fig. 10.13 shows the variation of the self-phase modulation Q_1 with input power for two guides with film thicknesses $d = 0.5\mu\text{m}$, and $2\mu\text{m}$ where the separation between the guides is assumed to be $w = 2.0\mu\text{m}$. It can be seen that whilst the $d = 0.5\mu\text{m}$ case (upper solid curve) is continuous at all input powers, the $d = 2.0\mu\text{m}$ case (see lower solid curve) is discontinuous at the threshold power. Below threshold, Q_1 is greater for the $d = 0.5\mu\text{m}$ case, because the fields in this case extend further into the nonlinear separation region and are affected more by the nonlinearity. Above threshold, the curves are similar since the fields are all surface modes, and affected by the same amount by the nonlinearity. It can be seen that above threshold the variation of Q_1 becomes linear with input power and the slope is much steeper than that below threshold.

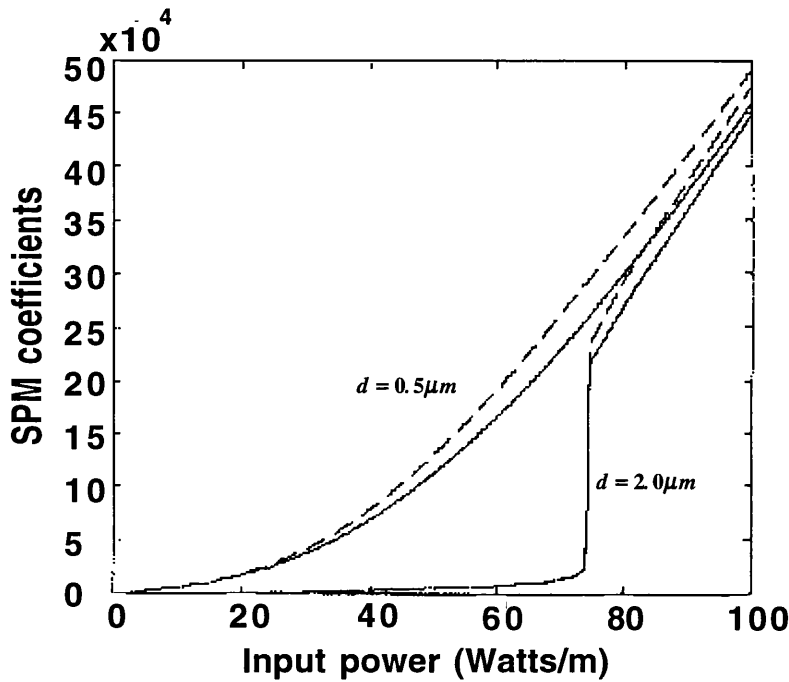


Fig. 10.13 Variation of Q_1 and Q_1^m with guide thickness and input power.

(i) Q_1 $d = 0.5\mu m$, $w = 2.0\mu m$ (upper solid curve), (ii) Q_1 $d = 2.0\mu m$, $w = 2.0\mu m$ (lower solid curve), (iii) Q_1^m $d = 0.5\mu m$, $w = 2.0\mu m$ (upper dashed curve), (iv) Q_1^m $d = 0.5\mu m$, $w = 2.0\mu m$ (lower dashed curve)

In Fig. 10.13 we can also see how the self-phase-modulation terms are modified by the overlap integral (Q_1^m 's) (see dashed curves and eqn 11.10 (next chapter) for the definition). For the $d = 0.5\mu m$ case, Q_1^m was found to be larger than Q_1 at all input powers. For the $d = 2.0\mu m$ case Q_1^m was observed to be similar to Q_1 below threshold, but slightly greater than Q_1 above threshold. It can also be seen that the modified coefficients (dashed curves) become similar at high powers.

10.5.4 The nonlinear cross-coefficients

Fig. 10.14 shows the variation of Q_2 with input power for $d = 2.0\mu m$, and various guide separations. We first notice the discontinuous change in Q_2 at the threshold power, which is characteristic of the $d = 2.0\mu m$ case. It can also be observed that the guide separation has an effect on Q_2 in contrast to what was observed for Q_1 . This is because Q_2 is a coupling coefficient, which depends on the interaction between two separate fields. Therefore it reduces when the separation between the fields is increased. In Fig. 10.14 we can see that above threshold, Q_2 initially increases with

input power, reaches a peak, and then reduces at higher powers due to field narrowing effects (see section 10.4.1). One remembers that in the Q_1 case (cf. Fig. 10.13) the relationship was linear with input power above threshold.

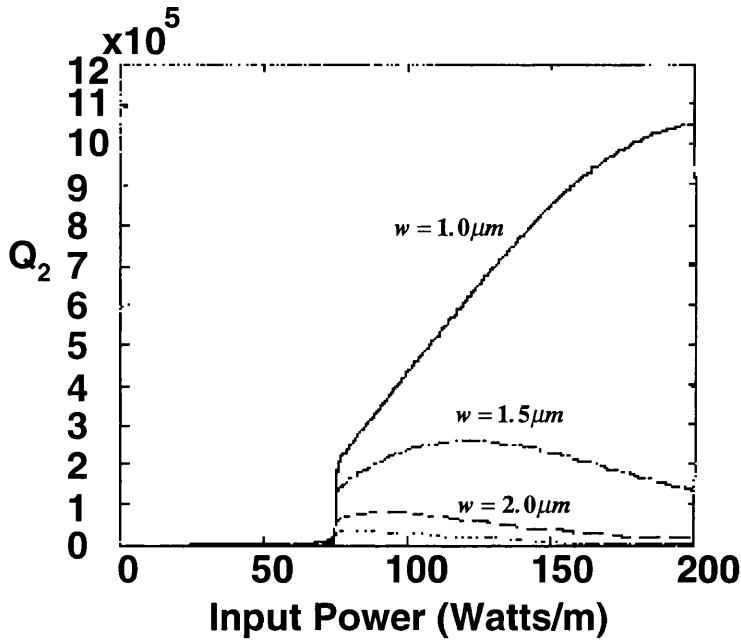


Fig. 10.14 Variation of Q_2 with input power $d = 2.0 \mu m$, (i) $w = 1.0 \mu m$ (solid) (ii) $w = 1.5 \mu m$ (chained), (iii) $w = 2.0 \mu m$ (dashed), (iv) $w = 2.4 \mu m$ (dotted)

We next investigated the effect of varying the film thickness. We saw that the film thickness did not have an effect above threshold, but below threshold Q_2 became larger with thinner films.

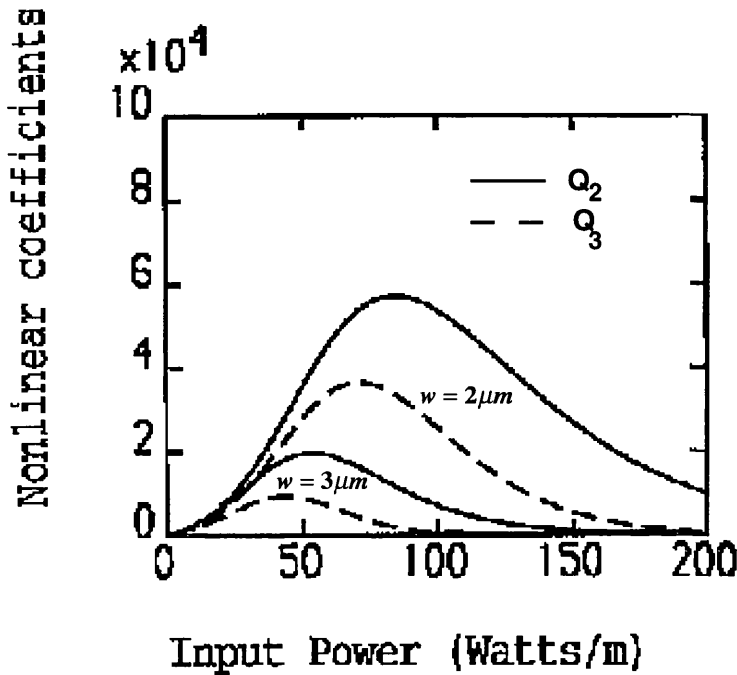


Fig. 10.15 (i) Q_2 $w = 3.0 \mu m$ (lower solid), (ii) Q_3 $w = 3.0 \mu m$ (lower dashed), (iii) Q_2 $w = 2.0 \mu m$ (upper solid), (iv) Q_3 $w = 2.0 \mu m$ (upper dashed)

The variation of Q_3 with input power and with guide separation is very similar to that of Q_2 . A comparison between Q_2 and Q_3 is shown in Fig. 10.15 for $d = 0.5 \mu m$ and the two separations $w = 3.0 \mu m$ and $w = 2.0 \mu m$. The upper solid (Q_2) and dashed (Q_3) curves refer to the smaller separation $w = 2.0 \mu m$. It can be seen that the peaks are at higher input powers for the smaller guide separations. This is because as the guide separation is decreased, the amount of nonlinearity also decreases and therefore more power is needed to compensate. It can be seen that $Q_2 > Q_3$ at all input powers. However, as we shall see in chapter 11, it is not the actual values Q_2 and Q_3 which affect the switching power, but the effect that the overlap integral has on these coefficients. It can be seen from the critical power formula (CPF) in eqn. 11.42 that, Q_2 becomes the overlap integral dependent $Q_{2,av}^m$ ($= (Q_2^m + Q_2^{m'})/2$) where Q_2^m and $Q_2^{m'}$ are defined in eqns. 11.10 and 11.9 respectively, and Q_3 becomes Q_3^m . We show in Fig. 10.16 the variation of $Q_{2,av}^m$ and Q_3^m with input power for $d = 0.5 \mu m$ for two guide separations $w = 2.0 \mu m$ (upper solid and dashed curves) and $w = 3.0 \mu m$ (lower solid and dashed curves). We saw that up to $50 W/m$, $Q_{2,av}^m$ was small but positive, but above that went negative. We observed that at low input powers, $Q_{2,av}^m > Q_3^m$ whereas at high input powers, $Q_3^m > Q_{2,av}^m$. Therefore it is dangerous to leave out Q_2 or Q_3 without careful attention to the effect of the overlap integral, guide thickness, and input power.

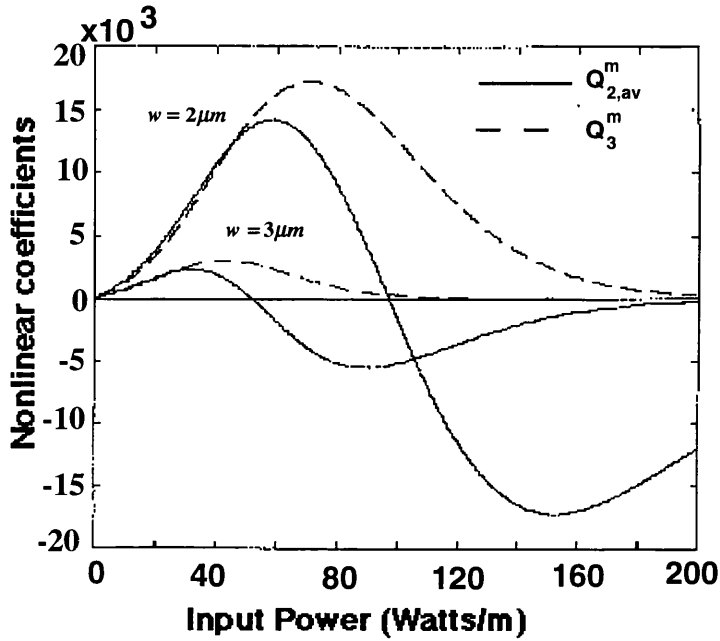


Fig. 10.16 Variation of $Q_{2,av}^m$ (solid curves) and Q_3^m (dashed curves) with input power for $d = 0.5 \mu m$ for two guide separations $w = 2.0 \mu m$ (upper solid and dashed curves) and $w = 3.0 \mu m$ (lower solid and dashed curves).

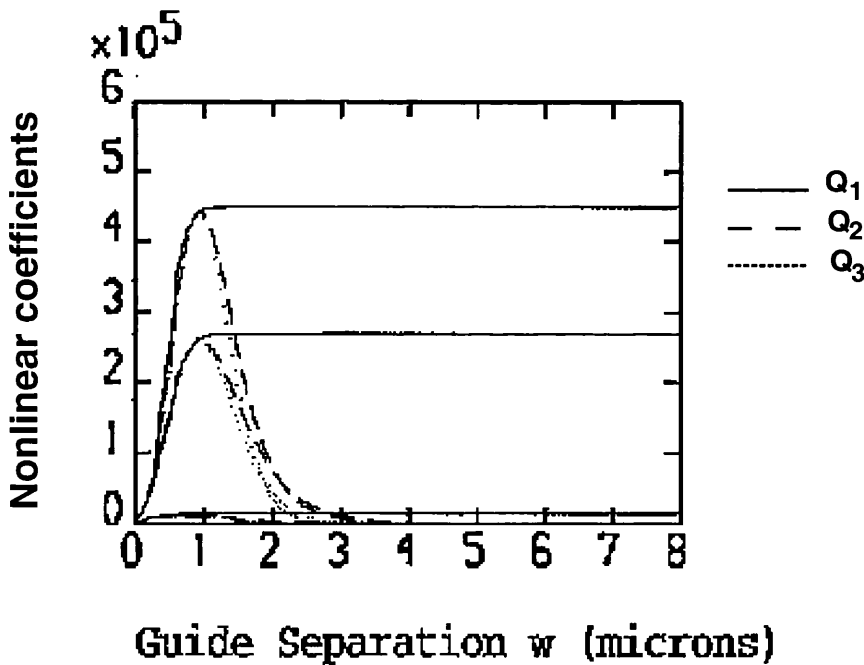


Fig. 10.17 variation of Q_1 (solid curves), Q_2 (dashed curves), and Q_3 (dotted curves) with guide separation for three input powers 70 W/m (lower curves), 80 W/m (middle curves), and 100 W/m (upper curves), assuming a film thickness of $d = 2.0 \mu m$.

In Fig. 10.17, we plot the variation of Q_1 , Q_2 , and Q_3 with guide separation for three input powers 70, 80, and 100W/m, assuming a film thickness of $d = 2.0\mu\text{m}$. It can be seen that for zero guide separation, where there is no nonlinearity, all three coefficients are zero. As the separation is increased, all the coefficients initially increase together. However around $1.0\mu\text{m}$ separation, they reach a maximum. With increase in separation Q_1 stays at the maximum level since it is a self-phase-modulation coefficient and not dependent on the other guide, whereas Q_2 and Q_3 reduce, since they are concerned with the interaction between two separate fields.

10.6 CONCLUSIONS FOR CHAPTER 10

It was shown in chapter 9 (previous chapter) that when power independent (linear) mode shapes are used, the overlap integral C_{pq} , and the coupling coefficient K_{pq} are constants with power, and the nonlinear coefficients and the nonlinear coefficients Q_1 , Q_2 and Q_3 are directly proportional to power.

In this chapter we calculated the power-dependent modes for a slab waveguide. We then used these to calculate the linear and nonlinear coefficients. We showed that incorporating power dependence not only causes a nonlinear variation of the coefficients with respect to input power, but also causes these coefficients to be dependent on the film thickness and the guide separation. At low powers, the power causes the fields to be skewed towards one another, which increases the overlap between the modes, and increases the coefficients above the power independent case. At much higher powers all the linear and nonlinear coefficients as well as the overlap integral are decreased because of field narrowing effects (this has not been mentioned elsewhere).

The film thickness is important below threshold power. Modes from thinner guides overlap more, and are affected more by the nonlinearity. Modes from thicker guides are unaffected by input power until near the threshold power, where they suddenly change into surface modes and all the coefficients become sharply affected at the threshold power.

It was also discussed that it is not the actual values of the coefficients which matter in strong coupling, but the modified form due to the overlap integral. For example although $Q_2 > Q_3$ may occur at all powers, it may be possible that the modified forms of these coefficients could show $Q_3^m > Q_{2,av}^m$. Therefore it is ill-advised to omit either Q_2 or Q_3 in strong coupling without knowing in advance how they change for different parameters.

REFERENCES

- [1] W. J. Tomlinson, J. P. Gordon, P. W. Smith, and A. E. Kaplan, "Reflection of a gaussian beam at a nonlinear interface", *Applied Optics*, Vol. 21, No. 11, June 1982
- [2] A. A. Maradudin, "Nonlinear surface electromagnetic waves", *Proceedings of international school condensed matter physics*, 1983, pp. 72-142.
- [3] W. J. Tomlinson, *Opt. Lett.*, Vol. 5, 323 (1980)
- [4] A. D. Boardman, P. Egan, T. Twardowski, and M. Wilkins, "Nonlinear surface-guided waves in self-focusing optical media", *Nonlinear waves in solid state physics*, Edited by A. D. Boardman et. al., Plenum Press, New York, 1990, pp. 1-50.
- [5] E. Wright and G. I. Stegeman, "Nonlinear Planar Waveguides", *Anisotropic and Nonlinear Optical Waveguides*, 1992 Elsevier Science Publishers B.V, pp.117-141
- [6] D. Michalache, M. Bertolotti, and C. Sibilia, "Nonlinear wave propagation in planar structures", *Progress in Optics*, vol. 27, 1989, pp. 229-313.
- [7] D. J. Robbins, "*TE* modes in a slab waveguide bounded by nonlinear media", *Optics Communications*, Vol 47, No. 5, October 1983, pp.309-312.
- [8] C. T. Seaton, Jesus D. Valera, R. L. Shoemaker, and G. I. Stegeman, J. T. Chilwell, and S. Desmond Smith, "Calculations of nonlinear *TE* waves guided by thin dielectric films bounded by nonlinear media", *IEEE Journal of Quantum Electronics*, QE-21, No. 7, July 1985, pp.774-783.
- [9] N. N. Akhmediev, "Novel class of nonlinear surface waves: asymmetric modes in a symmetric layered structure", *Sov. Phys. JETP*, Vol 56, No. 2, August 1982, 299-303.
- [10] F. Lederer, U. Langbein, and H.-E. Ponath, "Nonlinear waves guided by a dielectric slab", *Appl. Phys. B*, Vol 31, 1983, pp.69-73.
- [11] G. I. Stegeman, C.T. Seaton, J. T. Chilwell, and S. Desmond Smith, "Nonlinear waves guided by thin films", *Appl. Phys. Lett*, Vol 44, No. 9, May 1984, pp.830-832.
- [12] U. Langbein, F. Lederer, and H. E. Ponath, "A new type of nonlinear slab-guided waves", *Optics Communications*, Vol 46, No. 3,4, July 1983, pp.167-169.
- [13] K. Ogusu, "*TE* waves in a symmetrical dielectric slab waveguide with a Kerr-like nonlinear permittivity", *Optical and Quantum Electron.*, vol. 19, 1987, pp. 65-72.
- [14] A. D. Boardman and P. Egan, "Optically nonlinear waves in thin films", *IEEE J. Quant. Electron.*, vol. QE-22, no. 2, 1986, pp. 319-324.
- [15] W. R. Holland, "Nonlinear guided waves in low-index, self-focussing thin films: transverse electric case", *J. Opt. Soc. Am. B*, vol. 3, no. 11, 1986, pp. 1529-1534.

- [16] J. V. Moloney, J. Ariyasu, C. T. Seaton, and G. I. Stegeman, "Stability of nonlinear stationary waves guided by a thin film bounded by nonlinear media", *Appl. Phys. Lett.*, Vol 48, No. 13, March 1986, pp.826-828.
- [17] L. Leine, Ch. Wachter, U. Langbein, and F. Lederer, "Propagation phenomena of nonlinear film-guided waves: a numerical analysis", *Optics Letters*, Vol 11, No.5, May 1986, pp. 315-317
- [18] J. V. Moloney, "Modulation instability of two-transverse-dimensional surface polariton waves in nonlinear dielectric waveguides", *Physical Review A*, Vol 36, No. 9, Nov 1987, pp.4563-4566
- [19] L. Leine, C. Wachter, U. Langbein, and F. Lederer, "Evolution of nonlinear guided optical fields down a dielectric film with a nonlinear cladding", *J. Opt. Soc. Am. B*, Vol 5, No. 2, February 1988, pp. 547-558.
- [20] N. N. Akhmediev, V. I. Korneev, and Yu. V. Kuzmenko, *Sov. Tech. Phys. Lett.*, Vol. 10, 327 (1984); *Sov. Phys. JETP*, Vol. 61, 62 (1985)
- [21] C. K. R. T. Jones and J. V. Moloney, *Phys. Lett. A* Vol. 117, 175 (1986)
- [22] N. N. Akhmediev and N. V. Ostrovskaya, *Sov. Phys. Tech. Phys.* Vol. 33, 1333 (1988)
- [23] A. A. Kolokolov, *Zh. Prikl. Mekh. Tekh. Fiz.* 3, 153 (1973); A. A. Kolokolov, *J. Appl. Soc. Mech. Tech. Phys.* 11,1975, pp. 426
- [24] J. V. Moloney, J. Ariyasu, C. T. Seaton, and G. I. Stegeman "Numerical evidence for nonstationary, nonlinear, slab-guided waves", *Optics Letters*, Vol 11, No.5, May 1986, pp. 315-317
- [25] J. Atai and Y. Chen, "Stability of the asymmetric nonlinear mode trapped in symmetric planar waveguides", *J. light. Technol.*, vol. 11, no. 4, 1993, pp. 577-581.
- [26] J-S Jeong et. al., "Optical properties of *TE* nonlinear waves in planar waveguides with two nonlinear bounding layers", *Optics Comms.*,vol. 116, 1995, pp. 351-357.
- [27] D. J. Mitchell and A. W. Snyder, "Stability of fundamental nonlinear guided waves", *J. Opt. Soc. Am. B*, vol. 10, no. 9, 1993, pp. 1572-1580.
- [28] V. M. Agranovich, V. S. Babichenko, and V. Ya. Chernyak, *Sov. Phys. JETP Lett.*, Vol.32, 513 (1980)
- [29] A. D. Boardman, A. A. Maradudin, G. I. Stegeman, T. Twardowski, and E. M. Wright, *Phys. Rev. A* Vol. 35, 1159, 1987
- [30] A. D. Boardman, T. Twardowski, A. Shivarova, and G. I. Stegeman, *IEEE Proc.*, Vol. 134, 154 (1987)
- [31] S. Vukovic and R. Dragila, *Opt. Lett.* Vol. 15, 168 (1990)
- [32] A. D. Capobianco, and G. F. Nalesso, "Determination and stability analysis of the

supermodes in nonlinear directional couplers through a variational approach", *Optical and Quant. Electron.*, vol. 27, 1995, pp. 1015-1026.

[33] N. N. Akhmediev, V. I. Korneev, and Yu. V. Kuz'menko, "Excitation of nonlinear surface waves by Gaussian light beams", *Sov. Phys. JETP*, Vol 61, No 1, January 1985, pp. 62-67.

[34] E. M. Wright, G. I. Stegeman, C.T. Seaton, and J.V. Moloney, "Gaussian beam excitation of TE_0 nonlinear guided waves", *Applied Physics Letters* 49 (8), pp. 435-436, 1986.

[35] H. Vach, C. T. Seaton, G. I. Stegeman, and I. C. Khoo, "Observation of intensity-dependent guided waves", *Optics Letters*, Vol 9, No. 6, June 1984, pp. 238-240.

[36] P. Varatharajah, J. V. Moloney, A. C. Newell, and E. M. Wright, "Stationary nonlinear waves guided by thin films bounded by nonlinear diffusive media", *J. Opt. Soc. Am. B*, vol. 10, no. 1, 1993, pp. 46-54.

[37] J. Ariyasu, C. T. Seaton, and G. I. Stegeman, "Power-dependent attenuation of nonlinear waves guided by thin films", *Appl. Phys. Lett.*, vol. 47, no. 4, 1985, pp. 355-357

[38] M. Gubbels, E.M. Wright, G.I. Stegeman, C.T. Seaton, J. V. Moloney, "Effects of absorption on TE_0 nonlinear guided waves", *Optics communications*, March 1987, 357-362

[40] K. Oguso, "Nonlinear wave propagation along a bent nonlinear dielectric interface", *Optics Letters*, vol. 16, no. 5, 1991, pp. 312-314.

[41] J. V. Moloney, A. C. Newell, and A. B. Aceves, "Spatial soliton optical switches: a soliton based equivalent particle approach", *Opt. Quant. Electron.*, vol. 24, 1992, pp. S1269-S1293.

[42] A. B. Aceves, J. V. Moloney, and A. C. Newell, "Theory of light-beam propagation at nonlinear interfaces I", *Phys. Rev. A.*, vol. 39, pp. 1809, 1989.

[43] A. B. Aceves, J. V. Moloney, and A. C. Newell, "Theory of light-beam propagation at nonlinear interfaces II. Multiple-particle and multiple-interface extensions", *Phys. Rev. A.*, vol. 39, pp. 1828-1840, 1989.

[44] P. Varatharajah, A. B. Aceves, and J. V. Moloney, "All-optical spatial scanner", *Appl. Phys. Lett.*, vol. 54, no. 26, 1989, pp. 2631-2633.

[45] E. M. Wright, G. I. Stegeman, C.T. Seaton, J. V. Moloney, and A. D. Boardman, "Multisoliton emission from a nonlinear waveguide", *Physical Review A*, Vol 34, No. 5, Nov 1986, pp.4442-4444.

[46] D. R. Heatley, E. M. Wright, and G. I. Stegeman, "Soliton coupler", *Appl. Phys.*

Lett., Vol 53, No. 3, July 1988, pp.172-174.

[47] C. De Angelis and G. F. Nalesso, "Spatial soliton switching modes of nonlinear optical slab waveguides", J. Opt. Soc. Am. B, vol. 10, no. 1, 1993, pp. 55-59.

[48] T-T Shi and S. Chi, "Beam propagation method analysis of transverse-electric waves propagating in a nonlinear tapered planar waveguide", J. Opt. Soc. Am. B, vol. 8, no. 11, 1991, pp. 2318-2325

[49] N. Akhmediev, N. Mitskevich, and R. Nabiev, "Amplification of nonlinear waves in a symmetric planar waveguide", Phys. Rev. A, vol. 45, 1992, pp. 2006-2011.

[50] Y. Chen, and J. Atai, "Stability of black, gray and bright nonlinear guided waves", IEEE Jnl of Quant. Electron., vol. 34, no. 12, 1995, pp.2095-2100

[51] X. J. Meng, N. Okamoto, "Improved coupled-mode theory for nonlinear directional couplers", IEEE J. Quant. Electron., Vol. 27, No. 5, May 1991, 1175-1181.

[52] P. E. Gill and G. F. Miller, "An algorithm for the integration of unequally spaced data", Comp Journal 15, pp. 80-83, 1972; NAG Reference manual

[53] A. Ankiewicz and G-D Peng, J. Opt. Soc. Am. B, vol. 9, 1992, pp. 1341.

[54] S. M. Jensen, "The nonlinear coherent coupler", IEEE Transactions on Microwave Theory and Techniques, MTT-30, no. 10, 1982, pp. 1568-1571.

CHAPTER 11

ANALYTICAL SOLUTION OF NONLINEAR COUPLED MODE EQUATIONS

In this chapter we calculate for the first time analytical solutions to the complete coupled mode equations for the strongly coupled two guide case, show that one constant of motion which is the Poincaré sphere changes into an ellipsoid in strong coupling (section 11.3.2.1), and calculate a new analytical formula for the critical power (eqn. 11.42).

11.1 INTRODUCTION

The critical (or switching) power is the most important parameter defining a nonlinear directional coupler (NLDC). It is the unstable input power which causes equal asymptotic power variation along the guides. In this state, the NLDC can be switched by slight variation in the input conditions.

Coupled mode theory can be used to calculate an analytic formula for the switching power, as well as to find the variation of the mode amplitudes with distance in terms of elliptical functions. The first attempt at solving the nonlinear coupled mode equations was made by Jensen [1]. This was later followed by Daino et. al. [2] and Trillo et. al. [3] who introduced a more elegant approach involving first converting the mode amplitudes into Stokes parameter formalism. Although these initial papers were important in demonstrating the techniques involved, the actual derived solutions were inaccurate, since over-simplified and inconsistent forms of the coupled mode equations were used.

Attempts at improving the accuracy of the solutions were later made by Chen [4] who included the overlap integral as well as many of the nonlinear and linear terms. However the main conclusion from that paper seemed to be that including all the terms causes the critical power to be lower than Jensen's analysis. We found the opposite case to be true (see chapter 12). The main problem with Chen's analysis however was that power dependent mode shapes were not incorporated. The analysis therefore only applied to very large guide separations. For small separations, as found by Meng and Okamoto [5], the power dependence of the mode shapes is the most important factor determining the accuracy of the coupled mode equations. Meng and Okamoto's analysis

on the other hand was deficient for two reasons. Firstly, the overlap integral was ignored. It is known that ignoring the overlap integral causes inconsistencies in linear coupled mode equations (see chapter 3). It has an even greater effect in nonlinear couplers. Secondly, Meng and Okamoto used the full power of the NLDC to calculate the mode shapes whereas in reality some of the power (the power carried in the overlap) does not contribute to the shape of the modes; only the power carried by the modes does. Meng and Okamoto's analysis is therefore not valid for strong coupling.

Ankiewicz and Peng [6] also incorporated power dependence, and included the overlap integral. However by omitting a large number of nonlinear coefficients, their equations were inconsistent and resulted in severe errors (see chapter 6 and 12). Their use of local mode theory also did not lead to a formula for the critical power.

In this chapter an accurate analytical formula for the switching power is derived and then checked using the beam propagation method (BPM)- see chapter 12- for various guide thicknesses and separations. To derive the formula, the coupled mode equations derived in chapter 6 are first converted into Stokes parameter formalism; two constants of motion (3D surfaces in Stokes parameter coordinates) are then extracted. We show for the first time that one of the constants of motion, the Poincaré sphere, changes into a (Poincaré) ellipsoid at strong coupling. The intersection between these two 3D surfaces gives rise to an analytical formula for the critical power. The formula incorporates power dependence of the mode shapes in the correct manner using the modal powers and not the total power (as in [5]). In the second part of the chapter, a complete solution for the powers as a function of distance is derived.

The analytical solutions for three or more guides is not attempted here. These are much more complicated to derive than the two guide cases. Several attempts for solutions have been made in the literature. The only complete solutions exist for centre guide excitation [7], which are easy to study because the symmetry allows the structure to be regarded as pseudo- two guide. For the outer excitation cases, although a full derivation is complicated, it is possible to derive an empirical formula for the critical power using simple physical arguments [8]. Graphical (phase-space) approaches have also been attempted [9].

11.2 TRANSFORMING TO STOKES' COORDINATES

The method in this section is first to re-express the mode amplitudes in terms of Stokes parameters (similar to [2-3] but using more complicated nonlinear coupled mode equations). Four differential equations then result. Two constants of motion can be extracted to derive a formula for the switching power. The constants of motion are

three-dimensional geometrical objects in Stokes parameter coordinate system. The intersection between the two constants of motion gives rise to the trajectories of motion, which represent the variation of the amplitudes and phases with distance along the coupler.

First the nonlinear coupled mode equations are calculated from the matrix form of the equations (eqn. 7.17), pre-multiplied by C^{-1} , and expanded out for the two guide case using the matrix definitions in eqns. 7.18-7.24. Assuming the symmetrical case where $K_{12} = K_{21}$, $K_{11} = K_{22}$, $Q_1 = Q_{11}^{(1)} = Q_{22}^{(2)}$, $Q_2 = Q_{12}^{(2)} = Q_{21}^{(1)}$, $Q_3 = Q_{11}^{(2)} = Q_{22}^{(1)}$, and $K_1^m = K_{11}^m + K_{11}^{NLm} - Q_1^m$, $K_2^m = K_{12}^m + K_{12}^{NLm} - Q_2^{m'}$, the nonlinear coupled mode equations become

$$-j \frac{da_1}{dz} = (\beta_1 + K_1^m + |a_1|^2 Q_1^m) a_1 + (K_2^m + |a_2|^2 Q_2^{m'}) a_2 + (2a_1 |a_2|^2 + a_1^* a_2^2) Q_3^m + (2a_2 |a_1|^2 + a_1^2 a_2^*) Q_2^m \quad (11.1)$$

$$-j \frac{da_2}{dz} = (\beta_2 + K_1^m + |a_2|^2 Q_1^m) a_2 + (K_2^m + |a_1|^2 Q_2^{m'}) a_1 + (2|a_1|^2 a_2 + a_1^2 a_2^*) Q_3^m + (2a_1 |a_2|^2 + a_1^* a_2^2) Q_2^m \quad (11.2)$$

where β_1 , and β_2 are the nonlinear propagation coefficients for the isolated nonlinear guide (we note that $\beta = \beta_1 = \beta_2$ since the guides are symmetrical). It is possible to separate the different terms in a similar way to the linear coupled mode equations into those which contribute to the propagation coefficients and those which contribute to the coupling coefficients as follows

$$-j \frac{da_1(z)}{dz} = \beta_1^{NL}(z) a_1(z) + \mathcal{K}_{12}^{NL}(z) a_2(z) \quad (11.3)$$

$$-j \frac{da_2(z)}{dz} = \beta_2^{NL}(z) a_2(z) + \mathcal{K}_{21}^{NL}(z) a_1(z) \quad (11.4)$$

where β_1^{NL} , β_2^{NL} and \mathcal{K}_{12}^{NL} , \mathcal{K}_{21}^{NL} are the nonlinear z -dependent propagation and coupling coefficients defined as

$$\beta_1^{NL} = \beta_1 + K_1^m + |a_1|^2 Q_1^m + (2a_1^* a_2 + a_1 a_2^*) Q_2^m \quad (11.5)$$

$$\beta_2^{NL} = \beta_2 + K_1^m + |a_2|^2 Q_1^m + (2a_1 a_2^* + a_1^* a_2) Q_2^m \quad (11.6)$$

$$\mathcal{K}_{12}^{NL} = K_2^m + |a_2|^2 Q_2^{m'} + (2a_1 a_2^* + a_1^* a_2) Q_3^m \quad (11.7)$$

$$\mathcal{K}_{21}^{NL} = K_2^m + |a_1|^2 Q_2^{m'} + (2a_1^* a_2 + a_1 a_2^*) Q_3^m \quad (11.8)$$

Although the propagation coefficients β_1^{NL} , and β_2^{NL} are complex quantities (see eqns 11.5 and 11.6), we note that this does not mean that the system is lossy or active as is usually the case when there are imaginary components in the propagation coefficients. Power conservation can still be satisfied exactly (see chapter 7). We note that the m superscripts for the coefficients refer to the modified forms of the coefficients due to the presence of the overlap integral. The coefficients are defined as

$$Q_2^{m'} = \frac{1}{1 - C_{12}^2} (Q_2 - C_{12} Q_1), \quad K_{11}^m = \frac{1}{1 - C_{12}^2} (K_{11} - C_{12} K_{21}), \quad (11.9)$$

$$Q_1^m = \frac{1}{1 - C_{12}^2} (Q_1 - C_{12} Q_2), \quad Q_2^m = \frac{1}{1 - C_{12}^2} (Q_2 - C_{12} Q_3), \quad (11.10)$$

$$K_{12}^m = \frac{1}{1 - C_{12}^2} (K_{12} - C_{12} K_{22}), \quad Q_3^m = \frac{1}{1 - C_{12}^2} (Q_3 - C_{12} Q_2), \quad (11.11)$$

$$K_{12}^{NLm} = \frac{1}{1 - C_{12}^2} (K_{12}^{NL} - C_{12} K_{11}^{NL}), \quad K_{11}^{NLm} = \frac{1}{1 - C_{12}^2} (K_{11}^{NL} - C_{12} K_{12}^{NL}). \quad (11.12)$$

To solve the nonlinear coupled mode equations (eqns 11.3-11.4), they are first decoupled by removing $\beta + K_1^m$ terms. Hence $a_1(z)$ and $a_2(z)$ can be expressed as

$$a_1(z) = A_1(z) e^{j(\beta + K_1^m)z}, \quad a_2(z) = A_2(z) e^{j(\beta + K_1^m)z} \quad (11.13)$$

where $A_1(z)$ and $A_2(z)$ are the slow varying (complex) amplitudes. Therefore eqns. 11.1-11.2 become

$$-j \frac{dA_1}{dz} = A_1 |A_1|^2 Q_1^m + (K_2^m + |A_2|^2 Q_2^{m'}) A_2 + (2A_1 |A_2|^2 + A_1^* A_2^2) Q_3^m + (2A_2 |A_1|^2 + A_2^* A_1^2) Q_2^m \quad (11.14)$$

$$-j \frac{dA_2}{dz} = A_2 |A_2|^2 Q_1^m + (K_2^m + |A_1|^2 Q_2^{m'}) A_1 + (2A_2 |A_1|^2 + A_1^2 A_2^*) Q_3^m + (2A_1 |A_2|^2 + A_1^* A_2^2) Q_2^m \quad (11.15)$$

The mode amplitudes A_1 and A_2 can be expressed in terms of Stoke's parameters S_0 , S_1 , S_2 , and S_3 as follows

$$S_0 = |A_1|^2 + |A_2|^2 \quad S_1 = |A_1|^2 - |A_2|^2 \quad (11.16)$$

$$S_2 = A_1 A_2^* + A_1^* A_2 \quad S_3 = j(A_1 A_2^* - A_1^* A_2) \quad (11.17)$$

Differentiating S_0 , S_1 , S_2 , S_3 wrt z , substituting the coupled mode equations (eqns. 11.14 and 11.15) and rearranging extensively, results in the following differential equations

$$\frac{dS_0}{dz} = (Q_2^{m'} - Q_2^m) S_1 S_3 \quad (11.18)$$

$$\frac{dS_1}{dz} = -2 \left(K_2^m + Q_3^m S_2 + \frac{S_0}{2} (Q_2^m + Q_2^{m'}) \right) S_3 \quad (11.19)$$

$$\frac{dS_2}{dz} = (Q_1^m - Q_3^m) S_3 S_1 \quad (11.20)$$

$$\frac{dS_3}{dz} = 2 \left(K_2^m + Q_3^m S_2 + \frac{S_0}{2} (Q_2^m + Q_2^{m'}) \right) S_1 + (Q_2^{m'} - Q_2^m) S_0 S_1 - (Q_1^m - Q_3^m) S_1 S_2 \quad (11.21)$$

If the overlap integral had been ignored however, the equations would have become [2]

$$\frac{dS_0}{dz} = 0, \quad \frac{dS_1}{dz} = -2(K_2 + Q_2 S_0 + Q_3 S_2) S_3 \quad (11.22)$$

$$\frac{dS_2}{dz} = (Q_1 - Q_3) S_3 S_1, \quad \frac{dS_3}{dz} = 2(K_2 + Q_2 S_0 + Q_3 S_2) S_1 - (Q_1 - Q_3) S_1 S_2 \quad (11.23)$$

It is instructive to study the similarity and differences between eqns. 11.18-11.21 and eqns. 11.22-11.23. Firstly it is noticed from eqn 11.22 that S_0 does not vary with z . This is because in weak coupling S_0 is equal to the total power in the NLDC, and is therefore a constant. In strong coupling however, some of the power is held in the overlap between the eigenmodes. Therefore in that case S_0 is not necessarily equal to the total power, and its variation with z is non-zero (as in eqn. 11.18). A further comparison of eqns. 11.18-11.21, and eqns. 11.22-11.23 shows that Q_2 becomes $(Q_2^m + Q_2^{m'})/2$, where $Q_2^m \neq Q_2^{m'}$, K_2 becomes K_2^m , Q_1 becomes Q_1^m , and Q_3 becomes Q_3^m .

11.3 CONSTANTS OF MOTION

By careful manipulation of the four differential equations above (eqns. 11.18-11.21) it is possible to find some constants of motion, ie. quantities which remain unchanged with propagation distance.

11.3.1 Calculation of the total power

We first calculate a relationship between S_0 and S_2 . This can be derived from total power calculation using Poynting's theorem (see Appendix 6, eqn A6.19). However it can also be derived from eqn. 11.18-11.21. Eliminating S_1, S_3 from eqns. 11.18 and 11.20 leads to the following relationship between S_0 and S_2

$$\frac{dS_0}{dz} = \left(\frac{Q_2^{m'} - Q_2^m}{Q_1^m - Q_3^m} \right) \frac{dS_2}{dz} \quad (11.24)$$

But $(Q_2^{m'} - Q_2^m)$ and $(Q_1^m - Q_3^m)$ can be derived from eqns. 11.9-11.11

$$Q_2^{m'} - Q_2^m = \frac{C_{12}}{1 - C_{12}^2} (Q_3 - Q_1) \quad Q_1^m - Q_3^m = \frac{1}{1 - C_{12}^2} (Q_1 - Q_3) \quad (11.25)$$

we can now substitute for $\left(\frac{Q_2^{m'} - Q_2^m}{Q_1^m - Q_3^m} \right)$ in eqn. 11.24. Substituting also the arbitrary initial conditions \bar{S}_2 and \bar{S}_0 into eqn. 11.24 gives

$$(S_0 - \bar{S}_0) = -C_{12} (S_2 - \bar{S}_2) \quad (11.26)$$

Using initial values $\bar{S}_2 = 0$ and $\bar{S}_0 = 1$ (guide 1 excitation), eqn. 11.26 becomes

$$S_0 = 1 - C_{12} S_2 \quad (11.27)$$

Eqn 11.27 can be shown to be exactly the same formula as the power conservation formula derived in Appendix 6 (eqn. A6.19). By substituting the definitions for S_0 and S_2 (eqns. 11.16 and 11.17) into eqn. 11.27 leads to

$$|A_1|^2 + |A_2|^2 + C_{12} (A_1^* A_2 + A_2^* A_1) = 1 \quad (11.28)$$

which agrees exactly with eqn. A6.19

11.3.2 The ‘Poincaré’ equations (spheres, ellipsoids, and paraboloids)

It is shown in this section that the Poincaré sphere is a constant of motion in weak coupling, but becomes an ellipsoid in strong coupling and finally a paraboloid. This has not been mentioned in the literature. The Poincaré equation (which describes spheres, ellipsoids, and paraboloids), can be calculated by noting that the quantities $(Q_2^{m'} - Q_2^m)$, $2(K_2^m + Q_3^m S_2 + S_0(Q_2^m + Q_2^{m'})/2)$, and $(Q_1^m - Q_3^m)$ in the definition of dS_3/dz (eqn. 11.21), are contained in eqns. 11.18, 11.19, and 11.20 respectively. Therefore by incorporating these equations into eqn. 11.21 and integrating (using arbitrary initial values for the Stokes parameters $\bar{S}_0, \bar{S}_1, \bar{S}_2, \bar{S}_3$) results in

$$(S_0^2 - \bar{S}_0^2) = (S_1^2 - \bar{S}_1^2) + (S_2^2 - \bar{S}_2^2) + (S_3^2 - \bar{S}_3^2) \quad (11.29)$$

Assuming that the initial amplitudes are $A_1(0) = |\bar{A}_1|e^{j\bar{\phi}_1(z)}$, and $A_2(0) = |\bar{A}_2|e^{j\bar{\phi}_2(z)}$, where $\bar{\phi}_1(z)$ and $\bar{\phi}_2(z)$ are the respective initial phases (the bar implies initial conditions) and for convenience letting $\bar{\phi}(z) = \bar{\phi}_1(z) - \bar{\phi}_2(z)$, the initial values of Stokes parameters become

$$\bar{S}_0 = |\bar{A}_1|^2 + |\bar{A}_2|^2, \quad \bar{S}_1 = |\bar{A}_1|^2 - |\bar{A}_2|^2 \quad (11.30)$$

$$\bar{S}_2 = \bar{A}_1 \bar{A}_2^* + \bar{A}_1^* \bar{A}_2 = 2|\bar{A}_1||\bar{A}_2|\text{Cos}\bar{\phi}, \quad \bar{S}_3 = j(\bar{A}_1 \bar{A}_2^* - \bar{A}_1^* \bar{A}_2) = -2|\bar{A}_1||\bar{A}_2|\text{Sin}\bar{\phi} \quad (11.31)$$

Inserting the initial conditions (eqns. 11.30-11.31) into eqn. 11.29 leads to the Poincaré equation

$$S_1^2 + S_2^2 + S_3^2 = S_0^2 \quad (11.32)$$

S_0 is in general not equal to the total power. Therefore in general it is not a constant. However for weakly coupled geometries where the overlap integral can be ignored, S_0 is equal to the total normalised power ($S_0 = 1$).

Weak coupling: Poincaré sphere

$$S_1^2 + S_2^2 + S_3^2 = 1 \quad (11.33)$$

Equation 11.33 represents the equation of a sphere, and is known as the Poincaré sphere [2] (see Fig. 11.1). The surface of the sphere represents all possible states corresponding with constant total power. Therefore a trajectory on the sphere represents the evolution of the magnitudes and states of polarisation of the mode amplitudes in a lossless system. Several regions on the sphere surface have physical meaning. The north pole ($S_1 = 1$) represents all power carried by mode 1. The south pole ($S_1 = -1$) represents all the power in mode 2. The equator (curve Γ_2) represents equal power in the modes. Points on the great longitude (curve Γ_1) correspond with equal phases between the mode amplitudes. Any other points on the sphere (ie those not on curve Γ_1) signify unequal phases and points $S_3 = -1$ and $S_3 = 1$ on the equator with orthogonal phases [10].

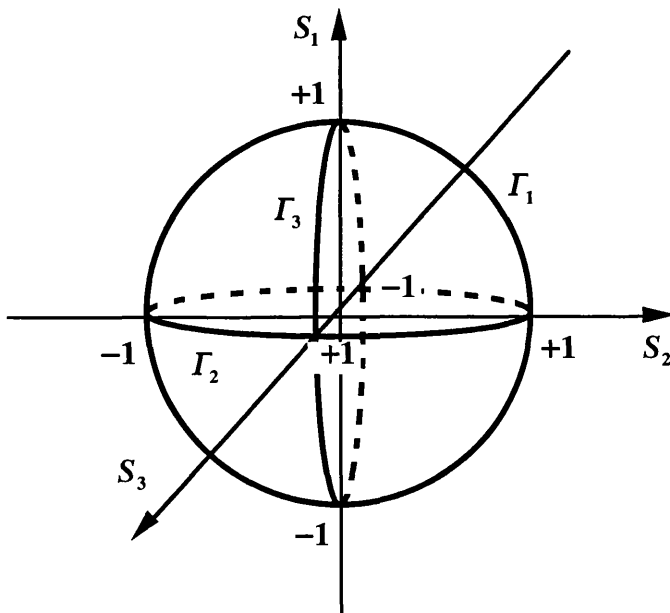


Fig.11.1 The Poincaré sphere

11.3.2.1 Strong coupling case

As explained before, for strong coupling S_0 is not a constant. It is the fourth variable in the Poincaré equation (eqn. 11.32). However, it can be eliminated from the Poincaré

equation by relating it to S_2 using the total power formula (eqn. 11.26). Therefore substituting the total power formula (eqn. 11.26) into the Poincaré equation (eqn. 11.32) leads to

$$S_1^2 + (1 - C_{12}^2)S_2^2 + 2C_{12}(S_2 - \bar{S}_2)(S_0 + C_{12}\bar{S}_2) + S_3^2 = \bar{S}_0^2 - C_{12}^2\bar{S}_2^2 \quad (11.34)$$

which is the equation for an ellipsoid. Considering guide 1 excitation only so that the initial conditions are $\bar{S}_1 = 1$, $\bar{S}_2 = \bar{S}_3 = 0$ simplifies eqn. 11.34 to

Strong coupling: Poincaré ellipsoid

$$S_1^2 + (1 - C_{12}^2)S_2^2 + 2C_{12}S_2 + S_3^2 = 1 \quad (11.35)$$

In summary, the effect of the overlap integral on the Poincaré sphere is to change it into an ellipsoid. It can also be seen from eqn. 11.35 that for very strong coupling ($C_{12} = 1$), the Poincaré ellipsoid itself then becomes a Poincaré paraboloid. Equation 11.35 is plotted in Fig. 11.2 below (in the $S_1 - S_2$ plane), for various values of the overlap integral. By simple geometry it can be shown from eqn. 11.35 that the ellipsoid crosses the S_2 axis at $1/(1 + C_{12})$ and $1/(C_{12} - 1)$, but crosses the S_1 axis always at $S_1 = \pm 1$. The point where the ellipsoid intersects the positive S_2 axis ($S_2 = 1/(1 + C_{12})$, $S_1 = S_3 = 0$) is a particularly important one, since it corresponds with the state where the mode amplitudes and phases are equal (ie this point corresponds with the final evolution state of the amplitudes if the NLDC is excited with the critical power).

The overall effect of the overlap integral on the Poincaré equation can be seen from Fig. 11.2. It is observed that $C_{12} \rightarrow 0$ corresponds with the shape of a sphere. As C_{12} increases, the shape changes into an ellipsoid and the ellipsoid 'expands' in the negative S_2 region (crossing the negative S_2 axis at $1/(C_{12} - 1)$). At $C_{12} = 1$ the result is a paraboloid.

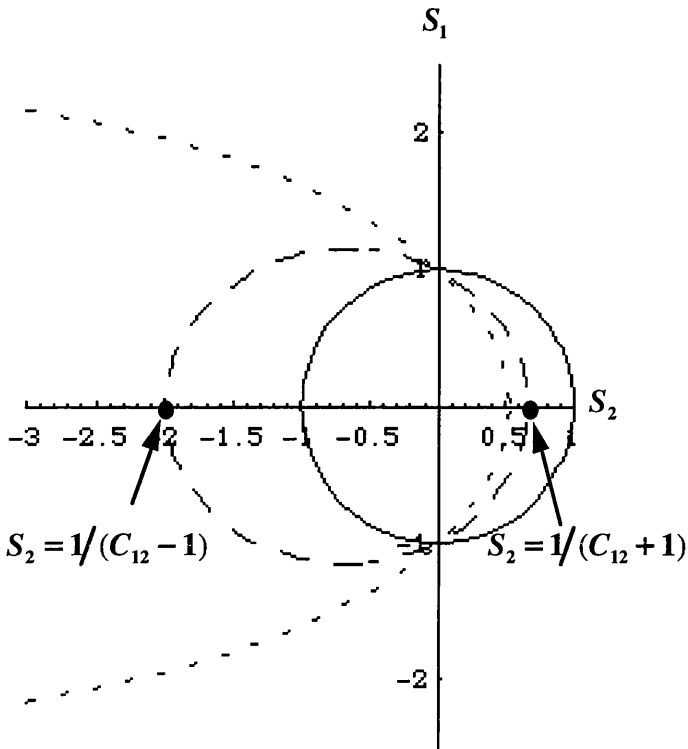


Fig. 11.2 The effect of the overlap integral on the ellipsoid. The overlap integral is varied from 0 (solid curve) to 0.5 (dashed curve) to 0.9 (dotted curve)

11.3.3 The parabolic surface

A second geometric surface in Poincaré coordinates can be derived by eliminating S_3 from eqns. 11.19 and 11.20 and rearranging to give.

$$S_1 \frac{dS_1}{dz} = \left[\frac{-2K_2^m}{Q_1^m - Q_3^m} - \frac{2Q_3^m}{Q_1^m - Q_3^m} S_2 - \frac{S_0(Q_2^m + Q_2^{m'})}{Q_1^m - Q_3^m} \right] \frac{dS_2}{dz} \quad (11.36)$$

By substituting the following into eqn 11.36

$$\mu^m = \frac{Q_1^m - Q_3^m}{4 \left(K_2^m + \frac{1}{2} (Q_2^m + Q_2^{m'}) \right)} \quad \delta^m = \frac{Q_3^m}{2 \left(K_2^m + \frac{1}{2} (Q_2^m + Q_2^{m'}) \right)} \quad (11.37)$$

$$\gamma^m = \frac{C_{12} (Q_2^m + Q_2^{m'})}{Q_1^m - Q_3^m} \quad (11.38)$$

and integrating results in the general equation for a parabolic surface.

$$(S_1^2 - \bar{S}_1^2) = \frac{-1}{\mu^m} (S_2 - \bar{S}_2) + \left(\gamma^m - \frac{\delta^m}{\mu^m} \right) (S_2^2 - \bar{S}_2^2) \quad (11.39)$$

Note that a ‘parabolic surface’ is not a paraboloid (which was mentioned in section 11.3.2). A paraboloid is cup-shaped whereas a parabolic surface is one where the parabola shape is unchanged in the third dimension. To be formally accurate, the shape (resulting from eqn. 11.39) is not a parabolic surface but an elliptical surface. However it approximates to a parabolic surface in the regions of interest on the Poincaré ellipsoid. Assuming guide 1 excitation, so that $\bar{S}_1 = 1$, $\bar{S}_2 = 0$, eqn. 11.39 becomes

Strong coupling: Parabolic surface

$$S_1^2 = 1 - \frac{1}{\mu^m} S_2 + \left(\gamma^m - \frac{\delta^m}{\mu^m} \right) S_2^2 \quad (11.40)$$

11.4 CRITICAL POWER FORMULA

11.4.1 Intersection between the two geometrical surfaces

The intersection between the parabolic surface discussed in the previous section and the ellipsoid derived in section 11.3.2.1 (see Fig. 11.3), gives rise to the trajectories of motion, ie the evolution of the mode amplitude and phases with propagation distance z .

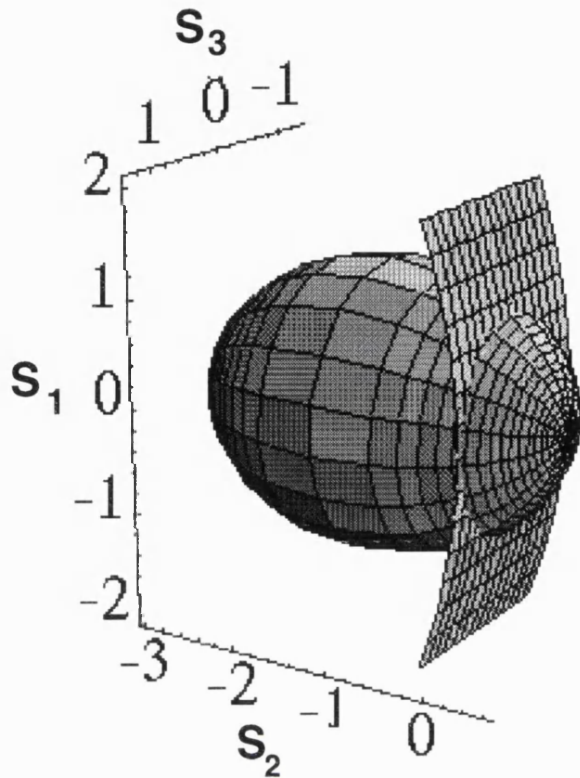


Fig 11.3 Showing the intersection between the two constants of motion. $d = 0.5\mu\text{m}$, $w = 2.0\mu\text{m}$, and $pow = 10\text{ W/m}$

The parabolic surface and the ellipsoid are drawn in three dimensions in Fig. 11.3. It can be seen that the two surfaces always intersect at $S_1 = \pm 1$ if guide 1 is excited. The intersection between these two surfaces gives rise to the trajectories of motion. At low powers, the base of the parabolic surface is at $S_2 = 0$. Therefore the intersection between the two surfaces is a large circle. As the power increases, the base of the parabolic surface shifts along the positive S_2 -axis. At the critical power the ellipsoid and the base of the parabolic surface intersect at the point $S_2 = 1/(C_{12} + 1)$. The trajectory is then a three dimensional separatrix, with a col at $S_2 = 1/(C_{12} + 1)$ (see Fig. 11.4). At higher powers, the separatrix then changes into two small loops in the north and south hemispheres. This results from the base of the parabolic surface being located outside the ellipsoid on the positive S_2 -axis. These loops shrink as the power is increased further.

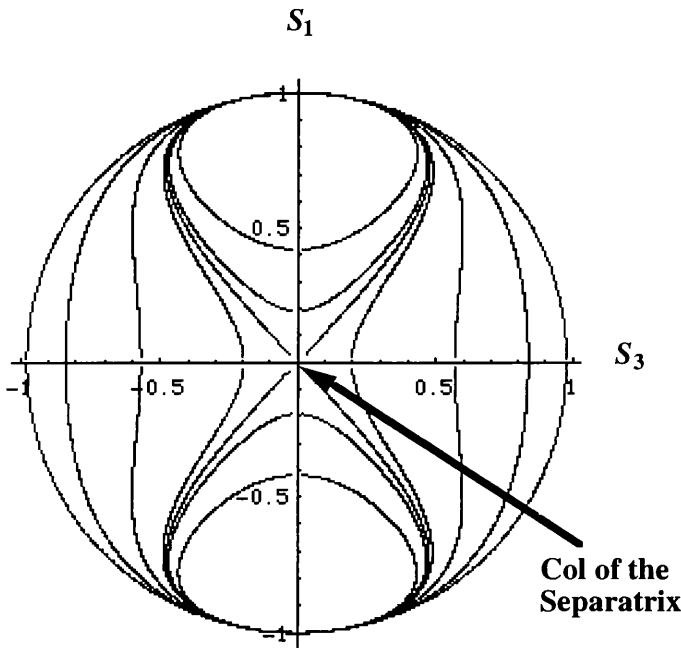


Fig. 11.4 Showing the trajectories resulting from the intersection between the two geometric surfaces for different input powers ($d = 0.5\mu m$, $w = 2.0\mu m$)

The trajectories are drawn in the $S_1 - S_2$ plane in Fig. 11.4. These trajectories are similar to those found in nonlinear dynamics. Movement along any particular trajectory [2] corresponds with the evolution of the mode amplitudes and phases with distance z . Closed trajectories correspond with oscillations of the mode amplitudes with distance, and separatrices with asymptotic evolution. At low powers, the trajectories are large loops which emanate from the north pole $S_1 = 1$ (corresponding with excitation of guide 1 at $z = 0$), which pass through the south pole after one coupling length (where all the power is then in guide 2). As the input power is increased, the loop narrows in the middle (in bow-tie fashion), until at the critical power it forms a separatrix. The separatrix trajectory starts from $S_1 = 1$ and ends at the col after an infinite distance. Above the critical power the separatrix splits into two closed curves in the top and bottom hemispheres.

To find the critical power, we are interested in the separatrix trajectory. Substituting the values for γ^m , μ^m , and δ^m (from eqn 11.37-11.38) into the general form of the parabolic surface equation (eqn 11.40) leads to

$$(Q_1^m - Q_3^m)(S_1^2 - 1) + 4(K_2^m + 1/2(Q_2^m + Q_2^{m'}))S_2 - (C_{12}(Q_2^m + Q_2^{m'}) - 2Q_3^m)S_2^2 = 0 \quad (11.41)$$

At the critical power, the final values for S_1 and S_2 are $S_1 = 0$, and $S_2 = 1/(1 + C_{12})$ respectively. Therefore eqn 11.41 can be rearranged to result in the critical power formula

Critical power formula

$$\frac{4K_2^m}{(1 + C_{12})Q_1^m - \left(2 - \frac{C_{12}}{1 + C_{12}}\right)(Q_2^m + Q_2^{m'}) - \left[(1 + C_{12}) + \frac{2}{1 + C_{12}}\right]Q_3^m} = 1 \quad (11.42)$$

This equation contains the critical power implicitly. All the coefficients incorporate fields with shapes which are power dependent. The critical power formula can be used to calculate the critical power iteratively, eg using the bisection method. The critical power is defined as that power which enables eqn. 11.42 to be satisfied.

The question arises as to which power should be used for the determination of the mode shapes. Meng and Okamoto used the full power P . However, for the symmetrical case, at strong coupling and after a large propagation distance, the power in the modes is $P/(1 + C_{12})$ (see section 11.5.1.2). The rest of the power $PC_{12}/(1 + C_{12})$ is held in the overlap. Therefore one should use the power $P/(1 + C_{12})$ in calculating the mode shapes rather than the full power P .

It is possible to extract the critical power explicitly from eqn. 11.42 if we assume power *independent* mode shapes, in which case when eqn. 11.42 is satisfied $Q_1^m, Q_2^m, Q_2^{m'}, Q_3^m$ are directly proportional to the critical power, and K_2^m , and C_{12} are constants with power. Therefore substituting $Q_1^m = P_c q_1^m$, $Q_2^m = P_c q_2^m$, $Q_2^{m'} = P_c q_2^{m'}$, $Q_3^m = P_c q_3^m$, where P_c is the critical power, and $q_1^m, q_2^m, q_2^{m'}$, and q_3^m are proportionality constants, eqn. 11.42 becomes

$$P_c = \frac{4K_2^m}{(1 + C_{12})q_1^m - \left(2 - \frac{C_{12}}{1 + C_{12}}\right)(q_2^m + q_2^{m'}) - \left[(1 + C_{12}) + \frac{2}{1 + C_{12}}\right]q_3^m} \quad (11.43)$$

11.4.2 Physical explanation for the coupled mode formula

11.4.2.1 Effect of linear and nonlinear coefficients

The various parameters which affect the critical power (eg. eqn 11.42 or 11.43) can be

explained physically. In summary, (ignoring the effect of the overlap integral) the main contributions are from those coefficients which are in essence coupling coefficients or propagation coefficients. The two contributions are explained as follows.

An increase in the coupling coefficient increases the critical power. This can be demonstrated from the following physical argument. Suppose that guide 1 is excited with the critical power \bar{P}_{cr} . The power would then emerge equally from the output ports, and (ignoring the effect of the overlap integral), they would each be 50% of the total power. This situation is plotted as point A in Fig. 11.5 below (assuming a one coupling length device). If the coupling coefficient were now to be increased slightly (still keeping the coupling length and input power unchanged) then more power would emerge from guide 2 than guide 1. This state is plotted as point B in Fig. 11.5. Since point B is below the 0.5 level, the new critical power P_{cr} for this new geometry must lie above the old critical power \bar{P}_{cr} . In summary, increasing the coupling coefficient slightly increases the critical power slightly. Since K_2 , Q_2 and Q_3 are all coupling coefficients, a small increase in any of them increases the critical power (and not decrease it as implied by Chen [4]).

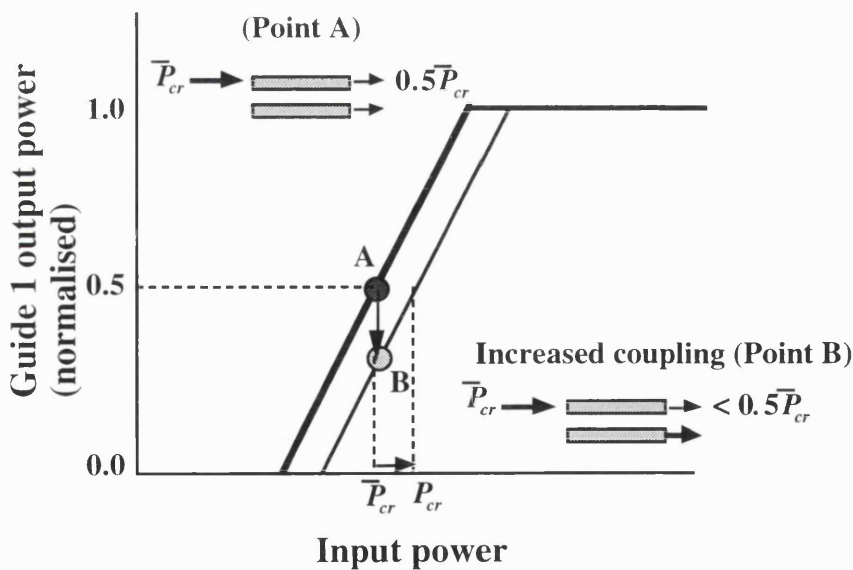


Fig. 11.5 Showing the effect of increased coupling on the critical power. The switching slope is exaggerated for discussion purposes

The self-phase-modulation (SPM) coefficient Q_1 on the other hand alters the critical power by affecting the nonlinear propagation coefficients. At the point where the NLDC is excited ($z = 0$), the input power mismatches the propagation coefficients, and

Q_1 determines the extent to which they are mismatched. If the input power were at critical (point A on Fig. 11.6) and Q_1 were to be increased at this stage, then the mismatch between the propagation coefficients at $z = 0$ would be greater than that necessary for asymptotic equal power output. Consequently an increase in Q_1 would lead to more power emerging from the output of guide 1 than guide 2 (point C in Fig. 11.6). Since point C is above the 0.5 level, the new critical power P_{cr} must be at a value below the old critical power \bar{P}_{cr} . Therefore in summary increasing Q_1 causes a decrease in the critical power.

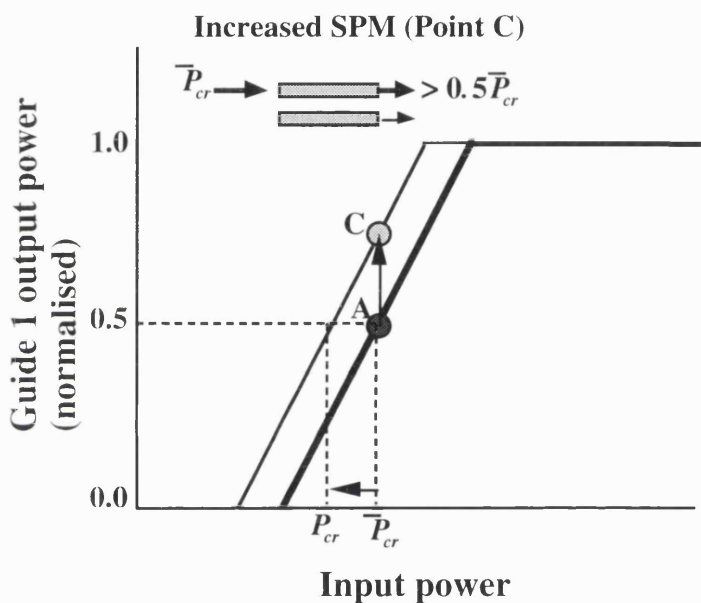


Fig. 11.6 Showing the effect of increased Self-Phase-Modulation on the critical power

11.5 POWER CURVES

11.5.1 Power as a function of distance

In this section the coupled mode equations are solved to calculate the variation of the power with distance. Squaring both sides of eqn. 11.20 gives

$$\left(\frac{dS_2}{dz}\right)^2 = (Q_1^m - Q_3^m)^2 S_1^2 S_3^2 \quad (11.44)$$

Substituting for S_1 and S_3 from eqns. 11.35 and 11.40 into eqn. 11.44 leads to

$$\left(\frac{dS_2}{dz}\right)^2 = (Q_1^m - Q_3^m)^2 \left(1 - \frac{1}{\mu^m} S_2 + \left(\gamma^m - \frac{\delta^m}{\mu^m}\right) S_2^2\right) \left(\frac{1}{\mu^m} S_2 - \left(\gamma^m - \frac{\delta^m}{\mu^m}\right) S_2^2 - (1 - C_{12}^2) S_2^2 - 2C_{12} S_2\right) \quad (11.45)$$

which can be rearranged to give

$$\left(\frac{dS_2}{dz}\right)^2 = \mu^{m^2} \left[4(K_2^m + 1/2(Q_2^m + Q_2^{m'}))\right]^2 \left(\frac{\delta^m}{\mu^m} - \gamma^m\right) \left(\gamma^m - \frac{\delta^m}{\mu^m} + (1 - C_{12}^2)\right) \times (S_2 - \alpha_1)(S_2 - \alpha_2) S_2 (S_2 - \beta_2) \quad (11.46)$$

where α_1 , α_2 , and β_2 are defined as

$$\alpha_1 = \frac{\frac{1}{\mu^m} + \sqrt{\left(\frac{1}{\mu^m}\right)^2 - 4\left(\gamma^m - \frac{\delta^m}{\mu^m}\right)}}{2\left(\gamma^m - \frac{\delta^m}{\mu^m}\right)}, \quad \alpha_2 = \frac{\frac{1}{\mu^m} - \sqrt{\left(\frac{1}{\mu^m}\right)^2 - 4\left(\gamma^m - \frac{\delta^m}{\mu^m}\right)}}{2\left(\gamma^m - \frac{\delta^m}{\mu^m}\right)} \quad (11.47)$$

$$\beta_2 = \frac{\frac{1}{\mu^m} - 2C_{12}}{\gamma^m - \frac{\delta^m}{\mu^m} + (1 - C_{12}^2)} \quad (11.48)$$

Eqn. 11.46 can be integrated as follows

$$\int_0^{S_2} \frac{dS_2}{(S_2 - \alpha_1)(S_2 - \alpha_2) S_2 (S_2 - \beta_2)} = \mu^m \left[4(K_2^m + 1/2(Q_2^m + Q_2^{m'}))\right] \sqrt{\left(\frac{\delta^m}{\mu^m} - \gamma^m\right) \left(\gamma^m - \frac{\delta^m}{\mu^m} + (1 - C_{12}^2)\right)} z \quad (11.49)$$

11.5.1.1 Below critical power

The solution to eqn. 11.49 depends on whether the power is above or below critical power. Below critical power, $\beta_2 > \alpha_2 > S_2 \geq 0 > \alpha_1$, and therefore (using Byrd and Friedman [11] formula 254, page 112) the solution is

$$S_2 = \frac{-\alpha_1 \alpha_2 sn^2 \left[\frac{\mu^m [4(K_2^m + 1/2(Q_2^m + Q_2^{m'}))]}{g} \sqrt{\left(\frac{\delta^m}{\mu^m} - \gamma^m \right) \left(\gamma^m - \frac{\delta^m}{\mu^m} + (1 - C_{12}^2) \right)} z |k \right]}{\alpha_2 cn^2 \left[\frac{\mu^m [4(K_2^m + 1/2(Q_2^m + Q_2^{m'}))]}{g} \sqrt{\left(\frac{\delta^m}{\mu^m} - \gamma^m \right) \left(\gamma^m - \frac{\delta^m}{\mu^m} + (1 - C_{12}^2) \right)} z |k \right] - \alpha_1} \quad (11.50)$$

where k is a modulus defined as

$$k = \sqrt{\frac{\alpha_2(\beta_2 - \alpha_1)}{\beta_2(\alpha_2 - \alpha_1)}}, \quad g = \frac{2}{\sqrt{\beta_2(\alpha_2 - \alpha_1)}} \quad (11.51)$$

and sn and cn are elliptical sine and cosine functions. Note that (see page 11 Byrd and Friedman [11]) Note that $k = 1$ where $K = F\left(\frac{\pi}{2}, k\right) F\left(\frac{\pi}{2}, 1\right) = K(1) = \infty$ leads to the critical power.

11.5.1.2 Above Critical Power

Above critical power, $\alpha_2 > \beta_2 > S_2 \geq 0 > \alpha_1$. Using formula 254 from Byrd & Friedman [11] (page 112) leads to

$$S_2 = \frac{-\alpha_1 \beta_2 sn^2 \left[\frac{\mu^m [4(K_2^m + 1/2(Q_2^m + Q_2^{m'}))]}{g} \sqrt{\left(\frac{\delta^m}{\mu^m} - \gamma^m \right) \left(\gamma^m - \frac{\delta^m}{\mu^m} + (1 - C_{12}^2) \right)} z |k \right]}{\beta_2 cn^2 \left[\frac{\mu^m [4(K_2^m + 1/2(Q_2^m + Q_2^{m'}))]}{g} \sqrt{\left(\frac{\delta^m}{\mu^m} - \gamma^m \right) \left(\gamma^m - \frac{\delta^m}{\mu^m} + (1 - C_{12}^2) \right)} z |k \right] - \alpha_1} \quad (11.52)$$

$$k = \sqrt{\frac{\beta_2(\alpha_2 - \alpha_1)}{\alpha_2(\beta_2 - \alpha_1)}}, \quad g = \frac{2}{\sqrt{\alpha_2(\beta_2 - \alpha_1)}} \quad (11.53)$$

S_2 can be related to the power carried in each guide. Using eqns. 11.16 gives

$$|a_1|^2 = (S_0 + S_1)/2 \quad |a_2|^2 = (S_0 - S_1)/2 \quad (11.53)$$

But S_0 can be related to S_2 through eqn. 11.27, and S_1 to S_2 through eqn. 11.40.

Therefore the amplitudes of the fields become

$$|a_1|^2 = \left(1 - C_{12}S_2 + \sqrt{1 - \frac{1}{\mu^m}S_2 + \left(\gamma^m - \frac{\delta^m}{\mu^m} \right) S_2^2} \right) / 2 \quad \text{and} \quad (11.54)$$

$$|a_2|^2 = \left(1 - C_{12}S_2 - \sqrt{1 - \frac{1}{\mu^m}S_2 + \left(\gamma^m - \frac{\delta^m}{\mu^m} \right) S_2^2} \right) / 2 \quad (11.55)$$

Eqns. 11.54 and 11.55 are plotted below

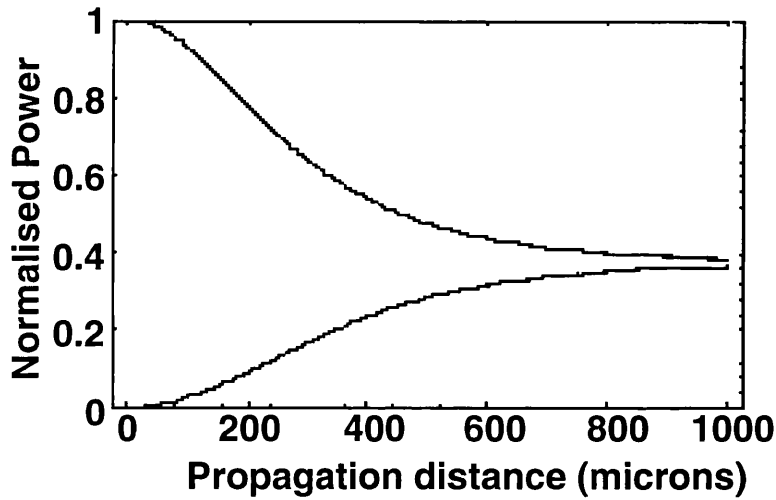


Fig. 11.7 Power vs propagation distance $d = 0.5\mu m$, $w = 3.95\mu m$, at critical power ($pow = 15.22Watts/m$). Note that since this is strong coupling the output powers are around 0.4 (and not 0.5 arising in weak coupling).

At the critical power, after an infinite propagation distance, the powers in the two guides are equal. At this point $S_1 = 0$, and $S_2 = 1/(1 + C_{12})$ (see section 11.3.2.1)

$$|a_1|^2 = |a_2|^2 = \frac{1}{2(1 + C_{12})} \quad (11.56)$$

Therefore it can be seen from eqn. 11.56 that when $C_{12} > 0$, the normalised mode powers are equal, with values each less than $1/2$, so that the sum of the normalised mode powers do not equal the total normalised power (ie 1). The remaining power is found in the overlap.

11.6 CONCLUSIONS

Analytical solutions for the full coupled mode equations in the strongly coupled regime were calculated for the first time. It was shown that one constant of motion which is the Poincaré sphere in weak coupling, changes to an ellipsoid in strong coupling. A new analytical formula for the critical power was derived. A physical explanation for this formula was given.

REFERENCES

- [1] S. M. Jensen, "The nonlinear coherent coupler", IEEE J. Quantum Electron, QE-18, 1580 (1982)
- [2] B. Daino, G. Gregori, and S. Wabnitz, "Stability analysis of nonlinear coherent coupling", J. Appl. Phys., vol. 58, no. 12, 1985, pp. 4512-4514.
- [3] S. Trillo and S. Wabnitz, "Nonlinear nonreciprocity in a coherent mismatched coupler", Appl.Phys. Lett., vol. 49, no. 13, 1986, pp. 752-754.
- [4] Y. Chen, "Solution to full coupled wave equations of nonlinear coupled systems", IEEE J. Quant. Electron., QE-25, No.10, pp. 2149-2153., 1987
- [5] X. J. Meng, and N. Okamoto: "Improved coupled-mode theory for nonlinear directional couplers", IEEE. J. Quant. Electron., Vol 27, No. 5, pp. 1175-1181, May 1991
- [6] A. Ankiewicz and G-D Peng, J. Opt. Soc. Am. B, vol. 9, 1992, pp. 1341.
- [7] L. J. Bernstein, "The three-waveguide nonlinear directional coupler: the center waveguide excitation", Opt. Comms., vol. 94, 1992, pp. 406-416.
- [8] N. Finlayson and G. I. Stegeman, "Spatial switching, instabilities, and chaos in a three-waveguide nonlinear directional coupler", Appl. Phys. Lett., vol. 56, no. 23, 1990, pp. 2276-2278.
- [9] C. Schmidt-Hattenberger, R. Muschall, F. Lederer, and U. Trutschel,"Phase-controlled switching in nonlinear multiport fibre couplers", J. Opt. Soc. Am. B, vol. 10, no. 9, 1993, pp. 1592-1599.
- [10] Born, M., and Wolf, E.: 'Principles of optics, electromagnetic theory of propagation, interference and diffraction of light', 1991, *Pergammon Press*.
- [11] P. F. Byrd and M. D. Friedman: "Handbook of Elliptical Integrals for Engineers and Physicists (Springer, Berlin, 1971).

CHAPTER 12

NUMERICAL COMPARISON OF COUPLED MODE THEORY WITH BPM

12.1 Introduction

In this chapter we compare and contrast our coupled mode model against other methods, and against BPM, and investigate the importance of terms which are ignored in other works (eg. [1]).

12.2 Critical power curves

The main parameter used in this chapter for comparison purposes is the critical power, which is the most important parameter defining a nonlinear directional coupler (NLDC). In chapter 11 we derived the 'critical power formula' (CPF) (see eqn. 11.42). In section 12.2.1 below we study the variation of the critical power with guide separation for various film thicknesses. A slab geometry is assumed for the guides mainly to compare against another work [2] and also because it is a structure where the mode shapes can easily be calculated. In order to study different strengths of coupling, either the strength of the guidance or the separation between the guides can be changed. One way to adjust the strength of the guidance is to vary the film thickness. In general the thicker the films become, the less the fields extend into the cladding regions, and the smaller the overlap between the fields (see Fig. 9.3). Conversely, the thinner the films become, the more the fields are spread out, and the larger the overlap between them. For comparison purposes we consider two extreme cases (see sections 12.2.2 and 12.2.3), a thick-film guide ($d = 2.0\mu m$), and a thin-film guide ($d = 0.5\mu m$). The other thicknesses are assumed to lead to results which are intermediate between these two. A thick film guide was studied by ref. 2. Their results were however only relevant for the weak coupling case. A thin film case would allow strong coupling to be studied, where differences between different methods can clearly be seen.

Our results are compared against BPM and against other methods, and the importance of various coefficients which affect the critical power investigated (see also chapter 10). We study some inconsistencies present in various papers, usually occurring as a result of the overlap integral and the nonlinear cross-coefficients not

appearing (or disappearing) together in the coupled mode equations. For example, in ref. 2, the overlap integral was neglected but the nonlinear cross-coefficients were kept. In ref. 1 the reverse occurred: the overlap integral was included but the nonlinear cross-coefficients neglected. This was also inconsistent and lead to inaccurate results as shown later in this chapter. A further defect with the use of the local mode theory as carried out in ref. 1 is that it does not lead to a theoretical solution for the coupled mode equations or allow the derivation of a formula for the critical power taking into account the power dependence of the fields as was possible in chapter 11. Also by using local mode theory some of the advantages of coupled mode theory are lost since the field shapes have to be calculated at every step. It could be argued that one might as well use BPM in that case.

Another approach is the nonlinear supermode approach. Dios et. al. [3] stated that their approach was more accurate than the coupled mode theory approach. However their results do not bear out their argument. Even though they studied a weakly coupled geometry where literally any method would have been accurate, their results were very poor.

12.2.1 Varying the guide thicknesses

The critical powers for four different guide thicknesses $d = 2.0, 1.5, 1.0,$ and $0.5 \mu m$ are compared in Fig. 12.1. As mentioned above we used the CPF formula (see eqn 11.42) to draw the curves. All the fields have shapes which are power dependent, and all the coefficients which appear in the CPF are also power dependent. The CPF formula contains the critical power implicitly. Therefore the critical power is calculated by first calculating the coefficients in eqn. 11.42 for a particular input power, and then inserting them into the equation, checking the equality, and iteratively repeating this for different input powers (eg by using the bisection method) until the equality is satisfied. The input power which allows eqn. 11.42 to be satisfied is then the critical power.

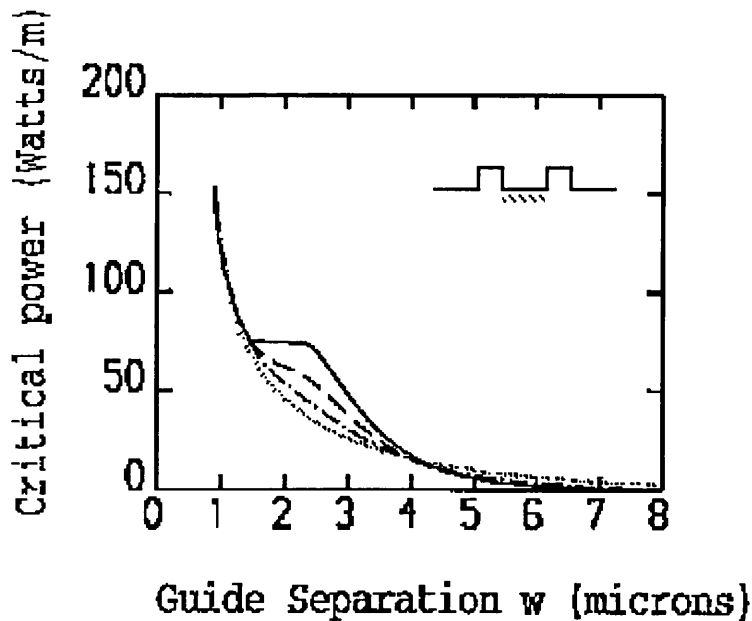


Fig. 12.1 Variation of the critical power with guide separation using our formula for various guide thicknesses (inset shows the location of the nonlinearity- hatched)
 (i) $d = 2\mu\text{m}$ (solid curve), (ii) $d = 1.5\mu\text{m}$ (dashed), (iii) $d = 1.0\mu\text{m}$ (chained), and (iv) $d = 0.5\mu\text{m}$ (dotted).

It can be observed from Fig. 12.1 that at large guide separations ($w > 4.0\mu\text{m}$) all the curves are similar. This is because for large guide separations, the modes of the two guides are so distant from each other that only the small portion of the evanescent tails overlap. Since the evanescent tails of modes at a distance are similar even if they are from guides of different thicknesses, the linear and nonlinear coupling coefficients are also similar at large separations irrespective of the guide thickness. Since these coefficients are similar, the critical powers are also expected to be similar. Actually it can be seen in Fig. 12.1 that the $d = 0.5\mu\text{m}$ curve is slightly higher than the others in the region $w > 4.0\mu\text{m}$. This is because the mode for the $d = 0.5\mu\text{m}$ guide has an increased spread in the cladding than the others, and separations of 6 to 8 μm considered here do not constitute as *large* separations. The larger overlap in this case causes the linear and nonlinear coupling coefficients to be slightly greater, resulting in a slightly higher critical power.

As the guide separation is reduced to $w = 4.0\mu\text{m}$ we notice that the critical powers for the different thicknesses become equal, and a further reduction in separation reverses the situation from what it was above $w = 4.0\mu\text{m}$: ie. the mode of the thickest guide ($d = 2.0\mu\text{m}$) (solid curve) now has the highest critical power. As the guide

separation is reduced, the critical power for all thicknesses increases. This is because the increased overlap between the fields means that all the linear and nonlinear coefficients (eg. Q_2 , Q_3 , and K_{pq}), with the exception of the self-phase-modulation term Q_1 , are increased. Therefore using this fact and considering the CPF formula (eqn. 11.42 or eqn. 11.43) (and bearing in mind the physical explanation given in section 11.4.2 for the dependence of the critical power on the coefficients) it can be seen that the critical power is also increased. It can also be seen that in this intermediate range of guide separations the critical power for the thickest guide rises more rapidly than the others as the guide separation is reduced. This is because the mode of the thickest guide is more tightly confined within the film region than the others and least influenced by the nonlinearity. Consequently more power is required to enable nonlinear effects to take place. The increase in critical power continues down to a separation of $w = 2.5\mu\text{m}$. where there is then a plateau. Meng and Okamoto [2] who studied the $d = 2.0\mu\text{m}$ case only, also observed the plateau, but labelled it as the 'maximum power' which it clearly is not so. They further implied wrongly that it occurs for all guide thicknesses. The reason for the existence of the plateau is because the mode of the thickest guide (ie $d = 2.0\mu\text{m}$) becomes a surface mode. Since surface modes are outside the film regions, they are not affected so much by the film region. Therefore the critical powers should also be much the same. Once the mode of the thickest guide becomes a surface mode, the critical power plateaus, and the plateau remains until the critical powers for the other thicknesses reach high enough values until all the curves then increase together. At that stage (around $d = 1.5\mu\text{m}$), there is then an asymptotic increase in the critical power for all thicknesses.

12.2.2 Comparison with BPM for a 'thick' guide

In this section we compare the critical powers obtained using our strong coupled mode theory (SCMT) against the beam propagation method (BPM). We consider the $d = 2.0\mu\text{m}$ case, which is an example of a 'thick' film guide. In Fig. 12.2 various comparisons are made between the different methods. It can be seen that all the methods lead to similar results for $w > 4.0\mu\text{m}$. Therefore this region is very weak coupling. BPM results are given by the thick solid curve in Fig. 12.2. Our CPF formula with all the terms included is given by the thin solid curve, which agrees almost exactly with BPM. As can be seen, the two curves are virtually coincident, and the plateau predicted by the CPF formula is also predicted by BPM. The dashed curve concerns the case where the overlap integral is omitted (ie the approach taken by Meng and Okamoto [2]). The results are fairly accurate for $w > 2.2\mu\text{m}$ but inaccurate for $w < 2.2\mu\text{m}$. We can see that in hindsight Meng and Okamoto [2] were quite fortunate

in studying the $d = 2.0\mu\text{m}$ $w = 2.4\mu\text{m}$ case, because as it happens the overlap integral which they neglected made very little difference to the critical power. However for the general case which is not necessarily extremely weak coupling, the overlap integral does make a difference.

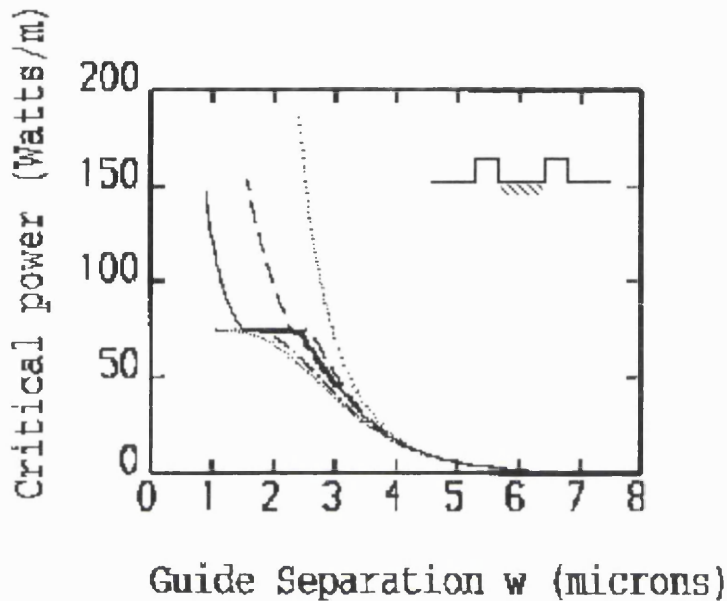


Fig. 12.2 $d = 2\mu\text{m}$. Our formula with (i) all the terms included (solid line), (ii) only overlap integral missing, (iii) the 'simple' case (chained), (iv) only nonlinear cross-coefficients missing (lower dotted), (iv) power independent curve (upper dotted), (v) BPM simulations (thick solid line).

The lower dotted curve is the approach taken by Ankiewicz and Peng [1] where the overlap integral is kept but the nonlinear cross-coefficients (Q_2 and Q_3) are omitted. It can be seen that the approach leads to very inaccurate results, even worse than the simple case (chained curve) which does not include the overlap integral. The absolute worst case is the power independent curve (upper dotted curve). Ignoring the power dependence causes large inaccuracies for small guide separations. There is no plateau with this curve, since plateau effects are due to surface waves. If power independent (linear) modes are used, then of course surface waves would not come into it and there would not be a plateau.

As mentioned above, a nonlinear supermode approach was used by Dios et. al. [3]. They analysed a weakly coupled NLDC with planar guides, the same as was done here. In one of their studies they used a structure with $d = 2.0\mu\text{m}$, and $w = 3.4\mu\text{m}$, which is

extremely weak coupling. From their Fig.4, it can be observed that their BPM simulation predicts a critical power of 29W/m, whereas their supermode analysis and nonlinear mode analysis shows a value of 36W/m, and 43W/m, an error of 24% and 48% respectively. Our CPF formula however agrees almost exactly with BPM for the same structure, as we have shown in Fig. 12.2. In addition, for the weak coupling geometry that they studied, even our coupled mode theory with power-independent fields seems to give better agreement than their formula.

Figure 12.3 shows the effect of the nonlinear cross-coefficients (Q_2 and Q_3) on the critical power. The CPF formula (with relevant terms missed out for each curve) was used to draw all these curves. It can be noticed that removing Q_3 (dotted curve) has the least effect on the critical power. Q_2 on the other hand (dashed curve) has a more significant effect, especially for small guide separations. Ignoring both Q_2 and Q_3 results in the chained curve, which is the most inaccurate case.

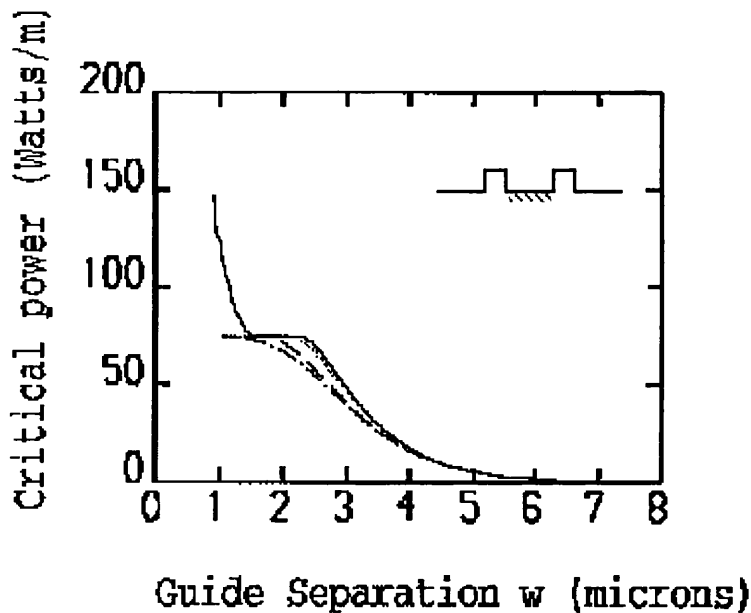


Fig. 12.3 $d = 2\mu m$. Our formula with (i) all the terms included (solid line), (ii) $Q_2 = 0$, and $Q_3 = 0$ (chained) (iii) $Q_3 = 0$ (dotted), (iv) $Q_2 = 0$ (dashed)

In summary, the most accurate cases seem to be those where either all the nonlinear cross-coefficients as well as the overlap integral are included in the equations (the 'full' case), or where the overlap integral as well as the nonlinear cross-coefficients are excluded from the equations (the 'simple' case). Ignoring either the overlap integral or the nonlinear cross-coefficients without ignoring both, leads to inaccurate results. It was also found that the power dependence of the fields was the most important

parameter in the accuracy of the equations.

12.2.3 Comparison with BPM for a ‘thin’ guide

Now we consider an example of a thin guide ($d = 0.5\mu\text{m}$). In this case the mode shape is spread out, and extends deeper into the nonlinear region. Therefore the modes overlap each other to a greater extent (see Fig. 9.3).

In Fig. 12.4 we compare the critical power curves obtained from coupled mode theory against BPM. The thick solid curve is BPM. The closest curve to BPM is the thin solid line which is the CPF curve. The next most accurate is the chained curve where both the nonlinear cross-coefficients and the overlap integral are ignored. The inaccurate cases are when the overlap integral is kept but the nonlinear cross-coefficients neglected (approach taken by Ankiewicz and Peng [1]), or where the overlap integral is neglected but the nonlinear cross-coefficients are kept (approach taken by Meng and Okamoto [2]). The absolute worst case is the power independent curve (upper dotted). These conclusions are exactly the same as Fig. 12.2, except in this case the differences can be seen more clearly.

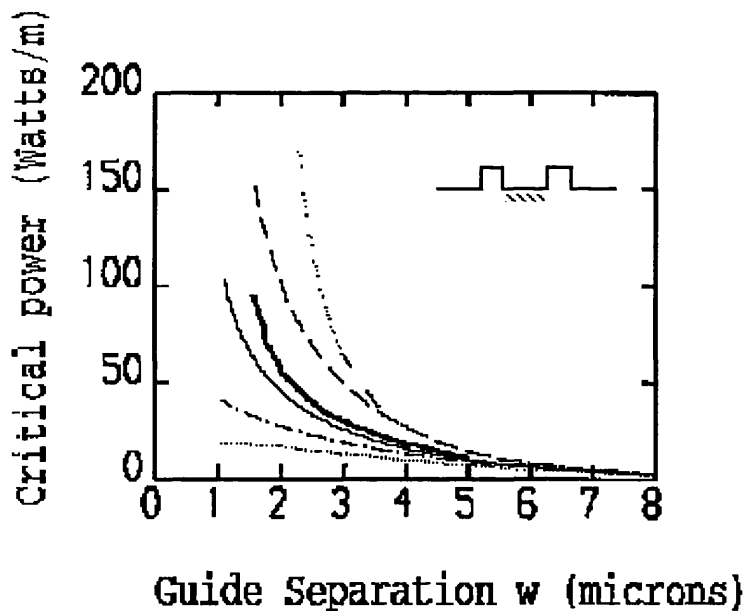


Fig. 12.4 $d = 0.5\mu\text{m}$. (i) BPM simulations (thick solid)

Our formula with (ii) All the terms included (solid), (iii) the ‘simple’ case (chained), (iv) overlap integral ignored (dashed), (v) nonlinear cross-coefficients ignored (lower dotted), (vi) Power-independent curve (upper-dotted).

In Fig. 12.5 we study the importance of the various cross-coefficients on the critical

power. The results are similar to those in Fig. 12.3. The solid curve is the curve with all the coefficients present in the formula. It can be seen that for large separations ($w > 2.5\mu\text{m}$) omitting Q_2 (dashed curve) has the greatest effect on the critical power, whereas for very strong coupling ($w < 2.5\mu\text{m}$) the situation reverses, and Q_3 (dotted) becomes the dominant coefficient. This reversal has not been pointed out before, and might seem slightly surprising (at first) because Q_2 should be greater than Q_3 for all separations. The reason for the interchange is that it is not the actual values of Q_2 and Q_3 that matter, but rather the effect that the overlap integral has on these coefficients. The overlap integral modifies Q_2 and Q_3 so that at large separations, the *modified* value of Q_2 is larger than the modified value of Q_3 , but the situation reverses at small separations ($w < 2.5\mu\text{m}$). Once again as in Fig. 12.3, the most inaccurate case occurs if both Q_2 and Q_3 are neglected from the equations (chained curve).

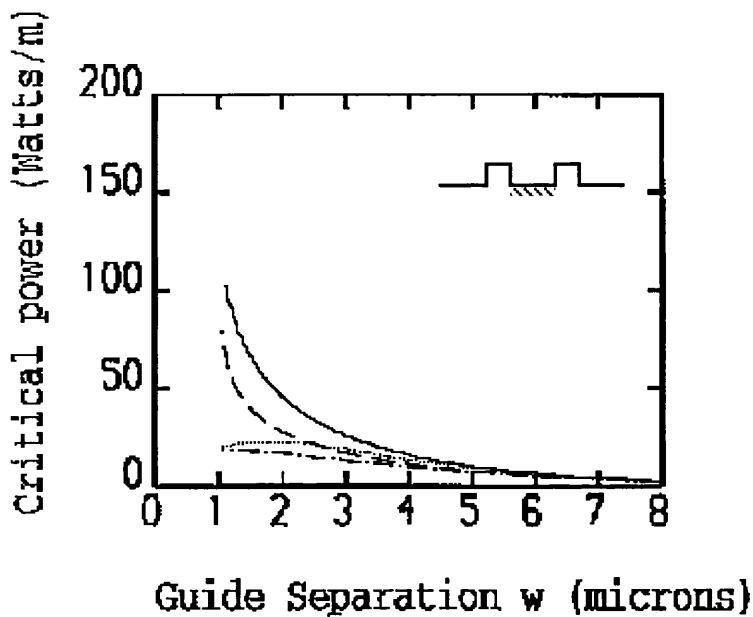


Fig. 12.5 $d = 0.5\mu\text{m}$, our formula with (i) all the terms included, (ii) $Q_2 = 0$, and $Q_3 = 0$ (chained), (iii) $Q_2 = 0$ (dashed), (iv) $Q_3 = 0$ (dotted)

In Fig. 12.6 we can see that the accuracy of the CPF curve can be improved by calculating the power dependent mode shapes by bearing in mind that the power in the overlap does not affect the mode shape, ie using $P/(1 + C_{12})$ instead of P for the mode shapes (see eqn. 11.56).

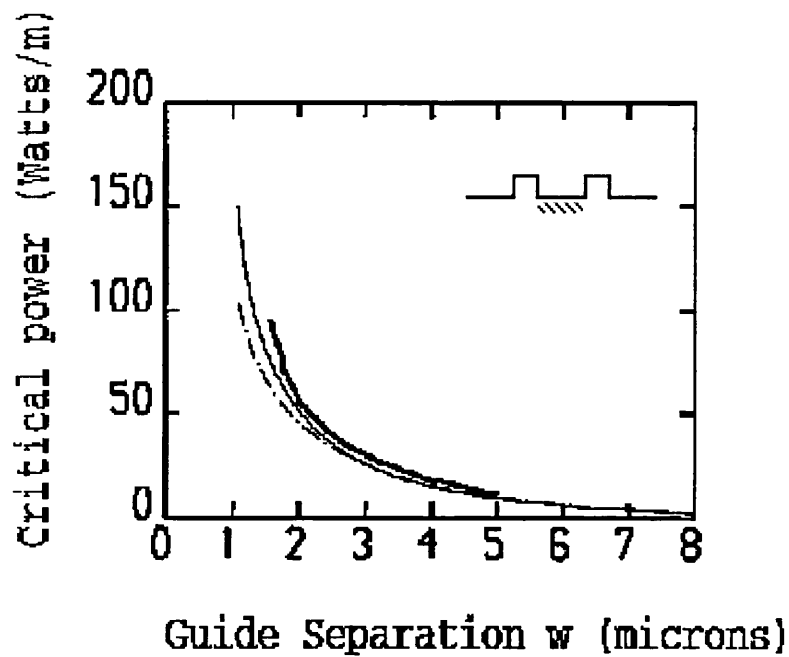


Fig. 12.6 $d = 0.5\mu\text{m}$, our formula with (i) full power fields (chained), (ii) normalised fields (solid), (iii) BPM (thick solid).

Fig. 12.7 below shows the case where the nonlinearity is in the outer cladding regions. It can be seen that once again, including the overlap integral without also including the nonlinear cross-coefficients leads to a result which is even worse than the 'simple' case.

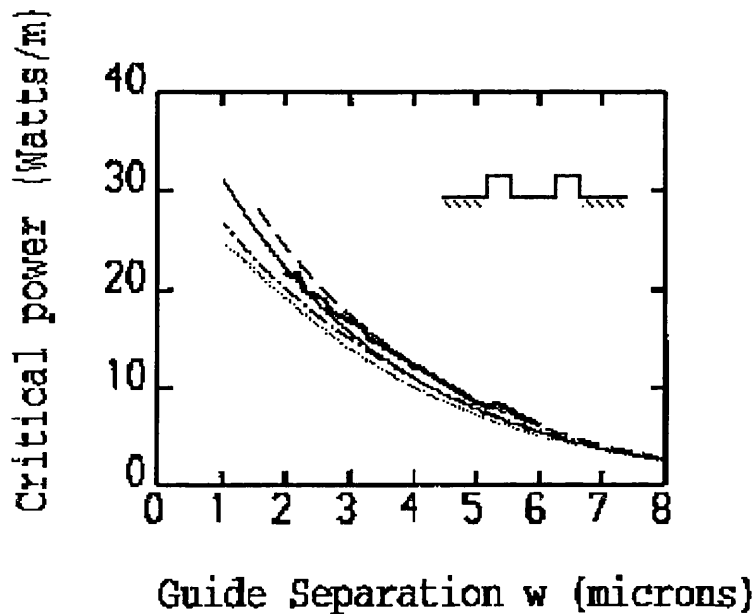


Fig. 12.7 Variation of critical power with guide separation for guide thicknesses $d = 0.5\mu\text{m}$. The nonlinearities are in the outer cladding regions
 (i) BPM (thick solid), (ii) Our formula with all the terms included (solid), (iii) The 'simple' case (chained), (iv) Overlap integral omitted (dashed), (v) nonlinear cross-coefficients omitted (similar approach to Ankiewicz and Peng [1]) (dotted)

12.3 Some notes on the BPM analysis

More discussion of the BPM analysis is now given. We excited the NLDC with the nonlinear mode (using the method in chapter 10), and used it also in the CPF formula to calculate the critical power. In a practical NLDC the nonlinear mode can be created by exciting a graded-nonlinear lead-in guide with a linear TE mode (see chapters 13 and 14). The lead-in guide adiabatically reshapes this linear mode so that it becomes the nonlinear mode when it reaches the NLDC.

In our BPM program we used 512 grid points and step sizes of $0.5\mu\text{m}$. Due to the large number of computations needed (to derive the critical power), we were restricted in using smaller step lengths. However we checked that the results did not change when the step sizes were reduced for several specific cases.

To calculate the powers in each guide, the field to the right of the middle of the separation region was attributed to the right hand guide, and the field to the left of the centre line to the left hand guide. This method introduces a slight error when calculating the guide powers. For example if one guide is supposed to contain the full power, our

program would calculate that one guide has perhaps 98% of the power and the other guide 2%. This is because our program apportions the part of the mode which extends into the other region as belonging to the other guide. This proportion naturally increases as the separation between the two guides is reduced.

The critical power is calculated in our program by plotting the output power versus the input power for a one coupling length device, and looking for the input power where a sharp transition in the output power occurs. Note that the critical power (which is the main parameter) was calculated here very accurately. This was due to the fact that in calculating it we were not concerned with the actual output powers, but only looking for when there was a sharp discontinuity in the output power. Therefore for example, at the critical power, the normalised output power could rise from 0 to 1, or from 0.3 to 0.8. It does not matter. The input power where this occurs is the important parameter.

It is difficult to calculate the actual output powers in strongly coupled guides with good accuracy. One solution might seem to be to provide diverging guides at the output so that the modes can be well separated before their powers are calculated. But this means that there will be some coupling in the diverging regions before the modes are separated sufficiently. Another method might seem to be to extend one guide at the end of the coupling region but not the other. However this introduces a difficulty because an abrupt end to one guide constitutes a large step change in refractive index and gives rise to backward reflections, which violates one of the assumptions of Feit and Fleck analysis.

12.4 CONCLUSIONS

We compared numerical solutions of our critical power formula (CPF) with those from accurate numerical simulations using the beam propagation method (BPM). We showed that the most accurate case arose whenever the overlap integral and the nonlinear cross-coefficients were present together or disappeared together from the equations (Figs. 12.2, 12.4, and 12.7). In conclusion either the full form of the equations, or the simple case with the nonlinear cross-coefficients and the overlap integral omitted should be used. The accuracy does not improve from the simple case by just adding the overlap integral as done by Ankiewicz and Peng [1]. The results would then be unreliable at the very least, or in some cases as in the geometry considered here even worse than the simple case.

We also discussed an improvement on the coupled mode theory model (Fig. 12.6). This was from an observation that the power carried by the overlap between the fields does not contribute to the shape of the modes. Therefore the actual power in the modes should be used to calculate the mode shapes, but not the full power as done by ref. 2.

REFERENCES

- [1] A. Ankiewicz, and G-D. Peng: "Effects of nonlinear mode field changes in optical switching using directional couplers", J. Opt. Soc. Am. B, Vol 9, No. 8, August 1992, pp. 1341-1349
- [2] X. Meng and N. Okamoto, "Improved coupled-mode theory for Nonlinear Directional Couplers", IEEE J. Quant. Electron., Vol 27, No.5, May 1991, pp. 1175-1181
- [3] F. Dios, X. Nogués, and F. Canal: "Critical power in a symmetric nonlinear directional coupler", Optical and Quantum Electronics, Vol 24, 1992, pp. 1191-1201

CHAPTER 13

NOVEL GRADED-NONLINEAR SCANNER AND SINGLE SOLITON GENERATOR

13.1 INTRODUCTION

Spatial solitons can be used to construct angular scanning elements. Two such devices have so far been proposed in the literature. The first is based on the power dependent refraction of a soliton penetrating the interface between two nonlinear media [1]. The soliton refracts at different angles depending on the input power, and this fact can be used for scanning applications. An alternative method is to make use of a nonlinear waveguide (with linear film and one nonlinear cladding) and excite it with a large power non-modal field shape. Since the waveguide cannot support this large power, it at once rejects much of it in the form of a soliton (or solitons at higher powers) [2]. This device is also a scanner because the soliton is emitted at an angle which depends on the input power. In this (latter) device, the first emitted soliton does not carry the whole power of the waveguide, except when the power happens to be at the threshold power for soliton generation. The device therefore has two major limitations. The first is that multisoliton emission occurs at higher powers degrading the performance of the device as a soliton generator, and the second is that incomplete power transfer occurs for the single soliton emission case, and since these types of waveguides are used in soliton couplers, the incomplete power transfer and multisoliton emission lead to inefficient soliton couplers [3].

This chapter discusses a new type of soliton generator and all-optical linear scanner based on *graded*-nonlinear waveguides (GNLWs). These devices employ a nonlinearity in one cladding which increases gradually with propagation distance. In contrast to uniform-nonlinear waveguides (UNLWs) [2-3], improved soliton emission occurs since most of the power of the waveguide is shed cleanly through the first emitted soliton. The launching length for soliton emission here is dependent on the input power (leading to design of other new devices, for example a three guide graded-nonlinear soliton coupler with switching based on propagation distance). Furthermore, in contrast to the angular scanners discussed above [2-3], the device is a linear scanner,

since the emission angle is constant and only the launching length is varied. The emitted soliton is then captured by one of a number of ports stationed perpendicular to the direction of its travel, by a parallel nonlinear film waveguide (as in soliton couplers) or by a parallel strip of high nonlinearity.

13.2 GRADED NONLINEAR WAVEGUIDES

The structure consists of a linear film with nonlinear cladding on one side and linear cladding on the other. The nonlinearity increases gradually with propagation distance z (see Fig.13.1). The graded nonlinearity can be formed, for example, by increasing the doping concentration gradually with distance. A linear TE mode is used to excite the waveguide. As the mode propagates along the waveguide, the nonlinear slope adiabatically changes the shape of the mode so that it always corresponds with the local, stable and stationary nonlinear mode. The variation of the mode shape with distance is analogous to the variation of the mode shape with increase in input power for a UNLW. The reshaping process is smooth and continuous so long as the dispersion characteristic for the stable mode of the waveguide is continuous. A discontinuity in the dispersion characteristics [2] would result in soliton emission since the change in the nonlinearity could not be made gradual enough to maintain adiabatic reshaping when there is a sudden discontinuity in the dispersion characteristics from a film-guided to cladding-guided mode. In a GNLW the soliton emission occurs at the value of propagation distance where the nonlinearity is just large enough for the threshold of soliton emission to occur for that particular power. At that distance, and for a large range of input powers, almost the whole power of the waveguide is transferred to the soliton. This is an improvement over the UNLW case, where for the single soliton emission case complete transfer occurs only at the threshold power, and incomplete transfer above, until the emission of the second soliton.

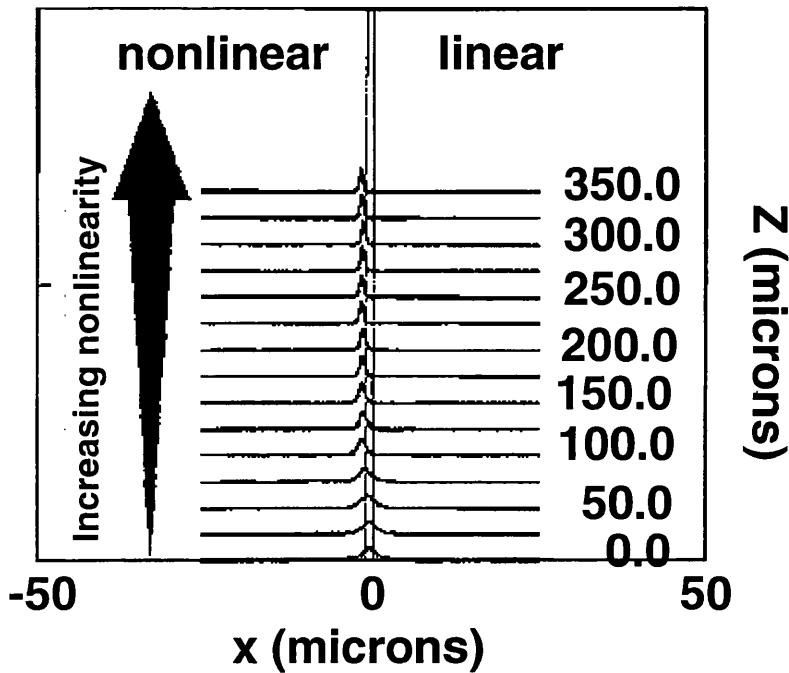


Fig. 13.1 The graded-nonlinear waveguide converting a linear TE mode to the nonlinear TE mode in a $d = 1.0\mu\text{m}$ waveguide (input power= 200 W/m). $n_f = 1.57$, and $n_{cl} = 1.55$

For the lossless GNLW geometry discussed here, with nonlinearity directly proportional to distance, the relationship $PL_s = C$ approximately holds, where P is the input power, L_s the soliton emission distance, and C a constant.

We used our BPM program with 1024 grid points and 5nm longitudinal sections. The section length was found by trial and error, so that variation of the section length did not change the results. The film and cladding indices for the waveguide were $n_f = 1.57$, and $n_{cl} = 1.55$ respectively. The nonlinear coefficient α was defined by the nonlinear permittivity $\epsilon_{NL} = \epsilon + \alpha|E|^2$, where E is the electric field, and ϵ is the linear permittivity, given by $\alpha = mz$ where $m = \alpha_{ref}/L_{ref}$, $\alpha_{ref} = 12.754 \times 10^{-12} \text{ m}^2/\text{V}^2$, and $L_{ref} = 500\mu\text{m}$.

In Fig. 13.1 it can be seen that for film width $d = 1.0\mu\text{m}$ the effect of the nonlinear cladding is gradually to change the field from a linear TE to a nonlinear TE mode even for such high powers as 200 W/m . The GNLW can therefore be used in the numerical calculation of the nonlinear mode [4], as well as for implementing a linear to nonlinear mode converter/launcher for practical nonlinear directional couplers. For $d = 2.0\mu\text{m}$ guides (with the same cladding and film indices as Fig. 13.1) there is a discontinuity in

the dispersion characteristics [2] (see chapter 10) which can be exploited for soliton generation (see Fig. 13.2). In Fig. 13.3 the variation of the power remaining in the guide as a function of propagation distance is shown for a UNLW. At lower powers, a larger launching length is required for soliton emission since a greater nonlinearity is needed. In UNLWs, complete power transfer occurs only at the threshold input power for soliton emission. Any increase in input power deteriorates the switching characteristics because of incomplete switching or multisoliton emission. In Fig. 13.4, significant improvement in switching is obtained using graded nonlinearity [5]. We observe that the switching curve is much sharper, and almost full transfer of power occurs for a wide range of input powers. The emission distance for the first soliton is increased, and the emission of the second soliton is not 'encouraged'[†] by the first soliton as in the UNLW case [2] (see Fig. 13.3), but occurs at a much larger distance. If a small amount of loss is present, the emission of the second soliton can be prevented altogether, resulting in single soliton emission.

[†]In [2] it was mentioned that although the first soliton is emitted at the threshold power, the second soliton is emitted below twice this power because the emission of the second soliton is 'encouraged' by the presence of the first emitted soliton when it is in the vicinity of the waveguide.

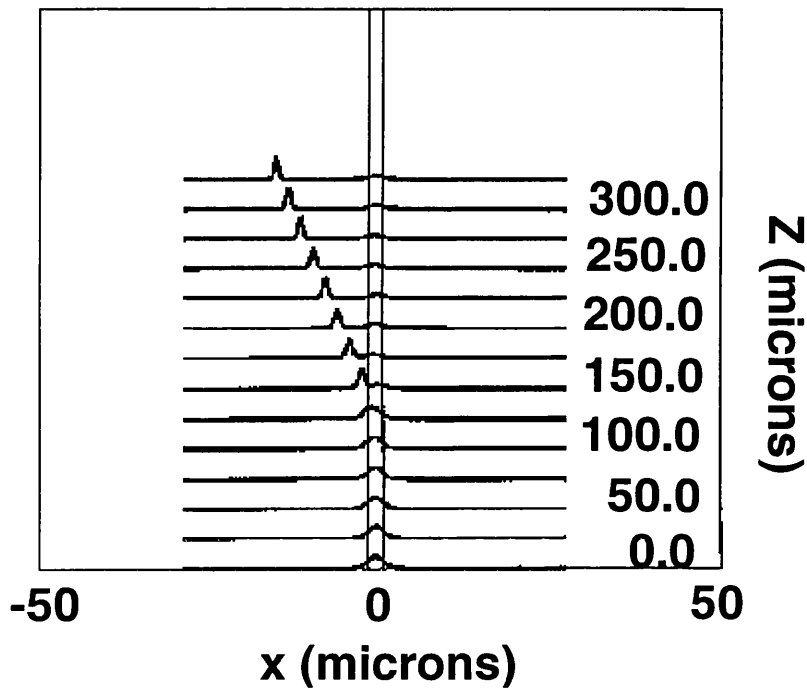


Fig. 13.2 Generation of a single soliton using the graded-nonlinear waveguide (input power=200 W/m).

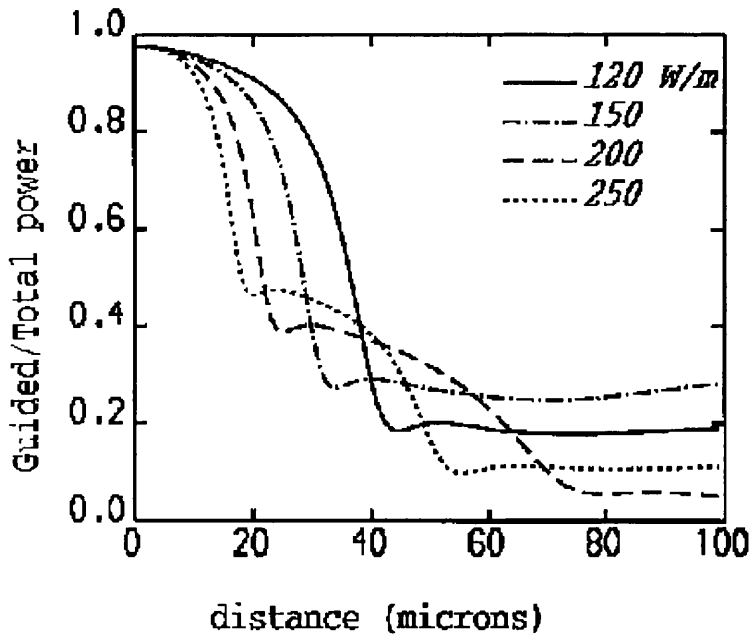


Fig. 13.3 Variation of waveguide power with propagation distance for different input powers in a uniform-nonlinear waveguide ($\alpha = 6.377 \times 10^{-12} \text{ m}^2/\text{V}^2$)

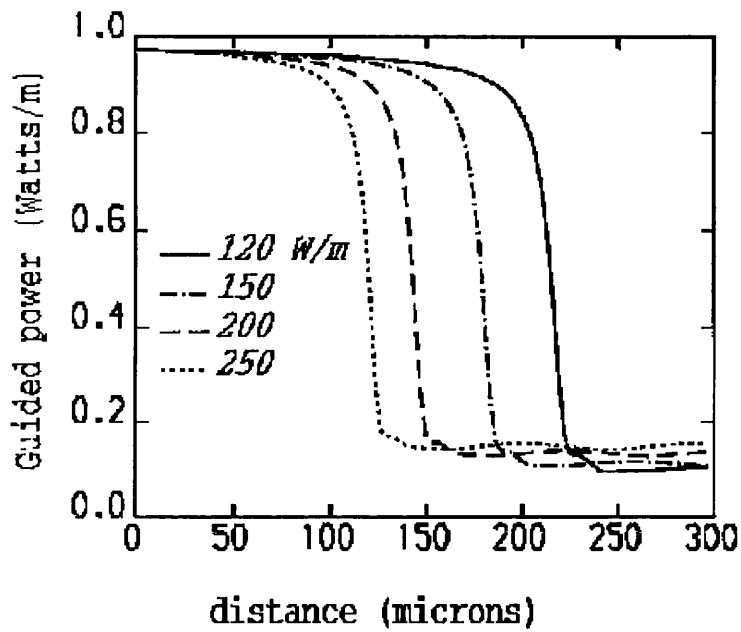


Fig. 13.4 Improved switching characteristics using a graded-nonlinear waveguide.

13.3 CONCLUSIONS

We have proposed a new linear scanner which complements the angular scanners discussed in previous publications. The use of graded-nonlinear waveguides allows for variable power, clean single-soliton generation, and more efficient soliton couplers.

REFERENCES

- [1] P. Varatharajah, A. B. Aceves, and J. V. Moloney, "All-optical spatial scanner", *Appl. Phys. Lett.*, vol. 54, pp. 2631-2633, 1989.
- [2] E. M. Wright, G. I. Stegeman, C. T. Seaton, J. V. Moloney, and A. D. Boardman, "Multisoliton emission from a nonlinear waveguide", *Phys. Rev. A*, vol. 34, pp. 4442-4444, 1986.
- [3] D. R. Heatley, E. M. Wright, and G. I. Stegeman, "Soliton coupler", *Appl. Phys. Lett.*, vol. 53, pp. 172-174, 1988.
- [4] F. Wijnands, H. J. W. M. Hoekstra, G. J. M. Krijnen, and R. M. de Ridder, "Numerical solution method of nonlinear guided modes with a finite difference complex axis beam propagation method", *IEEE J. Quant. Electron.*, vol. 31, pp. 762-790, 1995.
- [5] F. Farjady, M. G. F. Wilson, and P. M. Radmore, "New All-Optical Linear Scanner and Variable Power Single Soliton Generator using Graded-Nonlinear Waveguides", *IEEE Photonics Technology Letters*, Vol. 8, no. 8, August 1996, pp. 1047-1048.

CHAPTER 14

NOVEL TRI-STATE SPATIAL SOLITON SWITCH USING GRADED NONLINEARITIES

14.1 INTRODUCTION

In this chapter we discuss a novel type of three guide soliton coupler. We consider soliton couplers because they have several advantages over conventional coherent couplers. Firstly they are easier to fabricate due to having more relaxed requirements on their guide separations and lengths. Secondly they exhibit sharper switching since the coupling is by means of whole packets of solitons rather than continuous power transfer. Thirdly they allow power to be switched almost fully to all three guides, whereas in coherent couplers the power does not emerge fully from the middle guide unless gains and losses are also incorporated [1]. Fourthly, power emerges from each of the three guides for a wide range of input powers (see later in the chapter) whereas in coherent couplers the power emerges from the middle guide only for a narrow range of input powers.

The essential part of any soliton coupler is the soliton generator. It consists of a guide composed of a linear film with one of the claddings being nonlinear. The guide is initially excited with a linear TE field which is approximately the true mode of the waveguide at low powers but not at high powers (the mode becomes nonlinear in the latter case). At high powers the field shape becomes affected by the nonlinearity, and the field shifts towards the positive nonlinear cladding. At threshold the shift is so abrupt that in the process a soliton breaks off and becomes launched into the cladding. The soliton does not carry with it the whole power of the field however but some residual power is always left behind in the guide. In chapter 13 it was mentioned that the amount of residual power is always minimum when the emission occurs at threshold. The proportion of residual power then increases above threshold and results in reduced efficiency of emission. If the input power becomes larger than a certain threshold, a second soliton can be emitted [2] from the residual power. However the threshold input power needed for two soliton emission is lower than might be expected (ie less than twice the threshold power needed for single soliton emission). This is because the first soliton affects the emission conditions for the second soliton when it is

in close proximity to the guide.

So far the nonlinearity has been assumed to be in one cladding only. If both claddings are nonlinear however, the soliton is emitted into the cladding which has the higher nonlinearity. When the nonlinearities in both claddings are equal then in theory solitons are launched simultaneously into both claddings. However this is a rather unlikely case to occur in practice, since any local imperfection breaks the symmetry and leads to emission into one cladding only. The symmetrical nonlinear cladding configuration has been used in a recent publication [3] to design a three guide soliton coupler. In this device the middle guide is excited with a below threshold input power. By adding an asymmetrical control beam on top of the input beam it was possible to choose the cladding for soliton emission. The asymmetrical beam increases the refractive index in one cladding encouraging soliton emission on that side and decreases the refractive index in the other cladding suppressing soliton emission there. By changing the phase of the asymmetrical beam the asymmetrical effect can be reversed, and the soliton directed into the other cladding instead.

This three-guide soliton coupler arrangement, although theoretically interesting, has unfortunately several drawbacks in practice. The most obvious disadvantage is the need for an additional control beam which makes the device complicated to operate. Another disadvantage is that the use of *uniform* nonlinearities in the claddings leads to inefficient switching. As mentioned above, soliton emission from uniform nonlinear guides is efficient only if the total power happens to be at threshold. Above that power the emission becomes less efficient, and at even higher powers multisoliton emission effects degrade the switching characteristics even further. Another disadvantage of the arrangement is that both claddings are equally nonlinear resulting in the the field being drawn in both transverse directions. Therefore the emission is less efficient than say if one cladding had a much greater nonlinearity than the other. Another problem is that although the asymmetrical control beam enables switching to the lateral guides, it does not allow the power to be kept in the middle guide except for a narrow range of phases. The arrangement is therefore practically a two-guide switch and not the three-guide switch which was claimed [3]. The only solution for keeping the power in the middle guide seems to be to switch off that control beam altogether, but this adds extra complications to the already complicated device.

14.2 NEW GRADED-NONLINEAR TRI-STATE SWITCH

In chapter 13 we proposed graded nonlinear guides [4] which we believe have superior performance to uniform nonlinear guides for soliton generation. In graded nonlinear

guides, the nonlinearity of one or both claddings changes gradually with propagation distance. These guides can be used as devices for linear-to-nonlinear mode conversion or soliton generation depending on whether the mode they support are weakly or strongly guided. In the case of the field being weakly-guided, a large proportion of it is in the nonlinear cladding region and consequently its shape is sensitive to changes in the nonlinearity or the input power. As the field propagates through such guides the nonlinearity changes and the field shape alters adiabatically with propagation distance, so that it always corresponds with the local nonlinear mode of the waveguide. These weakly-guided graded nonlinear devices are therefore useful as mode converters (see chapter 13). In the case of the field being strongly-guided, it is mostly concentrated within the linear film region, and therefore not affected by the nonlinearity in the cladding. Consequently so long as the nonlinearity does not become large enough to affect the field shape, the linear TE mode shape is preserved. When the nonlinearity reaches a certain threshold, there is a sharp swing of the field towards the nonlinear cladding, and in the process a soliton breaks away from the field and becomes launched into the cladding. The emission is more efficient than uniform nonlinear devices because it always occurs at exactly the threshold point, so that the residual power left behind in the guide happens to be minimum. It should be noted that the distance where the soliton emission occurs is determined by the input power. For example, for large input powers, a smaller threshold nonlinearity is required. Since smaller nonlinearities are situated near the start of the grading, the soliton emission occurs there.

In summary there are two effects regarding well-guided graded-nonlinear guides which might be useful for a potential new device. Firstly, below threshold the mode shape does not alter with propagation distance (ie the field retains its linear TE mode shape). Secondly, the input power determines the value of the threshold nonlinearity and therefore the emission distance. In this chapter we propose a novel three-guide soliton coupler which makes use of these two effects. The implication of the first effect is that the nonlinearity in either cladding can be arbitrary so long as it is below threshold. The implication of the second effect is that the soliton is emitted into the cladding which contains the threshold nonlinearity first (for example a soliton is launched into the left hand cladding if the threshold nonlinearity is first encountered there). If the field does not break up during its transit through the guide then it remains in the guide.

14.3 DEVICE GEOMETRY

A schematic of the device geometry is shown in Fig. 14.1 and the variation of the cladding nonlinearities with propagation distance in Fig. 14.2. The middle guide is

excited with a linear TE mode, and there are two lateral nonlinear guides for capturing the emitted solitons. As the field propagates through the guide, initially there is a positive graded nonlinearity in the left hand cladding and zero nonlinearity in the right hand cladding. The nonlinearity at the start of the grading can be zero, or non-zero as is the case in Fig. 14.2. A non-zero nonlinearity has the advantage of leading to short grading lengths. So long as the input power is below the threshold associated with that nonlinearity it is permissible to use a non-zero nonlinearity. The length of the grading (more specifically the maximum nonlinearity reached) determines the minimum cut-off power required to excite a soliton into the left hand cladding. At the end of the left hand grading, further on along the guide, there is a grading in the right hand cladding. The initial value of the nonlinearity for the right hand grading continues from the maximum reached in the left hand grading. The generation of a soliton in either the left hand or the right hand grading depends on whether threshold nonlinearity is first reached in the left or the right hand cladding. Otherwise the field maintains its shape and remains in the input guide as a linear TE mode.

It can be noticed from Fig. 14.2 that there are *negative* graded nonlinear regions immediately following the positive graded nonlinear regions. As mentioned above, soliton emission is more efficient if the nonlinearities in the different claddings are sufficiently different. The purpose of the left hand negative grading in this case is therefore to ensure that the nonlinearities in the two claddings become sufficiently different so that the soliton is emitted efficiently into the right hand cladding. Another reason for the negative gradings is that there is a problem arising from high power solitons being emitted earlier in each positive grading than the low power solitons. Therefore they narrow more because they have to travel through the rest of the grading whilst in the cladding. Narrow solitons are captured less efficiently by the lateral guides. On the other hand using negative graded nonlinear regions immediately after the positive graded nonlinear regions allows these high power solitons to be widened before capture. However it should be remembered that the low power solitons are widened also, and in the limit they can become so wide that they collapse as solitons. Therefore the nonlinearity should not be decreased so much that low power solitons cannot complete their journey in the cladding towards the lateral guide. In Fig 14.2 it can be seen that the positive graded nonlinearity in the right hand cladding starts immediately once the negative graded nonlinearity ends in the left hand cladding. It can also be seen that at the end of the negative nonlinear regions, the nonlinearity becomes uniform in both claddings.

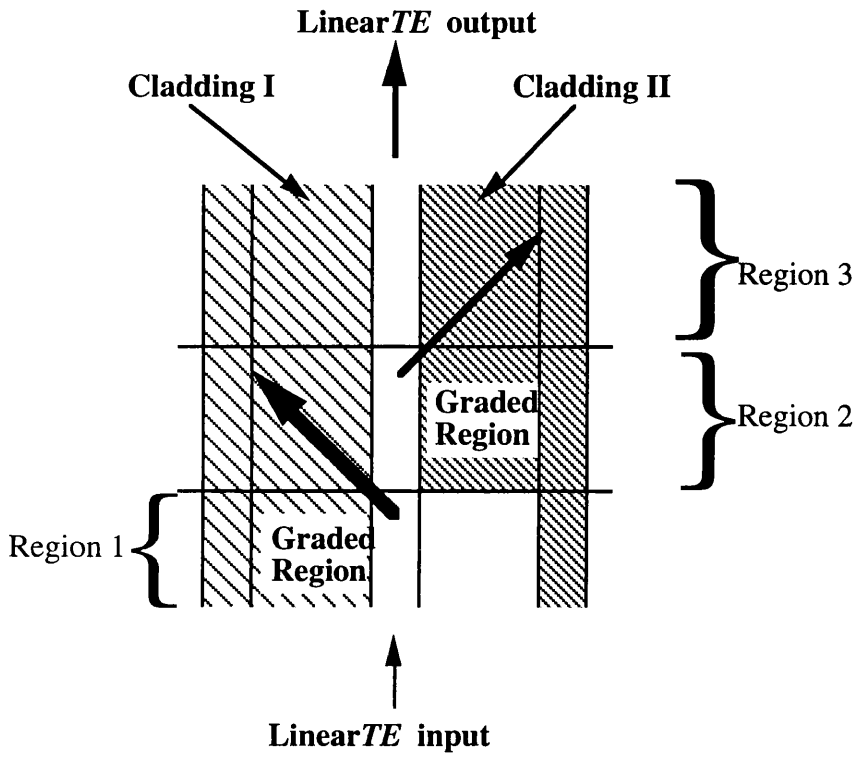


Fig. 14.1 A schematic of the device geometry

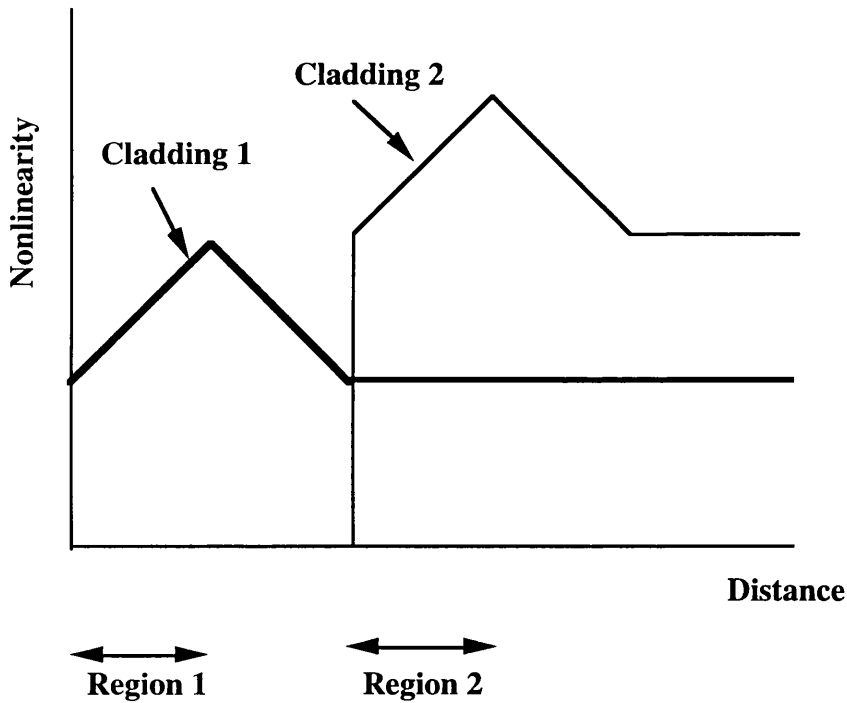


Fig. 14.2 The variation of the nonlinearities in the two cladding with distance.

The lateral guide should be carefully designed so that the incoming soliton is captured efficiently. Sometimes radiation is generated when the soliton is captured and upon capture whenever it reflects from the walls of the guide. This radiation reduces the capturing efficiency and leads to the degradation of the switching response. To minimise the amount of radiation, the transverse changes of the nonlinearity should be made gradual. Therefore as a first step the nonlinearity of the capturing film can be made the same as that of the cladding. In the longitudinal direction, the variation of the nonlinearity should depend on the distance where the soliton is captured. If the soliton is captured in the graded nonlinear region, then the film of the lateral guide should be graded. If it is captured in the uniform nonlinear region, the nonlinearity should be uniform. The latter is probably easier to implement in practice. To ensure that the soliton is captured in the uniform nonlinear section, the separation between the guides should be large enough so that the soliton emerges from the graded nonlinear region. The refractive index of the film should be such that the soliton is captured and not reflected or transmitted. To maximize the capturing efficiency a novel idea might be to make the lateral guides diverging with respect to the input guide so that the soliton is captured at a virtually grazing angle.

14.4 RESULTS

Fig. 14.3-14.5 show beam propagation method (BPM) simulations for different input powers respectively. The geometry includes a left hand graded nonlinearity with the nonlinearity starting at $0.4 \times 10^{-9} m^2/W$ (see Fig. 14.2) and increasing to a peak of $0.8 \times 10^{-9} m^2/W$ over $100 \mu m$. A negative graded nonlinearity then follows which decreases the nonlinearity down to $0.4 \times 10^{-9} m^2/W$ over the next $100 \mu m$. The nonlinearity subsequently becomes uniform with propagation distance. When the nonlinearity in the left hand cladding becomes uniform, the graded nonlinearity in the right hand cladding starts at $0.9 \times 10^{-9} m^2/W$, increases to a peak value of $1.3 \times 10^{-9} m^2/W$ over $100 \mu m$, and then decreases down to $0.9 \times 10^{-9} m^2/W$ over the next $100 \mu m$, subsequently becoming uniform.

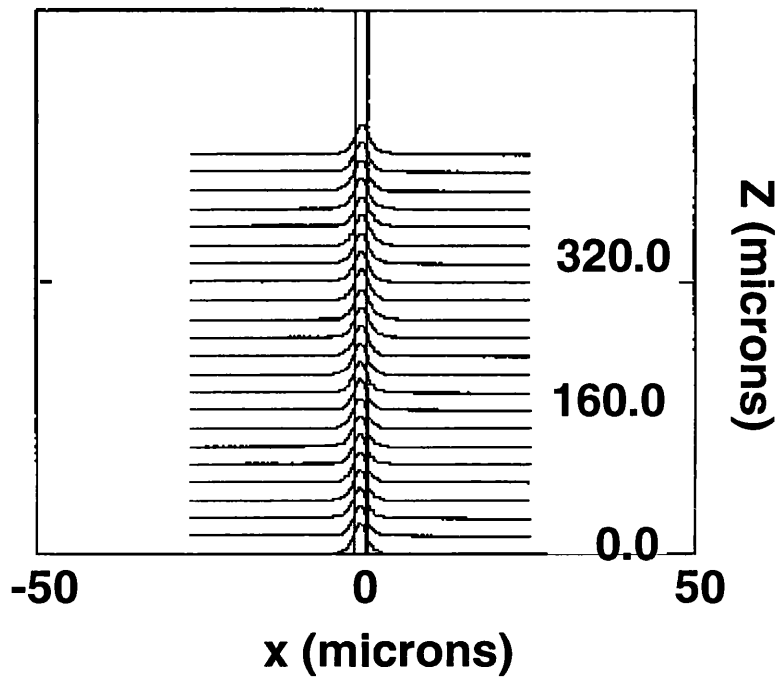


Fig. 14.3 BPM diagram showing straight through output at 50 Watts/m input power

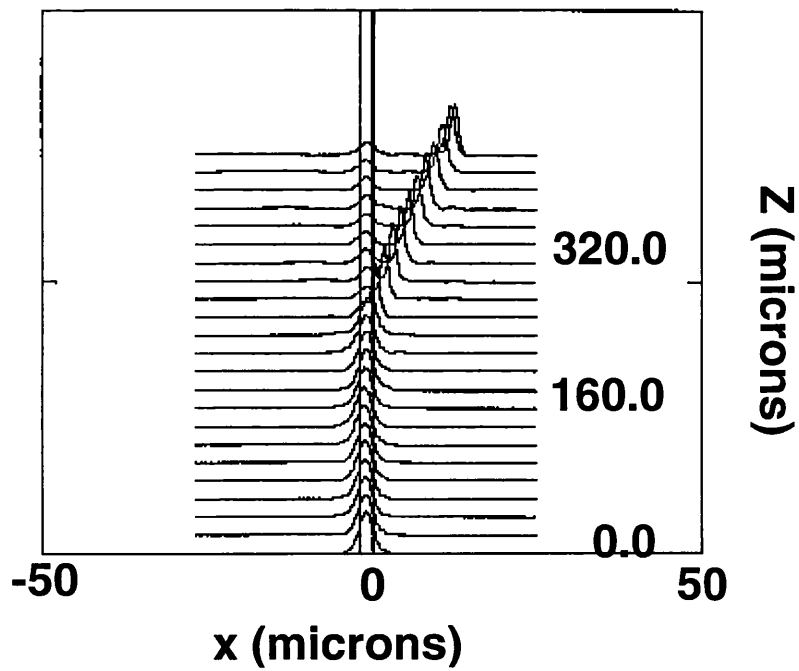


Fig. 14.4 Power switches to the right hand guide at 90 Watts/m

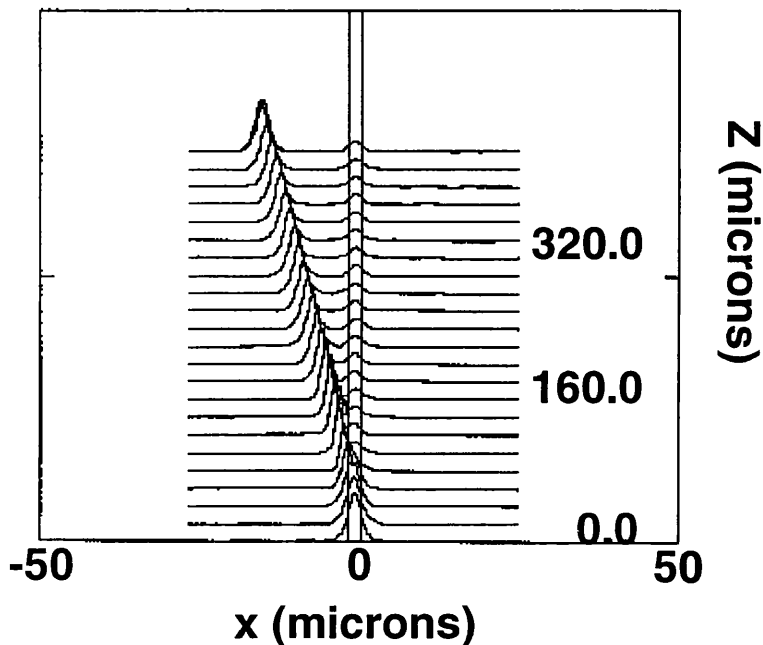


Fig. 14.5 Power switches to the left hand guide at 130 Watts/m

As can be seen from Fig. 14.3, at low powers (eg. 50 Watts) the power emerges from the middle guide. At higher powers (90 Watts) a soliton is emitted into the right hand cladding (see Fig. 14.4), and at still higher powers (130 Watts) (see Fig. 14.5) a soliton is emitted into the left hand cladding. The switching characteristics (input power vs output power) are summarized in Fig. 14.6. It can be seen that the switching edges are sharp, and almost full switching occurs between all three guides. The width of the switching can be arbitrarily wide by careful adjustment of the slope and length of the grading whereas in coherent couplers the switching to the middle guide occurs over a narrow range of powers [5]. It can be seen from Fig. 14.6 that the output characteristics for the left hand guide is that of a high pass power filter, for the right hand guide a bandpass power filter and the middle guide a low pass power filter. The minimum power for which the soliton is switched to the left hand guide is determined by the length of the left hand grading. The range of powers for which the soliton is emitted into the right hand guide is determined by the length of the right hand grading. It should also be mentioned that the slope of the graded nonlinear regions is limited by the discretised step length used in the BPM program. If the slope is too large then the step length has to be small, otherwise large index changes from one step to the next results in backward reflections violating the basic assumption of our BPM program. A step length of $0.05\mu m$ was used in our BPM program. It should be mentioned that the

lateral capturing guides have not been incorporated in our results. They are straightforward to design with a little experimentation (some design suggestions were proposed in the previous subsection).

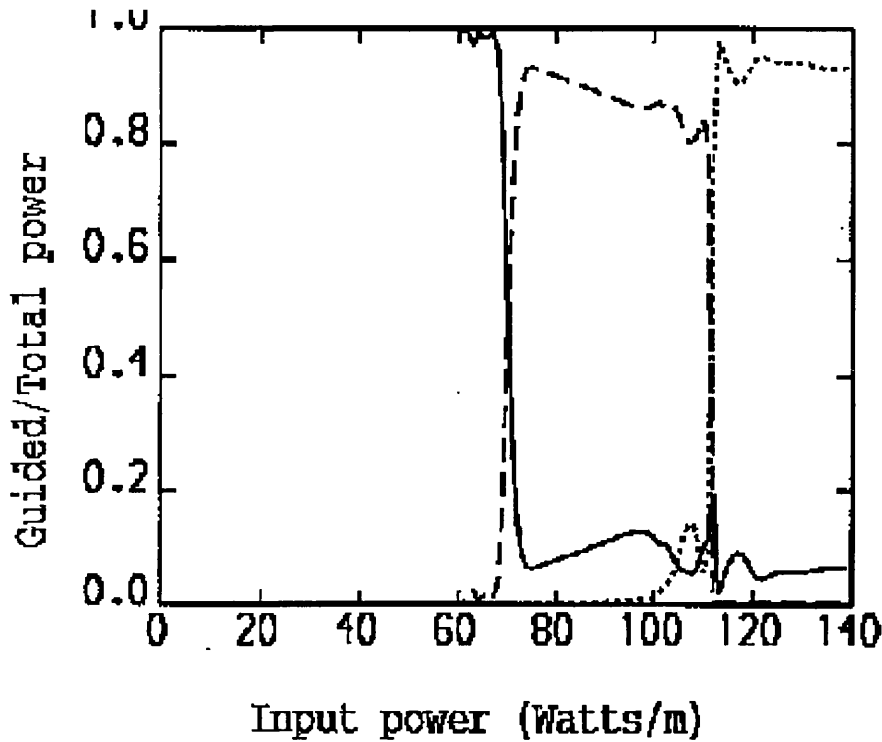


Fig. 14.6 Switching characteristics

14.5 CONCLUSIONS

In conclusion we have proposed the basis of a novel three guide soliton coupler based on graded nonlinearities. The device is more efficient and easier to implement than a previous proposed arrangement [3] based on uniform nonlinearities. The switching is simpler because it does not rely on an additional control beam but is entirely controlled by the input power and grading parameters.

REFERENCES

- [1] F. Di Pasquale and H. E. Hernández-Figueroa, "Improved all-optical switching in a three-slab nonlinear directional coupler with gain", *IEEE J. Quant. Electron.*, vol. 30, no. 5, 1994, pp. 1254-1258.
- [2] D. R. Heatley, E. M. Wright, and G. I. Stegeman, "Soliton coupler", *Appl. Phys. Lett.*, vol. 53, pp. 172-174, 1988.
- [3] H. E. Hernández-Figueroa, F. Di Pasquale, R. D. Ettinger, F. A. Fernández, and J. B. Davies, "Controlled spatial bright soliton emission from a nonlinear waveguide", *Opt. Lett.*, vol. 19, no. 5, 1994, pp. 326-328.
- [4] F. Farjady, M. G. F. Wilson, and P. M. Radmore, "New all-optical linear scanner and variable power single soliton generator using graded-nonlinear waveguides", *IEEE Photonics Technology Letters*, Vol. 8, no. 8, August 1996, pp. 1047-1048.
- [5] N. Finlyson and G. I. Stegeman, "Spatial switching, instabilities, and chaos in a three-waveguide nonlinear directional coupler", *Appl. Phys. Lett.*, vol. 56, no. 23, 1990, pp. 227677-2278

CHAPTER 15

CONCLUSIONS AND FUTURE WORK

15.1 SUMMARY OF RESULTS AND CONCLUSIONS

A summary of the work done, and the main conclusions reached are given below. We covered three main topics in this thesis. The first concerned coupled mode theory for the nonlinear directional coupler (section 15.1.1 below), the second the graded nonlinear soliton generator (section 15.1.2), and the third, the three guide soliton coupler (section 15.1.3).

15.1.1 Conclusions (part 1): Coupled mode theory for the multiwaveguide nonlinear directional coupler

The first aim was to derive the full coupled mode equations for the strongly coupled multiwaveguide nonlinear directional coupler (NLDC) (chapter 6). The word ‘full’ here signifies that all the linear and nonlinear coefficients are included in the equations. The ‘simple’ case on the other hand refers to the weak coupling assumption where all the nonlinear coefficients except the self-phase-modulation term are neglected and the overlap integral is not present. The full case is more accurate than the simple case since it has been derived directly from the original perturbation assumptions. We considered a general geometry which consisted of an arbitrary set of parallel guides with nonlinearity positioned arbitrarily in the cross-section of the system. In the literature it is assumed that only adjacent guides interact. Here we allowed for the first time for all the guides to interact.

To allow the equations to be in a more structured form, we introduced a new matrix notation (chapters 5 and 7). It was found that the matrix form greatly simplified the form of the equations. For example the entire set of equations for the all-guide interaction case was reduced to one line! (eqn. 7.17) The matrix form enabled a clearer understanding of the physical effects and allowed general patterns in the equations to be observed.

The second aim of our investigations into coupled mode theory for the NLDC was to study in detail the two guide case. We derived two new identities (chapter 5). We used them to derive the nonlinear propagation coefficient for an isolated nonlinear guide, and to show that one of the identities actually links the coupled mode equations of two different papers which assumed different unperturbed systems in their

derivations. We solved the full coupled mode equations analytically for the two guide case (chapter 11). We showed for the first time that one of two constants of motion which happens to be a Poincaré sphere in weak coupling changes into an ellipsoid in strong coupling (sections 11.3-11.4). We also derived a new formula for the ‘critical’ (or switching) power (eqn. 11.42), taking into account the power dependence of the mode shapes and the effect of all the nonlinear coefficients. This formula is not derivable from the local mode theory model suggested in a recent paper [1].

The third aim was to numerically investigate the two-guide case (chapter 12) in order to check the accuracy of the equations and to ascertain the importance of the various coefficients appearing in the equations (section 10.5 and chapter 12). The theory was shown to be more accurate than those of prior theories for both weak and strong coupling cases (Figs. 12.2 and 12.4). Since our equations included all the terms, they were free from inconsistencies. In the literature however, some terms were omitted from the coupled mode equations without careful consideration of their significance. For example, there has written a series of papers [1-3] where the overlap integral is included in the equations but the nonlinear cross-coefficients left out. We proved that this was inconsistent by using power conservation (section 7.4), reciprocity (section 5.4.2.4), and by performing numerical simulations and comparing the switching powers obtained using the different methods against those from the beam propagation method (chapter 12). We found that if the overlap integral were included without including the nonlinear cross-coefficients, the results would be even less accurate than the ‘simple’ case which does not contain the overlap integral at all (Figs. 12.2, 12.4, and 12.7). Therefore if the objective of the above papers was to improve the accuracy of the coupled mode equations by including the overlap integral, it failed in this regards since the results were made worse than the simple case which does not include the overlap integral. We also assumed in our simulations that the mode shapes were power dependent (chapter 10), resulting in all the linear and nonlinear coefficients also being power dependent. We studied in detail the variation of the linear and nonlinear coefficients with input power and guide separation. We also proposed an improvement in the accuracy of the coupled mode equations by taking into account the power carried by the overlap between the fields. Meng and Okamoto [4] used the full power to calculate the field shapes. Since the power carried in the overlap does not contribute to the shaping of the modes, we stated that this power must be removed from the total power before calculating the mode shapes (Fig. 11.56, chapter 12). We found in numerical investigations that the results became more accurate.

15.1.2 Conclusions (part 2): Graded nonlinear soliton generator

Secondly we proposed a new device, the graded-nonlinear soliton generator (see chapter 13). Graded-nonlinear guides have nonlinearity in one cladding which increases linearly, or changes otherwise with propagation distance. When the guide is excited with a field possessing a linear mode shape, the field propagates along the guide until it reaches a point where nonlinearity is at threshold, and at this point the field suddenly shifts towards the cladding and in the process a soliton breaks off from it and is emitted into the cladding (see Fig. 13.2). Some residual power is always left behind in the guide. In prior uniform nonlinear guides, whenever the input power was varied above threshold, the emission became less efficient, and the soliton emerged at varying angles. These guides were therefore applicable for angular scanning [5]. In graded-nonlinear guides on the other hand, the emission always occurs at threshold and therefore is more efficient than in uniform-nonlinear guides (see Figs. 13.3 and 13.4). The soliton is also emitted at the same angle regardless of the input power. This device can therefore be used as a linear scanner. Since the residual power left behind in the (graded nonlinear) guide is small, another soliton is not usually formed unless the length of the grading is very long. Therefore graded nonlinear guides can be employed as efficient single-soliton generators, whereas previous uniform nonlinear guides lead to inefficient emission, and multi-soliton emission at higher powers.

15.1.3 Conclusions (part 3): Graded nonlinear three-guide soliton coupler

We also designed, using the graded nonlinear concept, a novel three guide soliton coupler (see chapter 14) which we believe has superior performance to that in a previous paper [6] which used uniform nonlinearities and required the use of an additional control beam for its operation. By employing graded nonlinear guides here, the inconvenience of employing a control beam is avoided altogether. Our device operates purely by means of the input power, and the different switching powers are determined solely by the length and the slope of the graded nonlinearity. The switching is more efficient than the switching in the uniform nonlinear soliton couplers because graded nonlinearity is used. Almost full switching between all three guides can be expected. Moreover, the previous device is in practice a two-guide switch whereas ours is a true three-guide switch.

15.2 FUTURE WORK AND SOME NOVEL CONCEPTS AND DEVICES

The work undertaken in this thesis has opened up new exciting possibilities for further

research.

1- Work can be done to further improve the efficiency of soliton emission from graded nonlinear guides. For example, the emission from curved-film graded nonlinear guides should be investigated, to determine whether the emission is more efficient than in straight-film graded nonlinear guides. The results would also lead to improved soliton generators and soliton couplers.

2- New devices using graded nonlinear guides can be explored. For example it may be possible to design an angular scanner element using the graded nonlinear concept. The angular scanning can be achieved by substituting a uniform nonlinearity in the cladding which is normally held linear. The angle with which the soliton emerges depends on the difference between the nonlinearities in the claddings. If the soliton is emitted early on, it emerges at a small angle since the nonlinearities in the two claddings are almost equal. If on the other hand the soliton is emitted further along the guide, it will emerge at a larger angle since there is a large difference in the nonlinearities by that point. By keeping the length of the device short and using a steep nonlinear grading, the soliton can appear to emerge from the same point along the guide, even though the angle changes with input power. Consequently this device operates as an angular scanner.

3- Temporal pulse propagation in graded nonlinear guides should be investigated. In normal circumstances it might be expected that the pulse breaks up, since different parts of the pulse would be emitted in the form of spatial solitons at different distances along the guide. It may be possible however to avoid pulse break-up by using temporal solitons. This approach has succeeded in the case of nonlinear directional couplers, where the use of temporal solitons enabled whole pulse switching. It would be of interest to check whether the same is true of graded nonlinear guides. If so, the device would presumably be a temporal to spatio-temporal soliton converter. This is because a temporal soliton inserted into the device, is emitted as a whole in the form of a spatial soliton into the cladding.

4- Another novel application using graded nonlinear waveguides would be as a wavelength demultiplexer. In this case each pulse effectively 'sees' a different nonlinearity, due to having a different wavelength, and is therefore emitted at a different location from the guide. It should of course be ensured that the time interval between the pulses is sufficiently long to avoid nonlinear interaction between them.

5- Future work in the coupled mode theory area would include comparing numerically the coupled mode theory results for the three guide nonlinear directional coupler with those from beam propagation method simulations. It is necessary to use a numerical routine for the integration of the coupled mode equations, since an analytical derivation would be far too involved in this case. In addition, published papers on the three guide nonlinear coupler do not yet consider the effect of linear and nonlinear interactions between the outer guides. These effects could be investigated, and also comparisons between the characteristics of aligned and triangular formation could be made.

6- We suggest a novel idea using the nonlinear directional coupler. It is a filter with a power dependent bandwidth and fixed centre wavelength. The device has one guide as linear and the other as nonlinear. The nonlinearity in the nonlinear guide is such that it has a positive value over a certain range of wavelengths and negative over an adjacent range. At an intermediate wavelength the nonlinearity would be zero. At this particular wavelength both guides are linear. Assuming the length of the coupler is one linear coupling length, 100% power transfer would be expected at that wavelength. At other wavelengths the device is a nonlinear directional coupler. Therefore the output characteristic is that of a wavelength filter with a power dependent bandwidth. At low input powers the bandwidth is large or infinite depending on the maximum magnitude of nonlinearity achievable in that material. As the input power is increased the filter bandwidth reduces, but the peak efficiency stays the same. Practical materials with a nonlinearity which goes from positive to negative can be found in semiconductors [7], where physically the positive nonlinearity is due to two photon absorption and the negative nonlinearity due to bandgap resonance. Intermediate between these two is a wavelength where the nonlinearity is zero. It is possible to tailor this wavelength by changing material parameters, for example by altering the resonance nonlinearity distribution or the two photon absorption peak distribution.

This intensity dependent bandwidth filter is reminiscent of an intensity dependent tunable filter we proposed recently [8] which was also based on the nonlinear directional coupler. In that device the centre wavelength and the peak efficiency varied with input power. However, it was shown that in certain cases, it was possible to tune the filter whilst maintaining the peak efficiency and bandwidth.

REFERENCES

- [1] A. Ankiewicz and G-D Peng, *J. Opt. Soc. Am. B*, vol. 9, 1992, pp. 1341
- [2] A. Ankiewicz, "Interaction coefficient in detuned nonlinear couplers", *Optics Commun.*, vol. 66, no. 5,6, 1988, pp. 311-314.
- [3] A. Ankiewicz, "Novel effects in non-linear coupling", *Optics and Quant Electron.*, vol. 20, 1988, pp. 329-337.
- [4] X. Meng and N. Okamoto, "Improved coupled-mode theory for Nonlinear Directional Couplers", *IEEE J. Quant. Electron.*, Vol 27, No.5, May 1991, pp. 1175-1181
- [5] P. Varatharajah, A. B. Aceves, and J. V. Moloney, "All-optical spatial scanner", *Appl. Phys. Lett.*, vol. 54, pp. 2631-2633, 1989.
- [6] H. E. Hernández-Figueroa, F. Di Pasquale, R. D. Ettinger, F. A. Fernández, and J. B. Davies, "Controlled spatial bright soliton emission from a nonlinear waveguide", *Opt. Lett.*, vol. 19, no. 5, 1994, pp. 326-328.
- [7] M. Sheik-Bahae, D. Crichton Hutchings, D. J. Hagan, and E. W. Van Stryland, "Dispersion of bound electronic nonlinear refraction in solids", *IEEE J. Quant. Elect.*, vol. 27, no. 6, 1991, pp. 1296- 1309.
- [8] F. Farjady and M.G. F. Wilson, "New application for the nonlinear directional coupler- intensity controlled tunable optical filter", *Electron. Lett.*, vol. 27, no. 24, 1991, pp. 2218-2219.

APPENDICES

APPENDIX 1

NONLINEAR PERMITTIVITY

In this appendix, the relationship between the nonlinear refractive index n_2 , and the nonlinear permittivity α is derived, and related to the third order susceptibility (Kerr effect). Let $\underline{E}(r,t)$ and $\underline{P}(r,t)$ be the real parts of the electric field and polarisation in a medium. $\underline{E}(r,t)$ can be split into amplitude and phase notation as follows

$$\underline{E}(r,t) = \text{Re}[\hat{E}(r)e^{j(k \cdot r - \omega t)}] = 1/2[\hat{E}(r)e^{j(k \cdot r - \omega t)} + c.c.] \quad (\text{A1.1})$$

Similarly for $\underline{P}(r,t)$, the polarisation response becomes

$$\underline{P}(r,t) = 1/2[\hat{P}(r)e^{j(k \cdot r - \omega t)} + c.c.] \quad (\text{A1.2})$$

where $\hat{P}(r)$ is the slow varying amplitude. If the electric field $\underline{E}(r,t)$ is small, the polarisation $\underline{P}(r,t)$ is directly proportional to the field, but for large fields, the polarisation is related to it in terms of a Taylor expansion [1]

$$\underline{P}(r,t) = \epsilon_0 \chi^{(1)} \underline{E}(r,t) + \epsilon_0 \chi^{(2)} \underline{E}^2(r,t) + \epsilon_0 \chi^{(3)} \underline{E}^3(r,t) + \dots = \sum_n \epsilon_0 \chi^{(n)} \underline{E}^n \quad (\text{A1.3})$$

where $\chi^{(1)}$, $\chi^{(2)}$, $\chi^{(3)}$ etc are the susceptibilities, and ϵ_0 the permittivity of free space.

$\chi^{(2)}$ is responsible for second order effects such as second harmonic generation. $\chi^{(3)}$ is responsible for third order effects such as the optical kerr effect. Substituting equations A1.1 and A1.2 into A1.3 and expanding the right hand side binomially gives,

$$1/2[\hat{P}(r)e^{j(k \cdot r - \omega t)} + c.c.] = \epsilon_0 \chi^{(n)} \frac{1}{2^n} \sum_{m=0}^n {}^n C_m (\hat{E}(r)e^{j(k \cdot r - \omega t)})^m (\hat{E}^*(r)e^{-j(k \cdot r - \omega t)})^{n-m} \quad (\text{A1.4})$$

Eqn. A1.4 gives the polarisation response of the medium to the electric field. It consists of many frequencies, but we are interested in ω . Matching the coefficients of $e^{j(k \cdot r - \omega t)}$ on both sides of eqn A1.4, we note that on the RHS, if 'm' were replaced by a number ' μ ', and 'n-m' were replaced by ' $\mu - 1$ ', then $e^{j(k \cdot r - \omega t)}$ could be extracted. Therefore $m = \mu$ and $n - m = \mu - 1$ gives

$$m = \frac{n+1}{2} \quad n - m = \frac{n-1}{2} \quad (\text{A1.5})$$

Substituting eqn A1.5 into eqn A1.4 and simplifying

$$\hat{P}(r) = \sum_n \varepsilon_0 \chi^{(n)} \frac{1}{2^{n-1}} {}^n C_{\frac{n+1}{2}} |\hat{E}(r)|^{n-1} \hat{E}(r) \quad (\text{A1.6})$$

Expanding eqn A1.6 as far as third order and multiplying both sides by $e^{j(k \cdot r - \omega t)}$ gives

$$\underline{P}^\omega(r, t) = \varepsilon_0 \chi^{(1)} \underline{E}^\omega(r, t) + \frac{3}{4} \varepsilon_0 \chi^{(3)} |\underline{E}^\omega(r, t)|^2 \underline{E}^\omega(r, t) \quad (\text{A1.7})$$

where $\underline{P}^\omega(r, t)$ and $\underline{E}^\omega(r, t)$ are defined by

$$\underline{P}^\omega(r, t) = \hat{P}(r) e^{j(\omega t - k \cdot r)} \quad \underline{E}^\omega(r, t) = \hat{E}(r) e^{j(\omega t - k \cdot r)} \quad (\text{A1.8})$$

The electric displacement is given by

$$\underline{D}^\omega(r, t) = \varepsilon_0 \underline{E}^\omega(r, t) + \underline{P}^\omega(r, t) \quad (\text{A1.9})$$

Therefore the electric displacement becomes (substituting eqns A1.8 into eqn. A1.9)

$$\underline{D}^\omega(r, t) = \varepsilon_0 \underline{E}^\omega(r, t) + \underbrace{\varepsilon_0 \chi^{(1)} \underline{E}^\omega(r, t)}_{P_{\text{linear}}^\omega(r, t)} + \underbrace{\frac{3}{4} \varepsilon_0 \chi^{(3)} |\underline{E}^\omega(r, t)|^2 \underline{E}^\omega(r, t)}_{P_{\text{NL}}^\omega(r, t)} \quad (\text{A1.10})$$

But $\underline{D}^\omega(r, t) = \varepsilon_0 n^2 \underline{E}^\omega(r, t)$ where n is the nonlinear refractive index. The linear refractive index n_0 is related to $\chi^{(1)}$ via $n_0^2 = 1 + \chi^{(1)}$.

$$n^2 = n_0^2 + \frac{3}{4} \chi^{(3)} |\underline{E}^\omega(r, t)|^2 = n_0^2 + \frac{3}{4} \chi^{(3)} |\hat{E}(r)|^2 \quad (\text{A1.11})$$

But for intensity dependent refractive indices $n = n_0 + n_2 I(r)$, where the intensity $I(r)$ is given by (see eqn. A6.12)

$$I(r) = 1/2 \varepsilon_0 n_0 c |\hat{E}(r)|^2 \quad (\text{A1.12})$$

Squaring n , and ignoring the n_2^2 term because it is small results in

$$n^2 \cong n_0^2 + 2n_0n_2I(\underline{r}) \quad (\text{A1.13})$$

Inserting the value for $I(\underline{r})$ from eqn. A1.12 into eqn. A1.13 gives

$$n^2 \cong n_0^2 + \varepsilon_0 n_0^2 n_2 c |\hat{\underline{E}}(\underline{r})|^2 \quad (\text{A1.14})$$

In terms of the nonlinear permittivity eqn. A1.14 becomes

$$\varepsilon_{NL} \cong \varepsilon^{(p)} + \alpha |\hat{\underline{E}}(\underline{r})|^2 \quad (\text{A1.15})$$

$$\alpha = \varepsilon_0 n_0^2 n_2 c \quad (\text{A1.16})$$

Also n_2 and α can be compared to the third order susceptibility. Comparing eqns A1.15 and A1.16 with A1.11.

$$\alpha = \frac{3}{4} \chi^{(3)} \quad n_2 = \frac{3}{4} \frac{\chi^{(3)}}{\varepsilon_0 n_0^2 c} \quad (\text{A1.17})$$

n_2 is found in the literature either expressed in MKS units or ESU units. The relationship between the two is given by [2],

$$n_2[mks] = \frac{4\pi}{3} \times 10^{-7} \times \frac{1}{n_0} n_2[esu] \quad (\text{A1.18})$$

REFERENCES FOR APPENDIX 1

- [1] P. N. BUTCHER, and D. COTTER, "Elements of Nonlinear Optics", Cambridge Studies in Modern Optics 9, Cambridge University Press, 1990
- [2] H.A. HAUS, "Waves and fields in Optoelectronics", Prentice-Hall, 1984

APPENDIX 2

Maxwell's equations are given by

$$\nabla \times \underline{E} = j\omega\mu_0 \underline{H} \qquad \nabla \times \underline{H} = -j\omega\varepsilon_0 \varepsilon \underline{E} \qquad (A2.1)$$

where μ_0 is the permeability, ε_0 the permittivity of free space, and ε the relative permittivity. Considering *TE* propagation $\underline{E} = (0, E_y, 0)$, and $\underline{H} = (H_x, 0, H_z)$, and expanding eqns. A2.1 gives

$$H_x = \frac{j}{\omega\mu_0} \frac{\partial E_y}{\partial z} \qquad H_z = \frac{-j}{\omega\mu_0} \frac{\partial E_y}{\partial x} \qquad (A2.2)$$

$$\frac{\partial H_z}{\partial x} - \frac{\partial H_x}{\partial z} = j\omega\varepsilon_0 \varepsilon E_y \qquad (A2.3)$$

Substituting eqns. A2.2 into eqn. A2.3 (assuming $\partial/\partial y = 0$), and simplifying by shortening $\omega^2\mu_0\varepsilon_0$ to k_0^2 . Also assuming that E_y has $e^{j\beta z}$ dependence (where β is the propagation coefficient), $\partial^2 E_y / \partial z^2$ becomes $-\beta^2 E_y$. Therefore the wave equation becomes

$$\frac{\partial^2 E_y}{\partial x^2} = -(k_0^2 \varepsilon - \beta^2) E_y \qquad (A2.4)$$

Eigenvalue equation [1]

In section 10.4, when the value for the constant *A* is calculated, the eigenvalue equation is needed in the following two forms,

$$\text{Sin}kd = \frac{\pm\kappa(\gamma + \delta)}{\sqrt{(\kappa^2 + \gamma^2)(\kappa^2 + \delta^2)}} \qquad \text{Cos}kd = \frac{\pm(\kappa^2 - \gamma\delta)}{\sqrt{(\kappa^2 + \gamma^2)(\kappa^2 + \delta^2)}} \qquad (A2.5)$$

where the signs in eqns A1.5 are either both positive or both negative.

REFERENCES FOR APPENDIX2

[1] D. Marcuse, "Theory of dielectric optical waveguides", Academic Press, 1991

APPENDIX 3

Z-REVERSAL CONCEPT [1]

The z-reversal concept is very useful for converting backward travelling waves into forward travelling notation. Splitting \underline{E} , \underline{H} , and ∇ into transverse and longitudinal parts gives

$$\underline{E} = \underline{E}_t + \underline{E}_z \quad \underline{H} = \underline{H}_t + \underline{H}_z \quad \nabla = \nabla_t + \hat{z} \frac{\partial}{\partial z} \quad (\text{A3.1})$$

By inserting eqns A3.1 into Maxwell's equations (eqns A2.1) results in the following

$$\nabla_t \times \underline{E}_t = j\omega\mu \underline{H}_z \quad \nabla_t \times \underline{H}_t = -j\omega\varepsilon_0 \varepsilon \underline{E}_z \quad (\text{A3.2})$$

$$\nabla_t \times \underline{E}_z + j\beta \hat{z} \times \underline{E}_t = j\omega\mu \underline{H}_t \quad \nabla_t \times \underline{H}_z + j\beta \hat{z} \times \underline{H}_t = -j\omega\varepsilon_0 \varepsilon \underline{E}_t \quad (\text{A3.3})$$

For -ve travelling wave, β changes sign. Therefore Maxwell's equations become (where the '-' superscript on the fields imply negative travelling waves)

$$\beta \rightarrow -\beta \quad \nabla_t \times \underline{E}_t^- = j\omega\mu \underline{H}_z^- \quad \nabla_t \times \underline{H}_t^- = -j\omega\varepsilon_0 \varepsilon \underline{E}_z^- \quad (\text{A3.4})$$

$$\nabla_t \times \underline{E}_z^- - j\beta \hat{z} \times \underline{E}_t^- = j\omega\mu \underline{H}_t^- \quad \nabla_t \times \underline{H}_z^- - j\beta \hat{z} \times \underline{H}_t^- = -j\omega\varepsilon_0 \varepsilon \underline{E}_t^- \quad (\text{A3.5})$$

Eqns A3.4-A3.5 can now be converted back to eqns A3.2-A3.3 if the following substitutions are made.

$$\underline{E}_t = \underline{E}_t^- \quad \underline{H}_t = -\underline{H}_t^- \quad \underline{H}_z = \underline{H}_z^- \quad \underline{E}_z = -\underline{E}_z^- \quad (\text{A3.6})$$

Therefore, in conclusion if we want to transform the time-invariant form of -z travelling wave to a +z travelling wave, we have to make the following substitutions,

$$\beta^- \rightarrow \beta, \quad E_t^- \rightarrow E_t, \quad E_z^- \rightarrow -E_z, \quad H_t^- \rightarrow -H_t, \quad H_z^- \rightarrow -H_z \quad (\text{A3.7})$$

REFERENCES FOR APPENDIX 3

[1] eg. D.L.LEE,"Electromagnetic Principles of Integrated Optics", Wiley, 1986.

APPENDIX 4

LORENTZ' RECIPROCITY THEOREM [1,2]

Assume $\underline{E}^{(1)}, \underline{H}^{(1)}$ satisfies Maxwell's equations, and all the boundary conditions in medium $\epsilon^{(1)}(x, y)$, and $\underline{E}^{(2)}, \underline{H}^{(2)}$ in medium $\epsilon^{(2)}(x, y)$ respectively.

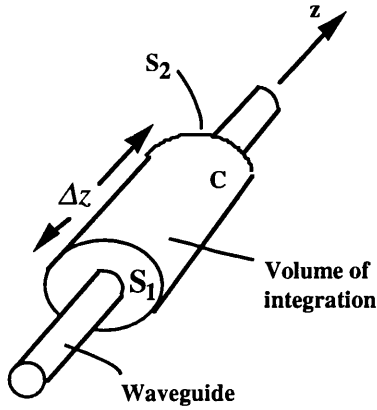


Fig. A4.1 illustrating Lorentz theorem

Maxwell's equations for medium 1 and 2 are:

$$\nabla \times \underline{E}^{(1)} = j\omega\mu_0 \underline{H}^{(1)} \quad \nabla \times \underline{H}^{(1)} = -j\omega\epsilon_0 \epsilon^{(1)} \underline{E}^{(1)} \quad (\text{A4.1})$$

$$\nabla \times \underline{E}^{(2)} = j\omega\mu_0 \underline{H}^{(2)} \quad \nabla \times \underline{H}^{(2)} = -j\omega\epsilon_0 \epsilon^{(2)} \underline{E}^{(2)} \quad (\text{A4.2})$$

Using the vector identity $\nabla \cdot (\underline{A} \times \underline{B}) = \underline{B} \cdot \nabla \times \underline{A} - \underline{A} \cdot \nabla \times \underline{B}$, and relating eqns. A4.1-A4.2 in the following way

$$\underline{H}^{(2)} \cdot (\text{A3.1}) - \underline{E}^{(1)} \cdot (\text{A3.4}) + \underline{E}^{(2)} \cdot (\text{A3.2}) - \underline{H}^{(1)} \cdot (\text{A3.3})$$

$$\text{gives } \nabla \cdot (\underline{E}^{(1)} \times \underline{H}^{(2)} - \underline{E}^{(2)} \times \underline{H}^{(1)}) = j\omega\epsilon_0 (\epsilon^{(2)} - \epsilon^{(1)}) \underline{E}^{(1)} \cdot \underline{E}^{(2)} \quad (\text{A4.3})$$

Integrating eqn A4.3 over a volume V and making use of the divergence theorem transforms the LHS from a volume integral to a surface integral

$$\oint_S [\underline{E}^{(1)} \times \underline{H}^{(2)} - \underline{E}^{(2)} \times \underline{H}^{(1)}] \cdot d\underline{S} = j\omega\epsilon_0 \iiint_V (\epsilon^{(2)} - \epsilon^{(1)}) \underline{E}^{(1)} \cdot \underline{E}^{(2)} dV \quad (\text{A4.4})$$

We now consider the integrand of eqn. A4.4. For clarity, let $\underline{F} = \underline{E}^{(1)} \times \underline{H}^{(2)} - \underline{E}^{(2)} \times \underline{H}^{(1)}$. If the volume of integration is that of a large cylinder of

infinitesimal length Δz (see Fig. A4.1), and the fields are small over the bounding area C (since the fields are in the region of the waveguide), the LHS of eqn A4.4 becomes,

$$\oiint_S \underline{F} \cdot d\underline{S} = \oiint_{S_1} \underline{F} \cdot d\underline{S} + \oiint_{S_2} \underline{F} \cdot d\underline{S} = \oiint_S (F_z(x, y, z + dz) - F_z(x, y, z)) d\underline{S} \quad (\text{A4.5})$$

For the RHS of eqn. A4.4, since the volume of integration is that of a cylinder $S\Delta z$, the volume integral $-j\omega \iiint_V dV$ can be expressed as $-j\omega\Delta z \oiint_S d\underline{S}$.
 $= \oiint_S (F_z(x, y, z + dz) - F_z(x, y, z)) d\underline{S}$. Therefore eqn. A4.4 now becomes

$$\lim_{\Delta z \rightarrow 0} \left[\oiint_S [F_z(x, y, z + dz) - F_z(x, y, z)] d\underline{S} = -j\omega\epsilon_0\Delta z \oiint_S (\epsilon^{(2)} - \epsilon^{(1)}) \underline{E}^{(1)} \cdot \underline{E}^{(2)} d\underline{S} \right] \quad (\text{A4.6})$$

Dividing both sides of eqn A4.6 by Δz gives

$$\oiint_S \left[\frac{\partial}{\partial z} F_z(x, y, z) \right] d\underline{S} = j\omega\epsilon_0 \oiint_S (\epsilon^{(2)} - \epsilon^{(1)}) \underline{E}^{(1)} \cdot \underline{E}^{(2)} d\underline{S} \quad (\text{A4.7})$$

But $F_z(x, y, z) = \underline{E}_i^{(1)} \times \underline{H}_i^{(2)} - \underline{E}_i^{(2)} \times \underline{H}_i^{(1)}$. Therefore eqn A4.7 becomes

$$\oiint_S \frac{\partial}{\partial z} (\underline{E}_i^{(1)} \times \underline{H}_i^{(2)} - \underline{E}_i^{(2)} \times \underline{H}_i^{(1)}) \cdot \hat{z} d\underline{S} = j\omega\epsilon_0 \oiint_S (\epsilon^{(2)} - \epsilon^{(1)}) \underline{E}^{(1)} \cdot \underline{E}^{(2)} d\underline{S} \quad (\text{A4.8})$$

where all the fields satisfy Maxwell's equations and all the boundary conditions for their respective systems. Substituting $ds = dx dy$ gives finally

$$\frac{\partial}{\partial z} \iint_{-\infty}^{+\infty} (\underline{E}_i^{(1)} \times \underline{H}_i^{(2)} - \underline{E}_i^{(2)} \times \underline{H}_i^{(1)}) \cdot \hat{z} dx dy = j\omega\epsilon_0 \iint_{-\infty}^{+\infty} (\epsilon^{(2)} - \epsilon^{(1)}) \underline{E}^{(1)} \cdot \underline{E}^{(2)} dx dy \quad (\text{A4.9})$$

REFERENCES FOR APPENDIX 4

- [1] A. W. Snyder and J. D. Love, "Optical waveguide theory", Chapman and Hall, 1983.
- [2] D.L.Lee, "Electromagnetic Principles of Integrated Optics", Wiley, 1986.

APPENDIX 5

The derivation of eqn 6.6 will be explained in more detail in this appendix.

The product of the sum of N numbers such that

$(a_1 + a_2 + a_3 + \dots + a_N)(a_1^* + a_2^* + a_3^* + \dots + a_N^*)(a_1 + a_2 + a_3 + \dots + a_N)$ is given by

$$\left(\sum_{q=1}^N a_q \right) \times \left(\sum_{r=1}^N a_r^* \right) \times \left(\sum_{\ell=1}^N a_\ell \right) = \sum_{\ell=1}^N a_\ell |a_\ell|^2 \quad (\text{A5.1a})$$

$$+ 2 \sum_{\ell=1}^N a_\ell \sum_{q=1}^N |a_q|^2 \quad \text{where } \ell \neq q \quad (\text{A5.1b})$$

$$+ \sum_{\ell=1}^N a_\ell^* \sum_{q=1}^N a_q a_r \quad \text{where } \ell \neq q \neq r \quad (\text{A5.1c})$$

$$+ \sum_{\ell=1}^N a_\ell^2 \sum_{q=1}^N a_q^* \quad \text{where } \ell \neq q \quad (\text{A5.1d})$$

Inserting $a_s \rightarrow a_s \underline{E}_i^{(s)}$ where s is any number, and $(1 - \delta_{pq})$ for $p \neq q$ into eqn A5.1, and substituting this into eqn 6.5, results in eqn 6.6

APPENDIX 6

POYNTING THEOREM

In this appendix, we will derive the Poynting theorem [1,2], which gives the power carried by an electromagnetic wave in terms of the fields.

Maxwell's equations in time-varying form for an isotropic medium are given by

$$\nabla \times \underline{E}(z, t) = -\frac{\partial \underline{B}(z, t)}{\partial t} \quad \nabla \times \underline{H}(z, t) = \frac{\partial \underline{D}(z, t)}{\partial t} + \underline{J}(z, t) \quad (\text{A6.1})$$

where $\underline{B}(z, t) = \mu_0 \underline{H}(z, t)$, and $\underline{D}(z, t) = \epsilon_0 \epsilon \underline{E}(z, t) = \epsilon_0 \underline{E}(z, t) + \underline{P}(z, t)$, μ_0 is the permeability, ϵ_0 the permittivity of free space, \underline{P} is the polarisation response of the medium, and \underline{J} is the current density. Substituting eqns. A6.1 into the following identity $\nabla \cdot (\underline{E} \times \underline{H}) = \underline{H} \cdot \nabla \times \underline{E} - \underline{E} \cdot \nabla \times \underline{H}$ and integrating over an infinite volume gives

$$-\int_V \nabla \cdot (\underline{E}(z, t) \times \underline{H}(z, t)) dV = \int_V \left[\underline{H}(z, t) \cdot \frac{\partial \underline{B}(z, t)}{\partial t} + \underline{E}(z, t) \cdot \frac{\partial \underline{D}(z, t)}{\partial t} + \underline{E}(z, t) \cdot \underline{J}(z, t) \right] dV \quad (\text{A6.2})$$

The first term in eqn. A6.2 can be transformed from a volume integral to a surface integral using the divergence theorem,

$$-\iint_S (\underline{E}(z, t) \times \underline{H}(z, t)) \cdot \hat{z} dS = \int_V \left[\underline{H}(z, t) \cdot \frac{\partial \underline{B}(z, t)}{\partial t} + \underline{E}(z, t) \cdot \frac{\partial \underline{D}(z, t)}{\partial t} + \underline{E}(z, t) \cdot \underline{J}(z, t) \right] dV \quad (\text{A6.3})$$

The first term on the RHS of eqn. A6.3 represents the rate of increase (with time) of the stored energy in the magnetic field, and the second term, the rate of increase of the stored electrical energy in the electrical field. The third term represents either ohmic power loss if \underline{J} is a conduction current density, or the power required to accelerate charges if \underline{J} is a convection current arising from moving charges. These rate of increase in energy are supplied by the $-\iint_S (\underline{E}(z, t) \times \underline{H}(z, t)) \cdot \hat{z} dS$ on the LHS, of eqn.

A6.3, which represents the external energy flow into the volume.

TIME AVERAGED INTENSITY

Since $\underline{P}(z, t)$ is the instantaneous intensity, we would like to find the time-averaged intensity, and to do this we have to somehow extract the time dependence from $\underline{P}(z, t)$. With fields, this is easy. We simply say

$$\underline{E}(z, t) = \text{Re}(\underline{E}(z)e^{-j\omega t}) \quad \underline{H}(z, t) = \text{Re}(\underline{H}(z)e^{-j\omega t}) \quad (\text{A6.4})$$

But we cannot express the Poynting vector $\underline{P}(z, t)$ in terms of amplitude $\underline{P}(z)$ and phase $e^{-j\omega t}$ as we can with the fields, ie $\underline{P}(z, t) \neq \text{Re}(\underline{P}(z)e^{-j\omega t})$, where $\underline{P}(z) = \underline{E}(z) \times \underline{H}(z)$. Therefore we are forced to multiply out as follows,

$$\underline{P}(z, t) = \underline{E}(z, t) \times \underline{H}(z, t) = \text{Re}[\underline{E}(z)e^{-j\omega t}] \times \text{Re}[\underline{H}(z)e^{-j\omega t}] \quad (\text{A6.5})$$

$$= \frac{1}{4} [\underline{E}(z) \times \underline{H}(z)e^{-2j\omega t} + \underline{E}(z) \times \underline{H}^*(z) + \underline{E}^*(z) \times \underline{H}(z) + \underline{E}^*(z) \times \underline{H}^*(z)e^{2j\omega t}] \quad (\text{A6.6})$$

The four terms in line A6.6 can be condensed to two terms as follows

$$= \frac{1}{2} \text{Re}[\underline{E}(z) \times \underline{H}^*(z) + \underline{E}(z) \times \underline{H}(z)e^{-2j\omega t}] \quad (\text{A6.7})$$

Now that the time component is separated from the Poynting vector in line A6.7, the time-averaged intensity can be found by integrating eqn. A6.7 over the time T and dividing by T . This will eliminate the fast varying component (containing $e^{-2j\omega t}$) since the period T is much larger than the period of oscillation. Using eqn A6.7, the time-averaged intensity \underline{I}_{av} is given by

$$\underline{I}_{av} = \frac{1}{T} \int_0^T \underline{P}(z, t) dt = \frac{1}{2} \text{Re}[\underline{E}(z) \times \underline{H}^*(z)] \quad (\text{A6.8})$$

Therefore in summary, $\underline{P}(z, t) = \underline{E}(z, t) \times \underline{H}(z, t)$ is called the Poynting vector, and is the instantaneous intensity vector, and $\underline{I}_{av} = \frac{1}{2} \text{Re}[\underline{E}(z) \times \underline{H}^*(z)]$ is the time averaged intensity vector. The vectors are in the direction of power flow (z direction).

Relating the intensity to the field

The time-averaged intensity, or irradiance is given by

$$I_{av} = \frac{1}{2} \text{Re}(\underline{E} \times \underline{H}^*) \cdot \hat{z} \quad (\text{A6.9})$$

Assuming *TE* propagation, $(0, E_y, 0)$, and $(H_x, 0, H_z)$, where E_y , H_x , and H_z are the time-independent fields.

$$I_{av} = \frac{1}{2} \text{Re}(-E_y H_x^*) \quad (\text{A6.10})$$

Assuming $\beta = \beta_r + j\beta_i$, where β_r , and β_i are the real and imaginary parts of the propagation coefficient, and making use of eqn. A2.2 (to relate H_x and E_y) eqn. A6.10 becomes

$$I_{av} = \frac{\beta_r |E_y|^2}{2\omega\mu_0} \quad (\text{A6.11})$$

Assuming $\beta_r \cong \omega\sqrt{\mu_0\epsilon_r\epsilon_0}$, eqn. A6.11 becomes,

$$I_{av} \cong \frac{n_0 |E_y|^2}{2\sqrt{\frac{\mu_0}{\epsilon_0}}} \cong \frac{1}{2} \epsilon_0 c n_0 |E_y|^2 \quad \text{where } n_0 = \sqrt{\epsilon_r} \quad (\text{A6.12})$$

Time-averaged power for a multiwaveguide system

The time-averaged power [3-4] is now calculated in terms of the overlap integrals. Let E_t and H_t be the total field for the multiwaveguide system, and that they can be approximately constructed from the eigenmodes of the guides. Therefore

$$E_t = \sum_{q=1}^N a_q \underline{E}_t^{(q)} \quad H_t = \sum_{p=1}^N a_p \underline{E}_t^{(p)} \quad (\text{A6.13})$$

The time-averaged power $P(z)$ is calculated by integrating the time-averaged intensity (eqn. A6.9) over infinite cross-section. (Note $P(z)$ should not be confused with Poynting vector).

$$P(z) = \frac{1}{2} \text{Re} \iint_{-\infty}^{+\infty} (\underline{E}_t \times \underline{H}_t^*) \cdot \hat{z} \, dx dy \quad (\text{A6.14})$$

Using the definition for \underline{E}_i and \underline{H}_i from A6.13, eqn. A6.14 becomes

$$= \frac{1}{2} \operatorname{Re} \int_{-\infty}^{+\infty} \sum_{q=1}^N \sum_{p=1}^N a_q a_p^* (\underline{E}_i^{(q)} \times \underline{H}_i^{(p)}) \cdot \hat{z} dx dy \quad (\text{A6.15})$$

but by definition $\iint_{-\infty}^{+\infty} (\underline{E}_i^{(q)} \times \underline{H}_i^{(p)}) \cdot \hat{z} dx dy = 2PC_{pq}$ (A6.16)

Substituting for P from eqn. A6.16 into A6.15 and rearranging gives $P = P \sum_{p,q} a_p^* C_{pq} a_q$. Therefore the total time averaged power is $P \sum_{p,q} a_p^* C_{pq} a_q$. Cancelling out the P gives $\underline{a}^+ C \underline{a} = 1$.

In prior weak coupled mode theories, it was thought that C was the identity matrix, which led to $\underline{a}^+ \underline{a} = 1$. For two guides, $\underline{a}^+ C \underline{a} = 1$ becomes

$$|a_1|^2 + |a_2|^2 + C_{12}(a_1^* a_2 + a_2^* a_1) = 1 \quad (\text{A6.17})$$

Therefore the power is carried by the first mode, the second mode, and the overlap between the modes (in prior theories, it was $|a_1|^2 + |a_2|^2 = 1$). For N guides, the total power is

$$\sum_{r=1}^N |a_r|^2 + \sum_{p,q} a_p^* C_{pq} a_q (1 - \delta_{pq}) = 1 \quad (\text{A6.18})$$

In terms of the amplitude coefficients $A_1(z)$, and $A_2(z)$ such that $a_1(z) = A_1(z)e^{j\beta_1 z}$, and assuming a symmetrical case so that $\beta_1 = \beta_2$, then eqn. A6.17 becomes

$$|A_1|^2 + |A_2|^2 + C_{12}(A_1^* A_2 + A_2^* A_1) = 1 \quad (\text{A6.19})$$

REFERENCES FOR APPENDIX 6

- [1] S. Ramo, J. R. Whinnery, and T. Vanduzer, "Fields and waves in communication electronics", Wiley, Second edition, 1984.
- [2] D. L. Lee, "Electromagnetic Principles of Integrated Optics", Wiley, 1986.
- [3] H. A. Haus and W. Huang, "Coupled mode theory", Proc. IEEE, vol. 79, no. 10, 1991, pp. 1505-1518.
- [4] H. Haus, W. P. Huang, S. Kawakami, and N. A. Whitaker, "Coupled-mode theory of optical waveguides", J. Light. Technol., vol. LT-5, no. 1, 1987, pp. 16-23.